# Monitoring a Pile - Supported Integral Abutment Bridge at a Site with Shallow Bedrock Phase II

## Technical Report
## ME 01-7
## August 2006

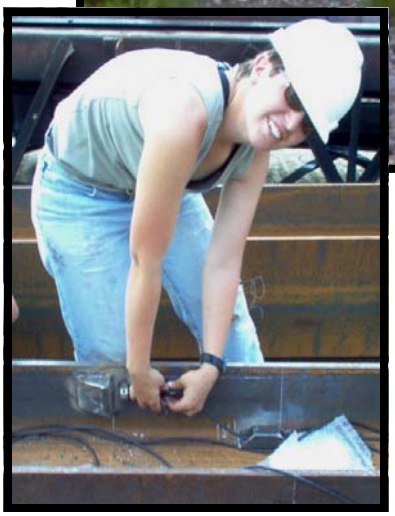

MaineDOT

A Publication from the Maine Department of Transportation's Research Division

Technical Report Documentation Page

| | | |
|---|---|---|
| 1. Report No.<br>ME 01-7 | 2. | 3. Recipient's Accession No. |
| 4. Title and Subtitle<br>Monitoring a pile-supported integral abutment.<br>Bridge at a site with shallow bedrock. Phase II | | 5. Report Date<br>August 2006<br>6. |
| 7. Author(s)<br>Sarah L. Hartt,<br>Thomas C. Sandford, PH.D., P.E.,<br>William G. Davids, PH.D., P.E. | | 8. Performing Organization Report No. |
| 9. Performing Organization Name and Address<br>Department of Civil & Environmental Engineering<br>University of Maine<br>Orono, ME 04469-5711 | | 10. Project/Task/Work Unit No.<br>11. Contract © or Grant (G) No. |
| 12. Sponsoring Organization Name and Address<br>Maine DOT<br>16 State House Station<br>Augusta, ME 04333-0016 | | 13. Type of Report and Period Covered<br>14. Sponsoring Agency Code |
| 15. Supplementary Notes | | |

16. Abstract (Limit 200 words)


Currently, pile supported integral abutments are limited to locations where the depth of overburden can provide fixed support conditions. In Maine, there are often integral abutment bridges site with a shallow depth to bedrock where piles must be drilled into bedrock to obtain fixity. The objective of this research is to expand the use of pile-supported integral abutment bridges bearing on bedrock at sites where the depth to bedrock is considered shallow, less than 4m (13 ft) from the ground surface.

The completed Phase 1 of this project (DeLano, 2004) has produced preliminary design guidelines for integral abutment bridges with piles to the top of bedrock at an overburden depth less than that required for developing fixity. The objective of Phase II of this two-part research project is to finalize the design and construction guidelines by incorporating the performance of a constructed, skewed integral abutment bridge on shallow bedrock into the guidelines. Part (a) of Phase II (this report) includes instrumentation installation, construction monitoring, and full-scale live load testing on the Nash Stream Bridge in Coplin Plantation, ME.

Observation made during both the construction sequence and live load testing are generally in agreement with those made during Phase 1. Maximum stresses at the end of construction from dead and live load were 59% of the nominal yield stress of -345 MPA (-50ksi). Bending stress was the largest component of the total stress, while axial stress made up an average of 31% of the total stress. There was significant variability in the axial loadings to piles with loads varying from 0.63 to 1.55 of the longer piles were fixed at some depth, while the shorter piles did not develop fixity. The stresses in the short piles were found to be no more severe than the stresses in the long piles.

Monitoring of the bridge will continue for more than a full year from the completion of construction to include seasonal thermal loadings. This data will be used to provide a calibration for finite element models developed in Phase 1 and to assess any limitations of the preliminary design guidelines. A final design guideline will be developed for all anticipated conditions in Maine.


| | | | |
|---|---|---|---|
| 17. Document Analysis/Descriptors<br>Integral Abutments, Pile-supported, Pile bedrock interaction. | | 18. Availability Statement | |
| 19. Security Class (this report) | 20. Security Class (this page) | 21. No. of Pages<br>234 | 22. Price |

# MONITORING A PILE-SUPPORTED INTEGRAL ABUTMENT

# BRIDGE AT A SITE WITH SHALLOW BEDROCK

By

Sarah L. Hartt

Thomas C. Sandford

William G. Davids

Civil and Environmental Engineering Department

The University of Maine

August, 2006

**MONITORING A PILE-SUPPORTED INTEGRAL ABUTMENT**

**BRIDGE AT A SITE WITH SHALLOW BEDROCK**

By Sarah L. Hartt

Thomas C. Sandford, Ph.D., P.E.

William G. Davids, Ph.D., P.E.

August, 2006

## ABSTRACT

Although the advantages of integral abutment bridges are widely known, design practices and assumptions vary extensively. Currently, pile supported integral abutments are limited to locations where the depth of overburden can provide fixed support conditions. In Maine, there are often integral abutment bridges sites with a shallow depth to bedrock where piles must be drilled into bedrock to obtain fixity. The objective of this research is to expand the use of pile-supported integral abutment bridges bearing on bedrock at sites where the depth to bedrock is considered shallow, less than 4 m (13 ft) from the ground surface.

The completed Phase I of this project (DeLano, 2004) has produced preliminary design guidelines for integral abutment bridges with piles to the top of bedrock at an overburden depth less than that required for developing fixity. The objective of Phase II

of this two-part research project is to finalize the design and construction guidelines by incorporating the performance of a constructed, skewed integral abutment bridge on shallow bedrock into the guidelines. Part (a) of Phase II (this report) includes instrumentation installation, construction monitoring, and full-scale live load testing. Part (b) of Phase II (future report) comprises responses to seasonal temperature changes, investigations into the effects of skew, and finalizing of construction and design guidelines.

The Coplin Plantation, ME site offered a unique opportunity to investigate possible differences in short and long pile behaviors. One abutment has a depth of overburden sufficient to achieve pile fixity, while the other abutment has insufficient overburden to achieve pile fixity. This allowed for the unique comparison of pile behavior for deep and shallow bedrock conditions at the same bridge. Finite element investigations during Phase I indicated that the performance of an abutment was little changed by changing the configuration of the other abutment. Monitoring of the bridge included pile and abutment movements, pile strains, soil and pore pressures, and temperatures. The sequence and procedure of construction was analyzed to assess its effects on stresses in the pilings. Upon completion, the bridge was subjected to a comprehensive live load test to assess the effects of truck loads on the structure.

Observations made during both the construction sequence and live load testing are generally in agreement with those made during Phase I. Maximum stresses at the end of construction from dead and live load were 59% of the nominal yield stress of -345 Mpa (-50 ksi). Bending stress was the largest component of the total stress, while axial stress made up an average of 31% of the total stress. There was significant variability in the

axial loadings to piles with loads varying from 0.63 to 1.55 of the mean load. Skew affected stress in the piles, especially bending stress with a movement perpendicular to centerline. The near-obtuse piles saw a larger percentage of the loads. The longer piles were fixed at some depth, while the shorter piles did not develop fixity. The stresses in the short piles were found to be no more severe than the stresses in the long piles.

Stresses encountered during construction including axial stress, weak axis bending stress, and strong axis bending stress should be considered in the design of piles.

Monitoring of the bridge will continue for more than a full year from the completion of construction to include seasonal thermal loadings. This data will be used to provide a calibration for finite element models developed in Phase I and to assess any limitations of the preliminary design guidelines. A final design guideline will be developed for all anticipated conditions in Maine.

**ACKNOWLEDGEMENTS**

We would like to acknowledge the Maine Department of Transportation through Dale Peabody, Research Engineer, for providing funding for this research project. Thanks go out to Jeff Tweedie for supplying information and arranging for assistance as needed and to Jerry Clark for answering field questions, on a daily basis. We would like to thank John G. DeLano for the support and insight he provided for this Phase II. Our appreciation goes to Chris Lyons for his help and patience in the field in untangling wires and then pulling them through miles of pvc. We would also like to thank the crew of Reed & Reed who were helpful in the field.

## TABLE OF CONTENTS

## LIST OF TABLES

## LIST OF FIGURES

## LIST OF SYMBOLS AND ABBREVIATIONS

$A_p$ …..……..…… Cross-sectional area of pile

AASHTO …… American Association of State Highway and Transportation Officials

AISC …….…… American Institute of Steel Construction

AISI …….…….…… American Iron and Steel Institute

ASTM …… American Society for Testing and Materials

AT …..……..……..……...… Alberta Transportation

$B_0$ …..……..……...……...Initial barometric pressure

$B_1$ …..……..……..……..Current barometric pressure

$c$ ……. Cohesion yield stress

$C0_t$ …… Thermistor calibration factor

$C1_t$ …… Thermistor calibration factor

$C2_t$ …… Thermistor calibration factor

$C3_t$ …… Thermistor calibration factor

$C4_t$ …… Thermistor calibration factor

$C1_{EX}$ ……Extensometer calibration factor

$C2_{EX}$ ……Extensometer calibration factor

$C3_{EX}$ ……Extensometer calibration factor

$C1_{PC}$ …… Pressure cell calibration factor

$C2_{PC}$ …… Pressure cell calibration factor

$C1_Z$ …… Piezometer calibration factor

$C2_Z$ …… Piezometer calibration factor

$CT_{PC}$ ……...Pressure cell thermal calibration factor

$CT_Z$ …… Piezometer thermal calibration factor

$D_{0EX}$ ……... Initial extensometer displacement

$D_{1EX}$ …… Current extensometer displacement

$D_{EX}$……..…… Displacement of extensometer

$D_{rel}$……... Relative displacement

DOT …….……..…… …Department of Transportation

$E_p$ ……...…….……. Young's modulus of pile

FE ……Finite Element

$F_y$ ……... Yield stress of pile

G1-S ……South pile supporting girder #1

G2-S ……South pile supporting girder #2

G3-S ……South pile supporting girder #3

G4-S ……South pile supporting girder #4

G1-N ……...North pile supporting girder #1

G2-N ……...North pile supporting girder #2

G3-N ……...North pile supporting girder #3

G4-N ……...North pile supporting girder #4

$l_c$ ……. Total length of equivalent cantilever ($l_u$+$l_e$)

$l_e$ …… Length of equivalent cantilever below ground surface

$l_u$ …… Length of pile above ground surface

$l_{inc}$……...Inclinometer measurement interval

$L$ ……...…… Length of pile below ground surface

$L_{IEX}$ ……Current extensometer reading

$L_{0PC}$…… Initial pressure cell reading

$L_{1PC}$……. Current pressure cell reading

$L_{0SG}$…….. Initial strain gage reading

$L_{1SG}$…… Current strain gage reading

$L_{0Z}$…… Initial piezometer reading

$L_{1Z}$……. Current piezometer reading

$L_S$……..……...…… Length of bridge span

LRFD ……...…… Load Resistance Factor Design

LU……Linear Unit

LVDT ……Lateral Variable Differential Transformer

MDOT ……...……...… Maine Department of Transportation

MTO ……...……. Ontario Ministry of Transportation

$p$ …….…….….. Soil pressure resistance

$R_{25}$ ……Thermistor resistance

$R_t$ ……Factor depicting thermistor type

$S_x$……Strong axis section modulus

$S_y$…….. Weak axis section modulus

$S_z$……...Torsional section modulus

$T_{0PC}$ ……Initial pressure cell temperature

$T_{1PC}$ …… Current pressure cell temperature

$T_{0Z}$ ……Initial piezometer temperature

$T_{1Z}$ ……Current piezometer temperature

$y$ ……. Lateral pile displacement

$\alpha$ ……. Coefficient of thermal expansion

$\Delta$ …… Lateral displacement of pile head due to temperature change

$\Delta_{lat}$ ……Lateral deviation

$\Delta\varepsilon$…….. Change in strain

$\Delta P_{PC}$ ……...Change in pressure determined from a pressure cell

$\Delta P_Z$……...Change in pore water pressure determined from a piezometer

$\varepsilon_{ave}$ ……...Average strain of a set of strain gages

$\varepsilon_y$ ……. Yield strain

$\phi$ …… Internal angle of friction

$\rho$ ……. Mass density

$\theta_{inc}$……Angle of inclination

# Chapter 1

# INTRODUCTION

## 1.1. Background

The majority of highway bridges are concrete slab-on-girder structures, utilizing either steel or concrete girders. Traditionally, such bridges are constructed with expansion joints and bearings at the abutments to accommodate movement due to thermal expansion and contraction. The associated hardware is expensive to buy, install, maintain and repair. Problems pertaining to the expansion joints and bearings include damage due to heavy vehicle traffic and snow plows as well as corrosion due to leaking expansion joints and seals permitting run-off, de-icing chemicals and sand to clog the joints and damage the bearings. Girder ends and reinforced concrete substructures can be damaged by the infiltration of de-icing chemicals. Also, all moveable deck joints are vulnerable to the destructive effects of approach pavement growth. As a means to counteract these problems, some bridges have been constructed integrally, or without joints.

Integral abutment bridges have a short stub-type abutment rigidly connected to the bridge deck without the use of joints and supported by a single row of flexible piling (see Figure 1.1). The rigid connection allows the abutment and superstructure to act as a single structural unit. Intermediate piers for multi-span integral abutment bridges may be constructed either integrally with or independently of the superstructure. Semi-integral bridges are defined as single or multiple span continuous bridges with rigid, non-integral foundations. Their movement systems are primarily composed of integral end

diaphragms, compressible backfill, and moveable bearings in a horizontal joint at the superstructure-abutment interface (Mistry, 2000).

Advantages of integral abutment bridges include the elimination of expensive and high-maintenance expansion devices, simpler construction, reduced construction related environmental problems due to the elimination of cofferdams, increased redundancy as the girders are cast into the abutment, reduced foundation costs, reduced construction tolerance problems, and better performance during seismic events since the bridge acts as a single structural unit.

**Figure 1.1. Typical components of an integral abutment bridge (Arsoy et al., 1999)**

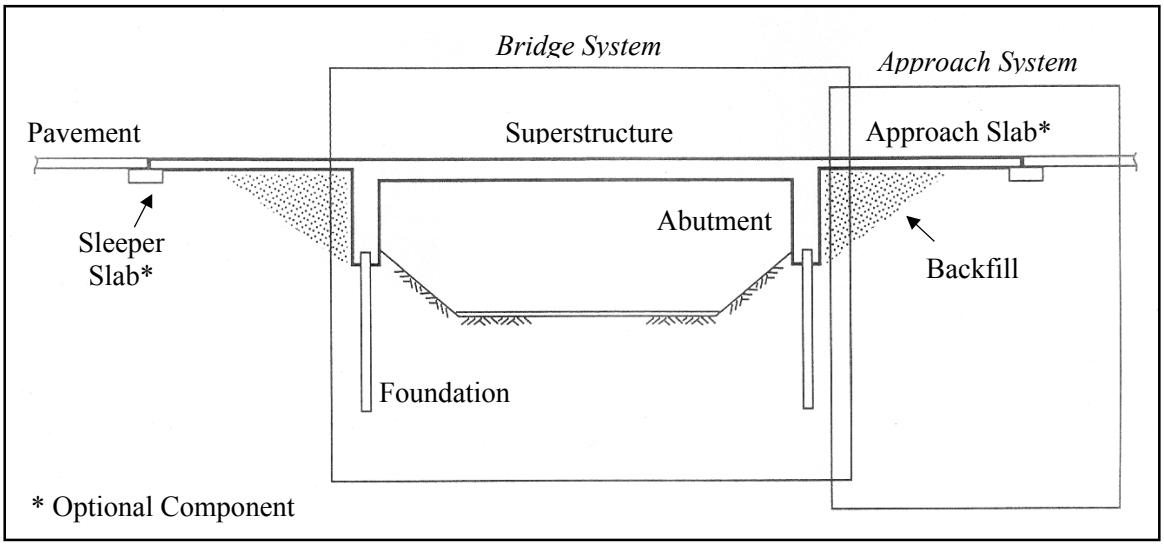


Currently, design practices in Maine and other states limit the use of pile-supported integral abutments to sites where there is sufficient soil overburden to provide a full fixed condition for a driven pile (Krusinski, 2002). The objective of this research is to expand the use of pile-supported integral abutment bridges to sites where the depth to bedrock is considered shallow, less than 4 m (13 ft) from the ground surface. Several questions remain that must be resolved before short pile-supported integral abutment

bridges can be designed and constructed with a high degree of confidence in Maine. Foremost is the need to quantify a minimum depth to bedrock and the degree of fixity required at the pile base to ensure abutment serviceability and safety. The research intended to address these issues is being completed in two phases:

Phase I:

a) Review of pertinent literature on the behavior and design of pile-supported integral abutments.

b) Completion of finite-element parametric studies to determine the effects of various design parameters, including pile length, on the bridge and foundation response.

c) Development of a preliminary set of design guidelines for short pile-supported integral abutment bridges.

Phase II:

a) Instrumentation and analysis of a short pile integral abutment bridge constructed in Coplin Plantation, Maine, both during and after construction.

b) Finite element model verification using data from instrumented bridge.

c) Development of final design guidelines for short-pile integral abutment bridges, incorporating data from both the finite element model and an actual bridge.

Phase I has been completed (DeLano, 2004), producing preliminary design guidelines for pile supported integral abutment bridges with overburden depth less than that required to develop fixity. This report focuses on the first task listed under Phase II of this project. Specific objectives pertaining to this task include determining:

- how the construction process affects the rotation of the abutment and the stresses in the piling caused by the dead load
- the effects of live load on stresses in the piling and the lateral distribution of live loads to the piles
- the effect of skew on abutment movements and individual pile stresses
- how stresses in piles without fixity compare to piles with fixity.

Monitoring of the bridge will continue for a full year after the completion of construction. This data will be used to provide calibration data for the finite element models and to assess any limitations of the preliminary design guidelines. A final design guideline will be developed for all anticipated conditions in Maine.

### 1.2. Organization of this Report

This report focuses on the work performed under the first task of Phase II, the instrumentation of an integral abutment bridge founded on short piles at the Coplin Plantation site. Chapter 2 contains a literature review that focuses on current practices as well as the behavior of integral abutment piles as examined in laboratory and field studies. Chapter 3 describes the instrument installation process, including the locations of each of the 11 instruments. Chapter 4 examines the monitored behavior of the integral

abutments, with particular emphasis on the construction sequence. The results of the live load test, conducted after the bridge was finished and prior to its opening, are given in Chapter 5. A summary of research findings, conclusions, and recommendations for future research is given in Chapter 6.

# Chapter 2

# LITERATURE REVIEW

Simple construction, reduced costs and maintenance and extended service life have made integral abutment bridges increasingly popular since the 1940's. The number of integral or continuous bridges constructed worldwide has increased significantly since the early 1960's. As of 1999, more than 30 American state and Canadian provincial transportation agencies have constructed over 9,700 bridges with integral abutments (Kunin & Alampalli, 2000).

Although their attributes are widely known, their limitations are less clear. Progress is constantly being made to unify design procedures. Currently, the American Association of State Highway and Transportation Officials (AASHTO) Load Resistance Factor Design (LRFD) Bridge Design Specification (AASHTO, 1998) does not directly address specific methods of analysis and design for integral abutment bridges. It does state, however, "integral abutment bridges shall be designed to resist and/or absorb creep, shrinkage, and thermal deformations of the superstructure." Many states have developed their own in-house methodologies for the design of integral abutment bridges. Several researchers have recommended techniques for design and used finite element models to check their validity.

This literature review investigates current design and construction practices in the United States, Canada and the United Kingdom. It examines some of the design procedures currently used including finite element modeling. Research conducted

regarding the behavior of piles supporting integral abutment bridges including both laboratory and field studies are reviewed, as are the preliminary design guidelines recently completed in Phase I of this research project by DeLano (2004).

## 2.1. Current Practices

Summarized below are results from surveys of transportation agencies in the United Kingdom (U.K.), Canada and the United States (U.S). The Canadian portion of the review pertains to the provinces of Alberta and Ontario. The survey of U.S. transportation agencies performed by Kunin and Alampalli (2000) includes over 30 states and Canadian provinces, excluding Alberta and Ontario.

### 2.1.1. United States

Kunin and Alampalli (2000) surveyed 39 states and Canadian provinces regarding their experience with integral abutment bridges, with eight states and provinces noting that they had no experience. For the most part, responses indicated that integral abutment bridges are performing as well as or better than their conventional bridge counterparts. Minimal difficulties were encountered including problems with minor cracking, drainage at abutments, and settlement of approach slabs. Despite this, the general opinion rated the performance of integral abutment bridges as good or excellent.

Construction of integral abutment bridges was reported dating back to 1905. The longest pre-cast concrete girder integral abutment bridge (358.4 m (1175 ft)) was constructed in Tennessee, while the longest steel girder integral abutment bridge (318.4 m (1044 ft)) and the longest cast in place concrete bridge (290.4 m (952 ft)) were both built in Colorado (Kunin and Alampalli, 2000). As of 1996, the Maine Department of

Transportation (MaineDOT) had constructed 18 integral abutment bridges between the years 1983 and 1994. A summary of state and provincial responses regarding the number of bridges, time frame and longest of each girder type is found in Table 1 in the article by Kunin and Alampalli (2000).

2.1.1.1. Planning

Several factors affect the applicability of constructing an integral abutment bridge at a particular site. In an effort to limit thermal movements, either the length of the bridge is limited, or the magnitude of movement is limited. Agencies that limit the girder length typically tolerate larger thermal movements. These thermal movements are based on the temperature ranges suggested for cold and moderate climates in Article 3.16 of the AASHTO Bridge Design Specifications (1998). Other limiting factors include skew, abutment and stem height. Most agencies, including MaineDOT, limit the skew of integral bridges to less than 30-degrees while one agency does not allow skew, and two others set no limits on skew. Maximum abutment height ranges from 0.9 m (3 ft) to no limit while the stem height ranged from 0.3 m (1 ft) to no limit. A summary of the maximum allowable limits for thermal movements, lengths, skew angle, pile location tolerance and abutment and stem height for the states and provinces surveyed is located in Table 2 in the article by Kunin and Alampalli (2000).

Another issue that must be addressed in the planning phase is the material used for the girders. Of the 17 agencies that confirmed that they had used both steel and prestressed concrete girders, only four observed differences in performance. Larger

movements have been noted when using steel, and shrinkage has occurred when concrete girders were used (Kunin and Alampalli, 2000).

2.1.1.2. Design

Soil pressure for abutment design is most commonly determined using passive soil pressure. Some agencies use a combination of both active and passive soil pressures pertaining to thermal contraction and expansion, respectively.

Approximately two-thirds of the agencies that responded expressed the view that the effects of skew are not considered with respect to soil pressure. The transportation agencies in Colorado and Quebec assume the soil pressure to be normal to the abutment. MaineDOT assumes loads on skewed abutments induce transverse forces and translation to the piles. Oregon DOT designers expressed concerns that large skew might result in a large torque with soil thrust loads not opposing one another (Kunin and Alampalli, 2000).

Wingwalls are either poured monolithically with the abutment or otherwise rigidly tied into the abutment. About two-thirds of those responding said that they used U-shaped wingwalls, while two indicated parallel extensions of the abutment (Kunin and Alampalli, 2000).

The most frequently used pile in integral abutment bridge construction is the steel H-pile, while cast-in-place concrete, prestressed concrete, steel pipe, and concrete-filled steel-shell piles have also been used. Slightly less than half the respondents design piles solely for axial loads, and of these, four agencies perform lateral analysis if the design does not meet certain requirements. The other half of the agencies design for both axial

and lateral loads. Some agencies assume abutment loads to be equally distributed over all piles, while others consider unequally loaded piles. Pile stresses are analyzed using various methods. Some agencies either consider the pile to be fixed at a certain depth, with a fixed, pinned, or free connection at the head, depending on the abutment connection detail (Kunin and Alampalli, 2000). The computer programs L-PILE (Ensoft, 2002) and COM624P (Wang & Reese, 1993), or an equivalent program, are used by some agencies to analyze the pile stresses. MaineDOT uses an allowable stress design based on rotation of the girder ends. If the pile is analyzed for flexure, either an accurate equivalent fixed length, $L_f$, must be known, or the pile-soil interaction must be considered explicitly using a program such as L-PILE or a more detailed geotechnical analysis. Although numerous studies examining the design of piles in integral abutment bridges have been done, the concept of an equivalent fixed cantilever is most commonly used which implies a substantial driven depth of pile (Abendroth et al, 1989).

Table 2.1, after Kunin and Alampalli (2000), summarizes the responses concerning pile orientation. To accommodate movement, a majority of the respondents orient the pile such that the weak axis is perpendicular to the direction of traffic. Three state agencies differ from the practices listed in Table 2.1. The Washington State DOT typically alternates orientation from pile to pile. Colorado DOT places the weak axis parallel to the skew direction but for larger movements the weak axis may be oriented parallel to the direction of movement. North Dakota DOT places the weak axis parallel to the abutment face (Kunin and Alampalli, 2000).

**Table 2.1. Pile orientation (after Kunin and Alampalli, 2000)**

| Pile Position | Agencies Responding |
|---|---|
| Weak axis perpendicular to direction of traffic | 10 |
| Weak axis in direction of traffic | 6 |
| Weak axis parallel to skew direction | 2 |
| Weak axis perpendicular to skew direction | 2 |
| Combinations: | |
| Weak axis in direction of traffic and perpendicular to skew direction | 2 |
| Weak axis perpendicular to direction of traffic and parallel to skew direction | 2 |
| Weak axis in direction of traffic and perpendicular to direction of traffic | 1 |

Most agencies employ approach slabs with appropriate cycle-control joints to accommodate movement without causing distress to the approach pavement. Typically the approach slab rests on a lip or corbel built into the abutment. Common problems with approach slabs include settlement, transverse or longitudinal cracking, and cracks in asphalt overlays at the ends of the approach slab. Despite this, most agencies rate the performance for their approach slabs as at least satisfactory (Kunin and Alampalli, 2000).

2.1.1.3. Construction

Construction processes can have significant influences on the behavior of the bridge and its substructure. Two-thirds of the respondents have no special procedures to

reduce soil pressure against abutments. The transportation agencies of New Hampshire and West Virginia have used loose, uncompacted fill; New Hampshire DOT now requires compaction due to unacceptable settlement of sleeper slabs caused by the loose fill. Illinois DOT has used uncompacted, porous, granular embankment with an underdrain. Kentucky DOT uses granular backfill both behind and in front of the abutment. Oregon DOT uses a soil-reinforced fill with a gap at the structure wall. Michigan DOT used a high-density foam backing on one bridge, but the evaluation of the performance of the foam is difficult since the designer was not convinced the backing was necessary (Kunin and Alampalli, 2000).

Eighteen of 30 agencies said they did not predrill oversized holes before pile driving and later backfill with granular material. Four agencies employed this technique if certain conditions exist including short piles, difficult driving conditions, piles in fill sections and bridge lengths of greater than 30 m (98.4 ft). Table 4 in Kunin and Alampalli (2000) summarizes details regarding predrilled hole criteria. None of the agencies use compressible material on the piles to reduce earth pressure, but Colorado DOT has used bitumen coating to reduce down drag on piles (Kunin and Alampalli, 2000).

Expansion between abutment and approach slab is controlled by either placing an expansion joint at the far end of the approach slab, between the abutment and approach slab, or no expansion joint. All three methods are considered to perform satisfactorily (Kunin and Alampalli, 2000).

### 2.1.2. Canada

The Ontario Ministry of Transportation (MTO) and Alberta Transportation (AT) both advocate for the use of integral abutment bridges when the conditions make it feasible. The uses of semi-integral or pinned-integral abutments are also options for these agencies. Semi-integral abutment bridges, like fully integral abutment bridges, eliminate the need for an expansion joint by using girders and decks that are continuous with the approach slab; the superstructure unit, however, is not continuous with the abutments. In a pinned-integral abutment, the superstructure is embedded in the diaphragm, a large concrete block. The diaphragm is then connected to an abutment seat using a steel pin and bearing pad system. Pinned-integral abutments eliminate the transfer of moments and rotations between the abutment and girder ends. Details of semi-integral and pinned-integral abutment configurations can be seen in Figure 2.1.

The MTO notes the first fully integral abutment bridges were built in Ontario in the early 1960's but did not become popular until the 1990's. The first semi-integral abutment bridges in Ontario were also built in the late 1960's. All of the jointless bridges (approximately 100 of them) have been continually monitored to increase designer confidence in Ontario. In general, both integral and semi-integral bridges are performing well with very little signs of deterioration or distress in any of the structures (Husain and Bagnariol, 2000). AT reports performance of pinned-integral bridges over the last 20 years has been excellent.

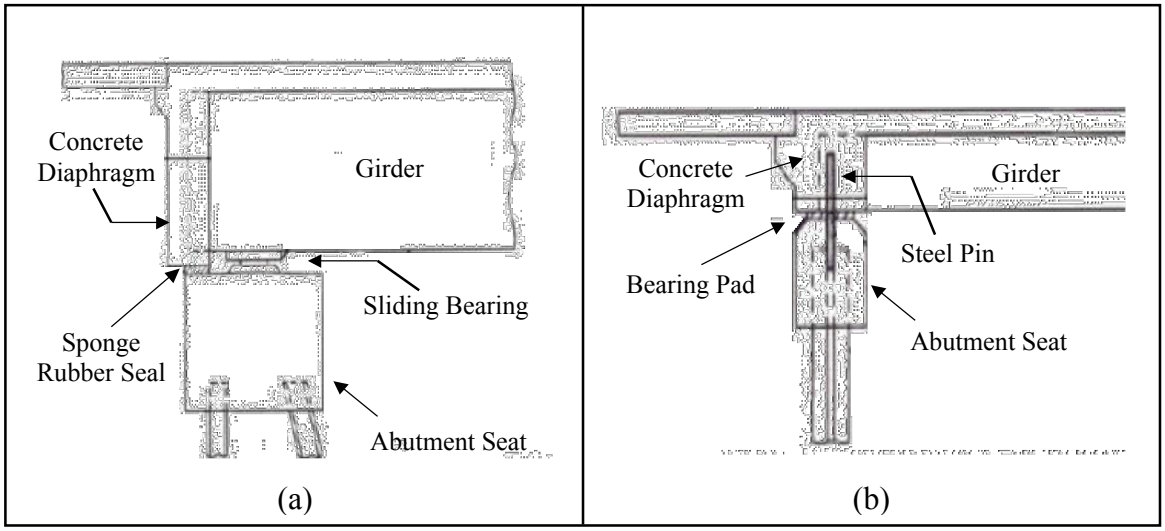


**Figure 2.1. Examples of (a) Semi-Integral and (b) Pinned-Integral abutment configurations (Alberta Transportation, 2003)**

2.1.2.1. Planning

AT (2003) recommends the use of "full monolithic integral abutments" whenever possible. Similarly, MTO suggests that semi-integral abutment details should be considered only in situations in which fully integral abutment bridges cannot be used (Husain and Bagnariol, 2000). Conditions that would warrant the use of semi-integral abutments would be sites with long spans, large skews or poor soil conditions.

The length of pinned-integral abutment bridges in Alberta is generally less than 50 m (164 ft) long, but lengths of up to 75 m (246 ft) exist. Ninety-five percent of all bridges in Alberta are shorter than 100 m (238 ft) in length (AT, 2003). Ontario limits the overall length of fully or semi-integral bridges to 150 m (492 ft) on the basis that satisfactory performance has been attained for structures of this length. The limitations placed on the total length are a function of seasonal temperatures variations, type of superstructure and the capacity and efficiency of the movement of the system (Husain and Bagnariol, 2000).

Another factor which plays an important role in determining the feasibility of integral abutments is the geometry of the bridge. AT limits skew to less than 30-degrees (AT, 2003). MTO typically limits skew to less than 20-degrees. Larger skews, up to 35-degrees, are allowed if an in-depth analysis is completed to determine the effects of the skew including the effects of torsion, unequal load distribution, lateral translation, pile deflection, and increase in length of abutment exposed to soil pressure (Husain and Bagnariol, 2000). Semi-integral abutments have no limit on skew provided that there is enough lateral restraint to prevent rotation of the superstructure caused by an eccentric lateral force.

MTO considers subsurface conditions important when considering the feasibility of an integral abutment bridge. If the depth to the load carrying stratum is less than 5.0 m (16.4 ft), such that short piles or caissons would be required, the site is considered unsuitable for integral type construction. When piles are driven in dense and stiff soils, pre-augured holes filled with loose sand are recommended to reduce resistance to lateral movement (Husain and Bagnariol, 2000).

2.1.2.2. Design

The MTO report SO-96-01 by Husain and Bagnariol (1996) established a basis for the planning and design of integral abutment bridges and is used by both MTO and AT. The report also assesses limitations of integral abutment bridges. The analysis and design of semi-integral abutment bridges are much the same as conventional jointed bridges with the addition of special design considerations that arise from the backfill pressure against the superstructure at the abutment location and the design of cantilevered

wing walls (Husain and Bagnariol, 2000). Both MTO and AT indicate that a single row of steel H-piles oriented for weak axis bending is typically preferred for their ductility and flexibility in cyclic bending, however, AT does allow integral abutments to be constructed on shallow footings in some cases. The web of the pile is oriented perpendicular to the direction of the girder in skewed bridges.

For fully integral abutment bridges MTO limits the abutment height and wing wall lengths to 6.0 m (19.7 ft) and 7.0 m (23 ft), respectively. The height of the abutments should be kept as short as possible, but the required depth should be adequate for frost protection. It is recommended to have abutments of equal heights so lateral loads are balanced and to protect against side sway (Husain and Bagnariol, 2000). AT suggests high abutment walls should be avoided (2003). Both agencies advise that wing walls should be constructed parallel to the roadway and their size should be minimized such that resistance to movement is also minimized. Also, wing wall lengths should be the same length, or shorter than the approach slab such that the cycle control joint is located beyond the end of the wing walls.

Even though fully integral and semi-integral abutment bridges allow for the elimination of deck joints, joints are still needed to facilitate thermal movements. Cycle control joints are located at the end of approach slabs where some leakage can be tolerated. Steel is more sensitive to temperature change than concrete; this difference in thermal response is accounted for when selecting the type of cycle control joint. The type of cycle control detail is chosen based on the girder material, overall structure length, seasonal variation and capacity for movement of the structural system.

2.1.2.3. Construction

Construction considerations are very similar for both agencies. Of utmost importance are the construction details and cycle control joints at the end of the approach slabs.

The construction sequence must not cause undue stresses to the structure; its stability and integrity should be maintained at all stages of construction. The concrete deck should be poured such that the structure becomes integral with no residual stresses. The ends of the deck should be placed last unless retarder is used to allow placement from one end to the other in a single pour. Backfilling of material behind abutments should not be done until the deck has reached 75% completion and should be done in a manner that minimizes unequal earth pressures on the abutment and differential settlement, i.e. backfill should be placed at either end at the same time, in nearly equal lifts (Husain and Bagnariol, 2000).

Drainage details must be incorporated to ensure a durable design. The amount of water from the bridge deck or approach pavement that passes over the approach slab should be minimized through the use of drains. Subsoil weep drains should be used to channel seepage away from the structure. Joints around the approach slab should be well sealed to prevent water infiltration.

### 2.1.3. United Kingdom

In 1989, a study was completed inspecting 200 randomly selected bridges in England. A major recommendation concerned the maintenance of bridge deck joints.

Although the report did not specifically recommend movement towards integral or continuous construction, the inference was obvious (Taylor, 1999).

The United Kingdom (U.K.) has more variation of integral abutment bridges than are seen in the United States (U.S.) and Canada. Six abutment configurations considered integral can be seen in Figure 2.2.

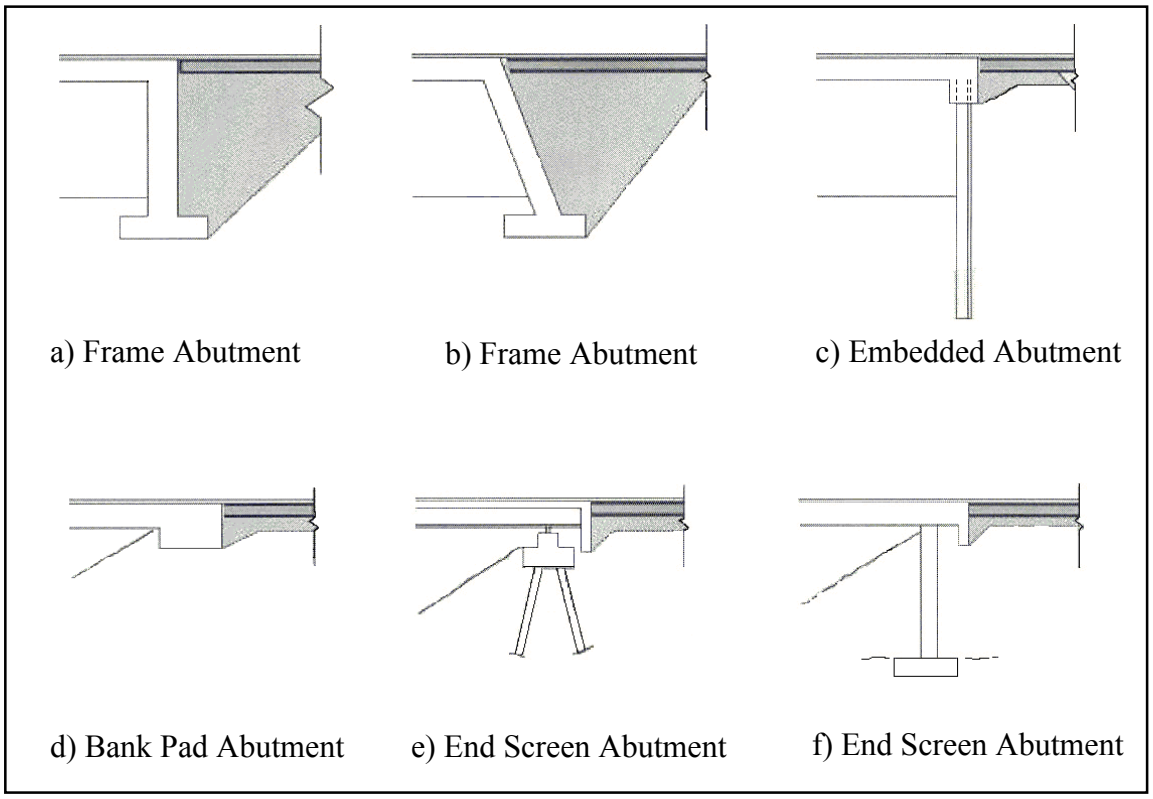


**Figure 2.2. Types of integral abutments (Highways Agency, 1996)**

The U.S. and Canada only use the frame, embedded, and bank pad abutments, or minor variations of these. The Highways Agency (1996) does not explicitly limit the sites at which integral abutment bridges can be constructed; instead bridge decks up to 60 m (196.8 ft) in length with skews not exceeding 30-degrees are generally required to be

continuous over intermediate supports and integral with their abutments. The only other limit set is thermally induced cyclic movements of each abutment is not to exceed 20 mm (0.8 in) in either direction (Highways Agency, 1996).

Integral bridges in the U.K. are designed essentially in the same manner as their jointed bridge counterparts, except that they must be able to accommodate thermal expansion and passive earth forces. U.K. bridges tend to be more expensive because of the higher anticipated vehicle speeds and more stringent road alignment requirements in the design. Bridge loading is also lower in North America than in the U.K., at times by 60 percent. Designers in the U.K. also pay more attention to appearance and detail. In the U.K., there is much more concern that bridge design and details are justified analytically rather than relying on experience (Taylor, 1999).

Integral abutments can be supported by either spread footings or piles. Piles must be designed to accommodate lateral movement while supporting axial loads and to support forces from movement of the piles and/or surrounding ground (Highways Agency, 1996).

Taylor (1999) summarizes a tour of integral abutments in North America taken by six engineers from the U.K. Department of Trade. The group concluded that the ride quality experienced over displaced and settled run-on slabs would not be acceptable in the U.K. As a result, the use of run-on slabs is neither endorsed nor prohibited, but rather recommendations were made to rely on the higher specifications of backfill material and consolidations in U.K. standards and to accept pavement damage that may result (Taylor, 1999).

## 2.2. Design of Integral Abutment Bridges

AASHTO has not yet directly addressed specific methods of analysis and design for piles supporting integral abutment bridges. Because of this, many states have developed their own in-house methodologies for the design of integral abutment bridges based on their past experiences. Much work has been done to develop simplified structural models and computer analyses to account for stresses and displacements in piles caused by thermal expansion of the bridge superstructure. This section discusses the two most widely accepted methods for integral abutment pile design. The "rational design method" by Abendroth et al. (1989) was refined from the design procedure created by Greimann and Wolde-Tinsae (1988). It is used by several state transportation agencies. The second method is the lateral analysis design method prepared for the American Iron and Steel Institute (AISI) by the Tennessee Department of Transportation (Wasserman & Walker, 1996).

### 2.2.1. "Rational Design Method"

Consideration of material nonlinearity for both piles and the surrounding soil play an important role in the design of integral abutment piles. The design methods presented by Abendroth and Greimann (1989) are an evolution of a method previously published by Greimann and Wolde-Tinsae (1988). The previous method was based on the Rankine equation for inelastic buckling, but did not address the problem of pile ductility associated with lateral movement of the pile head. The new design method, known as the "rational design method" replaces the actual pile with an equivalent cantilever for design purposes. A pile embedded in soil is modeled as an equivalent beam-column without transverse loading between the ends, having a fixed base at a certain depth. The head of

the pile can be modeled as either a fixed, for a fully integral abutment, or a pinned connection, for pinned or semi-integral abutments. Figure 2.3 shows an idealization of fixed cantilever, with both types of restraint at the head. It should be noted that the equivalent cantilever is a common, although imprecise idealization of laterally loaded piles.

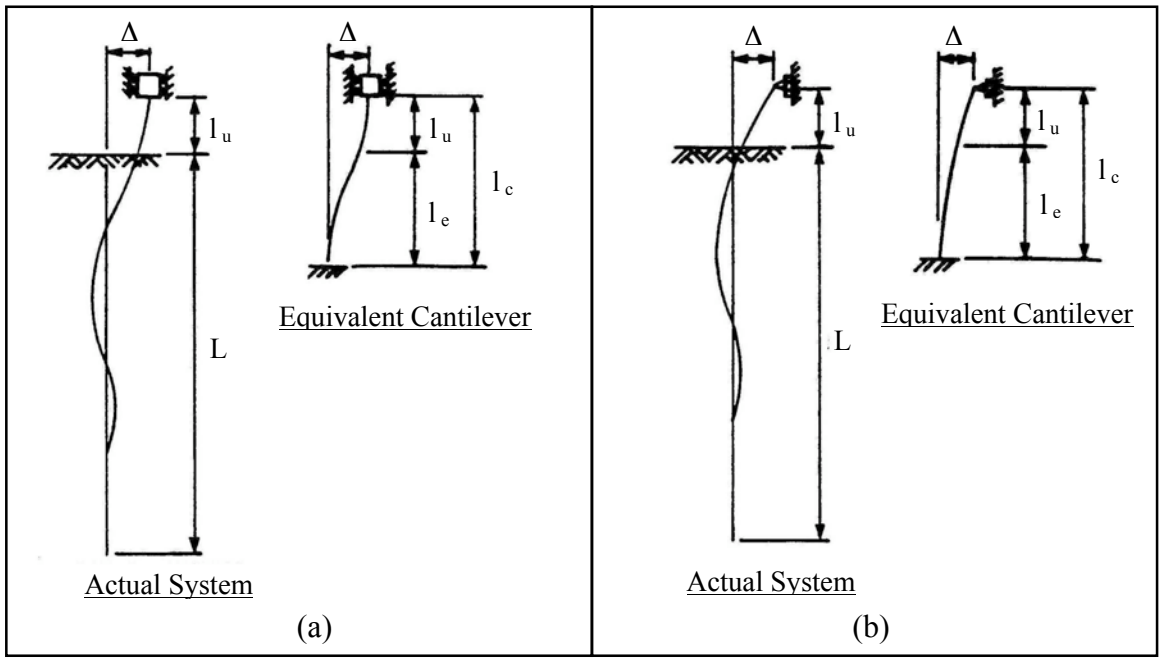


**Figure 2.3. Equivalent cantilevers for: (a) fixed-head condition (b) pinned-head condition (Greimann et al., 1987)**

The rational design method consists of two alternatives that address the three AASHTO Specification design criteria: the capacity of the pile as a structural member, the capacity of the pile to transfer the load to the ground, and the capacity of the ground to support the load. The first alternative is an elastic approach that should be applied to piles with limited ductility, such as timber and concrete. The second alternative is an inelastic approach that can be applied to recognize redistribution of internal forces caused by plastic hinge rotation.

In Alternative One, the lateral displacement, _, at the pile head, caused by thermal expansion and contraction of the bridge superstructure, produces an end moment. Since failure is assumed to occur when any internal stress reaches the yield value, this end moment can be expected to cause a dramatic reduction in member strength associated with lateral displacement of the pile head (Abendroth et al., 1989).

Alternative Two was developed to permit plastic redistribution of forces due to the formation of plastic hinges induced by thermal movements. The stresses induced by the horizontal pile head movement are considered to not significantly affect the pile's ultimate strength, as long as the corresponding strains can be accommodated through adequate pile ductility. The axial pile load generates a bending moment due to the lateral displacement at the pile head (Abendroth et al., 1989). In addition to strength and stability criteria, both design alternatives must satisfy local buckling and ductility criteria. Pile ductility affects the ultimate strength and behavior of piles subjected to combine lateral displacement and vertical load.

Both design alternatives gave conservative results for the vertical load capacity of the pile when the pile head was displaced horizontally when compared to a finite element solution (Abendroth et al., 1989). Alternative One was excessively conservative in the practical range of the design parameters. The finite element solutions confirmed the redistribution of pile forces required with Alternative Two. When the piles have sufficient ductility, Alternative Two will permit the safe design of integral abutment bridges that are longer than those designed using Alternative One (Abendroth et al., 1989).

Abendroth et al. (1989) also determined that lateral displacement of the pile could affect the capacity of the pile to transfer load to the ground. This displacement, however, should not affect the end bearing resistance of flexible piles, nor the capacity of the ground to support the load.

### 2.2.2. Lateral Analysis Design Method

This design method was prepared for the American Iron and Steel Institute (AISI) by Wasserman and Walker (1996) of the Structures Division of the Tennessee Department of Transportation. It incorporates the use of a computer program COM624P which models and analyzes laterally loaded piles (Wang and Reese, 1993). Since the deflected shape of the loaded pile is dependent upon the soil response, and in turn, the soil response is a non-linear function of pile deflection, the system response cannot be determined by the traditional rules of static equilibrium. The analysis and design of laterally loaded piles requires an iterative solution of a non-linear fourth-order differential equation using finite-difference techniques. The soil response is described by a system of non-linear curves that compute the soil pressure resistance, p, as a function of pile deflection, y.

First, the thermal movement is calculated based on the length of the structure, temperature range and coefficient of expansion. A pile section is selected such that it is flexible enough to achieve double curvature within the design length under the thermal movement calculated. Then, two key calculations are performed to assess the capability of the pile and abutment system to behave as needed. The first calculation determines whether the calculated thermal displacement is sufficient to cause a plastic hinge at the

top of the pile. The second calculation confirms the ability of the pile to develop the plastic-moment capacity within the embedded length of the pile penetrating the cap.

Once the ability to develop the plastic-moment capacity of the pile at its top has been established, the COM624P program is used to develop the deflected shape of the pile under specified conditions. For the thermal displacements calculated initially, *p-y* curves are generated based on the soil properties. A thorough discussion of the procedure for the determination of *p-y* curves is given by Wang & Reese (1993). The pile is analyzed with the plastic moment and thermal displacement applied at the head of the pile. The unfixed length of the pile is determined from identification of the points of zero moment at varying depths of pile embedment, and the longest of these distances is used in subsequent calculations.

### 2.2.3. Finite Element Modeling

Numerous finite element models of integral abutment bridges have been developed and studied by researchers in the past decade. Both two-dimensional, e.g. DeLano (2004), Diceli and Albhaisi (2003), Duncan and Arsoy (2003), Lehane et al (1999), and three-dimensional models, e.g. Faraji et al (2001), Mourad and Tabsh (1998), have been developed. Some of these models have been produced using commercially available software packages, while other models are comprised of original code written by the researchers. In these models, the structure and soil are modeled using either continuum elements, or specialty elements, such as beams and springs.

The two-dimensional (2D) finite element analysis of integral abutments is very popular, because 2D models require fewer computational resources. A typical 2D model

of an integral abutment bridge can be seen below in Figure 2.4. A summary of the work completed in Phase I of this study, including the finite element model created by DeLano (2004) is discussed in Section 2.4.

The soil response is most commonly modeled as a series of linear or non-linear spring elements. However, this approach is considered unrealistic by some, as these elements do not account for the fact that the springs are uncoupled, while the actual soil behaves more like a continuum. In addition, there is no widely accepted theory from which the spring constant, or modulus of subgrade reaction, can be derived (Krusinski, 2002). Hence, researchers have used continuum elements to model the soil using easily determined properties, such as internal angle of friction ($\phi$), density ($\rho$), and cohesion ($c$).

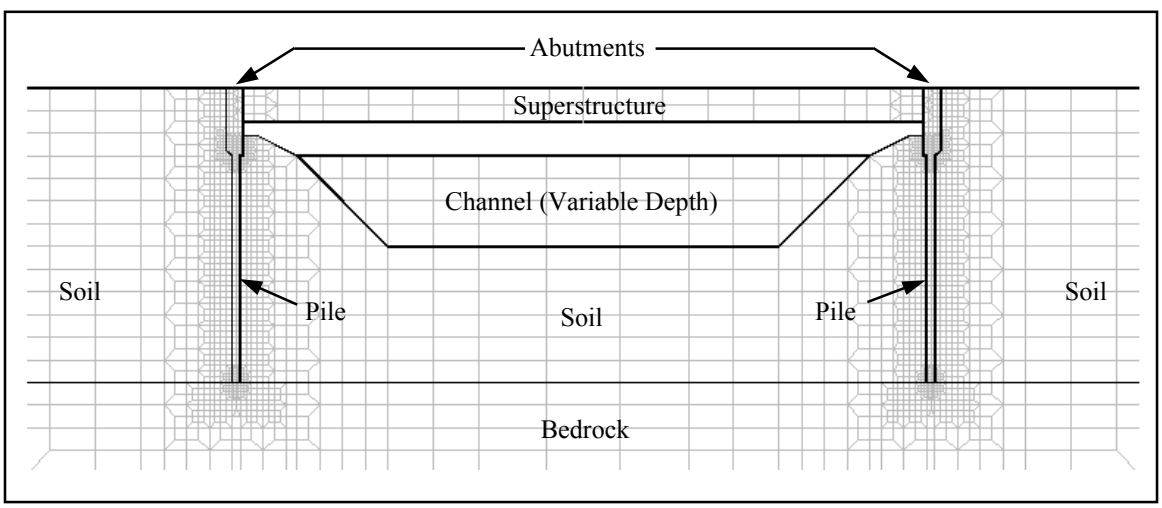


**Figure 2.4. Typical finite element model of integral abutment bridge (DeLano, 2004)**

Three-dimensional (3D) finite element models of integral abutment bridges are not as prevalent as two-dimensional models. This is due to their increased complexity as

well as increased computational requirements. However, unlike 2D models, 3D models can account for skew effects and discrete piles, as well as effects of off-center loading.

## 2.3. Behavior of Integral Abutment Bridges

Piles are the most common foundation for integral abutments due to their ability to resist lateral loading while maintaining their axial capacity. Published field and laboratory studies regarding the behavior of integral abutment piles are reviewed in this section. In the past, research pertaining to the behavior of integral abutment piles had been limited to field studies of in-service integral abutment bridges and driven test piles. Laboratory studies of integral abutment piles, using either full-size or scaled-down models, have become increasingly popular. Most of the experimental studies involve the use of steel H-piles as the foundation type, although the study performed by Arsoy, Duncan, and Barker (2002) examined steel pipe and prestressed concrete piles as well.

### 2.3.1. Laboratory Studies

Studies done in the laboratory, whether full-sized or scaled-down, are an excellent way to investigate specific behaviors of piles supporting integral abutment bridges due to the controlled conditions. Two laboratory studies are examined in this section.

#### 2.3.1.1. Full Scale Test without Soil

Arsoy, Duncan, and Barker (2002) investigated the performance of various types of piles used to support integral abutment bridges. Full-scale tests were performed on a steel H-pile, a steel pipe pile, and a prestressed concrete pile. The purpose of the test program was to simulate the effects of lateral loading induced by temperature changes

over the expected life of integral bridges and to evaluate damage to the piles and pile caps under typical working stress conditions. As shown in Figure 2.5, the test setup is inverted from orientation in the field for ease of testing. Only the behavior of the pile under cyclic displacements due to temperature fluctuations is represented in this test setup; the soil-pile-bridge interaction is not modeled.

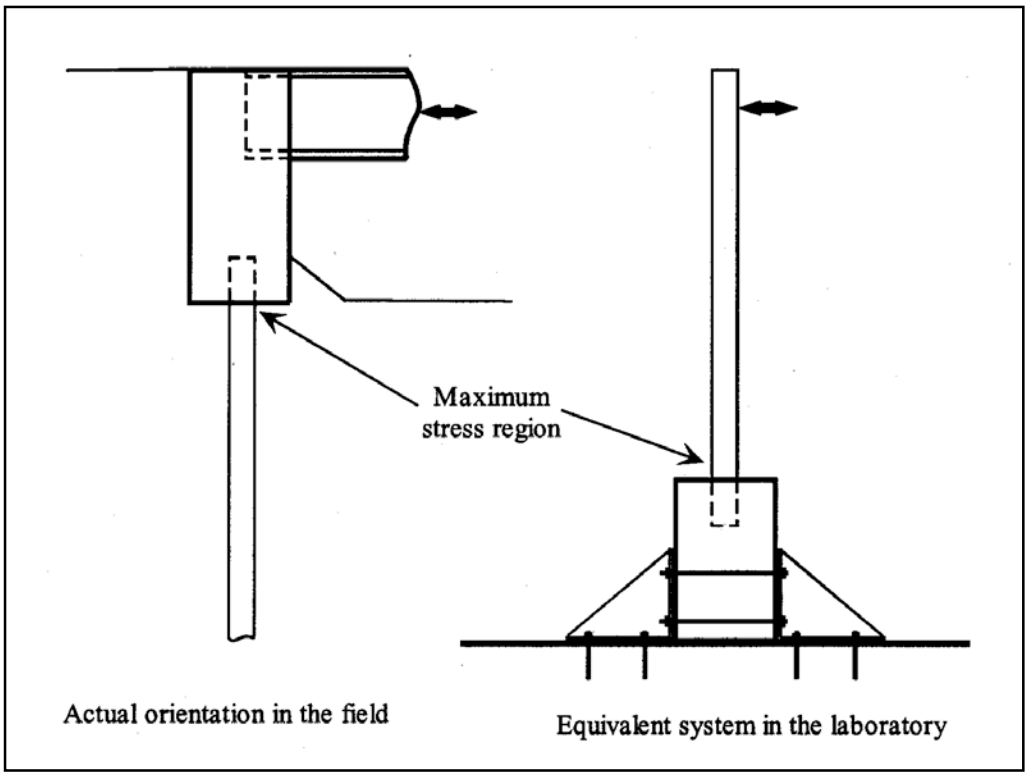


**Figure 2.5. Equivalent laboratory test setup (Arsoy, Duncan, and Barker, 2002)**

The type of H-pile tested was an HP254x63 (10x42) fabricated from grade A572-50 S50 steel. The pipe pile was made from ASTM A252 Grade 3 steel, and had a 350 mm (14 in) outside diameter, with a 12.7 mm (_ in) wall thickness. The prestressed concrete pile was a 305 mm (12 in) square pile with five 12.7 mm (_ in) diameter low relaxation steel strands, with a yield stress of 1.86 GPa (270 ksi). The prestress in the

pile was 6.3 MPa (920 ksi). The piles were cast into pile caps constructed from Virginia DOT Class A4 concrete with a minimum 28-day strength of 27.6 MPa (4000 psi). Early strength accelerators were added to achieve the 28-day strength in 7 days due to time constraints. Both the H-pile and prestressed pile were embedded 460 mm (18 in) into the pile cap, while the pipe pile was only embedded 150 mm (6 in). However, reinforcement of the pipe pile extended another 305 mm (12 in) into the pile cap to achieve the same embedment as the other two piles (Arsoy et al., 2002).

The pile caps were fastened to a reaction floor beneath a load frame. A gravity load simulator was used to apply a constant vertical load to the pile as it deflected laterally. Approximately 27,000 cycles of lateral load were applied by a displacement-controlled actuator to simulate the thermal loading over a 75-year bridge life. Pile displacements were measured using wire pot transducers. Three transducers were affixed to the pile, while two were used to measure the lateral displacement and rotation of the pile cap. Load cells were used to monitor the vertical and horizontal loads being applied to the pile. Four strain gages were attached to the H-pile near the pile cap, at the tip of each flange. The pipe pile had two strain gages near the cap, one 1397 mm (55 in) above the pile cap, and one 1778 mm (70 in) above the cap. The prestressed concrete pile had only two gages, both at the pile cap, on opposite sides of the pile.

The H-pile, tested with bending about its weak axis, exhibited the best behavior of the three piles tested. For the entire test, the maximum stress level was set to 50% of the nominal yield capacity of the pile. Overall, the H-piles sustained stresses in excess of 138 MPa (20 ksi) in cyclic loading and 241 MPa (35 ksi) in static loading without any

sign of distress. The steel pipe pile was significantly stiffer than the H-pile. Consequently, the cap of the pipe pile rotated more than that of the H-pile. As was the case with the H-pile, the pipe pile did not sustain any damage during testing. The concrete pile was tested with no vertical load. In the first cycle, tension cracks developed at the interface with the pile cap. The tension cracks in the test pile developed progressively from the bottom (cap) towards the top (toe). The cracks gradually enlarged as the cycles continued. At the end of the test, it was observed that the contact area was only 20% of the original cross-sectional area of the pile.

Arsoy, Duncan, and Barker (2002) conclude that steel H-pi1es oriented in weak-axis bending are a good choice for support of integral abutment bridges. Pipe piles are less suitable for support of integral abutments, because they have significantly higher flexural stiffness than H-piles, for a given width or diameter. Because of this, stresses in an abutment supported by pipe piles will be higher than stresses in an abutment supported by steel H-piles in weak axis bending, leading to increased loading on the abutment. Concrete piles appeared to be the least suitable choice for support of integral abutments because of the formation of tension cracks which progressively worsen under cyclic loading. This can greatly reduce their vertical load carrying capacity. While this study provides valuable data on the relative performance of different pile types, the results do not account for soil/structure interaction.

2.3.1.2. Scaled Model Test with Soil

Amde, Chini, and Mafi (1997) performed experiments on model steel H-piles driven into dry silica sand to calibrate a finite element program. The model H-piles

underwent simulated thermal expansions and contractions of a bridge abutment to determine the influence of lateral displacement on the vertical load-carrying capacity of the piles. Small-scale tests were performed, as the cost of tests increases as the size of the pile increases. In most physical models, scaling correlations are necessary to determine the equivalent full-scale values from experimental data. In the case of soil, which behaves non-linearly, model soil would require increased unit weight. In addition, if complete similitude is desired, the model piles must be tested under increased gravitational acceleration in a centrifuge to match stresses present at full-scale. Scaling relations were not required in this study, since the model test results were compared with finite element models that used actual geometric and material properties existing in the model piles and soil.

The model H-piles used in this study were fabricated from A36 structural steel, with the width-to-thickness ratios of the web and flange conforming to American Institute of Steel Construction (AISC) specifications for 'compact sections'. This was done to allow the sections to develop their plastic moment without any local buckling of the compression flanges occurring. Consideration of the height and diameter of the soil test tank led to the sizing of the H-piles to minimize the effect of soil boundary conditions on the behavior of the pile-soil model.

The testing apparatus is depicted in Figure 2.6. The tank was filled with dry silica sand in 15 layers. The first two layers were compacted to maximum density, and the other layers of soil were placed, leveled, and compacted to a unit weight of 16 $kN/m^3$ (102 $lb/ft^3$). To model end bearing conditions, a piece of steel plate was added at the pile

locations during the filling of the tank. Each test pile was marked in 25 mm (1 in) increments, placed over the desired position, plumbed, and driven to the required depth. In the locations that end-bearing tests were performed, the pile was driven until it encountered the steel plate. The number of blows required for driving the pile each increment using a 3.7 kg (2.2 lb) hammer dropped from 305 mm (12 in) was recorded (Amde et al., 1997).

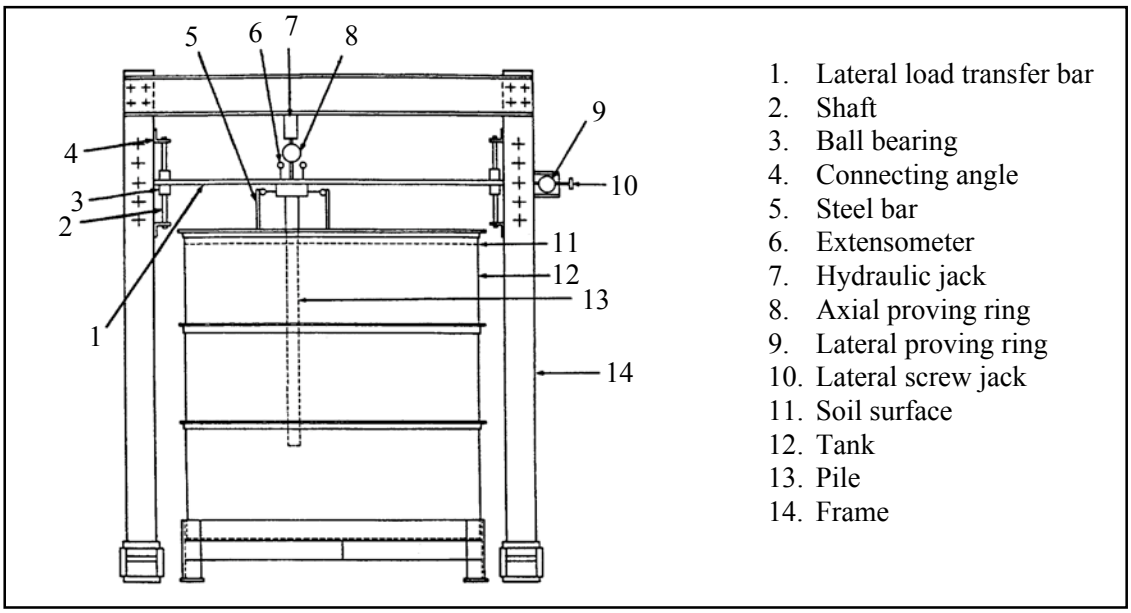


**Figure 2.6. H-pile testing apparatus (after Amde et al., 1997)**

The axial load test consisted of a vertical load applied to each model test pile in 445 N (100 lb) increments. Settlement and strain were recorded for each load increment by means of dial and strain gages. The displacement was the average of measurements from two dial gauges located on the pile cap. The loading continued until the change in displacement increased rapidly over a small change in the applied load.

Lateral load testing consisted of a load applied in 133.5 N (30 lb) increments. Displacement was measured by two lateral deflection gauges installed on the pile cap,

and flexural strains were measured through strain gauges installed on opposite sides of the web. As in the case for the axial test, failure was considered as the point where displacement began to increase rapidly over a small change in the applied load. There was no mention as to whether the piles were subjected to weak or strong axis bending.

The combined load tests were a combination of both the axial and lateral testing procedures. The procedures discussed for the lateral load test were used to displace the pile cap to the required lateral displacement, and then the procedures of the axial load test were conducted until the ultimate pile capacity was reached. The lateral and vertical loads as well as the displacement for each direction were recorded. The test on the end bearing pile was run to the limit of the test set-up for vertical load, which was equal to 4.45 kN (1000 lb).

The experimental data was compared to results from the finite element model. The finite element model used for comparison was developed by Greimann et al. (1986). The two-dimensional program uses a beam element idealization for the pile and an equivalent spring idealization for the soil which includes vertical springs, lateral springs and a vertical point spring at the pile tip. Curves for horizontal displacement versus lateral load for test pile A-3 obtained experimentally and from the finite element model are shown in Figure 2.7. Although the finite element results are conservative, for small horizontal displacements the discrepancy between the two curves is smaller than at higher displacements. In addition, piles 1140 mm (3.7 ft) in length were found to have more resistance to lateral load than those that were 990 mm (3.2 ft) long. The thickness of the webs and flanges was also found to have an effect on lateral resistance of the pile.

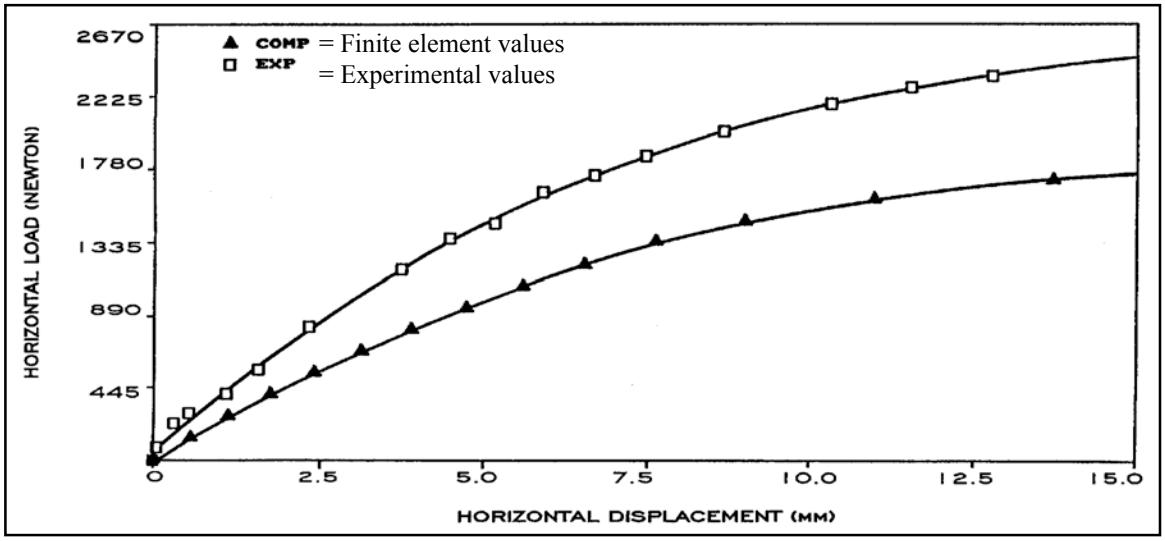


**Figure 2.7. Horizontal load/displacement curves (after Amde et al., 1997)**

A review of the vertical load-settlement data shows that all the piles failed through a vertical-type failure, occurring when the applied load exceeded the ultimate soil frictional resistance. The load settlement curves became horizontal as the load reached the ultimate pile load for all prescribed lateral displacements. When experimental data was compared to the results of the finite element program, the finite element model program underestimated the ultimate capacity of piles.

Amde et al. (1997) concluded that the results from their nonlinear finite element computer program were found conservative when compared to the experimental results. The experimental results showed greater pile capacities and lower bending moments than were predicted by their finite element program.

### 2.3.2. Field Studies

Instrumented in-service integral abutment bridges provide valuable information about the behavior of integral piles due to loading from traffic, earth forces, and temperature change. Four field studies are summarized in this section.

2.3.2.1. Cass County Bridge, North Dakota

Jorgenson (1983) completed a study on the Cass County Bridge in North Dakota between 1978 and 1979. Jorgenson examined the effects of air and deck temperature on the length of a 137.2 m (450 ft) long concrete bridge with integral abutments and piers and no skew. No live load testing was reported.

The 33.5 m (110-ft) long HP254x63 (10x42) H-piles were founded in very dense silty sand. The abutment piles and piles in the piers adjacent to the abutments were oriented with the weak axis in the longitudinal direction of the bridge. The piles for the three center piers were oriented with their strong axis in the longitudinal direction of the bridge. A pressure relief system was set up between the back side of the abutment and the backfill soil to allow for measurement of the abutment movement relative to the backfill soil. To allow longitudinal movement of the abutment piles without creating considerable resistance, a 50 mm (2 in) thick layer of compressible material was glued to the web of the piles.

Measurements of the bridge's movements were made on a monthly basis, for one year. The length of the bridge was measured directly with a steel tape which was corrected for temperature change. Measurements were also taken of the void space between the back side of the abutment and the backfill soil, as well as the size of the opening in the expansion joint in the approach slab, which was located about 6.1 m (20 ft) from the end of the bridge. Slope indicator casings were installed on each corner pile of each abutment and also read on a monthly basis. The slopes of the piles were used to measure pile movement as well as bending stresses in the pile. The maximum measured

abutment movement of 49.8 mm (1.96 in) induced a moment that was sufficient to cause yielding within the top 305 mm (1 ft) of the pile. However, while strains exceeded the yield strain of the pile, the plastic hinge moment was not reached.

Jorgenson (1983) concluded that the maximum change in bridge length due to thermal expansion is a function of the air temperature at dawn on the hottest day, the air temperature at dawn on the coldest day, and the maximum air temperature on the hottest day. The change in length determined from this function corresponded well to the changes in length determined from tape measurements and measurements of the openings in the expansion joints. It was also concluded that the total change in bridge length did not result from equal movements of the two abutments. The vertical movements of the abutments and piers were determined to be nearly zero.

2.3.2.2. Rochester, Minnesota

Lawver, French and Shield (2000) instrumented and monitored an integral abutment bridge near Rochester, Minnesota from the beginning of construction through several years of service. The bridge was designed according to the 1992 AASHTO design specifications by the load factor design method. The 66 m (216.5 ft) long prestressed concrete girder bridge was constructed in three spans which were made continuous at the piers only through the deck. One row of six HP254x85 (10x57) H-piles was placed under each pier oriented for strong axis bending. A 0.4 m (15.7 in) diameter steel tube filled with concrete to protect and stiffen the piles was placed around each pier pile down to a depth of 1.5 m (4.9 ft) below grade. The girders were set on elastomeric pads set on top of the bridge abutments. Diaphragms were cast around the end of the

girders directly on top of the bridge abutments at the same time that the deck was poured. Wingwalls extended back from the bridge at 45-degree angles. The abutments were supported by a single row of six, approximately 24 m (78.7 ft) long, HP305x79 (12x53) piles oriented in weak axis bending. The approach slabs on each end of the bridge rested on the diaphragm at one end and on a concrete sill at the other end, with select granular borrow backfilled beneath the rest of the slab.

One hundred eighty instruments were installed to measure abutment horizontal movement, abutment rotation, abutment pile strains, earth pressure behind abutments, pier pile strains, prestressed girder strains, concrete deck strains, thermal gradients, steel reinforcement strains, girder displacements, approach panel settlement, frost depth and weather. The behavior of the bridge components was monitored throughout the construction process and during live load testing and agreed with anticipated behavior. It was concluded that the instrumentation was working as intended with exception of the earth pressure cells which were found to respond nonlinearly with temperature variations.

The bridge behavior was found to be driven by changes in air temperature and solar radiation. Ambient air temperatures for the first two years of monitoring ranged from -33 to 27ºC. The solar radiation of the sun was about two and a half times stronger in the summer than in the winter. Whereas the air temperature affected the entire bridge, the solar radiation heated the top of the bridge deck. Changes in temperature cause the superstructure of the bridge to expand and contract in the summer and winter, respectively. As the bridge deck expands in the summer and contracts in the winter due to temperature changes, the abutments also move. Movements of the abutments cause

changes in strains of the piles supporting the abutments, movement of the approach slabs and changes in earth pressures on the abutments, diaphragms and wing walls. If the abutments and supporting piles are too stiff and movement is resisted, higher than design stresses can be encountered in the superstructure. Orienting the abutment piles to allow longitudinal bending along the weak axis increases the flexibility of the system.

Two abutment piles were each instrumented with two sets of three arc-weldable strain gages located on the insides of three of the flange tips so that biaxial bending and compression could be measured.

Lawver, French and Shield (2000) concluded that the effects of the loads from solar radiation and changing ambient air temperature were found to be as large as or larger than live-load effects. The abutment was found to accommodate superstructure expansion and contraction through horizontal translation rather than rotation. Also, the pile strains on the approach panel side of the piles indicated the onset of yielding, and the piles appeared to be deforming in double curvature. No mention was made of the effects of the construction process.

2.3.2.3. Tennessee

Burdette, Wasserman, Goodpasture, and Deatherage (1999) report on research, supported by the Tennessee Department of Transportation, that investigated the behavior of integral abutments. Although field monitoring was conducted, no full-scale field testing was reported. Figure 2.8 shows a typical setup for field tests to examine the embedment zone of the pile in the concrete abutment and the embedment zone of the pile in the soil. Weldable strain gages were affixed 457 mm (18 in) apart for the top 6.1 m

(20 ft) of the BP254x63 (10x42) pile which was driven 11.6 m (38 ft). Pressure sensors were also installed at regular intervals in the vicinity of expected points of zero lateral pressure. Rotation of the end of the pile was limited to the range of a typical bridge. Lateral Variable Differential Transformers (LVDT's) were used to monitor lateral movements of the bottom of the abutment and the pile.

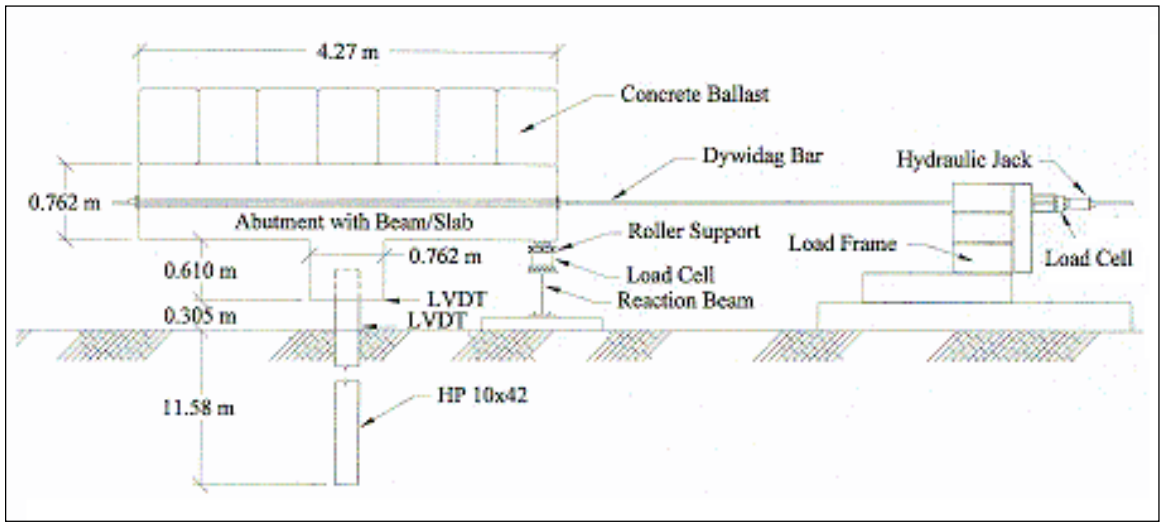


**Figure 2.8. Test set-up for field tests (Burdette et al., 1999)**

The data from the strain gages was converted to stresses then to bending moments of each section of the pile. The typical distribution of moment versus depth for a particular lateral pile displacement is shown in Figure 2.9. The equation for this plot was differentiated twice to obtain an equation for lateral pressure. Figure 2.10 is the lateral pressure versus pile depth for the bending moment distribution presented in Figure 2.9.

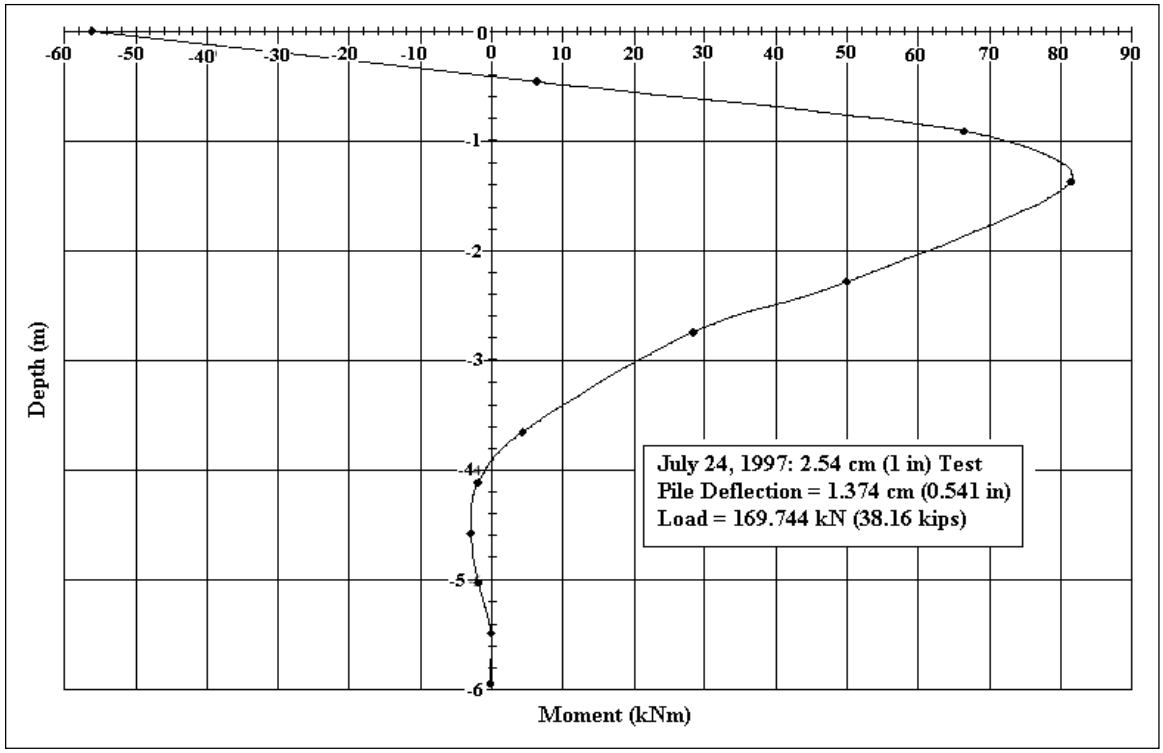


**Figure 2.9. Moment vs. depth (Burdette et al., 1999)**

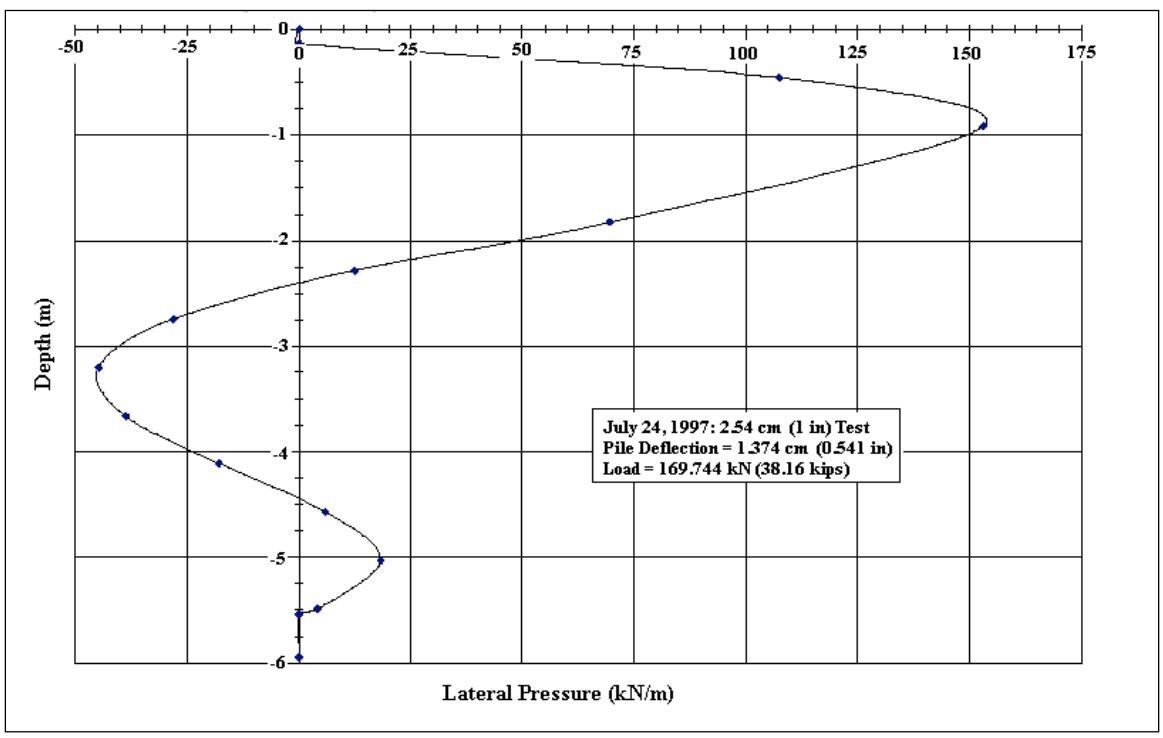


**Figure 2.10. Lateral pressure vs. depth (Burdette et al., 1999)**

As large lateral displacements were induced, the response of the pile-abutment interface was one of the most important observations made during the research at the time of publication of the article (Burdette et al, 1999). A lateral displacement of the pile near the ground surface of 25 mm (1.0 in) resulted in very minor cracking of the abutment in the vicinity of the pile head. Additionally, more rapid displacements led to more cracks and opening of existing cracks. Induced displacements of 38 mm (1.5 in) caused cracking in the abutment, but the cracks were not considered to compromise the abutment integrity. Removal of load significantly closed many cracks. Lateral displacements of 63 mm (2.5 in) caused significant cracking, and the test was stopped. However, the abutment was not considered to have "failed" (Burdette et al, 1999).

2.3.2.4. Iowa

Girton, Hawkinson, and Greimann (1991) instrumented and monitored two pile-supported integral abutment bridges in Iowa. Experimental data were collected for two years and compared to previously developed design equations. Refined design recommendations were made based on the results. Experimental data consisted of air temperatures, bridge temperatures, bridge displacements and pile strains. In addition, concrete core samples were collected from the bridges and laboratory measurements of the coefficient of thermal expansion were made. No live load testing was completed.

The Boone River Bridge is a prestressed girder bridge, 12.2 m (40 ft) wide, spanning 98.9 m (324.5 ft). It is a continuous, four-span bridge in which two of the piers are located approximately 24.4 m (80 feet) from each abutment; the third pier is located at the center of the bridge. The prestressed girders are not integral with the piers but sit

on neoprene pads approximately 25 mm (1 in) thick. The rest of the structure is monolithically constructed, with a skew angle of 45-degrees. The reinforced concrete deck is 190 mm (7.5 in) thick, with a compressive strength of 20.7 MPa (3000 psi). The prestressed concrete girders are C80R type as specified by the Iowa DOT with a design strength of 34.5 MPa (5,000 psi). The H-piles, HP254x65's (10x42)'s, were driven in predrilled holes approximately 2.7 m (9 ft) deep with the strong axis parallel to the longitudinal direction of the structure and battered at a slope of 4:1 in the lateral direction. A cross-sectional view of the Boone River Bridge abutment and pile is shown below in Figure 2.11.

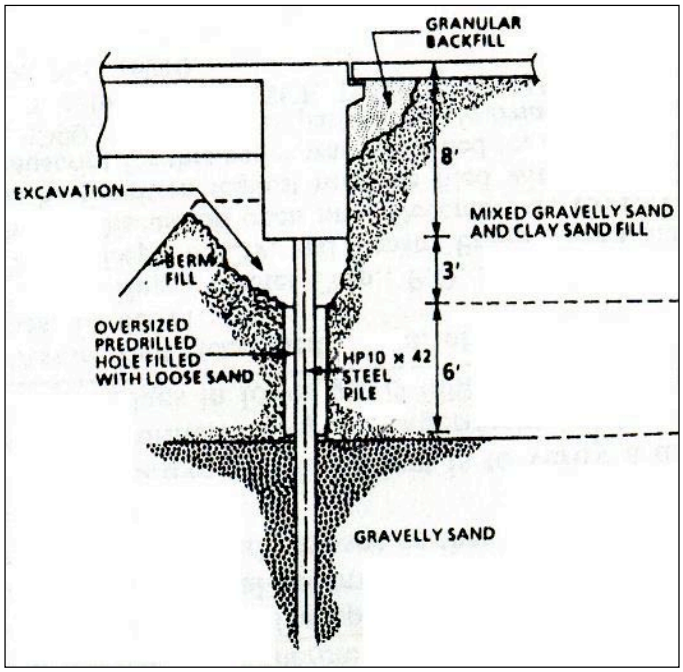


**Figure 2.11. Cross section of abutment and pile of Boone River Bridge (Girton et al., 1991)**

The Maple River Bridge is a steel girder bridge, 97.5 m (320 ft) long by 9.8 m (32 ft) wide. It is a continuous, three-span bridge with two piers located approximately 230 m (98 ft) from each abutment. The bridge was skewed 30-degrees. Abutments and girders were cast integrally with the deck, which is reinforced concrete, 216 mm (8.5 in) thick with a concrete strength of 24.1 MPa (3500 psi). The steel girders are welded plate girders approximately 1245 mm (49 in) deep and placed on bearing pads over the piers. The piles, HP254x65's (10x42)'s, were driven in predrilled holes approximately 3.7 m (12 ft) deep with the strong axis parallel to the longitudinal direction of the bridge and battered at a slope of 3:1 in the lateral direction. A cross-sectional view of the abutment and pile of the Maple River Bridge is seen below in Figure 2.12.

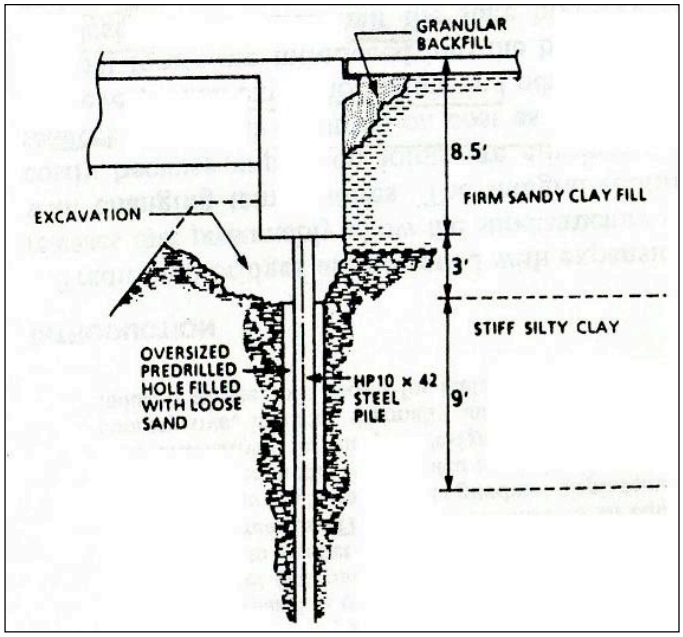


**Figure 2.12. Cross section of abutment and pile of Maple River Bridge (Girton et al., 1991)**

Instrumentation included two LVDT's installed on the Maple River Bridge and one on the Boone River Bridge to monitor the longitudinal expansion. Air and superstructure temperatures were monitored with thermocouples at the locations shown in Figure 2.13. At the Boone River Bridge, holes were drilled in the pre-cast girders, thermocouple wires were placed inside the holes then sealed with grout. At the Maple River Bridge, the thermocouple wires were soldered to the exterior surface of the steel girders and enclosed in electrical junction boxes. Holes were drilled in both bridge decks; thermocouple wires were placed inside and sealed with grout.

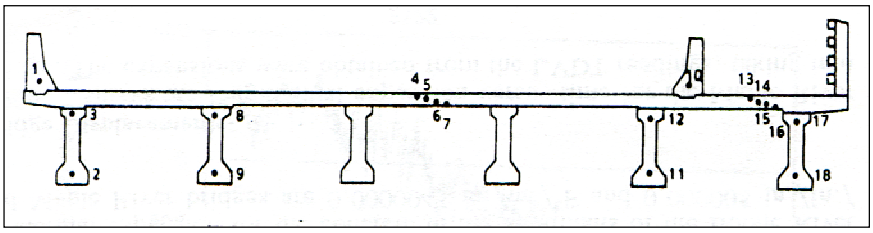


**Figure 2.13. Typical thermocouple locations (Girton et al., 1991)**

The pile-abutment interface of one pile at each bridge was excavated for the installation of four strain gages, about 152-203 mm (6-8 in) below the bottom of the abutment. The strain gages were placed on the outside faces of the flanges, about 44 mm (1.75 in) in from the flange tips. The excavated area was left unfilled for the testing.

Air temperature ranged from 6º C to 45º C (-21º F to 113º F) and 4º C to 39º C (-25º F to 103º F) at the Maple River Bridge, and the Boone River Bridge, respectively. The bridge deck temperatures ranged from 9º C (-16º F) at both sites, to 49º C (120º F) near the upper surface of the Boone River Bridge and 50º C (122º F) at the Maple River Bridge. The temperature distribution through the depth of the deck and concrete girder is

shown in Figure 2.14 for the Boone River Bridge at the time of the hottest temperature. The distribution at the Maple River Bridge was similar.

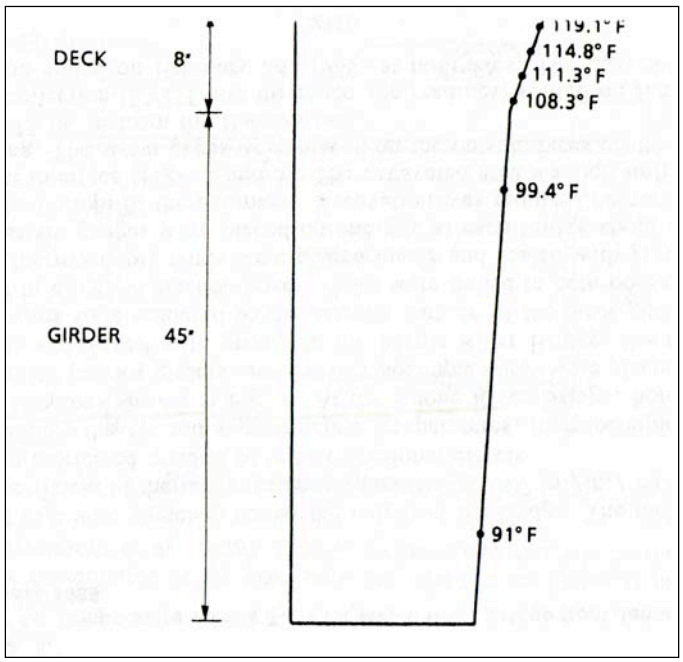


**Figure 2.14. Temperature distribution through depth of Boone River Bridge (Girton et al., 1991)**

The coefficient of thermal expansion (_) is not the same in all concrete as it is a function of cement mix, aggregate type, mix proportions, temperature, and concrete age (Girton et al., 1991). The coefficient of thermal expansion, _, was experimentally determined in this study to be 0.000008 1/ºC (0.0000045 1/ºF) and 0.000009 1/ºC (0.000005 1/ºF) for the Boone River and Maple River bridges, respectively. AASHTO specifies a coefficient of thermal expansion for concrete as 0.000011 1/ºC (0.000006 1/ºF), which is considerably higher than experimentally determined.

The longitudinal expansion versus time for the Maple River Bridge is shown in Figure 2.15. The Maple River Bridge and Boone River Bridge had total displacement ranges of approximately 64 mm (2.5 in) and 50 mm (2 in), respectively.

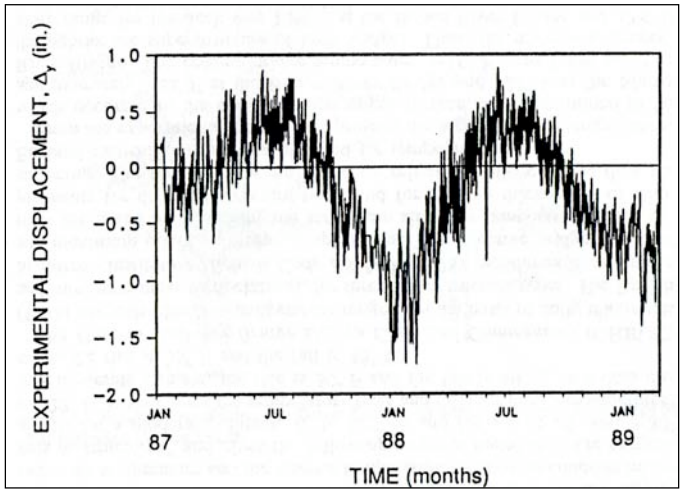


**Figure 2.15. Experimental longitudinal bridge displacement versus time for Maple River Bridge from January 1987 to February 1989 (Girton et al., 1991)**

Pile strains were separated into four components: axial, strong axis bending, weak axis bending, and torsional strain. Axial and torsional strains were relatively small. The maximum strains were approximately 700 and 900 micro-strains for weak axis (longitudinal) bending at Boone River and Maple River bridges, respectively, and 200 to 300 micro-strains for strong axis (transverse) bending.

Girton, Hawkinson, and Greimann (1991) concluded that for design purposes, the coefficient of thermal expansion for bridges should be experimentally determined or predicted by some other means, as the AASHTO specification values for the coefficient of thermal expansion were determined in this study to be too high. For design purposes, a temperature range of 66º C (150º F) should be used for a concrete deck and a range of

60º C (140º F) for concrete and steel girders. They also recommend that piles be driven in oversized, predrilled holes and oriented such that bending occurs predominately about the weak axis. For skewed bridges, they suggest battering the piles in the lateral direction to limit lateral motion.

## 2.4. Work Completed in Phase I of this Study

A summary of Phase I of this research project, completed by DeLano (2004), is presented in this section. A finite element model was created and used to examine the behavior of pile-supported integral abutment bridges, including those at sites with shallow bedrock. Based on the parametric studies completed, a preliminary design guideline was developed as an addendum to MaineDOT's current design procedure.

### 2.4.1. Finite Element Model

A two-dimensional finite element model was created using complex constitutive and surface interaction models in order to provide a more realistic illustration of the soil/structure interaction. Material properties were based on test data and theoretical values, and then adjusted to more closely resemble the anticipated conditions at bridge sites in Maine. The expected elastic-plastic behavior and response of the soil and piles were verified using simplified models. Several load cases to be used in the parametric study were created based on design recommendations from MaineDOT and AASHTO (DeLano, 2004).

Preliminary finite element models were created and analyses were performed to resolve any abnormal model behavior. Factors such as the out-of-plane thickness of the two-dimensional elements, and varying the depth of the channel beneath the girder had

unexpected influence on the behavior of the model. Once issues pertaining to these factors had been resolved or mitigated, critical model responses were examined more closely in the parametric studies. Changes were made in the level of mesh refinement in order to provide a more accurate numerical solution for the selected model responses (DeLano, 2004).

### 2.4.2. Parametric Studies

Parametric studies using the model previously described were performed in order to determine the effect of several variables on three major structural responses: pile stresses, pile kinematics, and pile/bedrock interaction. A primary parametric study, consisting of 630 combinations, was performed, investigating how changes in girder length, pile length, subsurface conditions, and loading affected the pile responses. DeLano's inspection of the pile kinematics showed that piles less than 4 m in length behave similarly to a laterally loaded, fixed-head pile of intermediate length, as defined by Broms (1964a, 1964b). The tip of the pile rotates, but does not translate horizontally or vertically, similar to a column with a pinned support. In addition to translation of the pile head due to thermal movement of the girder, dead and live loading of the girder induce a rotation of the abutments, causing additional pile head displacement, which is not typically accounted for in design (DeLano, 2004), nor found in monitoring (Lawver et al., 2000).

DeLano's model showed the magnitudes of the pile strains to be independent of the pile length, but dependent on girder length (and therefore loading), as well as the subsurface conditions (2004). Consequently, piles embedded in clay soils are more likely

to experience plastic deformation than those in granular soils. Similarly, for piles in a given soil type, those supporting longer spans can be expected to experience some degree of plastic deformation (DeLano, 2004).

The ratio of the shear force to the normal force acting at the pile/bedrock interface was compared to the coefficient of friction determined for this interface, as a means to validate the assumptions of pinned support conditions (DeLano, 2004). The normal force at this interface is controlled by loading and girder length, although downdrag resulting from certain soil conditions had a small effect. The magnitudes of shear forces at the pile tip are influenced by subsurface conditions and pile length.

Smaller parametric studies were performed in order to investigate less significant changes in loading, geometry, and member properties. DeLano (2004) concluded that positioning the design truck at different locations along the girder had no adverse effect on the pile behavior. He also determined that the larger live loading used by MaineDOT increased strains at the head of the pile, which may further reduce the allowable girder lengths used in design (2004). The structure was shown to accommodate cyclic live and thermal loading without any major consequences. Under annual temperature cycles, the abutment backfill is shown to deform, illustrating the need for approach slabs behind integral abutments (DeLano, 2004). Under combined cyclic live and thermal loading, plastic strains did not accumulate under load cycling, provided the strains at the pile head were less than 1.25 times the yield strain, $\varepsilon_y$, (DeLano, 2004).

Since conditions at bridge sites rarely consist of equal depths to bedrock at each abutment, a finite element model bridge with different length piles at each abutment was

created and subjected to the same load cases used for the models in the primary parametric study. Results of the bridge model with each abutment having different pile lengths were compared to the results obtained from the primary parametric study which had the same length of pile at each abutment. DeLano (2004) confirmed that pile head strains predicted at each of the abutments with different length piles compared well to the results from the primary parametric study.

A major concern about the behavior of an integral abutment bridge with a short pile on one abutment, and a pile with adequate overburden on the other abutment, was the deflection of the piles. Specifically the concern was that the entire short pile would experience increased translation because of the presence of the fixed support conditions of the longer pile on the other abutment. DeLano's model showed deflections along the entire lengths of both the short and long piles to be relatively unaffected by the presence of different lengths of piles on the other abutment. The results were consistent with the deflections from the models that had the same lengths on both abutments (2004). There was no lateral deflection at the tip of either pile, and the support conditions at the tip of the shorter pile still allowed for rotation to occur. Displacements of the pile head under dead and live loading were identical to the values from the primary study, while values in load cases involving temperature change were within 1% agreement for both the short and long piles (DeLano, 2004). Since there were no major differences in any of the pile responses between bridges with equal and unequal length piles, it was presumed that changes in girder length and soil type will affect the response of a bridge with unequal length piles in the same way that they would a bridge with equal pile lengths at both abutments (DeLano, 2004).

A separate small study showed that stiffer piles experience smaller strains at the pile head. Due to insufficient soil support, short, stiff pile sections were found to be less likely to develop double curvature than other pile sections. Thus, stiffer piles experience more lateral translation along the entire length of the pile; larger shear forces are generated at the tips of stiffer piles in order to compensate for the lack of lateral support provided by the soil. The bridge length and soil conditions may dictate the section of pile that can be used for a particular bridge, especially if the limiting strain at the pile head is considered to be a critical factor. Therefore, there are some cases where simply specifying a larger pile section will not improve design (DeLano, 2004).

### 2.4.3. Preliminary Design Guidelines

The current MaineDOT design procedure for piles supporting an integral abutment assumes the pile to be an equivalent cantilever, based on loading and soil conditions. Therefore, sufficient pile length must be provided in order to achieve support conditions approximating a cantilever with a fixed end. DeLano (2004) proposed an addendum to the current design procedure which could be used for sites in which the depth to bedrock is less than the depth required to achieve pile fixity. Based on results of the parametric studies, a relationship between the moment at the head of the pile and the axial load was created for various soil conditions and loadings. The proposed guidelines limit the strain in the pile to a maximum value of 1.25 times the yield strain, which was shown to be the point where plastic deformation accumulates under the most severe loading conditions (dead, live, and negative temperature change) (DeLano, 2004). The current guidelines limit the stress in the piles (due to live load only) to 0.55 $F_y$.

Unlike the current guidelines, the proposed guidelines idealize the support conditions at the pile tip as a pinned support, i.e., the pile tip cannot translate horizontally or vertically but is free to rotate. This is drastically different from the assumption of fixed conditions commonly used for longer piles. Forces at the pile tip are calculated in order to determine if this idealization is valid for the proposed pile/soil/load combination. The ratio of shear forces and normal forces are compared, along with a factor of safety, to the coefficient of friction between the pile and bedrock.

The moments at the pile head predicted using the proposed design method are, on average, 16% greater than those predicted from the finite element model. Thus the proposed design method is somewhat conservative. The values of the shear force at the top of the pile obtained with the design procedure are also conservative since they exceed the model predictions by 44% on average (DeLano, 2004).

### 2.5. Summary

Planning, design and construction practices employed by the United States, Canada and the United Kingdom for integral abutments have been summarized in this section. No universally accepted design practices currently exist. Several research studies have examined the behavior of piles supporting integral abutment bridges, both in the field and in the laboratory. Only one full-scale live load test has been reported. Very little work, however, has been done concerning integral abutments founded on short piles. Current design assumptions are invalid for lengths of pile less than that required to achieve fixed conditions. Additionally, these methods generally do not take into account

any interaction between pile and bedrock, nor do they predict rotation of the abutment as predicted for the short pile.

The Coplin Plantation, ME site offers a unique opportunity to investigate possible differences in short and long pile behaviors. One abutment has a depth of overburden sufficient to achieve pile fixity, while the other abutment has insufficient overburden to achieve pile fixity. The finite element analysis has shown that the behavior of each abutment is relatively unaffected by the behavior of the other abutment. With monitoring and live load testing, this bridge will provide an assessment of short pile-supported abutments. The data gathered from this study will also be valuable for applying to other bridge configurations. This will be accomplished by calibrating the finite element model to Coplin Plantation's results and using the calibrated model for predictions of other configurations.

# Chapter 3

# SITE CONDITIONS AND INSTRUMENTATION

## 3.1. Introduction

Integral abutment bridges are being built more frequently in the United States. Current practices in Maine limit the use of pile-supported integral abutment bridges to sites where there is sufficient overburden to provide a fully fixed condition for a driven pile. This allows the designer to treat the pile using an equivalent cantilever length, a conservative and simplifying assumption.

Subsurface conditions in Maine vary considerably; depth to bedrock varies from zero to more than 60 m (200 ft) below the ground surface. At sites with shallow bedrock, current design provisions require that the bedrock be drilled to the depth of fixity; the pile is then placed in the drilled hole backfilled with granular material. However, finite element (FE) modeling conducted during phase I of this project has shown that it may be feasible to construct a pile-supported integral abutment bridge when the depth of overburden is less than the depth of fixity and that stress conditions in these piles would be no more severe than in longer piles (DeLano, 2004). To confirm this, Phase II of this project involves monitoring the construction of an integral abutment bridge founded on short piles driven to bedrock. The chosen site, Nash Stream in Coplin Plantation, Maine, affords a unique opportunity to compare pile behavior for deep and shallow bedrock at the same bridge, as well as the effects of a relatively large skew, 35-degrees. This chapter summarizes the relevant site features, project construction and instrumentation.

### 3.2. Project Description

An integral abutment bridge with H-piles to bedrock was recommended for the crossing of Nash Stream on Route 16 in Coplin Plantation, Franklin County, Maine. The bridge spans 30 m (98 ft) and is 10 m (32.8 ft) wide. Each abutment is supported by four- HP360x132 (HP14x89) grade 50 steel H-piles oriented with the weak axis perpendicular to the direction of traffic and driven to bedrock. The H-piles were welded to the steel plate girders; the connection was encased in concrete to form the abutments. The concrete deck was cast monolithically with the concrete abutments, without the use of expansion joints. See Figure A.1 in Appendix A for a plan view and elevation view and Figure A.2 in Appendix A for a typical cross sectional view of the Nash Stream Bridge.

### 3.3. Subsurface Characteristics

Subsurface explorations were completed by the Maine Department of Transportation (MaineDOT) between May 21 and May 23, 2002. Five borings were completed throughout the site, including a cased washboring behind each abutment location. Further drilling was done during construction on Days 215 – 217 (August 2 - 4, 2004) at each test pile location to determine the depth to bedrock and thus the length of pile and the strain gage locations on the pile.

Soil profiles with depth to bedrock for Abutments 1 (South) and 2 (North) are shown in Figures 3.1 and 3.2, respectively. These figures were compiled based primarily on the borings done at each pile location but also on the exploratory drilling completed in May, 2002. The washborings (from May, 2002) were used to define the various soil types; the

recorded casing blows from the May borings were compared to casing blows from the August borings at the test pile locations to differentiate between soil layers.

Abutment 1 has a thick layer of medium dense to dense sand with traces of silt and gravel as shown in Figure 3.1. This deposit is underlain by a very dense silty sand with gravel, which was considered to be glacial till. The thickness of the glacial till layer at one of the pile location is unclear (see Figure 3.1). The casing blows suggest that the top of this layer is approximately at the same elevation as the pile tip, which implies a drastic reduction in thickness of this layer compared to the adjacent pile locations. A dashed line with question marks was made in Figure 3.1 connecting the top of the till layer at two nearby pile locations, this line reflects the logic that the layer would be moderately uniform and would imitate the pitch of the bedrock. Abutment 2 (Figure 3.2) has a very dense gravel layer near the surface, likely to be fill material from the construction of the previous bridge. This layer is underlain by a very dense layer of silt, followed by a medium dense sand, which is thought to be glacial till.

The elevation of bedrock was taken as the lower of the elevation determined from the boring at the test pile location or the pile tip elevation after driving; it is unreasonable to believe the pile tip penetrated intact bedrock. Table 3.1 summarizes the elevations of bedrock as determined from the borings at each test pile location, and the elevations of the pile tip after driving. At least 1.5 m (5 ft) of bedrock was cored at every boring location; the bedrock was observed to be medium grained metamorphosed pelite. Boring logs for the subsurface exploration as well as the drilling at each pile location can be seen in Appendix A.

**Table 3.1. Bedrock and pile tip elevations**

| Abutment #1 (South) - Elevation, m | | | |
|---|---|---|---|
| | Bedrock | Tip | Difference |
| G1-S | 368.930 | 369.283 | 0.353 |
| G2-S | 368.870 | 369.743 | 0.873 |
| G3-S | 371.000 | 370.859 | -0.141 |
| G4-S | | 371.729 | |
| | | | |
| **Abutment #2 (North) - Elevation, m** | | | |
| | Bedrock | Tip | Difference |
| G1-N | | 373.841 | |
| G2-N | 373.31 | 373.545 | 0.235 |
| G3-N | 373.56 | 373.551 | -0.009 |
| G4-N | 374.23 | 373.676 | -0.554 |

Earthwork for the project was completed by Jordan Excavation. The backfill material was supplied from Fotter's pit in Wyman Township. Sieve analyses were completed on the well-graded granular borrow by the Technical Services Division of the MDOT.

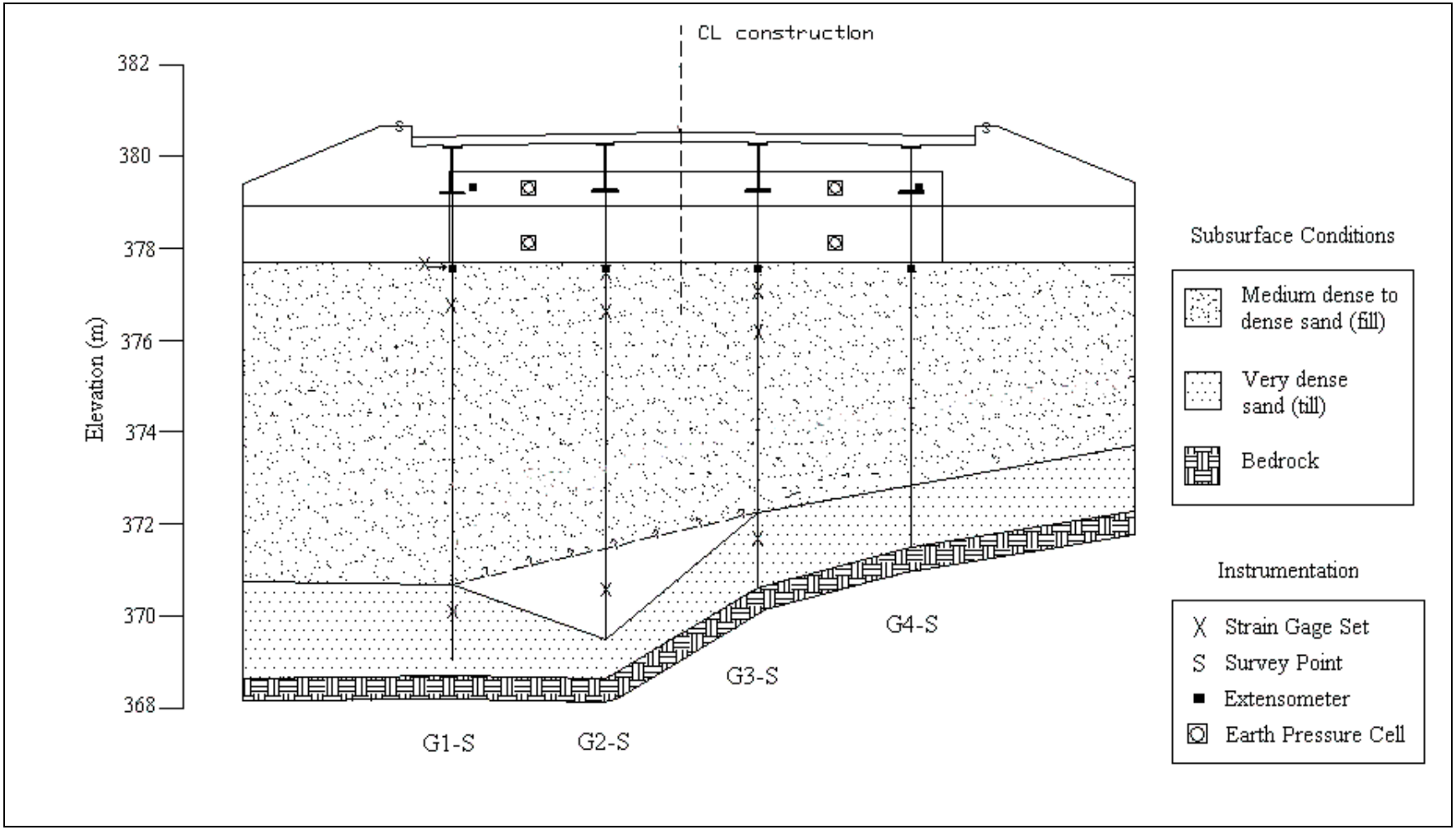


**Figure 3.1. Profile view of Abutment 1 (South) of Coplin Plantation Bridge, looking north**

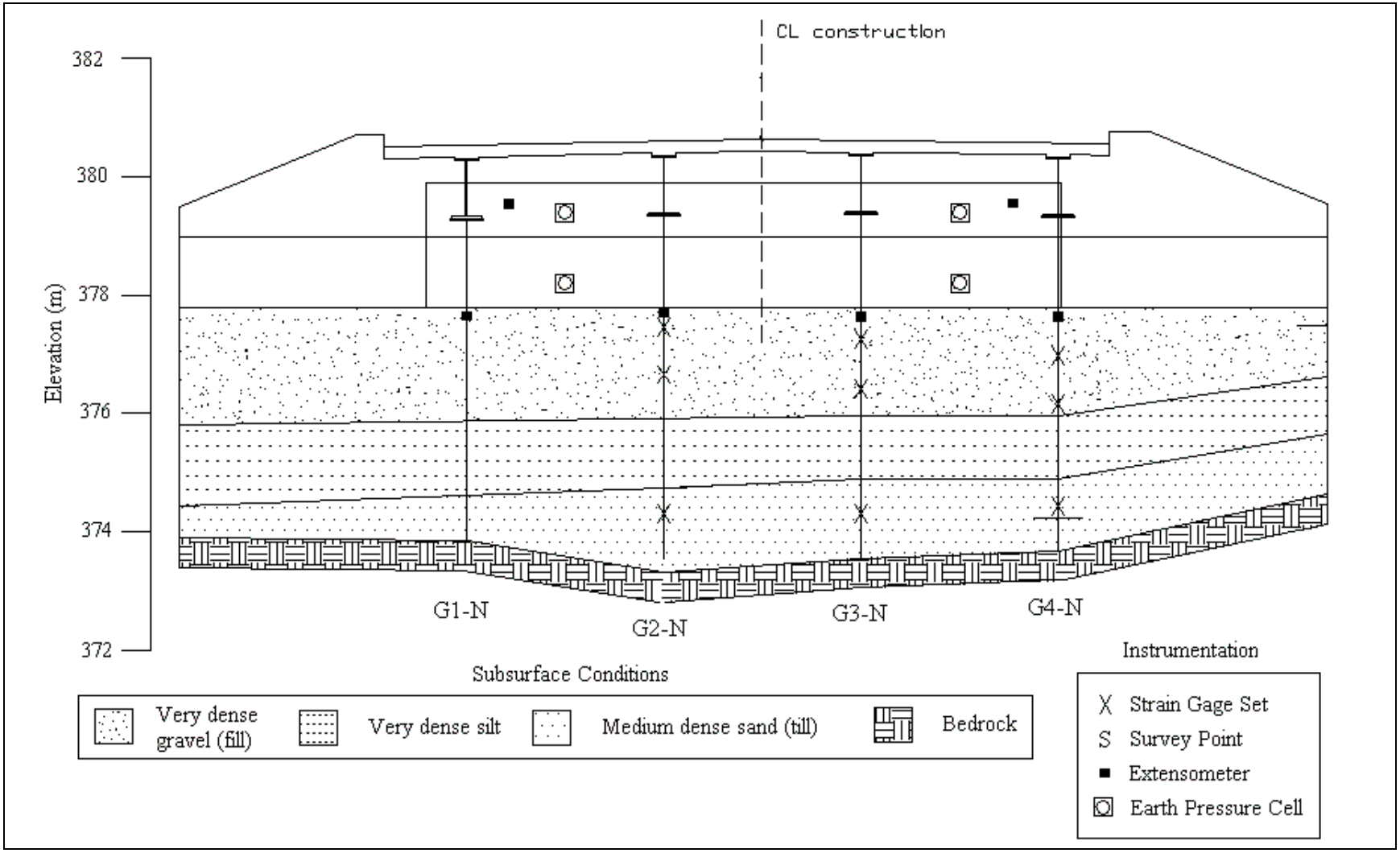


**Figure 3.2. Profile view along Abutment 2 (North) of Coplin Plantation Bridge, looking north**

### 3.4. Construction Schedule

Prior to construction, the site contained a truss bridge with sliding plate bearings. The abutments were founded on spread footings. The bridge had been severely distressed over the years and required replacing. Site work commenced on Day 127 (May 6) with erosion control, putting up signs, and constructing a temporary bridge over Nash Stream. Demolition of the existing bridge took place on Day 202 (July 20), after traffic was diverted to the temporary bridge. Four 18.3 m (60 ft) long HP360x132 (HP14x89) grade 50 steel H-piles arrived on site on Day 201 (July 19). The pile sections were cut, creating two pile sections, one to be driven under Abutment 1 and one to be driven under Abutment 2. Immediately after installation of strain gages and protection for the strain gages and inclinometers, the Abutment 1 piles and Abutment 2 piles were driven on Day 222 (August 9) and Day 224 (August 11), respectively. A hydraulic vibratory driver was used to insert and stabilize the piles in the soil, after which a Delmag 32-16 diesel hammer was used to drive the piles to refusal. Figure 3.3 and 3.4 illustrate piles being driven with the vibratory and diesel drivers, respectively.

**Figure 3.3. Vibratory driving of pile G1-S**

**Figure 3.4. Diesel hammer driving of pile G3-N**

The concrete for the lower portion of Abutments 1 and 2 was cast on Day 230 (August 17) and Day 232 (August 19), respectively. The bridge girders arrived on Day 239 and 240 (August 26 and 27). Two cranes, each supporting an end, set the girders in place on sole plates on Day 240. The diaphragms and cross bracing were bolted in place on Day 243 (August 30); the girders were then welded to the sole plates on Day 245 (September 1). The upper portion of both abutments and the deck were cast continuously on Day 258 (September 14). The approach slabs were cast on Day 266 (September 22) and backfilled on Day 271 and 272 (September 27 and 28) for Abutment 1 and 2, respectively. The bridge and approaches were paved on Day 275 and 276 (October 1 and 2). Immediately following the completion of the live load testing of the bridge on Day 281 (October 7), it was opened to the public.

## 3.5. Instrumentation

### 3.5.1. Overview

Instrumentation on each of the six test piles consisted of twelve strain gages, with four mounted at each of three elevations, and inclinometer casings to allow for manual inclinometer readings. Each of the eight piles was instrumented with an extensometer. Both abutments were instrumented with four earth pressure cells, with two mounted at each of two elevations, and an extensometer at each of the four abutment corners. Four thermistors were embedded in the concrete deck, three thermistors were attached to the two middle steel girders, and an air thermistor was placed at either end of the bridge. An inclinometer casing was installed in the slope behind each abutment. Two vibrating wire piezometers were installed; one at either end of the bridge, and a standpipe was also

installed. Every vibrating wire instrument (strain gages, extensometers, pressure cells, piezometers) and every thermistor was connected to a solar-powered automated data retrieval system that allows remote access to the data via modem. A manual readout unit was used to take initial readings as well as subsequent readings until the data acquisition systems were functional. A plan view of the instrument locations is shown in Figure 3.5. A profile view of the instrumentation on Abutment 1 and 2 is shown in Figure 3.1 and 3.2, respectively, and a pile cross-section with location of instrumentation is shown in Figure 3.6.

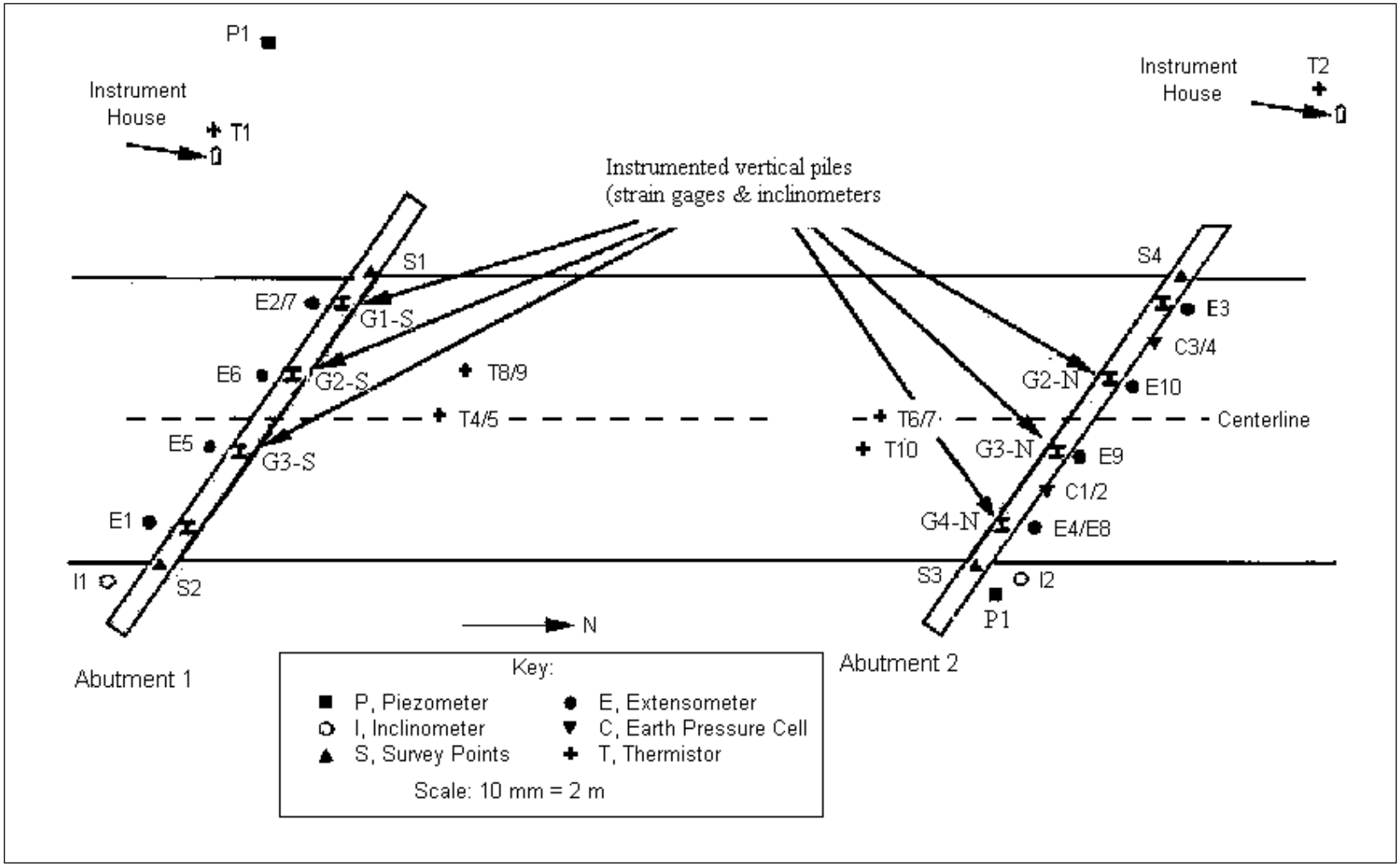


**Figure 3.5. Plan view of instrumentation on Coplin Plantation Bridge**

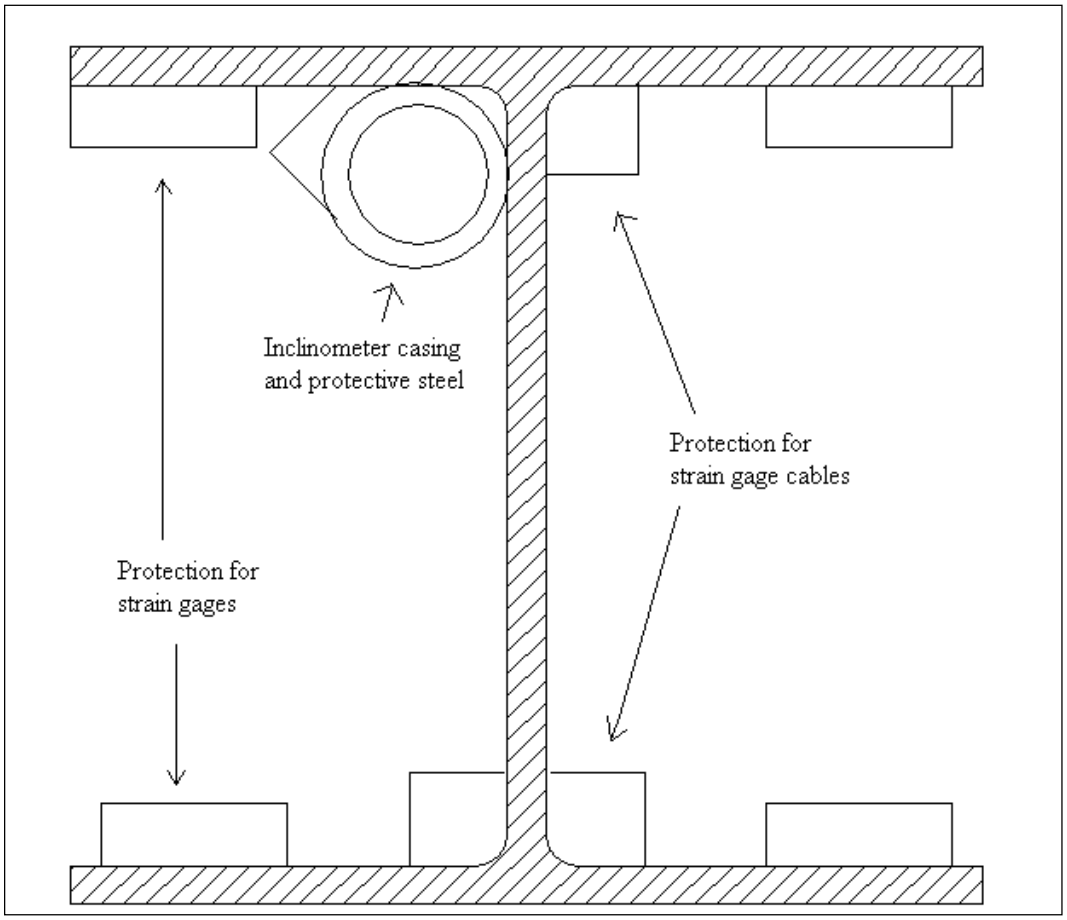


**Figure 3.6. Instrumentation layout on piles**

### 3.5.2. Strain Gages

The foundation piles of the bridge crossing Nash Stream were oriented primarily for weak axis bending, however, the large skew will cause the piles to also bend in the strong axis as well as experience torsion. Strain gages were installed on the piling to determine the effects of abutment lateral and rotational movements on the strains in the piles. The strain gages were positioned so that axial and bending stresses could be differentiated, and also to determine the strain distribution with depth.

Roctest model SM-5A vibrating wire strain gages were installed on each of six test piles with a set of four at each of three elevations. Each set consisted of four strain gages welded to each inner face of the flanges, approximately 50 mm (2 in) from the edge (Figure 3.6). This layout allowed for distinguishing between bending stresses and compression stresses at each elevation. The strain gages are equipped with a spring that pre-tensions a high strength wire which is clamped in two end blocks which were welded to the flanges of the steel pile. Changes in the distance between the two end blocks modify the tension in the wire, and therefore the resonant frequency. To read the gages, voltage pulses at various frequencies are generated in an electromagnet, forcing the wire to oscillate. A readout unit converts the resonant frequency to a linearized value in microstrains, referred to as LU. The readable strain range is 3000 microstrains with an operating temperature range of -50ºC to 60ºC (-122ºF to 140ºF).

The bottom set of strain gages was positioned 1.0 m (40 in) and 0.7 m (28 in) above the pile tip for piles under Abutment 1 and 2, respectively. Ideally, the strain gages would have been located directly at the tip, but it was feared that damage to the steel protection over the strain gages as well as the strain gages may occur during hard driving. The hardest driving was anticipated in the 1 m to 2 m thick glacial till above bedrock; the strain gages were therefore positioned to reduce the exposure of the instruments to hard driving. The top set of strain gages was initially located such that after driving, they would be 305 mm (12 in) below the bottom of the concrete abutment. The middle set was placed 1 m (39 in) below the top set.

A summary of the as-built elevations of strain gage sets for each pile is summarized in Table 3.2. The elevations of the bottom of the concrete for Abutment 1 and 2 are 377.950 and 377.780, respectively.

**Table 3.2. Elevation of strain gage sets**

| Abutment #1 (South) - Elevation, m | | | |
|---|---|---|---|
| Pile | Bottom | Middle | Top |
| G1-S | 370.299 | 376.930 | 377.845 |
| G2-S | 370.759 | 376.831 | 377.670 |
| G3-S | 371.888 | 376.360 | 377.274 |
| | | | |
| **Abutment #2 (North) - Elevation, m** | | | |
| Pile | Bottom | Middle | Top |
| G2-N | 374.269 | 376.619 | 377.432 |
| G3-N | 374.262 | 376.371 | 377.197 |
| G4-N | 374.387 | 376.115 | 376.928 |

A section of each H-pile was retrieved for tensile testing in the laboratory to determine the properties of the pile for use in analysis. Piles G1-S and G4-N, G2-S and G3-N, and G3-S and G2-N were cut from the same H-pile. A sample from the web and the flange from each section of pile were testing according to ASTM A370-97a. The specimen dimensions were 305 mm x 13 mm x 13 mm (l2 in x 0.5 in x 0.5 in). The modulus of elasticity and yield stress were determined for each sample and are presented in Table 3.3.

**Table 3.3. Results from Tensile Testing of Steel H-Piles**

| | **G1-S/G4-N** | | **G2-S/G3-N** | | **G3-S/G2-N** | |
|---|---|---|---|---|---|---|
| | **Web** | **Flange** | **Web** | **Flange** | **Web** | **Flange** |
| **Modulus of Elasticity, E (GPa)** | 209.3 | 212.4 | 203.1 | 192.5 | 160.1 | 195.5 |
| **Yield Stress, _y (MPa)** | 407.2 | 437.9 | 395.4 | 394.6 | 404.0 | 403.2 |

The average modulus for each pile was used in analysis. The modulus determined from the web of piles G3-S/G2-N was omitted in analysis as it was determined to be too

low, probably due to testing error. The modulus from the flange of these piles was used in calculations. Plots of the test results are presented in Appendix C.

Protection for the strain gages and their cables was provided by welding steel covers (38 mm x 76 mm x 150 mm) over them with a tapered protection block at the bottom (Figure 3.7). The cables were also anchored within the steel channel to protect against damage during driving. Preformed baskets were welded to the piles; the strain gage cables were wrapped in this device which acted like a "Chinese finger" and prevented the cable from pulling out of the instrument due to inertial forces during driving. The inclinometer protection pipe was also reinforced during driving by a tapered end block welded to the bottom of the pipe. Expanding insulation foam was used to seal any openings and to give additional resistance to developing cable inertial forces.

**Figure 3.7. Strain gage and inclinometer casing protection**

The depth to refusal encountered by the piles was found to be different from the top of bedrock depths determined by prior drilling at each test pile location as indicated

in Table 3.1. Piles that met refusal at elevations higher than expected caused strain gages sets to be at elevations that would be later encased in concrete. To compensate for the discrepancy, the elevation of the bottom of the concrete abutments was raised by 305 mm (12 in). This design modification resolved the problem for all but one set of strain gages. The remaining set, the top set on Pile G2 under Abutment 1, was removed and reinstalled 840 mm (33 in) below the original middle set. Thus the original middle set became the top set on this pile.

### 3.5.3. Extensometers

The pile extensometers monitored the lateral movement at the top of each pile which provided a datum for the pile inclinometer movements. Since the piles are not socketed into bedrock, the tips of the pile may move slightly, and thus the bottom of the inclinometers can not be used as a non-moving reference. The abutment extensometers indicate lateral movement and rotation resulting from temperature induced expansion and contraction of the bridge deck, as well as the effects of skew on the movements. Information from both the pile and abutment extensometers was compared to reveal the rotation of the abutment in the vertical plane.

A Roctest Model ERI extensometer (measurement range of 25 mm) was installed on each of eight piles as shown in Figure 3.8. A hole was drilled through the web of the each pile 150 mm (6 in) below the bottom of the concrete abutment (98 mm below bottom of concrete on pile G2 of Abutment 2). The elevations of the extensometers connected to the piles are 377.798 for the south abutment, and 377.646 for the north

abutment except for pile G3-N which is at elevation 377.700. The threaded end of the extensometer rod extended through the pile and was fastened with a nut.

**Figure 3.8. Installation of pile extensometer**

A total of four additional extensometers were installed in the concrete abutments at elevation 379.55 to assess abutment rotation vertically and horizontally. A 50 mm (2 in) hole was drilled into the concrete at each corner of the two abutments (Figures 3.2 and 3.3); the extensometer rod was secured in the hole with epoxy. All extensometers were aligned parallel to the direction of traffic with the ends anchored in the soil 3 m (10 ft) beyond the back face of the abutment, which was assumed to be unaffected by abutment movement and remain fixed.

### 3.5.4. Pressure Cells

A total of eight Roctest model TPC earth pressure cells (measurement range of 350 kPa (75 psi)) were installed to establish the changes in soil pressure with abutment movement. Two pressure cells were installed at elevation 378.20 and two more at elevation 379.40 on Abutment 1. Two pressure cells were installed at elevation 378.05 and two more at elevation 379.25 on Abutment 2. Each set of two pressure cells consisted of a cell 3.3 m (11 ft) to the right and one 3.3 m (11 ft) to the left of the centerline of construction on the approach fill face of the abutment. This configuration (Figure 3.1 and 3.2) is expected to reveal the effects of skew, as well as the change in soil pressure with depth.

The pressure cells were embedded in a 75 mm (3 in) thick concrete bed which served as protection for the cell during concrete pouring. Four nuts were set into the concrete block which allowed for the block to be attached to the formwork. After the formwork was removed, steps were taken to ensure that neither concrete nor sand wedged the space between the cell and the concrete bed in which it rested. Special calibrations of the pressure cells in the concrete bed were conducted in the laboratory prior to field installation.

### 3.5.5. Thermistors

Roctest model TH-T thermistors, with a measurement range of -50ºC to 150ºC (-122 ºF to 302ºF), were used to monitor the temperature of the concrete deck, steel girders and the ambient air temperature. These thermistors will allow a correlation to be made between the ambient air temperature, the bridge temperature, and the magnitude of

movement of the bridge. These thermistors supplement the internal thermistors contained in all vibrating wire instruments including strain gages, extensometers, piezometers and pressure cells. The internal thermistors will measure primarily ground and water temperatures.

#### 3.5.5.1. Concrete

Two thermistors were placed in the concrete deck 7.6 m (25 ft) north of Abutment 1 and two were placed 7.6 m (25 ft) south of Abutment 2. Thermistors were placed at 75 mm (3 in) and 150 mm (6 in) below the concrete surface at each location. The thermistors were encased in concrete cylinders with a diameter of 50 mm (2 in) and a length of 150 mm (6 in) and secured to deck reinforcing to protect them during the deck pour.

#### 3.5.5.2. Steel

Three thermistors were placed on the middle two steel girders. Two thermistors were located at 7.6 m (25 ft) north of Abutment 1 on Girder 2, one at the top intersection between the web and the flange, and one two-thirds of the way up the web (Figure 3.9). One thermistor was located at 7.6 m (25 ft) south of Abutment 2 on Girder 3, at the top intersection between the web and the flange (Figure 3.7). The thermistors were set inside 150 mm (6 in) long galvanized pipes welded to the downstream side of the girders to protect them and to have a closer attachment to the steel girder.

3.5.5.3. Air

A thermistor was located on each post supporting the two data acquisition systems to measure the ambient air temperature. The thermistors were protected with solar radiation shields.

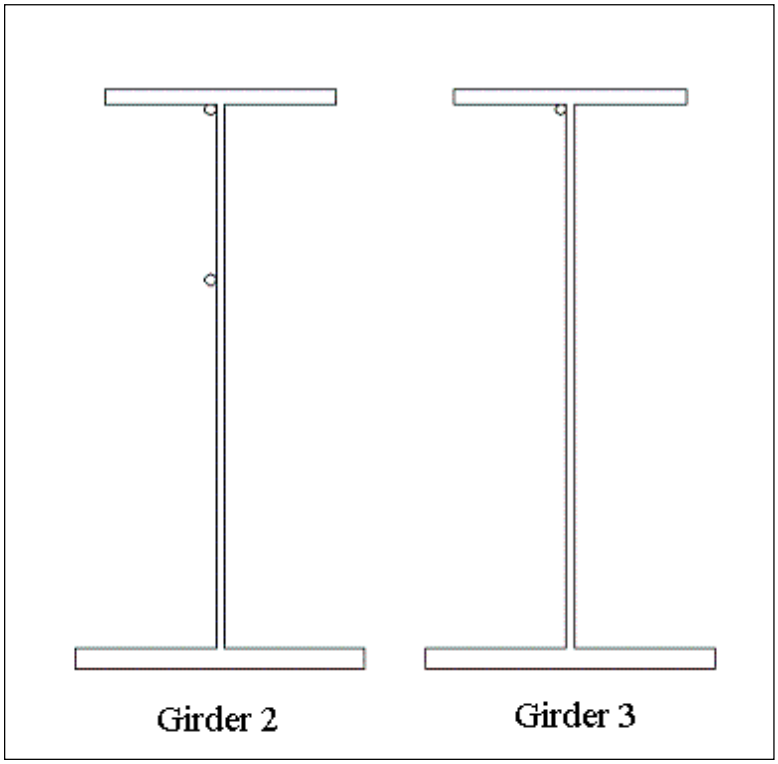


**Figure 3.9. Steel thermistors on downstream face of girders**

### 3.5.6. Piezometers

Two Roctest Model PWS vibrating wire piezometers were installed on Day 271 (September 27) to measure pore water pressure which can be used to interpret effective stresses in the soil which relate to the strength of the soil. The pore pressures will primarily indicate the level of water in Nash Stream. One piezometer was installed in a

borehole drilled 1 m (3 ft) north of Abutment 2, behind the upstream guardrail at an elevation of 375.72. A second piezometer was installed in a borehole located 2 m (6.5 ft) south of Abutment 1. This piezometer was located 1.2 m (4 ft) beyond the toe of the slope on the downstream side at an elevation of 375.20. A standpipe was installed in a borehole approximately 0.6 m (2 feet) west of the second piezometer to monitor the groundwater level. A 0.6 m (2 ft) section of 38 mm (1_ in) pvc piping was drilled with holes, then wrapped with geotextile to prevent fine grained material from infiltrating the pipe. The bottom of the standpipe is at elevation 378.25. All boreholes were backfilled with sand immediately around the piezometer, then a sand and cement mixture was backfilled up to the ground surface

### 3.5.7. Inclinometers

Inclinometers were installed to monitor lateral movements in the side slope embankments and also to monitor the deflections of the piles. Inclinometer casings are typically installed in a near vertical borehole that passes through suspected zones of movement into stable ground. The casing is installed such that one set of grooves is aligned with the expected direction of movement, the A-axis. The inclinometer probe employs two force-balanced servo-accelerometers to measure tilt. One accelerometer measures tilt in the plane of the inclinometer wheels (A-axis), while the other accelerometer measures tilt in the plane perpendicular to the wheels (B-axis). A typical inclinometer survey consists of four readings at each elevation, two in the A-direction and two in the B-direction; readings are taken every 2 ft from the bottom of the borehole upward. Although technology allows for the inclinometer sensor to be connected directly

to a computer for automatic recording, all data was taken manually due to problems with the computerized data acquisition system.

One inclinometer casing was installed along the web of each test pile to determine the longitudinal and lateral movements of the pile (Figure 3.6). As indicated previously, it was anticipated that the bottom of the pile may move, therefore, the inclinometer datum was established by the movement of the extensometer. Protection for the inclinometer casing consisted of a welded steel pipe with an outside diameter of 76 mm (3 in). The steel pipe extended through the sole plate, girder, abutment and deck such that after construction, the inclinometer casing can be accessed from the deck surface. Figure 3.10 shows the inclinometer capping system after the bridge was completed. The space between the inclinometer casing and steel pipe was grouted with a mixture of 1.3 parts bentonite, 7.5 parts Portland cement, and 17.6 parts water.

**Figure 3.10. Inclinometer capping system**

An inclinometer was installed behind each abutment in boreholes in the upstream shoulders (Figure 3.3). The inclinometer casing was installed to a depth of 370.33 and 374.5 for Abutment 1 and 2, respectively. A sand and cement mixture was used to

backfill the area around the inclinometer casings as the borehole casing was withdrawn to achieve good contact between the casing and the surrounding soil.

All inclinometer casings were oriented so that their principal axis (A-axis) would be parallel to the centerline of the roadway. Azimuth corrections were applied to the two pile inclinometer casings that depart from the desired orientation. Inclinometer readings were taken on an as needed basis initially, then every other week; readings were taken with a Digitilt 09plus manufactured by Slope Indicator, Co.

### 3.5.8. Survey Points

Four survey points were established at the corners of the bridge such that periodic checks of bridge movement could be made. Locations and elevations of the survey points can be seen in Figures 3.1 and 3.2 for Abutments 1 and 2, respectively.

### 3.5.9. Data Acquisition Systems

A data acquisition system was set up beyond the toe of the slope on the downstream side of both ends of the bridge. Vibrating wire instruments from the piles and abutment on the south end, as well as the thermistors, were connected to a Campbell Scientific CR-10x datalogger (Figure 3.11). The instruments on the piles and abutment on the north end of the bridge were connected to a Campbell Scientific CR-23x datalogger (Figure 3.12). Both dataloggers were powered by 12 V, 7 Ahr batteries which are charged by solar panels. Each system had a telephone line and modem so that remote access can be made to collect data. The systems allow for adjustment of the data reading interval. The interval is set to read the instruments hourly; during specific events in

which loads and stresses may be changing rapidly, the system can monitor the instruments as frequently as every three minutes.

The systems were installed shortly after pile driving. Both dataloggers were fully functional as of Day 259 (September 15). Prior to system installation, readings of the vibrating wire instruments were taken with a Roctest MB-6T manual readout unit.

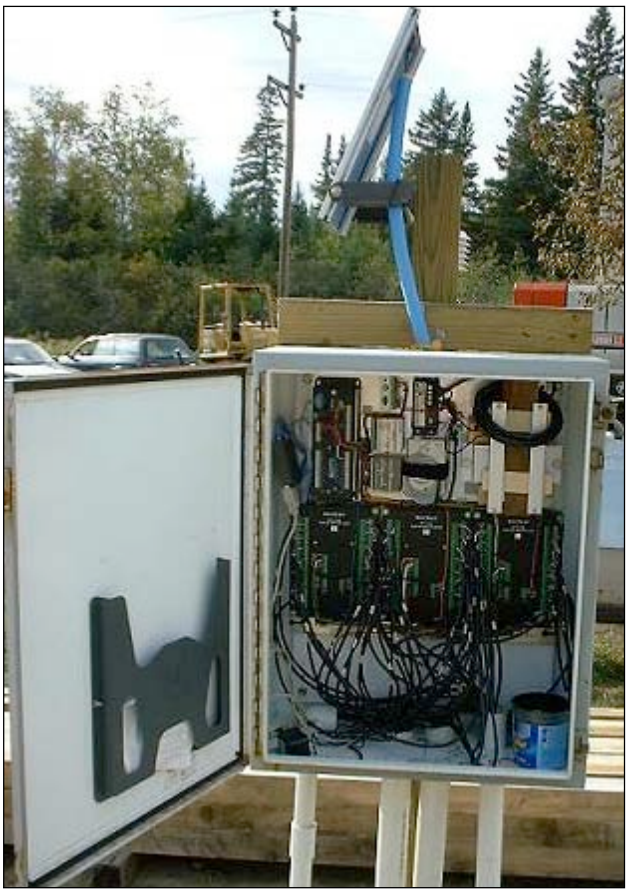

**Figure 3.11. Data acquisition system for Abutment 1**


**Figure 3.12. Data acquisition system for Abutment 2**

# Chapter 4

# PROCESS FOR DATA INTERPRETATION AND THE EFFECTS OF THE CONSTRUCTION PROCESS

## 4.1. Introduction

The first sections of this chapter examine how the electronic measurements from each type of instrument are translated into engineering measurements. The frequency output from each vibrating wire instrument must be converted to some meaningful unit of strain, pressure, or length. The resistance reading of the thermistor must be converted to temperature. The angle of inclination read from the probe of the slope indicator must be converted to movement. Since readings for strain gages, extensometers, pressure cells, piezometers and inclinometers are relative, the initial condition for these instruments are detailed including reasons for selecting a particular initial condition. The issue of correcting, or ignoring, faulty instruments is also addressed in the first portion of this chapter.

The second part of this chapter examines the effects of the construction process on the stresses in the piles, the movements of the piles and the abutments, and the soil pressures. The process is broken down into significant events, such as placement of the girders and support bracing, casting the deck, casting and backfilling the approach slabs, casting the curbs, and paving the deck. Due to the sequence of bridge construction and technical difficulties encountered while setting up the data acquisition systems, some instruments were not read, resulting in an incomplete data set for some initial construction events. Thus some instruments measured the effect of a particular construction event, while other instruments were not fully operational.

## 4.2. Initial Conditions

The most significant assumption made during the analysis process was the selection of the initial conditions. The strain gages, extensometers, pressure cells, piezometers and inclinometers required a reference reading to which subsequent readings were compared. Since instruments were installed throughout the construction of the bridge, each set of instruments had their own initial condition. Temperature readings did not require an initial value.

The strain gages proved to be the most challenging when selecting an initial condition. The change in strain between the installations of the strain gages and after driving is not considered in this research, as there is insufficient data to draw significant conclusions. Therefore, it was originally assumed that the initial condition for the strain gages would be immediately after driving. Several problems arose from this preliminary assumption. The time lapse between driving and taking the readings after driving varied from pile to pile. This appeared to affect the calculation of change in strain. The north side was read the day after driving, while the times at which the south side's readings were taken were inconsistent. Half of the strain gages on Pile G1-S were not read the day after driving, as they were inaccessible due to the required protection during driving. Pile G2-S also had inconsistent times for 'as-driven' readings, since one set of gages was removed and relocated after driving (see section 3.5.2).

In addition to finding a consistent time for 'as-driven' readings, it was difficult to establish the expected magnitude of downward force applied to the piles due to the casting of the first portion of the abutments. When the abutment was cast, the concrete

was poured directly on the foundation soil. The ground carried the majority (perhaps all) of the load from this initial pour. When the ground beneath the abutment settled, the pile must support the load once carried by the ground. Addition of fill and its compaction could push material into any voids that may have formed below the abutment, thereby transferring some load back to the ground from the pile.

The inconsistent 'as-driven' readings and uncertainty of the induced loads due to the first portion of the abutment pour caused the initial condition to be chosen as the point in time after the first portions of the abutments were cast, but before the girders were set in place. This allowed the strain gages to all have the same initial condition. The total weight of the first portion of the two abutments was calculated to be 823 kN (185 kips), or 103 kN (23.1 kips) per pile. Since the abutments were relatively symmetrical, the stress applied to the piles will be primarily uniform axial compression of -5.3 MPa (-0.77 ksi). The residual stresses due to pile driving as well as the stresses due to the casting of the lower portion of the abutment were back-calculated from the strain gages on the piles. Table 4.1 summarizes the measured stresses is the fully functional strain gage sets. These stresses are not included in subsequent reported results.

**Table 4.1. Summary of stresses (MPa) after driving and the casting of the lower portion of the abutment along the length of the pile**

| | Stresses (MPa) | | |
|---|---|---|---|
| | **Minimum** | **Maximum** | **Average** |
| **Driving:** | | | |
| **High Set** | -105.7 | 39.9 | -16.0 |
| **Middle Set** | -122.2 | 188.2 | 51.9 |
| **Low Set** | 44.3 | 95.2 | 67.1 |
| **Lower Abutment:** | | | |
| **High Set** | -17.2 | -13.4 | -15.6 |
| **Middle Set** | -20.8 | -8.7 | -16.4 |
| **Low Set** | -28.5 | -5.9 | -15.0 |

The initial condition for strain gages and extensometers on the piles of the South Abutment was established as Day 238, at 12:00 PM; the initial condition for strain gages and extensometers on the piles of the North Abutment was established as Day 240, at 7:00 AM.

## 4.3. Process for Data Interpretation

The process for analyzing each instrument is explored in detail in the following sections. The rationale behind the determination of the initial condition for each instrument is also given. Readings are induced by the portable readout unit or data acquisition systems by signaling for the vibrating wire to be plucked. The frequency of the vibrating wire is recorded by the portable readout unit or the data acquisition system and is then output in Linear Units, LU, which must then be converted to a meaningful unit.

### 4.3.1. Strain Gages

The strain gages are all calibrated to a standard level of accuracy by the manufacturer, +/- 0.5% of working range. Each strain gage is supplied and installed with its vibrating wire at varying pre-tension. The pre-tension is based on the anticipated strains during the life of the project. It was anticipated that the piles would experience both tensile and compressive stresses; therefore the gages were installed at pre-tensions in the middle of the measuring range to adequately capture a broad spectrum of stresses. The strain gages are read in LU's by the readout unit or data acquisition systems, then converted to strains according to Equation 4.1 (Roctest: Model SM-5A, 2000). All calculated strains are changes in strain with reference to a specified initial condition.

$$\Delta\varepsilon = (L_{1SG} - L_{0SG}) \qquad \text{(Equation 4.1)}$$

where __ is the change in strain, in micro-strains, $L_{1SG}$ and $L_{0SG}$ are the current and initial strain gage readings (LU). Initial readings for strain gages on the south and north piles, are considered to be the readings taken on Day 238 at 12:00 PM and on Day 240 at 7:00 am, respectively.

The thermal strains of the pile are not included in the calculated strains used for stress calculation. The steel vibrating wire will expand and contract the same amount as the steel pile under temperature changes and thus eliminates thermal strains in its monitoring. The range of temperatures reported from the strain gages during construction of the bridge was 6 ºC to 17 ºC.

Each pile had three sets of four strain gages per set with each set at a different elevation on the pile; each set consisted of one gage on each flange of the H-pile (see Figure 3.6). Since each pile would potentially be subjected to axial load, strong-axis bending, weak-axis bending and a torsional moment, the use of four gages allowed the four internal member forces to be back-calculated. A set of four linear equations was written to express these four internal pile forces as a function of strains, the pile elastic modulus, and cross-sectional member properties. The four equations were solved for the four member forces using the four strains from a set of gages. The system of linear equations is only valid if the stresses in the pile do not exceed the yield stress of the pile, which was always the case. See Appendix B for derivation of this analysis method. The positive direction for bending moments is different for each abutment. Expansion of the bridge will produce positive moments about the weak axis, for both abutments; compression of the obtuse corner of an abutment will produce positive moments about

the strong axis, for both abutments. Figure 4.1 illustrates the positive sign convention for a pile from the south and north abutments. The numbered locations (1, 2, 3, 4) in Figure 4.1 are the outer tips of the flanges, where the maximum stress will occur.

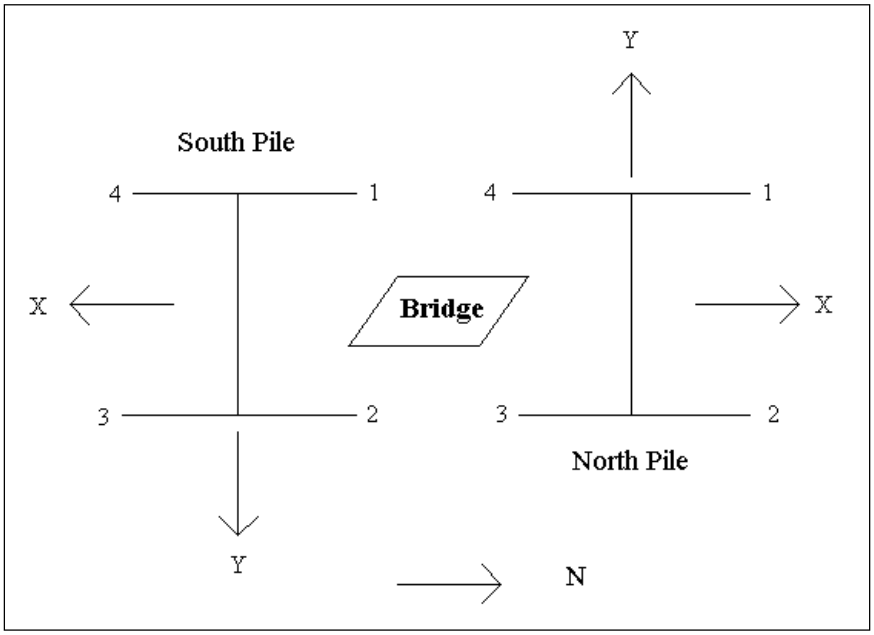


**Figure 4.1. Sign convention for stresses in the south and north piles**

The required properties for the analysis include the area of the pile ($A_p$), the modulus of elasticity of the pile ($E_p$), and the section modulii for weak axis bending ($S_y$), strong axis bending ($S_x$) and torsion ($S_z$). The area of the pile included the area of the protective steel pipe for the inclinometer and angle welded to the pile to protect the instrument cables; the areas of the channels welded over each strain gage were not included as they were not continuous along the length of the pile. The modulus of elasticity was determined by tensile testing of a coupon from each pile, as discussed in Section 3.5.2. Piles G1-S and G4-N, G2-S and G3-N, G3-S and G2-N were each cut from the same section of H-pile and therefore had the same modulus of elasticity. All piles came from the same heat number. The strong axis and weak axis section modulii of

the piles included the protective steel angle and steel pipe. However, since the steel pipe was not a continuous piece and only stitch welded to the pile, it was not included in the calculation of the torsional section modulus.

Out of a total of 72 strain gages installed on six piles, only four were considered faulty. Strain gages were considered faulty when either an error message was recorded, rather than a reading, or when the plots of the readings were erratic compared to the well-behaved gages. All gages were in working order when they were installed on the pile, prior to driving. Three of the faulty gages were in a top strain gage set and one was in a middle set. Strain gages #3 on G1-S, #4 on G2-N, and #1 on G4-N, all located in top sets, were each considered faulty. Strain gage #2 of the middle set on pile G3-S was also considered faulty. Since the top level of strain gages is considered critical in this study, much effort was invested to determine a means of estimating the strain for each faulty gage. A least squares regression was used to compare an incomplete set to all other complete sets at the same strain gage level. The three functioning gages of an incomplete set were compared to the same three gages of a complete set. The set of strain gages that produced the least error when compared to the incomplete set was used to determine strains for the faulty gage. See Appendix B for a sample calculation.

The process was first applied to trial data from five days after the bridge was completed. Each incomplete set was found to be the most similar to one particular complete set, during the trial. The trial, however, was only during dead loading. It was unclear whether or not these results would be repeated during live loading.

The process was then expanded to all of the data. It was again found that each incomplete set emulated a particular set most of the time. The instances when the error

was smaller for a different set appeared to be due to an erratic reading either from the incomplete set, or the emulated set, and not because another set was a better match. It was therefore assumed that the incomplete set always imitated one particular complete set. Each of the top sets of strain gages with a faulty gage emulated the top set of strain gages on pile G2-S. The middle strain gage set on pile G3-S was most similar to the middle strain gage set on pile G4-N. Figure 4.2 shows a typical incomplete set of strain gages with the corrected faulty gage (pile G1-S, gage #3). Typical magnitudes of error (see in Appendix B for calculation) for this process ranged from 0.183 to 9.724, with the average being 0.996. In the following analysis, when a strain gage set that has been corrected is referenced, it will be denoted with an asterisk, *.

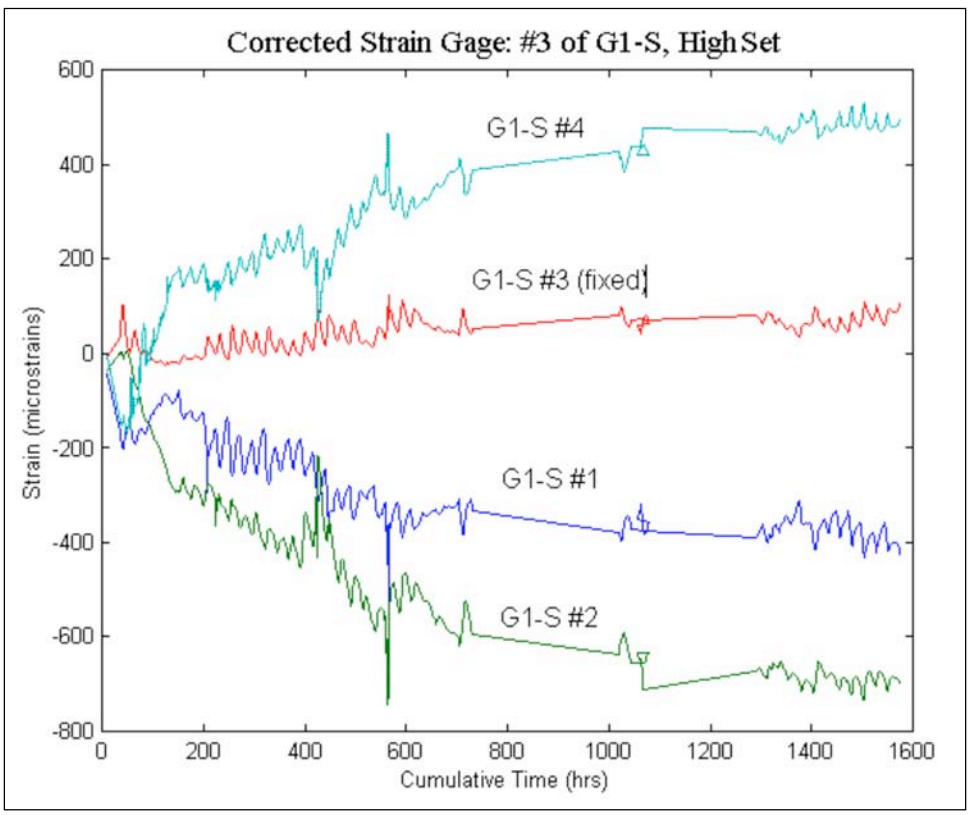


**Figure 4.2. Adequate correction for strain gage G1-S, #3***

One of the faulty gages, after being corrected, appeared to be inconsistent with the expected trend. Figure 4.3 shows the three functional strain gages of the high set on Pile G2-N, and the corrected readings for the faulty gage, #4. The corrected readings do not appear as smooth as the corrected gage in Figure 4.2.

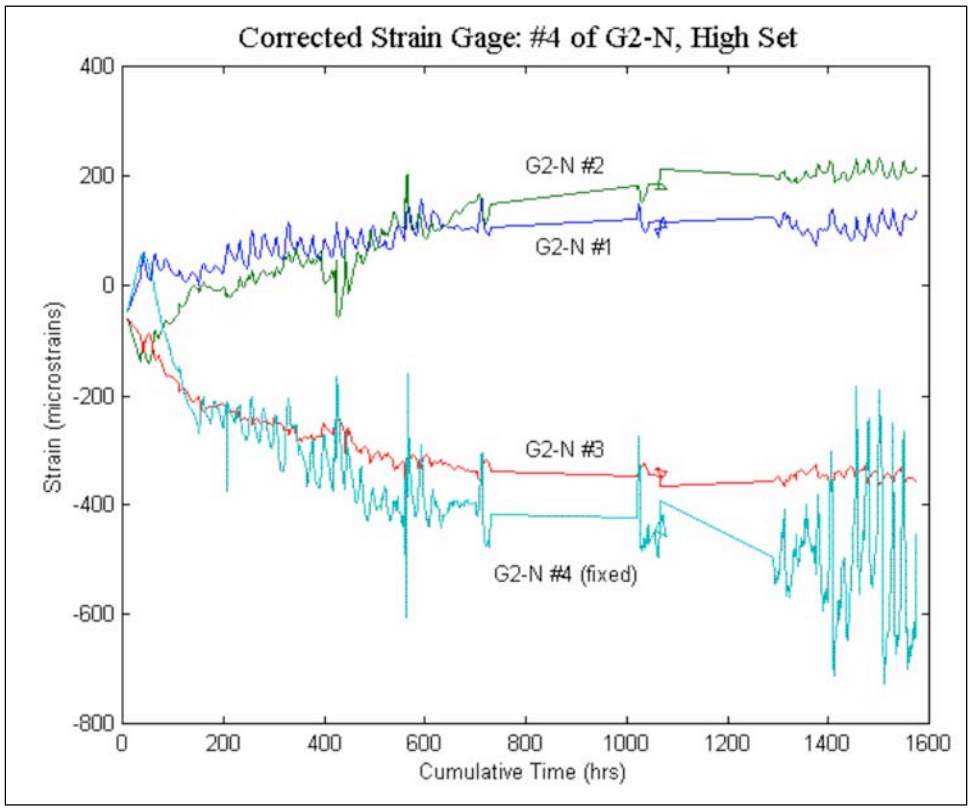


**Figure 4.3. Inadequate correction for strain gage, G2-N, #4**

This method was deemed inadequate to correct strain gage #4 on pile G2-N. However, an examination of the results from the other strain gages showed that the effects due to torsion were very small, typically less than 1% of the total stress due to dead load and live load. The three known strains were therefore used to solve for axial load, weak axis moment and strong axis moment, ignoring the effects of torsion. The results from this method and the least squares method were compared for the other three faulty gages. The results from the least squares method gave results which compared

better to complete sets at the same level. Therefore, for gage #3 of G1-S (high set), #2 of G3-S (middle set), and #1 of G4-N (high set), the least squares method was used to correct for the faulty gage. To correct for strain gages #4 on G2-N (high set), the effects of torsion were ignored.

As a separate means to verify the strain gage readings, and to detect faulty gages, the axial load for each pile was back-calculated and the sum of the loads was then compared to the weight of the bridge. It was critical, when comparing the weight of the structure to the load as determined by the strain gages, to know the exact stage of bridge construction. The weight due to the bridge deck forms, curbs or guardrails can significantly alter bridge weight. It was also important to know of any factors that might alter the strain readings, whether it is thermally induced strains that increase the load, or bearing surfaces that reduce the pile load. The calculated as-built weight of the bridge was 4034 kN (907 kips), neglecting the lower portion of the abutments which total 823 kN (185 kips). Each pile, if equally loaded, should support 504 kN (113.4 kips). Thus, the sum of the loads on the six instrumented piles should theoretically be 3024 kN, excluding the lower portion of the abutments.

On the morning of the live load testing, before any additional load was applied to the bridge, the sum of the loads on the six instrumented piles was 3309 kN (744 kips), 9.4% greater than the expected tributary load (based on an equally distributed load). It must be noted, however, that the measured pile loads were not equal, ranging from 389 kN to 780 kN (87.4 kips to 175.4 kips). The total calculated weight of the bridge is 4034 kN (907 kips). A reasonable assumption would be that the weight of the bridge would be equally distributed to each abutment; cumulatively, the south piles would see 2017 kN

(453.4 kips), as would the north piles. Subtracting the measured axial loads in the instrumented piles allows for an estimate to be made of the uninstrumented, acute piles. Based on this reasoning, on the morning of live load testing, piles G4-S and G1-N were estimated to be carrying 300 kN and 425 kN, respectively. G4-S compares well with the expected trend; the acute piles are expected to see less axial loads than the other piles. G1-N, however, does not compare well with this trend. The estimate of G1-N is the same as the near-acute pile, and larger than the obtuse pile. The calculation of the weight of the bridge can be seen in Appendix B. Table 5.8 in Section 5.2 gives a summary of the effects of the dead load on the morning of live loading.

### 4.3.2. Extensometers

Extensometers were installed on the test piles, and also in the face of the abutment to reveal the movement of the bridge. The layout of the extensometers allows for differentiation between translational, rotational and bending movement of the abutments. The extensometers were installed so that they could measurement up to 12.5 mm (0.5 in) of movement in either direction. The frequency of the vibrating wire is read by the portable readout unit or data acquisition system and output in LUs. The LUs were then converted to displacement using Equation 4.2 (Roctest: Model ERI, 2000):

$$D_{EX} = C1_{EX} * L_{1EX}^{2} + C2_{EX} * L_{1EX} + C3_{EX} \qquad \text{(Equation 4.2)}$$

Relative displacement is then calculated using Equation 4.3:

$$D_{rel} = D_{1EX} - D_{0EX} \qquad \text{(Equation 4.3)}$$

where $D_{EX}$ is displacement, in mm, $C1_{EX}$, $C2_{EX}$ and $C3_{EX}$ are extensometer calibration factors unique to each instrument, $L_{1EX}$ is the current extensometer reading in LU, $D_{rel}$ is

the relative displacement between the current displacement ($D_{1EX}$) and the as installed displacement ($D_{0EX}$).

The preset condition for each extensometer at installation was at the mid-point of the movement range. This allowed the extensometer to measure up to 12.5 mm (0.5 in) in either direction. The sign convention for the south and north extensometers and inclinometers was established as bridge contraction resulted in positive movement, while bridge expansion resulted in negative movement.

The initial condition for the extensometers installed on the piles was chosen to be the same as for the strain gages, Day 238, at noon and Day 240, at 7:00 am for the south and north abutments, respectively. The initial condition for the extensometers installed in the abutment face was the first reading taken after the instruments were installed and backfilled, Day 264 at noon and Day 265 at 8:00 am, for the north and south abutments, respectively.

The extensometer installed on pile G3-N was considered faulty and was not corrected. It was assumed that due to its rigidity, the abutment remained planar, and therefore the missing data could be linearly interpolated from other extensometer readings.

#### 4.3.3. Earth Pressure Cells

Earth pressure cells were installed at two levels in each abutment (Figures 3.1 and 3.2) to monitor the variation in soil pressures, both along the abutment face and with depth. The pressure cells were calibrated by the manufacturers using a fluid pressure surrounding the cell. Since the cells were to be installed at the interface of the concrete abutment and the backfill, concrete blocks were cast to protect the cells during pouring of

the abutment concrete and to provide a bed for the cells. The cells were re-calibrated in the laboratory simulating field conditions; one face was the concrete block and the other was a granular material. A polynomial regression supplied by the manufacturer was used to determine the new calibration factors for each earth pressure cell.

Based on the new calibration factors, Equation 4.4 was used to calculate the change in pressure (Roctest: Model EPC, 2000):

$$\Delta P_{PC} = C1_{PC}(L_{1PC} - L_{0PC}) + C2_{PC}(L_{1PC} - L_{0PC})^2 - CT_{PC}(T_{1PC} - T_{0PC}) - (B_1 - B_0)$$

(Equation 4.4)

where $C1_{PC}$ and $C2_{PC}$ are the pressure cell's calibration factors, $CT_{PC}$ is the pressure cell's thermal calibration factor, $L_{1PC}$ and $L_{0PC}$ are the current and initial pressure cell readings (LU), $T_{1PC}$ and $T_{0PC}$ are the current and initial temperatures determined by the pressure cell's internal thermistor, and $B_1$ and $B_0$ are the current and initial barometric pressures.

The initial condition for the set of earth pressure cells cast in the lower portion of the abutment was established as after removal of the abutment forms and after backfilling up to the construction joint. No readings were taken with the forms off and no backfilling. The pressure due to backfill up to the construction joint was estimated and added to the initial reading. The upper portion of the abutment was not backfilled as quickly as the lower portion due to the construction of the approach slab. This allowed for the initial condition to be with the abutment forms off, and no backfilling.

The sign convention for the earth pressure cells is positive changes in pressure correspond to the abutment moving into the backfill, or deck expansion. Negative

changes in earth pressure correspond to the abutment moving away from the backfill, or deck contraction.

### 4.3.4. Thermistors

Thermistors were used to monitor the ambient air, concrete deck, and steel girder temperatures. Additionally, all vibrating wire instruments had internal thermistors. When connected to the portable readout unit, the temperature can be read directly in ºC or ºF. When using a data acquisition system, the readout units are in voltage then converted to ohms using Equation 4.5 (Roctest: Model TH-T, 2000).

$$R_t / R_{25} = (A / Vout) - B \qquad \text{(Equation 4.5)}$$

where $R_t$ is the resistance in ohms, $R_{25}$ is the type of thermistor, and A and B are conversion factors dependent on the type of thermistor. The temperature reading is then obtained using the polynomial approximation in Equation 4.6 (Roctest: Model TH-T, 2000).

$$T(°C) = CO_t + C1_t(X) + C2_t(X)^2 + C3_t(X)^3 + C4_t(X)^4 \qquad \text{(Equation 4.6)}$$

where X is the natural log of the ratio of $R_t$ to $R_{25}$, and $CO_t$, $C1_t$, $C2_t$, $C3_t$, and $C4_t$ are constants.

### 4.3.5. Piezometers

Vibrating wire piezometers with a 0 to 200 kPa range were used to monitor the pore water pressure on either side of Nash Stream. Factory calibration using a polynomial regression was used for the vibrating wire piezometers. The pressure is therefore calculated using Equation 4.7 (Roctest: Model PWS, 2000).

$$\Delta P_Z = C1_Z(L_{1Z} - L_{0Z}) + C2_Z(L_{1Z} - L_{0Z})^2 - CT_Z(T_{1Z} - T_{0Z}) - (B_1 - B_0)$$

(Equation 4.7)

where $\_P_Z$ is the change in pore water pressure, $C1_Z$, $C2_Z$ are the piezometers' calibration factors unique to each instrument, and $CT_Z$ is the piezometer's temperature factor, $L_{0Z}$ and $L_{1Z}$ are the initial and the current piezometer readings, $T_{0Z}$ and $T_{1Z}$ are the initial and the current piezometer temperatures, and $B_0$ and $B_1$ are the initial and the current barometric pressures.

A standpipe piezometer, using a 38 mm (1.5 in) pvc pipe, was also installed. This piezometer is monitored manually.

### 4.3.6. Inclinometers

An inclinometer casing was installed in each of the protective steel pipes on the six test piles. Two additional inclinometer casings were installed on the east side of the bridge in the embankments, one behind each abutment. Inclination of the piles and slopes was detected with regular inclinometer readings. Inclination parallel to the direction of traffic was established as the A-direction, while inclination perpendicular to the direction of traffic was established as the B-direction. Movement in the A-direction is considered critical in this study.

The measured inclinations were converted to lateral movement using two software applications by Slope Indicator Co., DMMwinn and DigiPro. Inclination readings were taken manually and later input into DMMWinn, which kept inclinometer data orderly. The files created in DMMWinn were later imported into DigiPro, which converted the readings of angle of inclination to lateral deviations by Equation 4.8,

$$\Delta_{lat} = l_{\text{int}} \sin(\theta_{inc}) \qquad \text{(Equation 4.8)}$$

where $\Delta_{lat}$ is the lateral deviation, $l_{int}$ is the measurement interval, and $\theta_{inc}$ is the angle of inclination, see Figure 4.4 for a sketch of the inclinometer system. DigiPro then compared the change in lateral deviation of the current survey to the initial survey.

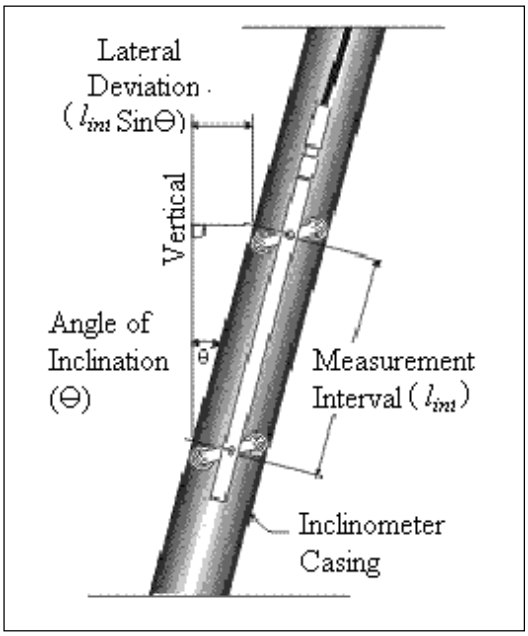


**Figure 4.4. Sketch of inclinometer probe**

The sign convention for the south and north extensometers and inclinometers was established so that bridge contraction resulted in positive movement, while bridge expansion resulted in negative movement. For inclinometer plotting purposes, the northern inclinometers show bridge expansion as positive. This allowed for better comparisons of movement between the two abutments. Graphs of cumulative displacement along the pile show the deformed shape of the pile relative to the initial reading.

DigiPro allowed the user to easily create numerous graphs. DigiPro also has a means to account for azimuth corrections; this was needed for piles G2-N and G4-N because the casings were twisted out of position during grouting. The azimuth

corrections are only applicable for data sets in which the initial survey consists of readings in both the A and B directions.

Initial readings were taken the night prior (and morning of) the casting of the second portion of the abutments and the deck. Subsequent readings include the day after and two days after the deck pour, then weekly thereafter. Readings were taken in the A0 and A180 directions for all sets of readings. Due to equipment malfunction, the B0 and B180 were read for the first time on Day 265 (September 21) and read consistently thereafter.

The lip of the inclinometer casing was used as a reference level from which to measure the depth in the casing. Initially, the protective pipe extended to some elevation above the deck. The protective pipes were cut to their final elevations on Day 274 (September 30). After Day 274, all readings used the lip of the casing cut to the deck elevations as a reference level. The surveys were therefore split into two sets according to their initial reference points. The readings prior to Day 274 consist of one set of data, while readings after this are considered a separate set. The depths of the first surveys were adjusted to reference the same initial elevation as the surveys taken from final grade. Since DigiPro cannot account for the non-consistent depths, the movements were determined for each set separately. The movements of the first set of surveys were taken relative to the initial inclinometer reading, on Day 257/258 (September 13/14). The movements of the second set of surveys were taken relative to the survey taken on Day 274, when the inclinometer pipes were cut to final grade.

To get a better sense of the entire construction process, it was important to consolidate the data into one set, with one reference. This was done by determining the movement of the piles between the last survey of the first set and the first survey of the second set, Days 265 and 274. Movement along the length of the pile was interpolated from the movement determined from the extensometers and from assuming no movement at the tip of the pile. This allowed the second set of surveys to reference the initial reading.

With all surveys referencing the initial survey, there was no way to correct for the azimuth discrepancy for piles G2-N and G4-N since there was no initial survey in the B-direction. Figures 4.5 and 4.6 show the differences between corrected and uncorrected surveys for Days 280 and 288, referencing Day 274.

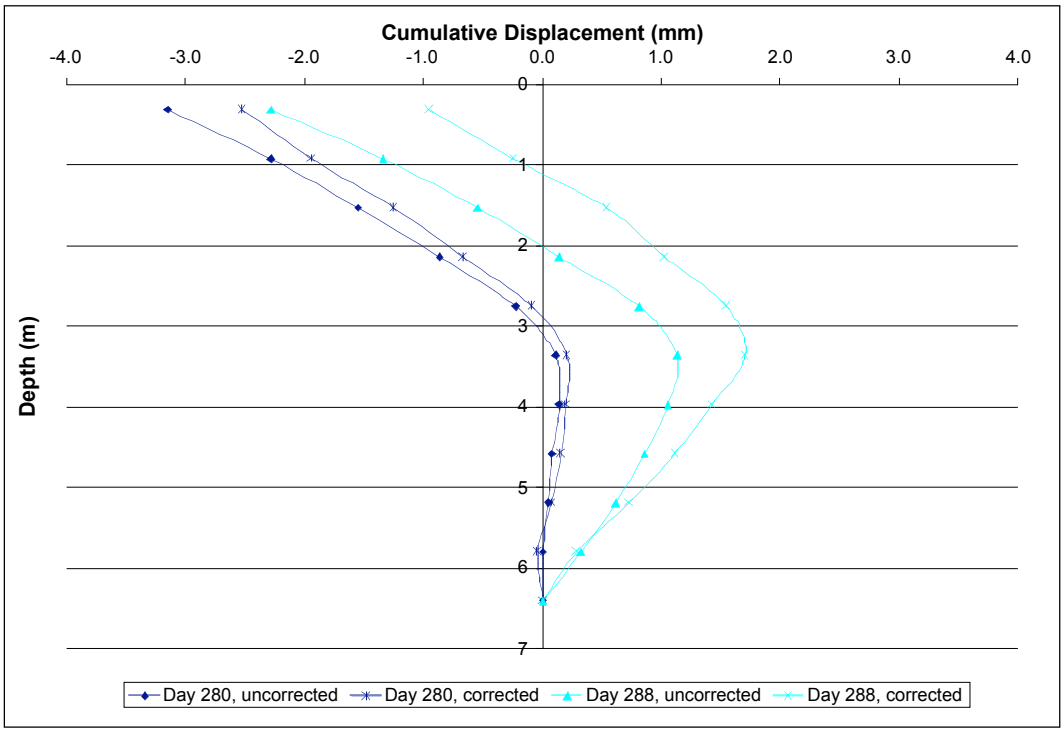


**Figure 4.5. The effect of azimuth correction for pile G2-N**

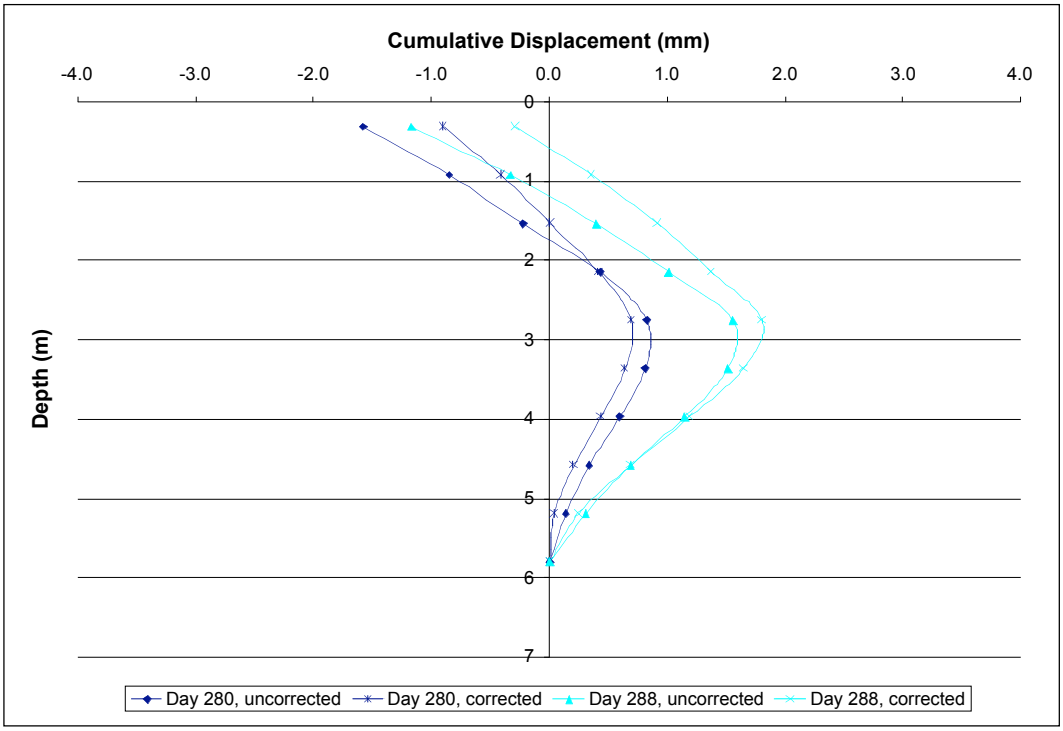


**Figure 4.6. The effect of azimuth correction for pile G4-N**

The azimuth correction shifts the deformed shape of the pile to the right (north) for both G2-N and G4-N since part of the longitudinal movement is read in the B-direction. In the following sections, when inclinometer results are presented, the movements for G2-N and G4-N have not been corrected, and thus actual movements correspond to more deck expansion.

The movement recorded by inclinometers at the location of the pile extensometers was compared to the movement recorded by the pile extensometers as a means of determining consistency between instruments. The movements were compared on two days after the bridge was fully constructed, Days 280 and 288 (October 6 and 14). There was an increase in concrete temperature between these two days of 3ºC (37.4ºF). Table 4.2 summarizes the movements at the pile extensometer locations.

**Table 4.2. Summary of movements (mm) between days 280 and 288**

| | Movement (mm) | | | | | | | |
|---|---|---|---|---|---|---|---|---|
| Location | G1-S | G2-S | G3-S | G4-S | G1-N | G2-N | G3-N | G4-N |
| Pile: elev. 377.7 | | | | | | | | |
| Inclinometer | -1.692 | -1.237 | -1.080 | | | -1.585 | -1.336 | -1.067 |
| Extensometer | -0.635 | -0.622 | -0.572 | -0.457 | -0.584 | -0.610 | -0.667 | -0.724 |
| Abut.: elev. 379.4 | | | | | | | | |
| Inclinometer | -3.909 | -1.405 | -1.173 | | | -0.980 | -1.417 | -0.577 |
| Extensometer | -0.279 | | | -0.127 | -0.216 | | | -0.292 |

The movements summarized in Table 4.2 are all deck expansion. The range of the coefficient of thermal expansion of concrete is about $9x10^{-6}$ /ºC to $13x10^{-6}$ /ºC for concrete constructed with siliceous aggregate (MacGregor and Wight, 2005). The expected expansion of the 30 m long bridge due to the 3ºC increase in temperature is thus 0.81 mm to 1.17 mm total, or 0.40 mm to 0.59 mm (0.0157 in to 0.0232 in) per abutment. This expansion is only an estimate; the bridge is a steel-concrete composite and there is a thermal gradient through the depth of the deck. However, the pile extensometer reflects this expansion very closely while the inclinometers show two to three times more movement at the same location as the extensometer. The abutment extensometers show less expansion than the pile extensometers; the inclinometers at this location show much larger movements. The movement at the abutment extensometer location near pile G1-S, as read by the inclinometer, is likely to be faulty.

### 4.4. Effects of Construction Process

Results and general trends which occurred during each step of the construction process are discussed in the following sections. As discussed in Section 4.2, the effects of pile driving on the pile stresses were not considered. The analysis of the strain gages was started after the casting of the first portion of the abutments since the readings were

too sporadic before that time. The major construction events discussed include placement of the girders and bracing, casting of the deck and second portion of the abutment, casting and backfilling of the approach slabs, casting of the curbs, and paving. Changes in pile stresses, pile and abutment movements and earth pressures resulting from each event will be discussed. Pile stresses were calculated at the tips of each flange on the pile, and the critical stress for a pile under a specific loading event is considered the largest negative stress of the four calculated stresses. This critical stress includes the sum of the stresses from axial loading, weak-axis bending, strong-axis bending and torsion. Unless otherwise noted, the pile stresses being discussed are the stresses at the top strain set location, approximately 1 m (3.3 ft) below the bottom of the abutment.

The effects of a particular construction event are determined by comparing the results from before the event and after the event. Whenever possible, the before and after readings were taken at 5:00 AM on both days to minimize the effects of diurnal temperature variation and to ensure no activity on the bridge. Since the data acquisition systems were not fully functional until Day 259 (September 15), the day after the bridge deck was cast, the before and after readings of the placement of girders and bracings as well as the casting of the deck and second portion of the abutments are not complete or were taken at times other than 5:00 AM. Table 4.3 summarizes the construction event timeline.

**Table 4.3. Timeline for construction sequence and cumulative critical stresses in piles**

| | | | | Critical Stress (MPa) | | | | | |
|---|---|---|---|---|---|---|---|---|---|
| **Day** | **Time** | **Ambient Temperature (ºC)** | **Event** | **G1-S** | **G2-S** | **G3-S** | **G2-N** | **G3-N** | **G4-N** |
| 238 | 12:00 | N/A | Initial condition, south piles | | | | | | |
| 240 | 7:00 | N/A | Initial condition, north piles | | | | | | |
| 245 | 5:41 | N/A | Girders and bracing in place (north only) | | | | -6.1 | -4.9 | -5.1 |
| 258 | 10:25 | 22.7 | Deck pour (north only) | | | | -12.0 | -24.9 | -23.3 |
| 259 | 13:00 | 29 | Day after deck pour | -6.1 | -6.2 | -5.0 | -27.5 | -39.0 | -33.6 |
| 260 | 5:00 | 7.5 | Before abutment forms removed | -45.2 | -27.2 | -26.3 | -31.5 | -40.8 | -33.6 |
| 261 | 5:00 | 17 | After abutment forms removed | -36.6 | -27.8 | -25.2 | -32.1 | -30.4 | -25.1 |
| 266 | 5:00 | 8 | Before approach slab cast | -39.8 | -34.7 | -21.7 | -50.5 | -44.7 | -16.4 |
| 267 | 5:00 | 10.3 | After Approach slab cast/ | -103.7 | -89.6 | -47.7 | -63.6 | -63.8 | -33.6 |
| | | | Before curb pour | | | | | | |
| 268 | 5:00 | 3.6 | After curb pour | -78.4 | -67.4 | -42.2 | -57.3 | -54.5 | -24.7 |
| 271 | 5:00 | 1.2 | Before south approach slab backfilled | -87.5 | -77.3 | -45.7 | | | |
| 272 | 5:00 | 4 | After south approach slab backfilled/ | -91.4 | -77.1 | -49.6 | -61.5 | -59.0 | -42.7 |
| | | | Before north approach slab backfilled | | | | | | |
| 273 | 5:00 | 2 | After north approach slab backfilled | | | | -66.6 | -69.2 | -40.4 |
| 275 | 5:00 | 3.6 | Before paving | -102.8 | -86.6 | -49.5 | -64.2 | -60.1 | -36.2 |
| 276 | 5:00 | -0.1 | After 1st layer of pavement | -91.4 | -77.1 | -49.6 | -61.5 | -59.0 | -42.7 |
| 277 | 5:00 | 0.6 | After 2nd layer of pavement | -117.4 | -98.5 | -54.5 | -69.8 | -67.2 | -49.0 |

See Tables C.1 through C.8 in Appendix C for comprehensive results of the effects of the construction process, including a summary of the critical stresses, and the percentage of the critical stresses due to each of the internal forces.

Figures 4.7 and 4.8 show the axial load for each of the instrumented piles of the south and north abutments, respectively, during the construction process.

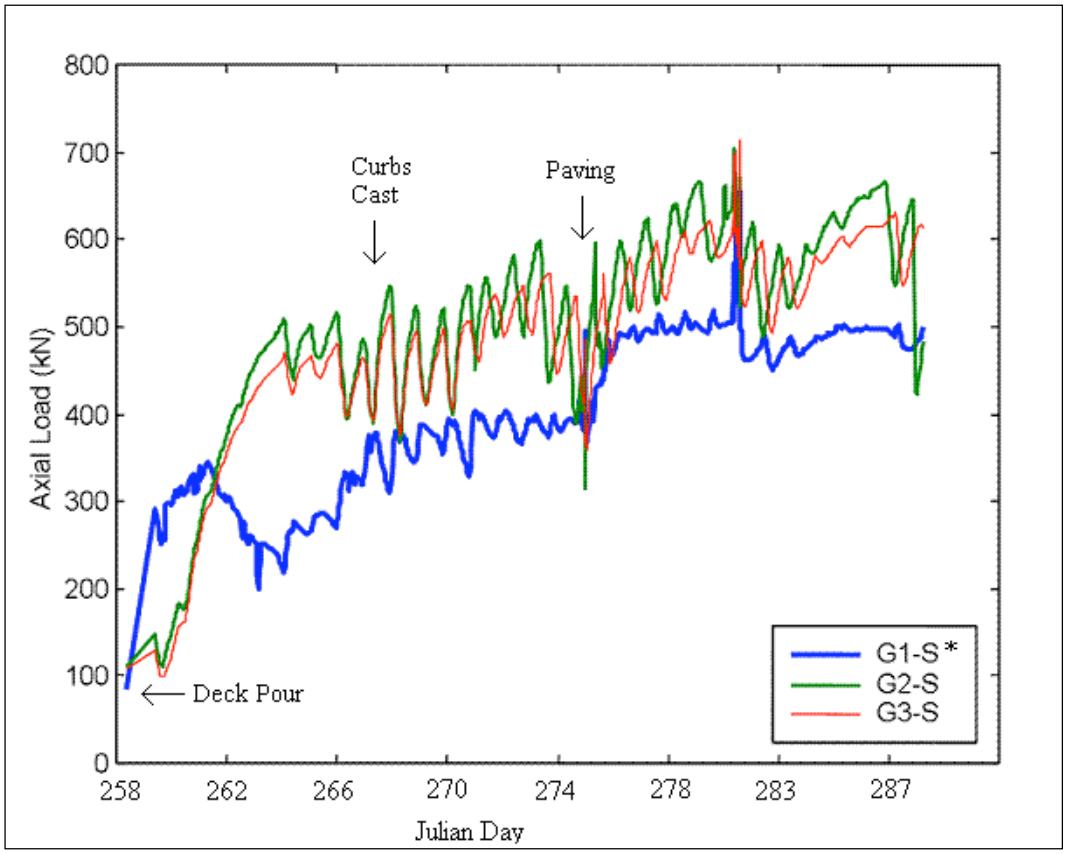


**Figure 4.7. Axial load (kN) for south piles during construction**

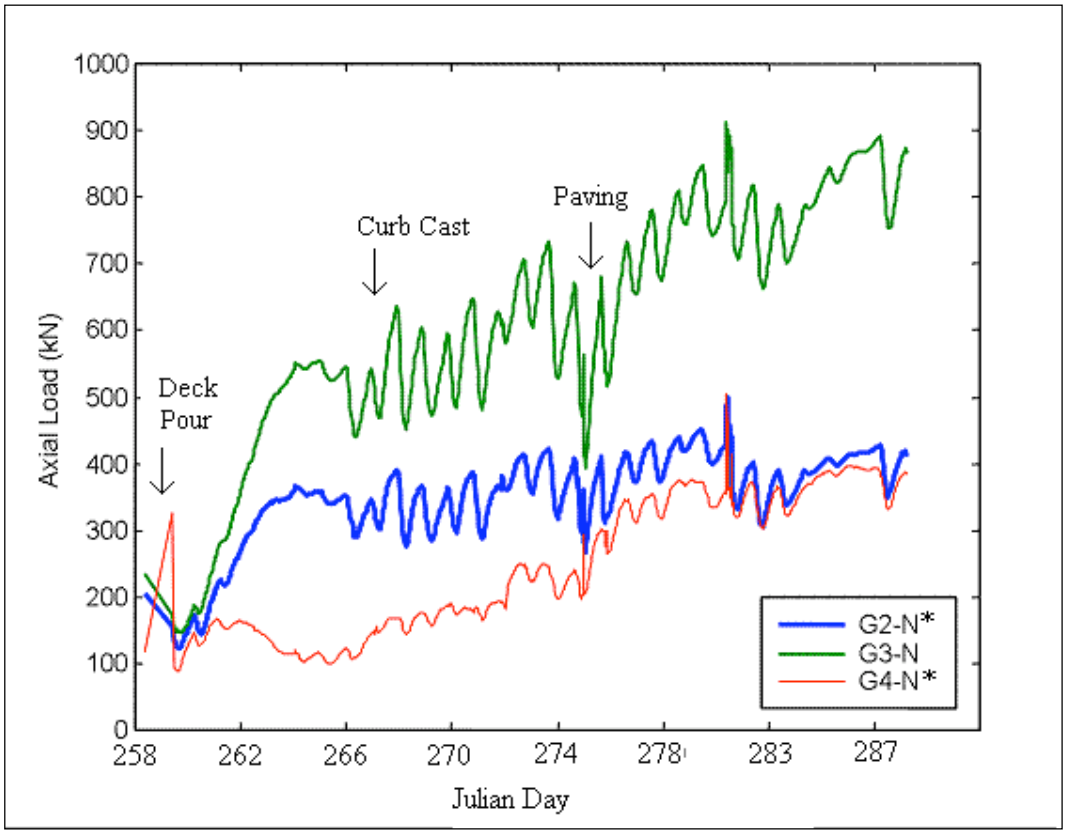


**Figure 4.8. Axial load (kN) for north piles during construction**

Figure 4.9 shows the total axial load of the instrumented piles during the construction process. The dashed lines in this figure represent the six-eighths of the total calculated load at the specified stage during construction; the dashed line assumes the weight of the bridge is distributed evenly to the piles. Figure 4.9 therefore compares the sum of the measured axial load in the instrumented piles with the portion of the load that would be seen in the piles if the load were distributed evenly. As seen in Figures 4.7 and 4.8, the load was not evenly distributed to the piles. The calculated as-built weight of the bridge neglects the weight of the abutment portion below the construction joint (refer to Section 4.2 for explanation).

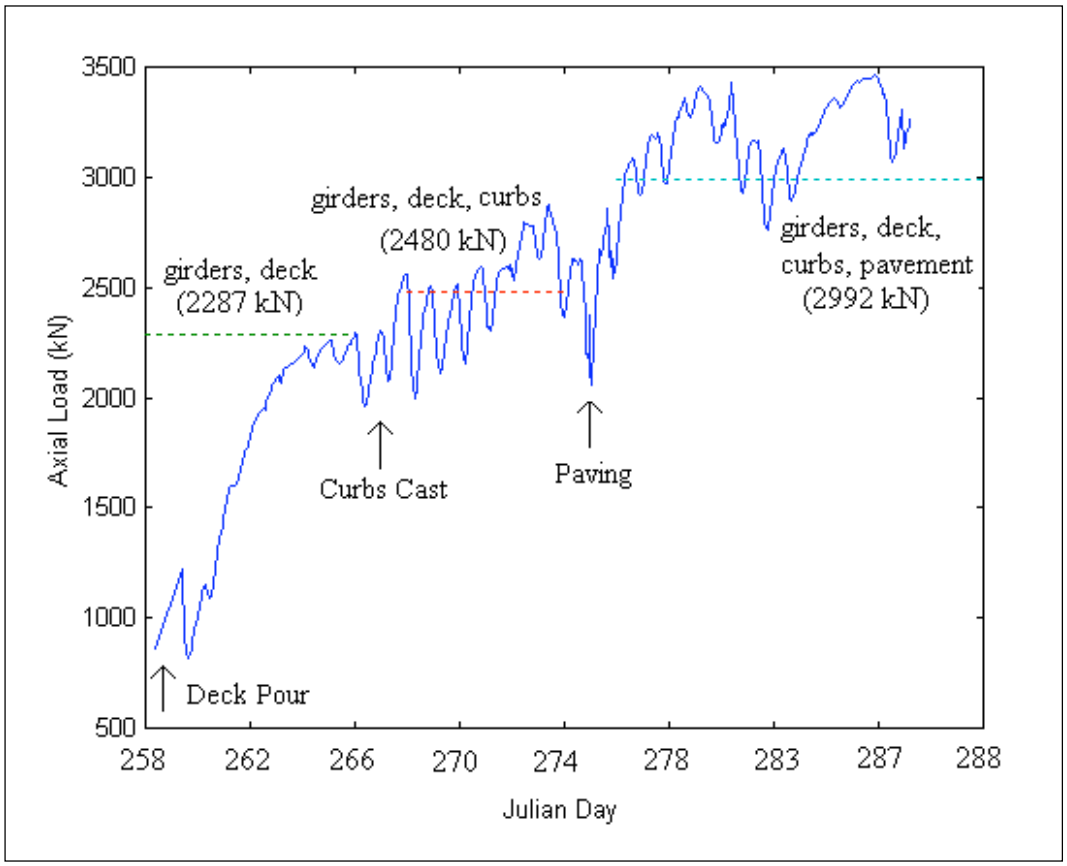


**Figure 4.9. Cumulative axial loads (kN) for instrumented piles during construction**

Figure 4.9 clearly shows that the sum of the loads in the instrumented piles increases during the construction sequence. It is also obvious that the applied loads due to a particular construction event are not immediately transferred to the piles, especially due to the deck pour.

### 4.4.1. Placement of Girders and Bracing

Girders arrived on site on Days 239 and 240 (August 26 and 27) and were hoisted into place on Day 240, one at a time. The girders were supported at each end by a crane, and then placed in position. The girders were welded into place and the diaphragms and cross bracing were installed Day 243 (August 30). The data acquisition system for Abutment 1 (south) was not fully functional at this time, and therefore no data regarding

the effects of girder placement was recorded for the south abutment. The data acquisition system for Abutment 2 (north) was functioning during this event.

The northern piles each experienced a maximum stress increase of approximately -4.8 MPa (-0.7 ksi). Piles G2-N* and G4-N* both have critical stresses at location #4, while pile G3-N's critical stress is at location #3 in Figure 4.1. Critical stress was determined to be the largest negative stress in the pile due to the combined effects of axial load, weak-axis moment, strong-axis moment and torsion. The three north instrumented piles cumulatively experienced a net compressive change in axial load of 100.1 kN (22.5 kips); this is 66% of the expected load. Three-eighths of the weight of the girders and support bracing is 152.5 kN (34.3 kips). The piles all experienced a negative change in weak axis bending with reference to the initial condition, which indicates the pile heads were rotating in towards the bridge due to the applied load of the girders. The weak axis moments vary from pile to pile.

The north pile extensometers registered movement of 1.7 mm (0.067 in) corresponding to deck contraction for pile G1-N, and -0.26 mm (-0.010 in) and -0.59 mm (-0.023 in) for G2-N and G4-N, respectively, corresponding to deck expansion. This trend suggests the abutment is trying to straighten out, or reduce the skew angle. There is no data for the south pile extensometers. There is also no earth pressure cell data for this event.

#### 4.4.2. Casting of the Deck and Second Portion of the Abutments

The deck and second portion of the abutments were cast on Day 258 (September 14). The north abutment was cast first, followed by the deck and finally the south

abutment. The placement began at 7:00 AM and was finished at 12:30 PM. Since the data acquisition systems were not yet fully functional, the readings before and after the deck pour were taken as the initial reading and the readings at 1:00 PM on the day after the deck pour (Day 259). Thus this data includes the girder placement as well as the deck placement. Data from Days 260 and 261 (September 16 and 17), which are the days before and after the abutment forms were removed, were also compared.

Both the north and south piles had comparable maximum stresses on the three days of comparison (Days 259, 260, and 261). All three north piles experienced the largest stresses at location #2 in Figure 4.1. Piles G2-S and G3-S experienced the largest stresses at location #4, which corresponds to location #2 for the north piles (see Figure 4.1). These critical stress locations are on the backfill side of the abutment, and on the side of the pile nearest the obtuse corner of the abutment. These were the critical locations for the piles on Days 259, and 260. Pile G1-S* had comparable stresses, but the critical stress was at location #1, which is on the bridge side and on the side of the pile nearest the obtuse corner of the abutment. The critical stress location changed for two of the piles after the abutment forms were removed. For these two piles, the critical location changed from the backfill side of the abutment to the bridge side of the abutment.

Critical stresses due to the deck pour ranged from -21.0 MPa (-3.05 ksi) to -39.1 MPa (-5.67 ksi), resulting in total stresses ranging from –26.3 MPa (-3.81 ksi) to -45.3 MPa (-6.56 ksi). For the three days after the deck pour, the percentage of the critical stress due to the four internal forces changed significantly. The percentage of the critical stress due to axial load increased by 20%, on average, for the six instrumented piles. The

axial loads steadily increased on the three days being examined. On Day 261 the total measured axial load on the six test piles, due to the girders and deck, was 1543 kN (346.8 kips). The calculated weight of the bridge at this point in the construction was 3049 kN (685.6 kips); if the load was equally distributed to the piles, the six test piles would see 2287 kN (514.2 kips). After Day 261, the axial load increased, suggesting that part of the load was initially carried by the ground below the abutments and perhaps some shear on the abutment backwall. Figures 4.7 – 4.9 clearly show this increase in axial force, which reached a nearly constant value prior to casting of the approach slabs; this agreed well with the 2287 kN, which is the load on six piles assuming an equal distribution.

For the days immediately following the deck pour, the strong axis moments were considerably larger than the weak axis moments. In nearly all piles, the moments were large and positive but decreased in the days after the deck pour. For these three days, the percentage of the critical stress due to strong-axis bending decreased by 18%, on average. The percentage due to weak-axis bending increased in piles G1-S, G2-S and G2-N, by an average of 17%, each; piles G3-S, G3-N and G4-N each saw decreases of approximately 19%. During these first three days, the strong-axis moments were larger than the weak-axis moments; on Day 266, this trend flipped. The weak axis moments became increasingly positive on the two days following the deck pour, with reference to the initial condition. When the abutment forms were removed, the weak axis moments decreased compared to readings in which the forms were still intact. The weak axis moments were considerably smaller than the strong axis moments during this period. This could be due to the fluctuations of temperature at the time of readings, which

worked against the changes. For example, the weak axis moment increased slightly, but the temperature at the time of the readings decreased significantly between Days 259 and 260. A temperature reduction would cause a decrease in weak axis moment, as the bridge contracts. The change in weak axis moment would have likely been larger if the temperature had been constant on the respective days.

The average percentages of the total stresses for the instrumented piles eight days after the deck pour, due to each of the internal forces are as follows: axial load 41%, strong-axis moment 9%, weak-axis moment 46%, and torsion 3%. See Figure C.8 in Appendix C for a complete summary of the critical stress breakdown due to the construction processes.

Inclinometer surveys were completed the day before the deck was cast and the two days following the placement. Figure 4.10 shows the cumulative displacement for each of the piles, as a result of the deck pour. Inclinometer surveys taken on Day 260 (September 16) illustrate very little movement relative to the surveys from Day 259. The general trend between Days 259 and 260 is slight contraction of the bridge deck.

The north and south abutment piles reflect each other's movement. All piles show contraction of the bridge deck at the top of the inclinometer pipe, and expansion below the construction joint. All piles show expansion from approximately 1.2 m (4 ft) below final grade to 5.2 m (17 ft) below final grade. Above 1.2 m (4 ft) each pile experiences a sudden change in movement. This corresponds to the length of inclinometer pipe that sticks up above the top of the girder and was not welded to anything. During the deck pour the tops of the pipes got pushed inwards. The top data

point within the initial reading on pile G1-S, is considered faulty, and does not accurately reflect the shape of the pipe.

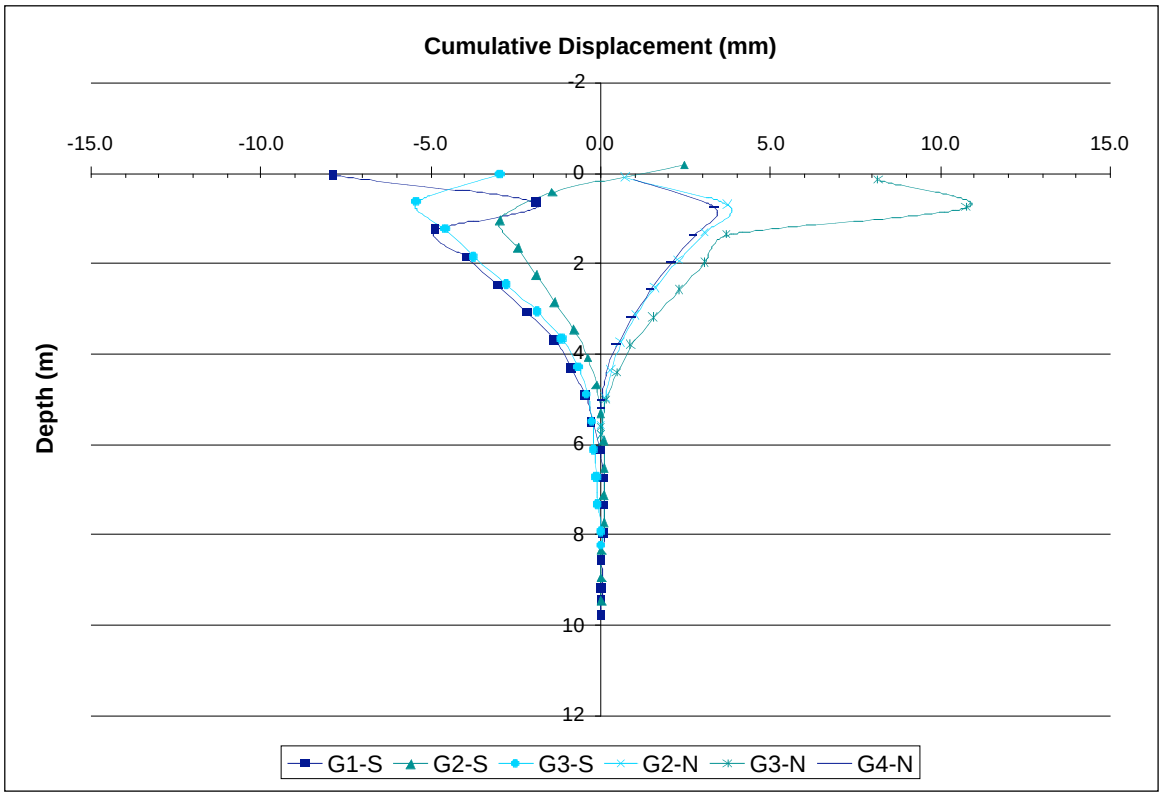


**Figure 4.10. Cumulative displacement of piles due to deck pour, Day 259 (A-direction)**

The extensometer data for this construction event is inconclusive because the data acquisition system was not fully functional until after the deck was cast; the "before" readings are incomplete.

The lower earth pressure cells saw an increase in earth pressure due to the casting of the deck and second portion of the abutments. The south obtuse and acute corners saw an increase of 3.35 kPa and 3.82 kPa (70 psf and 79.8 psf), respectively. The north obtuse and acute corners saw an increase of 1.92 kPa and 2.81 kPa (40 psf and 58.7 psf),

respectively. The acute corners saw the larger increases in pressures; the south abutment saw larger increases than the north abutment. The inclinometers (Figure 4.10) showed more movement into the soil on the south abutment than on the north abutment and were thus consistent with a larger increase in soil pressure on the south abutment.

### 4.4.3. Approach Slabs

Both approach slabs were cast on Day 266 (September 22). They were 10.7 m (35 ft) wide, by 5 m (16 ft) long, and 205 mm (8 in) thick. They each rested on a seat on the backfill side of each abutment which is 0.8 m (2.6 ft) below the top of pavement. The effects of the approach slabs are generally ignored by designers. Initially, the approach slab sat on the soil beneath it. As the soil settled, more of the weight was applied to the approach slab seat on the abutment. This was also the case when 0.8 m (2.5 ft) of backfill was placed on top of the approach slab.

The critical pile stresses occur at the outermost edges of the flanges closest to the bridge both before and after the approach slabs are cast, and before and after the approach slabs are backfilled. The south piles experience slightly higher increases in critical stress than their northern counterparts. The load transferred to the piles due the weight of the approach slabs and backfill was estimated to be a portion of the total weight. The largest loading the approach slab was estimated to apply to the piles would be from one-half of the length of the approach slab, i.e. all soil beneath it settled and it was simply supported by the abutment on one end and by soil at the other end. This would induce a load of 336 kN (75.5 kips) to each abutment for the concrete, backfill and pavement. The portion

carried by the three test piles on each end would be 252 kN (56.6 kips), assuming an equally distributed load.

However, there was very little change in pile stresses on the day after the approach slabs were cast or backfilled. The critical stresses do not increase significantly, nor do the percentages due to the internal forces change significantly due to the casting and backfilling of the approach slabs. The casting of the approach slabs had no change on the axial load of the piles. The weak axis moments revealed a negative change for this event. The strong axis moments revealed a positive change.

The south piles and north piles registered an increase in axial load of 69.4 kN (15.6 kips) and 181.5 kN (40.8 kips), respectively, when the approach slabs were backfilled. These loads correspond to 1 m (3.2 ft) and 2.5 m (8.5 ft) of the total approach slab length applying a load to the abutment seat. The weak axis moments, again, revealed a negative change for the backfilling for all piles. The south piles showed a positive change in the strong axis moment during this event while the north piles show a negative change in the strong axis moment. The change was larger in magnitude for the south piles than the north piles.

The inclinometer surveys before and after the approach slabs were cast and backfilled reference different elevations and thus cannot be compared. Overview of movements during the entire construction sequence can be seen in Section 4.5. A summary of the movements for this event, as determined by the extensometers, is located in Table 4.4. Neither the casting nor backfilling of the approach slabs caused much

movement in the pile or abutment extensometers. All of the movements correspond with deck expansion.

**Table 4.4. Summary of piles and abutment movement (mm) due to the casting and backfilling of approach slabs as determined by extensometers**

| | Movement (mm) | | | | | |
|---|---|---|---|---|---|---|
| | **G1-N** | **G2-N** | **G3-N** | **G4-N** | **G1-N Abut.** | **G4-N, Abut.** |
| **Cast** | -0.257 | -0.234 | N/A | -0.203 | -0.679 | -0.338 |
| **Backfilled** | -0.003 | -0.077 | N/A | -0.137 | -0.212 | -0.228 |
| | | | | | | |
| | **G1-S** | **G2-S** | **G3-S** | **G4-S** | **G1-S, Abut.** | **G4-S, Abut.** |
| **Cast** | -0.188 | -0.187 | -0.261 | -0.207 | N/A | N/A |
| **Backfilled** | -0.216 | -0.239 | -0.153 | -0.114 | -0.197 | -0.343 |

Table 4.5 summarizes the change in earth pressures due to the casting and backfilling of the approach slabs. The upper cells for the south and north abutments are 0.6 m and 0.4 m (2 ft and 1.6 ft) below the bottom of the approach slabs, respectively.

**Table 4.5. Summary of change in earth pressures due to casting and backfilling the approach slabs**

| | Change in Earth Pressure, kPa | | | |
|---|---|---|---|---|
| | **SE** | **SW** | **NE** | **NW** |
| | **(obtuse)** | **(acute)** | **(acute)** | **(obtuse)** |
| **Lower** | | | | |
| **Casting** | 3.959 | 4.277 | 2.014 | 1.798 |
| **Backfilling** | 2.454 | 4.094 | 0.861 | 0.264 |
| **Upper** | | | | |
| **Casting** | N/A | N/A | 1.803 | 0.607 |
| **Backfilling** | -0.426 | 0.339 | 2.753 | 0.852 |

The acute earth pressure cells saw larger increases in pressure than their obtuse counterparts. The upper pressure cells on the north side saw larger increases in pressure than the south cells due to backfilling; this corresponds to the larger applied load in the north approach slab seat as measured in the piles. The lower cells saw a larger increase

in pressure due to casting than backfilling, on both abutments. The increase in pressure of the cells corresponds to the movement of the abutment into the soil.

#### 4.4.4. Curbs

Prior to the casting of the curb, the effect of the deck and second portion of the abutments had been almost completely transferred to the piles. The total calculated weight of the bridge at this point in construction was 3145 kN (707 kips). The instrumented piles registered 2267 kN (509.6 kips), or 96% of the weight of the bridge tributary to six of eight piles (six-eighths of the total load).

The bridge curbs were cast on Day 267 (September 23). The total calculated weight of the curbs was 161.5 kN (36.3 kips), with 121 kN (27.2 kips) representing six-eighths of the total load. The change in axial load as recorded by the test piles (262 kN (58.9 kips)) was much larger than the calculated added weight.

The critical stresses in the piles changed, on average, -6.9 MPa (-1.0 ksi) as a result of the casting of the curbs; the total stresses in the instrumented piles ranged from -24.5 MPa (-3.56 ksi) to -86.2 M9a (-12.5 ksi). See Table C.8 for a breakdown of the critical stresses before and after the casting of the curbs. Both the north and south piles experienced a negative change in weak axis bending as a result of the addition of the curbs. This indicated rotation towards the bridge which is consistent with expectations. The strong axis bending for both abutments also had a negative change. This indicated rotation towards the acute corners.

Similar to the results for the approach slabs the inclinometer surveys before and after the curbs were cast had different reference elevations and thus cannot be compared. Overview of movements during the entire construction sequence can be seen in Section 4.5. The pile extensometers show very little movement due to the casting of the curbs. The largest movement, seen in piles G4-S and G1-N, was 0.13 mm (0.005 in), corresponding to deck contraction. The movements recorded by the abutment extensometers near these piles, also corresponding to deck contraction, were 0.25 mm and 0.33 mm (0.010 in and 0.013 in), respectively. The abutment extensometers near pile locations G1-S and G4-N showed slight expansion, less than -0.025 mm (-0.001in) away from the bridge.

All earth pressure cells saw a decrease in pressure due to the casting of the curbs. The decrease in pressures ranged from 0.55 kPa to 4.13 kPa (11.5 psf to 86.3 psf). The lower cells had larger decreases in the obtuse corners than the acute corners.

#### 4.4.5. Paving

The bridge and approaches were paved on Day 275 and 276 (October 1 and 2), in two equal lifts. Despite the similarity of construction events over the two days, the pile stresses reveal different effects for the two days.

The comparison between the before and after readings for the first lift of pavement show slightly smaller critical pile stresses for all but one pile. The interior piles of each abutment show a decrease in axial load after paving, while the exterior piles show an increase in axial load. The net change in axial load for both abutments is slightly positive for the first layer of pavement. Weak axis moments undergo a positive

change during the placement of the first layer of asphalt, indicating rotation away from the bridge. Strong axis bending is also positive indicating rotation towards the obtuse corner. See Table C.8 for the breakdown of critical stresses due to paving.

The second layer of pavement resulted in a larger, more negative critical pile stress increase for all piles, and a corresponding increase in axial loads. The weak axis and strong axis moments both experience a negative change for the placement of the second layer of asphalt.

Inclinometer surveys taken on Day 280 (October 6) with reference to Day 274 (September 30) illustrate the effects due to paving the bridge as well as a -9ºC (-48.2ºF) change in concrete temperature (see Figure 4.11). The piles tops are moving towards the bridge near the deck surface, due to the added weight of pavement, as well as the contraction of the bridge due to a decreased deck temperature. The piles move outwards at approximately 3 m (10 ft) below final grade, indicating rotation of the abutments.

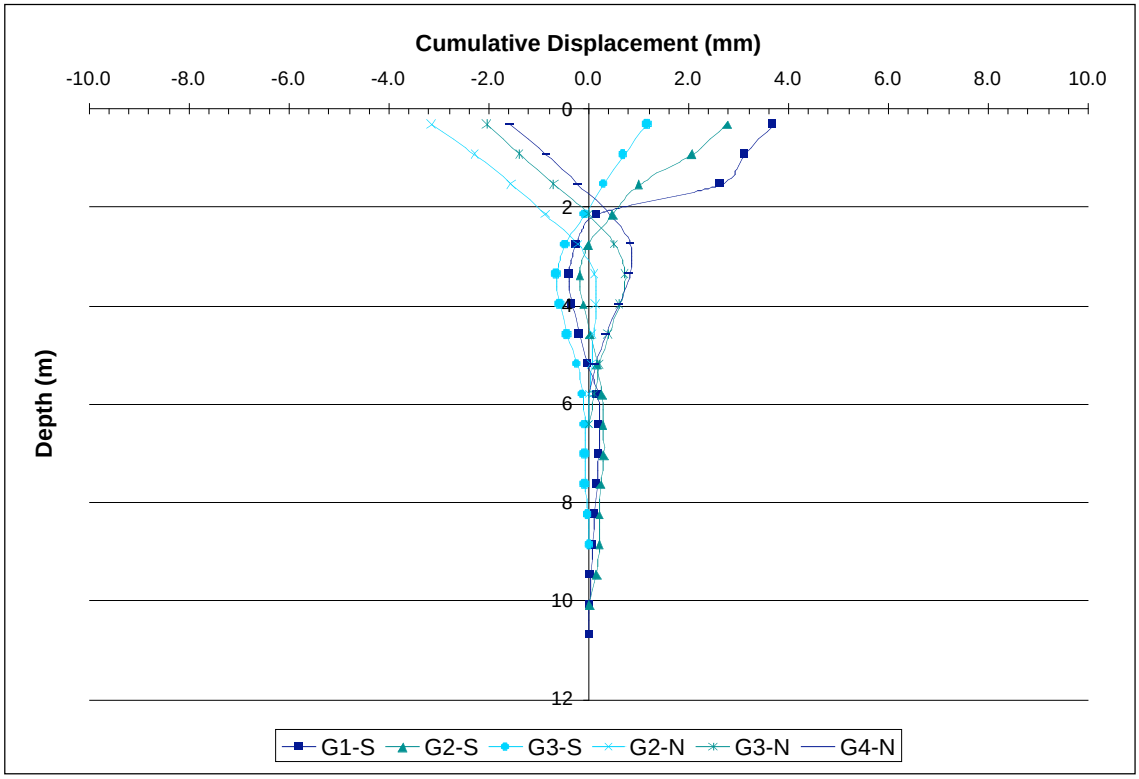


**Figure 4.11. Pile movement (mm) due to paving**

Table 4.6 gives a comparison of the movements of the piles and abutments due to paving as determined by the inclinometers and the extensometers (positive movement corresponds to deck contraction). The extensometers movements as a result of paving are, for the most part, larger than the results from the inclinometer, at comparable locations and times.

**Table 4.6. Summary of movements due to paving**

| | Movement (mm) | | | | | | | |
|---|---|---|---|---|---|---|---|---|
| | **G1-S** | **G2-S** | **G3-S** | **G4-S** | **G1-N** | **G2-N** | **G3-N** | **G4-N** |
| **Abutment:** | | | | | | | | |
| **Incl.** | 2.875 | 0.099 | 0.488 | | | 1.847 | 0.599 | 0.511 |
| **Ext.** | 0.254 | | | 1.194 | 1.041 | | | -0.064 |
| **Pile:** | | | | | | | | |
| **Incl.** | -0.305 | -0.099 | -0.566 | | | -0.010 | -0.599 | -0.673 |
| **Ext.** | -0.584 | -0.686 | -0.508 | -0.178 | -0.140 | -0.597 | N/A | -0.737 |

The abutments show contraction (positive movement), except for pile G4-N, which shows slight expansion, while the pile movements 150 mm (6 in) below the bottom of the concrete abutment all show expansion (negative movement) of the bridge. These directions are consistent with the expected rotation of the abutments under the weight of the pavement. The movement at the abutment extensometer location near pile G1-S is likely to be faulty.

The lower earth pressure cells had increases in pressure due to paving, with the acute corners seeing larger increases than the obtuse corners. The upper earth pressure cells all had decreases in earth pressure due to paving. Table 4.7 summarizes the changes in earth pressure due to paving. The earth pressure cells indicate rotation of the abutment with the top moving into the deck and the bottom moving into the soil.

**Table 4.7. Changes in earth pressure due to paving**

| | Change in Earth Pressure, kPa | | | |
|---|---|---|---|---|
| | SE (obtuse) | SW (acute) | NE (acute) | NW (obtuse) |
| **Lower** | 4.127 | 5.791 | 2.910 | 2.417 |
| **Upper** | -0.442 | -0.453 | -0.462 | -1.275 |

### 4.4.6. After Bridge Completion

Upon completion of paving the bridge crossing Nash Stream in Coplin Plantation, the sum of the measured axial loads for the six test piles is 3046 kN (685 kips). The corresponding calculated weight of the bridge for the six test piles, assuming equal load distribution, is 2991.4 kN (672.5 kips), a 2% difference. The piles were found to not be loaded equally. The total calculated weight of the bridge is 3990 kN (897 kips). A

reasonable assumption would be that the weight of the bridge would be equally distributed to each abutment; cumulatively, the south piles would see 1995 kN (448.5 kips), as would the north piles. Subtracting the measured axial loads in the instrumented piles allows for an estimate to be made of the uninstrumented, acute piles. Based on this reasoning, at the end of construction, piles G4-S and G1-N were estimated to be carrying 377 kN and 567 kN, respectively. G4-S compares well with the expected trend; the acute piles are expected to see less axial loads than the other piles. G1-N, however, does not compare well with this trend.

### 4.5. Discussion and Conclusions

The critical pile stresses due to dead load did not exceed -118 MPa (-17.1 ksi); this critical stress does not include the residual stress due to pile driving, nor the stresses due to the portion of the abutment below the construction joint, which were summarized in Table 4.1. The average residual stress due to driving in the upper part of the pile was –16.0 MPa (-2.32 ksi), with a maximum value of -105.7 MPa (-15.3 ksi). The average stress due to the casting of the portion of the abutment below the construction joint was -15.5 MPa (-2.27 ksi), with a maximum value of -17.2 MPa (-2.49 ksi). The measured additional stresses may not be representative since measurements of these events were incomplete. Based on the critical stress plus the combined average residual stress and lower abutment stress of -149.5 MPa in the instrumented piles, there still remains significant capacity to carry live loading and thermally induced loads. Further, all piles remained well within the linearly elastic range.

The average critical stress breakdown at the end of construction for the instrumented piles is as follows: percentage due to axial load 37%, percentage due to strong-axis moment 6%, percentage due to weak-axis moment 56%, and percentage due to torsion 1%. The largest component of the critical stress is due to weak axis moment, which is significant.

The near-obtuse piles (G2-S and G3-N) carried the largest axial load during the construction sequence. These piles have the largest tributary loading area. The obtuse piles would normally have the most induced load, but the width of the cantilevered part of the deck is less than half the distance between girders. The effects of skew on load distribution appeared larger for the north abutment than the south abutment during the construction process. Pile G2-S was loaded -2 to 19% more than pile G3-S. Pile G3-N was loaded 7 to 72% more than pile G2-N*.

Although the sum of the final axial loads of the instrumented piles are about the same as the loads assuming equal distribution, during the construction process the measured loads did not always match the loads calculated assign equal load distribution to the piles. It was found that it took a while (as much as eight days) for the six-eighths of the weight of the deck and second portion of the abutments to be transferred to the piles. A possible explanation for this observation is that initially, the piles only carry a fraction of the load, while the rest of the load is compensated for in abutment shear and/or bearing. The day after the deck pour, the instrumented piles saw 30% of the total weight of the deck, eight days after the deck pour (with no additional dead load added), the piles saw 74% of the total weight of the deck.

For days of constant dead load, the extensometer movements more accurately reflected the estimated thermally induced movements calculated for the deck than did the inclinometer movements. It is believed that accurate comparisons of the deflected shape of the pile can be made using the results from the inclinometer surveys. Inclinometer surveys taken during the construction sequence illustrate similar movements for the south and north abutments. Figures 4.12, 4.13 and 4.14 compare the south piles with their northern counterparts (all movements relative to Day 259). The three figures illustrate that the corresponding piles from each abutment experience consistent movements during the construction sequence. The tops of the inclinometers contract with the bridge deck as dead loads are added to the bridge during construction and also as the temperatures of the concrete decrease. The inclinometer data suggests the top of the abutment rotates inward, while the lower section of the abutment and top of the pile kick outward. The long piles are fixed at some depth 6m to 9 m (20 to 30 ft) below final grade. As seen in the following figures, the lower part of the short piles are starting to develop curvature, this indicates that the short piles are beginning to develop some fixity. The short piles are also rotating significantly.

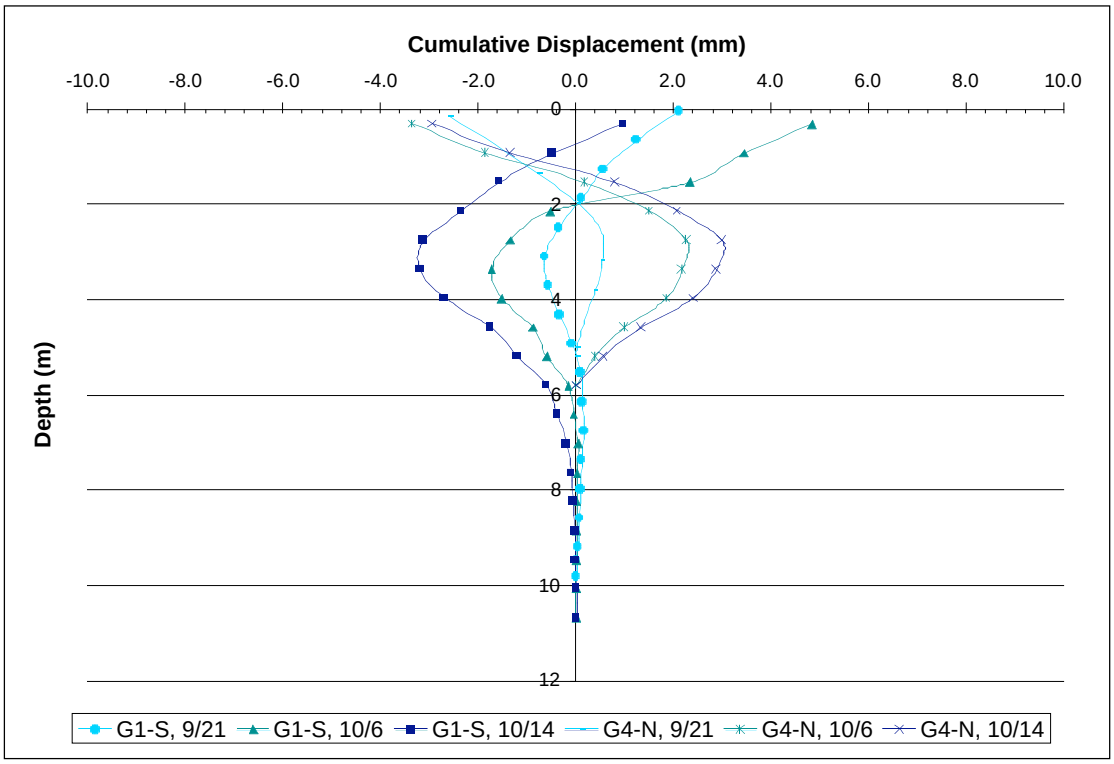


**Figure 4.12. Cumulative displacement of piles G1-S and G4-N, relative to Day 259**

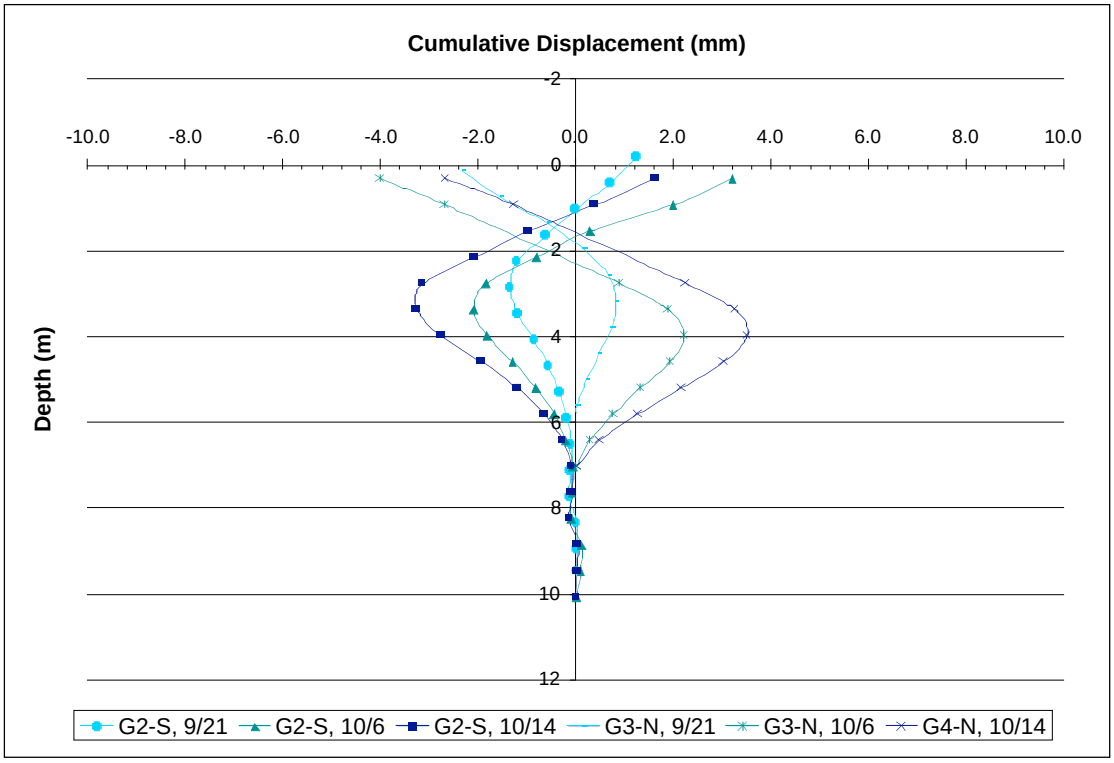


**Figure 4.13. Cumulative displacement of piles G2-S and G3-N, relative to Day 259**

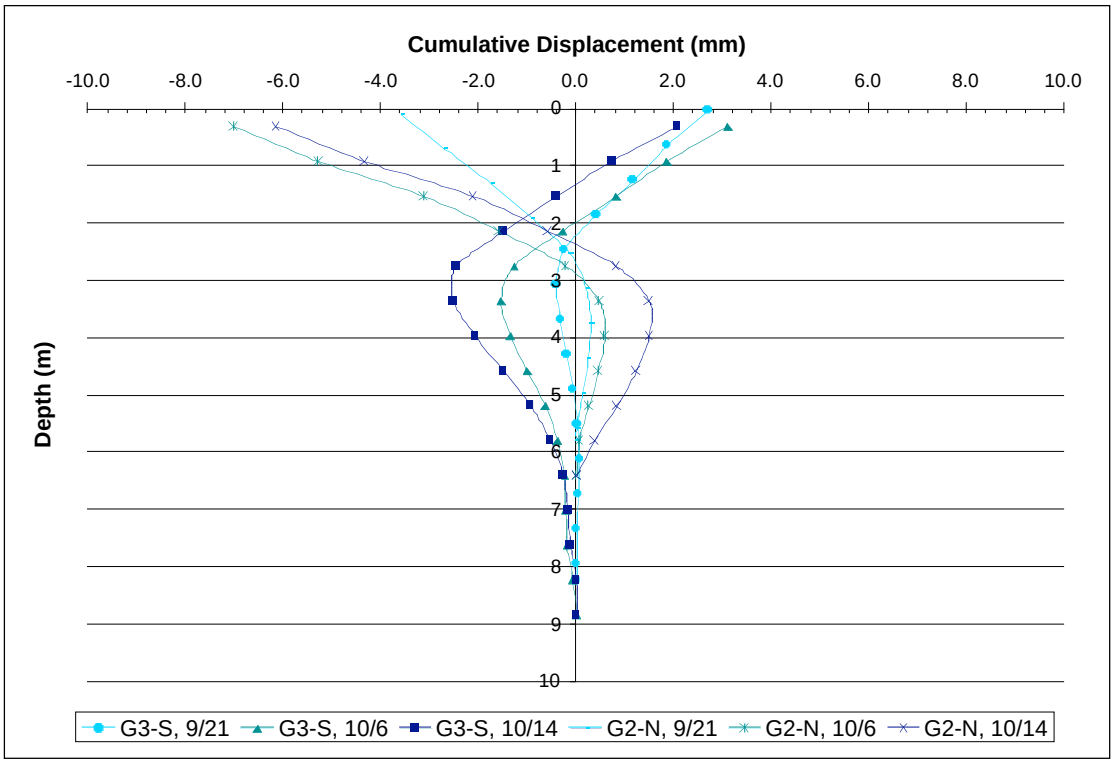


**Figure 4.14. Cumulative displacement of piles G3-S and G2-N, relative to Day 259**

# Chapter 5

# LIVE LOAD TESTING

## 5.1. Introduction

Upon completion of bridge construction, live load testing was conducted on the bridge. The results of live load testing can provide a basis for predicting responses under other loadings. Thirteen cases were utilized to examine differences in responses between the long and short piles, as well as the effects of the large skew.

Live load testing was completed on the bridge on Day 281 (October 7, 2004). The two Maine Department of Transportation (MaineDOT) dump trucks used for live loading were fully loaded with gravel and weighed 297.8 kN (66.95 kips) and 273.6 kN (61.5 kips) each, for a total of 571.4 kN (128.45 kips). The dimensions of each truck including the contact area of each tire, the length of the wheel base, and distance between wheels were taken (see Figure 5.1). The deck was loaded by the two trucks in thirteen different positions; the approach slab was also loaded, in position fourteen (see Figure 5.2). The two data acquisition systems were adjusted to read every three minutes at concurring intervals. Each loading position was held for at least nine minutes so that three complete sets of readings were taken for each position.

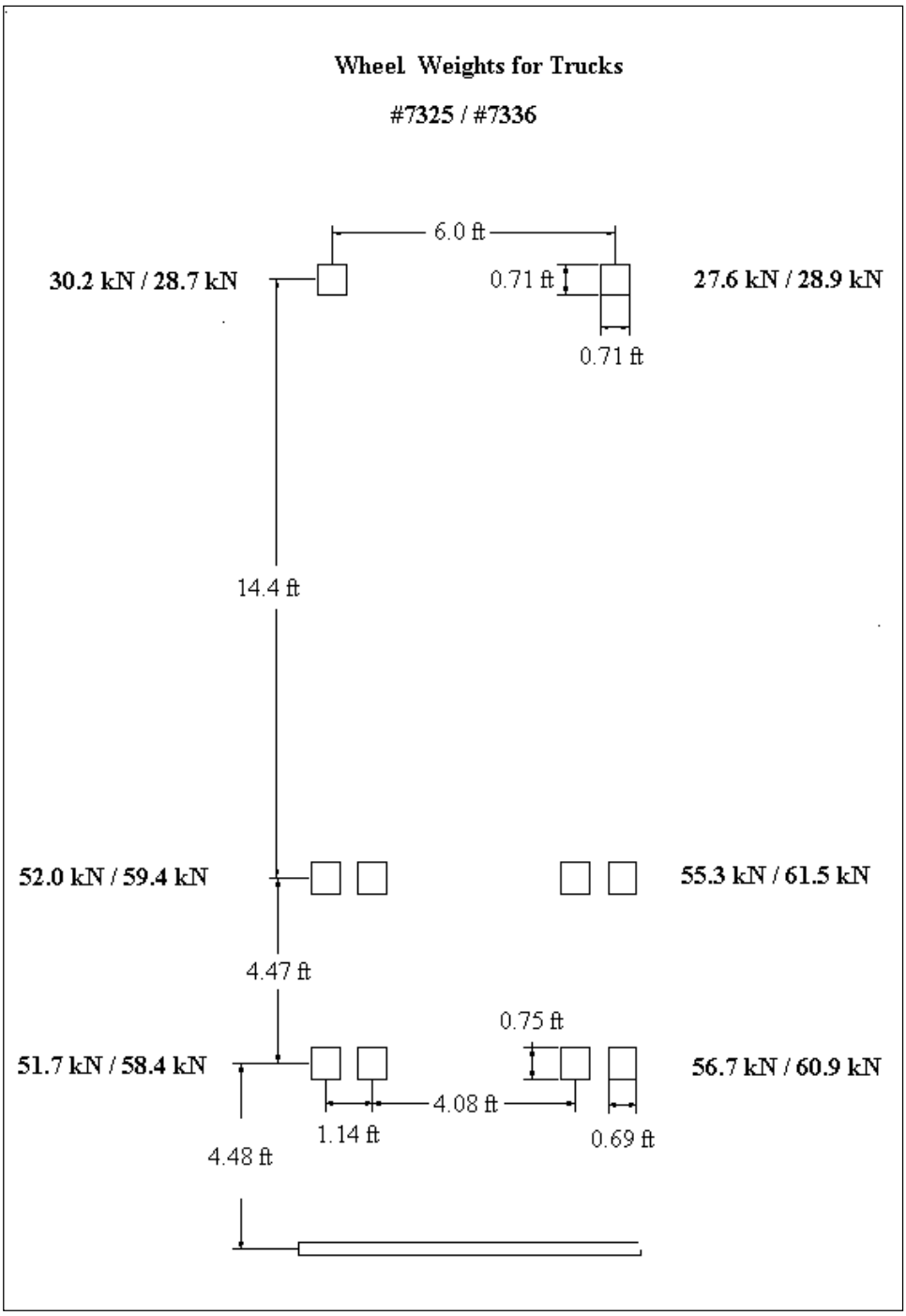


**Figure 5.1. Truck dimensions and wheel weights**

Live loading positions were chosen to simulate and magnify the effects of traffic moving across the bridge. Several series of progressions were completed with each consisting of three positions - at the one-quarter, one-half and three-quarter points along the length of the span. To create a worst case loading on a single pile, the two dump trucks were positioned facing opposite directions, with their rear bumpers touching (cases #4 - #9). In these worst load cases, the weight of the rear axles is concentrated within an area of 12.8m$^2$ (138.2 ft$^2$). The trucks were progressed down each curb line, with readings at the one-quarter, one-half and three-quarter points of the span length ($L_s$). These loadings magnified the effects of the skew.

The trucks were also progressed down the length of the bridge, positioned side by side (cases #1, #2, #3 and #10). They were shifted towards the eastern curb line, which loaded girders #3 and #4. This distributed the load to two girders rather than concentrating the load on one girder as was done in the bumper to bumper loadings.

The final series of positions consist of a truck centered in each lane with both facing southward and progressing together along the bridge (cases #11, #12 and #13). The south approach slab was loaded in case #14. Figures 5.2. a) and b) layout the loading positions which will be referenced often in the subsequent sections. The location of the truck with reference to the edge of the deck is given for each case. For side-by-side loadings, the dimension is to the center of the rear axle, while for bumper-to-bumper loadings, the dimension is to the touching bumpers. In Figure 5.2 truck # 7336 is denoted with a (*); the other truck is #7325.

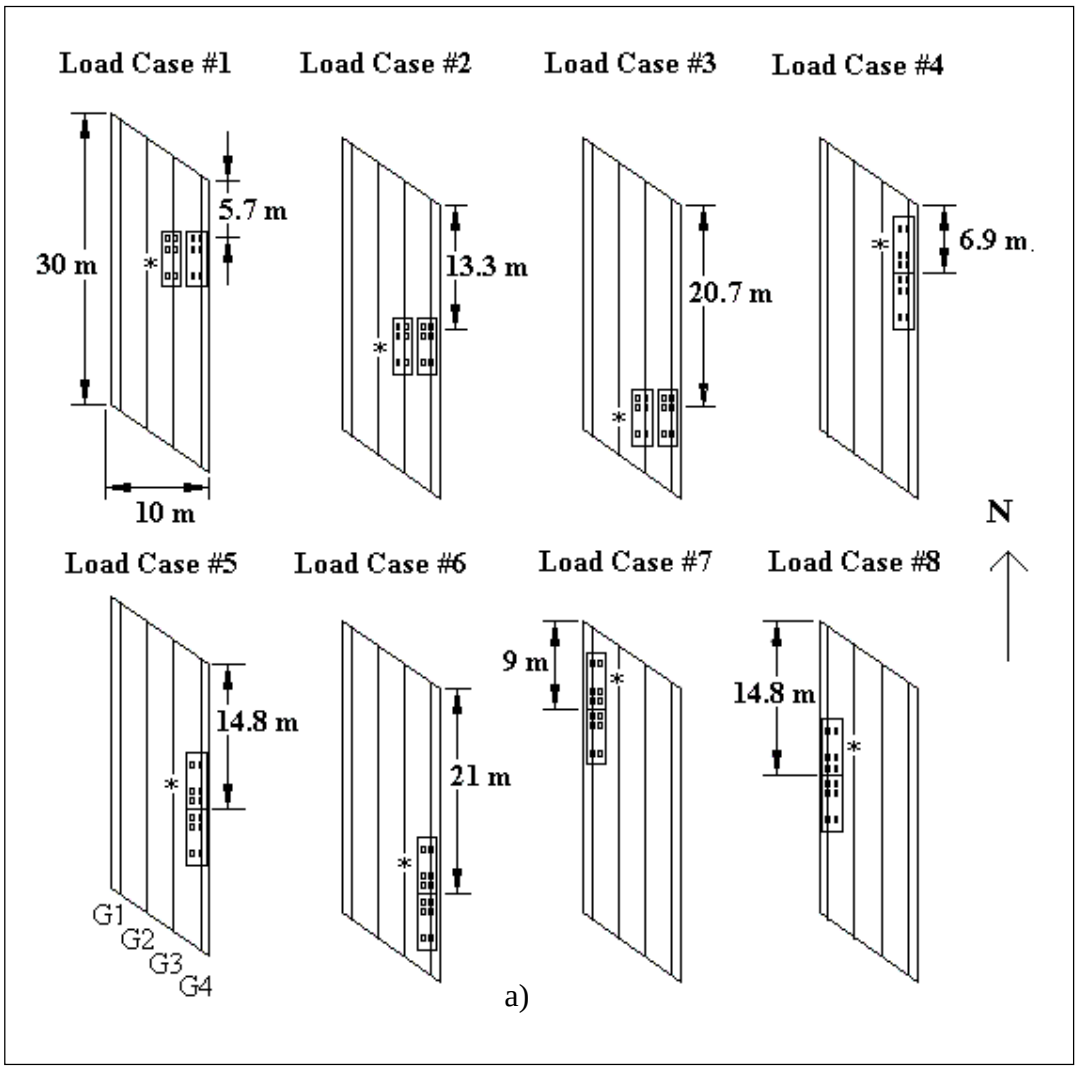


**Figure 5.2. Live loading positions**

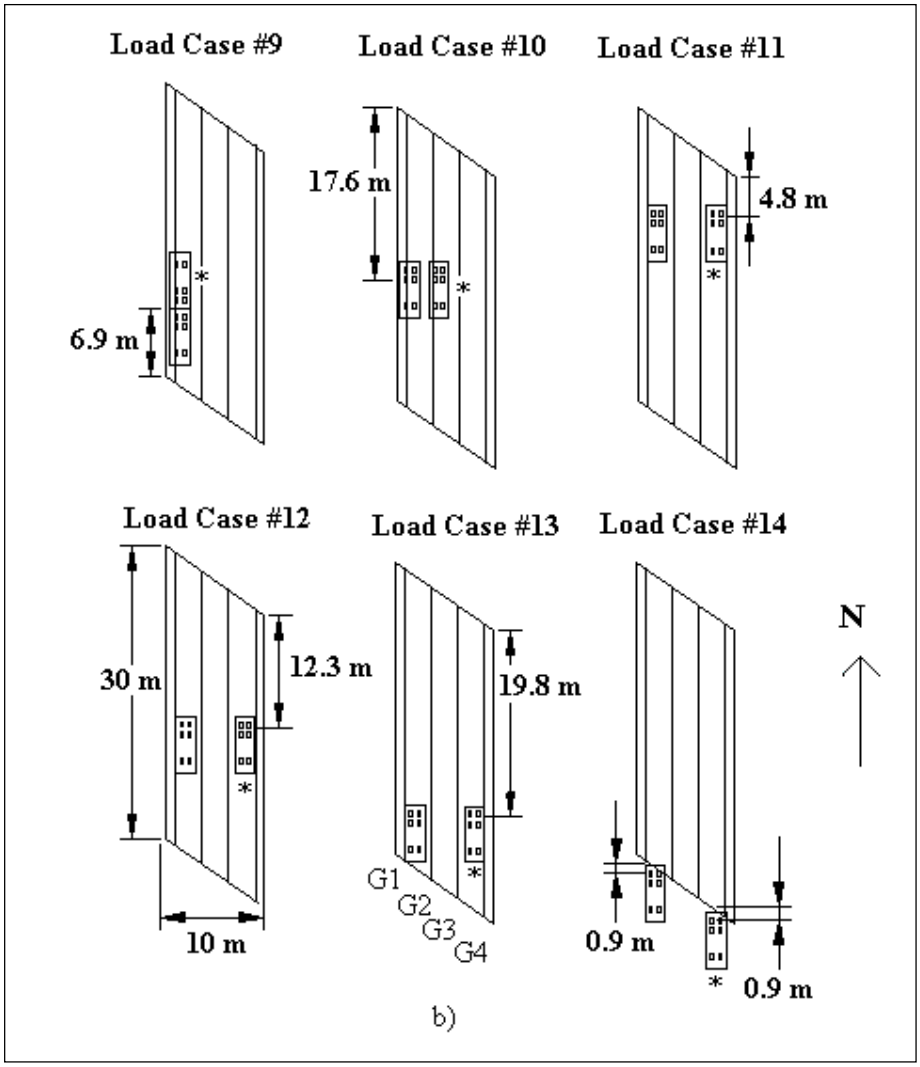


**Figure 5.2. continued**

In the following sections, thirteen loading positions will be examined according to pile stresses, pile and abutment movement and soil pressure. The southern approach slab was loaded in loading case #14; the results are not discussed as this loading did not have a significant effect on the bridge (the results are reported in Appendix C).

The following topics will be addressed in the subsequent sections: stresses in the piles derived from the strain gages readings, pile and abutment movement (extensometers and inclinometers), soil pressure on abutments (earth pressure cells), and in some cases pore pressures (piezometers).

## 5.2. Overview of Live Load Results

Data was processed in a manner consistent with that described in Chapter 4. Slope indicator readings were completed before testing and during only two loading cases (cases #5 and #8). However, strain gages, extensometers, pressure cells, thermistors, and piezometers were monitored for all loadings.

### 5.2.1. Diurnal Temperature Changes

The live load data was significantly influenced by diurnal thermal variations. The deck temperature was found to vary by 10 ºC (50 ºF) on the day of live load testing, Day 281. Figure 5.3 shows the variation of deck temperature on Day 281 as recorded by the four thermistors in the deck. The lower thermistors were slightly cooler than the upper thermistors, and the thermistors in the southern part of the deck were slightly cooler than the thermistors in the northern part of the deck. All thermistors decrease in temperature until approximately 10:00 AM, and then increase until approximately 7:00 PM.

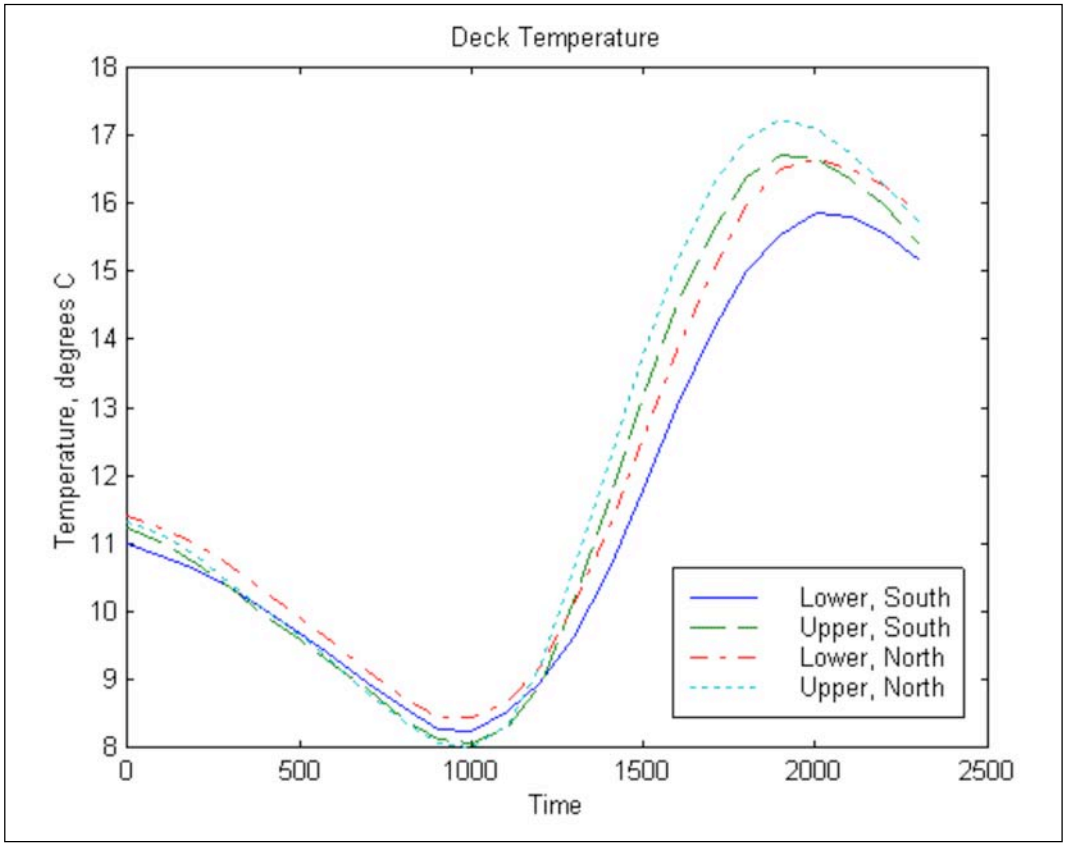


**Figure 5.3. Deck temperature on the day of live load testing**

The variation in deck temperature, and thus deck length, throughout the day causes changes in pile stresses as well as abutment movement. The effects due to diurnal thermal variation of the bridge were compensated for in the live load testing results. To compensate for temperature changes on the day of the test loading, the effects of temperature changes on days without test loading were obtained. Days 282 and 287 (October 8 and 13), days with no live load testing, have deck temperatures slightly higher and slightly lower, respectively, than Day 281. The general trends apparent in Figure 5.3 are also seen in Days 282 and 287. Figure 5.4 shows the average deck temperatures for the three days.

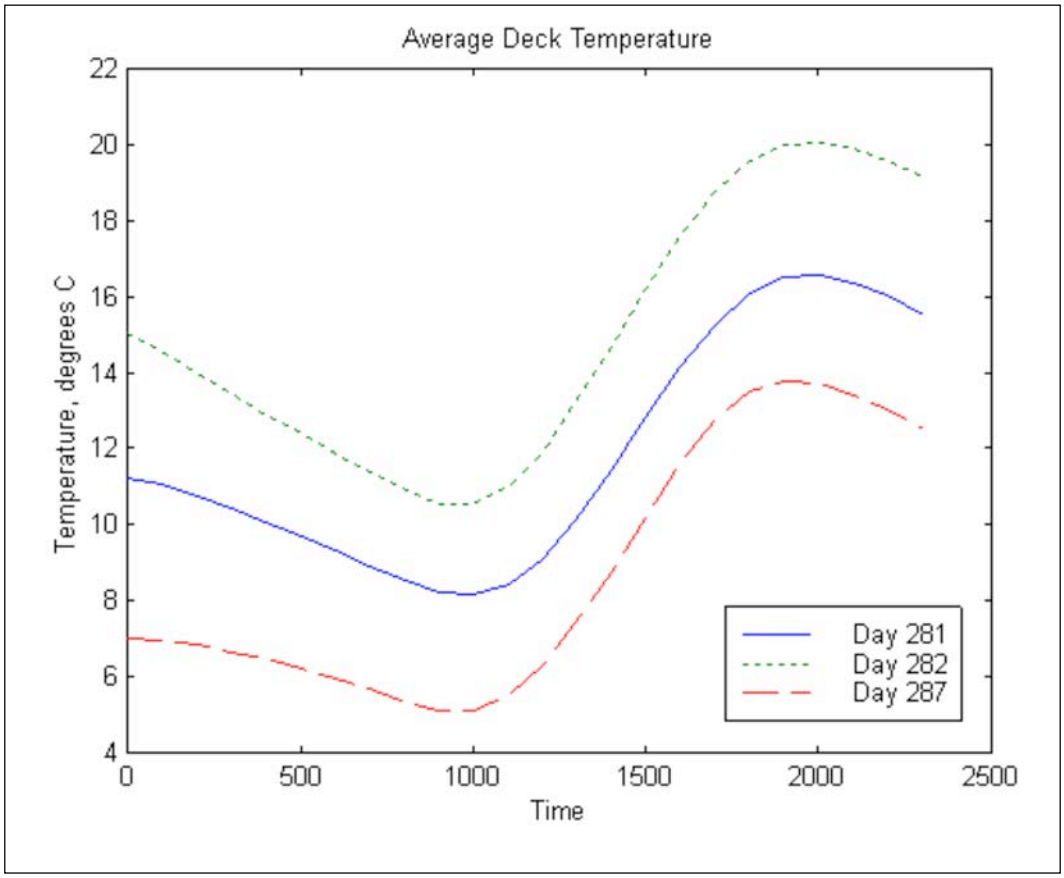


**Figure 5.4. Average deck temperatures for interpolation**

Data for all vibrating wire instruments was interpolated for Day 281 between the readings from Days 282 and 287 on the basis of the temperatures. These values were considered to reflect the in situ bridge conditions, if live loading had not taken place. The difference between the readings during the test loadings and the interpolated values for no live load at the same deck temperature was taken to be the result of live loading.

### 5.2.2. Pile Stresses

Strain gages installed on each flange, at each of three elevations on the HP 360x132 (14x89) were used to determine the stresses in the piles. The axial load, weak axis moment, strong axis moment and torsional moment were calculated for each strain

gage set location. Stresses for each loading condition were calculated at the outermost edge of each flange using the pile section properties since this is the location of maximum stress. In the following section, unless otherwise stated, the strain gage set being discussed is the one located at the highest elevation on the pile.

The sign convention for the pile stress analysis was outlined in Section 4.3.1 and is shown again in Figure 5.5. Expansion of the bridge creates positive weak axis bending, and bending towards the obtuse angle of the abutment is considered positive strong axis bending. Figure 5.6 summarizes the locations of piles.

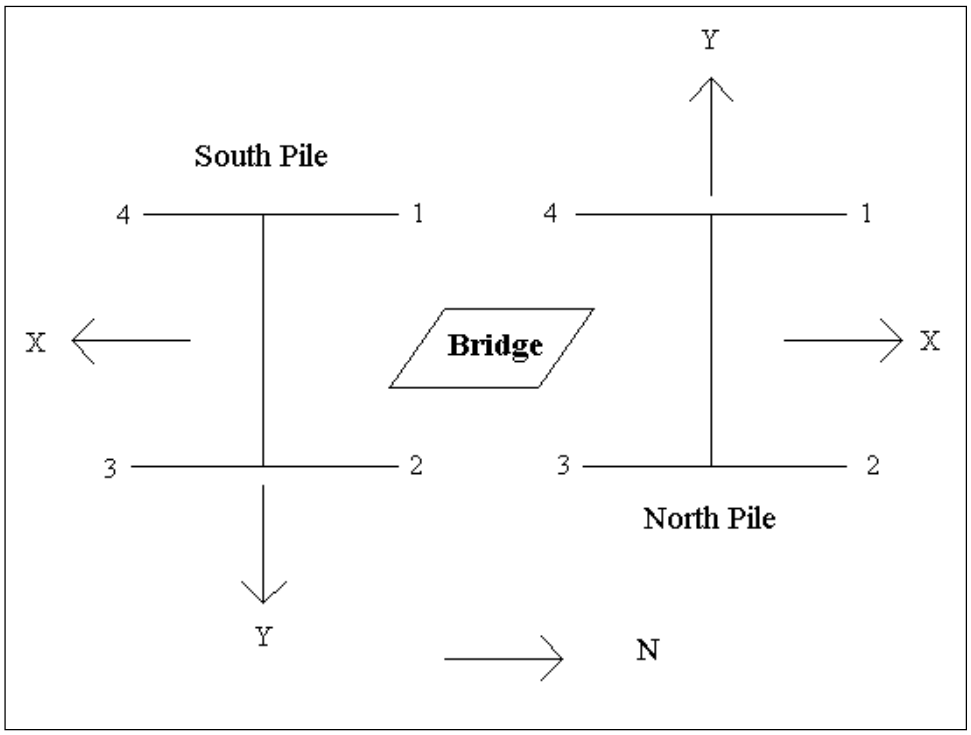


**Figure 5.5. Sign convention for analysis of pile stresses**

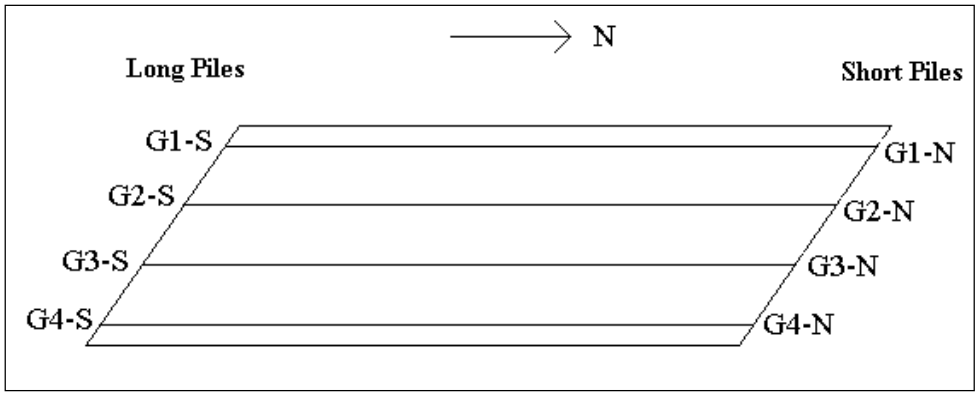


**Figure 5.6. Summary of pile locations**

The distribution of live load to each pile is important in determining which load situation produces the largest stress in the piles. The different nature of pile support at each abutment and the skew angle affects the magnitude of axial load, bending moments and torsion transmitted to the piles. The stresses due to loads and moments applied to the piles must be evaluated in design. Tables 5.1, 5.2, 5.3 and 5.4 summarize the axial loads, weak axis, strong axis and torsional moments, respectively, on the piles directly below the abutment concrete for each live loadings condition. Note: the asterisks denote a strain gage set with a faulty strain gage.

**Table 5.1. Axial loads (kN) due to each live load case**

| | Axial Pile Loads (kN) | | | | | | |
|---|---|---|---|---|---|---|---|
| **Case** | **G1-S*** | **G2-S** | **G3-S** | **G2-N*** | **G3-N** | **G4-N*** | **sum** |
| **1** | -60.6 | -8.3 | -18.5 | -49.2 | -63.7 | -87.8 | -288.1 |
| **2** | -91.2 | -44.4 | -54.7 | -25.3 | -22.5 | -59.9 | -298.1 |
| **3** | -85.9 | -64.4 | -82.8 | -14.0 | 17.5 | -20.9 | -250.6 |
| **4** | -36.0 | 0.6 | -19.4 | -26.0 | -59.0 | -124.8 | -264.7 |
| **5** | -51.4 | -33.7 | -67.7 | -10.0 | -23.5 | -81.9 | -268.3 |
| **6** | -53.8 | -40.5 | -93.4 | -2.0 | 7.2 | -37.7 | -220.1 |
| **7** | -72.8 | -5.4 | 3.9 | -93.7 | -63.7 | 9.0 | -222.7 |
| **8** | -114.2 | -30.6 | -3.1 | -58.7 | -54.2 | 6.6 | -254.2 |
| **9** | -162.0 | -68.4 | -16.0 | -14.3 | -6.8 | 10.6 | -256.9 |
| **10** | -113.0 | -59.7 | -28.4 | -43.8 | -64.4 | -25.8 | -335.1 |
| **11** | -41.8 | -20.0 | -9.7 | -58.3 | -100.0 | -65.5 | -295.4 |
| **12** | -84.8 | -53.0 | -38.2 | -22.3 | -55.2 | -50.7 | -304.2 |
| **13** | -100.1 | -85.2 | -70.7 | 1.6 | -7.3 | -23.0 | -284.7 |

The sum of the measured loads is typically only two-thirds of the total truck weight. The sum of the axial loads for the six instrumented piles in Table 5.1 are well below 427 kN (96 kips), which is 6/8 of the total live load, 571.6 kN (128.5 kips). This is consistent with the pile forces observed during the deck pour (as discussed in Chapter 4), which were initially about two-thirds of the total deck weight but increased with time. This is attributed to soil bearing and shear initially carrying significant load. With the live loading, however, the short duration of loads does not permit load redistribution. Analysis of these results is done below in Section 5.3.1.1.

**Table 5.2. Weak-axis moments (kN-m) due to each live load case**

| | Weak-Axis Moment (kN-m) | | | | | |
|---|---|---|---|---|---|---|
| **Case** | **G1-S*** | **G2-S** | **G3-S** | **G2-N*** | **G3-N** | **G4-N*** |
| **1** | -4.93 | 0.31 | 2.72 | -6.23 | -1.43 | -2.26 |
| **2** | -9.88 | -4.16 | 1.54 | -5.65 | -1.21 | -1.11 |
| **3** | -7.54 | -3.27 | 0.93 | -1.33 | 1.28 | 1.61 |
| **4** | -2.70 | 1.29 | 1.57 | -3.80 | -1.39 | -4.04 |
| **5** | -5.25 | -2.59 | 0.61 | -4.06 | -1.78 | -2.52 |
| **6** | -5.73 | -2.89 | 0.20 | -3.25 | -0.81 | -0.55 |
| **7** | -10.39 | -1.77 | 1.04 | -8.30 | -1.47 | 0.51 |
| **8** | -18.23 | -7.35 | 0.65 | -9.61 | -2.36 | 0.37 |
| **9** | -20.10 | -8.58 | 0.30 | -4.08 | -0.41 | 1.99 |
| **10** | -16.52 | -8.92 | 0.05 | -8.12 | -2.99 | -0.50 |
| **11** | -6.28 | -3.59 | 0.64 | -8.06 | -3.87 | -3.12 |
| **12** | -11.99 | -7.87 | 0.11 | -7.10 | -3.58 | -2.17 |
| **13** | -10.26 | -8.02 | -0.33 | -2.66 | -1.27 | 0.43 |

**Table 5.3. Strong-axis moments (kN-m) due to each live load case**

| | Strong-Axis Moment (kN-m) | | | | | |
|---|---|---|---|---|---|---|
| **Case** | **G1-S*** | **G2-S** | **G3-S** | **G2-N*** | **G3-N** | **G4-N*** |
| **1** | -1.38 | 0.43 | 0.02 | -5.71 | -0.02 | 4.64 |
| **2** | -6.70 | -4.57 | -3.96 | -4.54 | -0.10 | 3.54 |
| **3** | -7.87 | -6.13 | -5.13 | -0.50 | 0.24 | 2.14 |
| **4** | 0.63 | 0.49 | -1.28 | -2.71 | 0.10 | 5.22 |
| **5** | -2.79 | -3.87 | -5.62 | -2.08 | 0.06 | 2.26 |
| **6** | -3.65 | -4.68 | -6.65 | -0.15 | 0.36 | 0.55 |
| **7** | -7.25 | -1.63 | 0.32 | -12.83 | 0.65 | -1.97 |
| **8** | -16.03 | -7.07 | -1.40 | -13.01 | 0.22 | -0.70 |
| **9** | -16.17 | -7.53 | -1.73 | -5.48 | 0.19 | 0.84 |
| **10** | -17.70 | -10.52 | -3.62 | -11.72 | 0.37 | -0.07 |
| **11** | -5.88 | -3.97 | -1.34 | -11.51 | 0.48 | 1.97 |
| **12** | -11.10 | -8.32 | -4.06 | -9.35 | 0.21 | 1.61 |
| **13** | -11.10 | -9.51 | -5.14 | -3.42 | 0.26 | 0.55 |

**Table 5.4. Torsional moments (kN-m) due to each live load case**

| | Torsional Moment (kN-m) | | | | | |
|---|---|---|---|---|---|---|
| **Case** | **G1-S*** | **G2-S** | **G3-S** | **G2-N*** | **G3-N** | **G4-N*** |
| **1** | 0.39 | 0.14 | 0.12 | N/A | 0.75 | -0.84 |
| **2** | 0.75 | 0.13 | 0.03 | N/A | 0.51 | -0.62 |
| **3** | 0.74 | 0.15 | -0.03 | N/A | -0.23 | 0.01 |
| **4** | 0.61 | 0.09 | -0.08 | N/A | 0.53 | -1.19 |
| **5** | 0.79 | 0.10 | -0.03 | N/A | 0.50 | -0.87 |
| **6** | 0.97 | 0.10 | -0.04 | N/A | 0.04 | -0.39 |
| **7** | 0.77 | 0.27 | -0.24 | N/A | 1.06 | -0.29 |
| **8** | 0.52 | 0.36 | -0.11 | N/A | 1.08 | -0.39 |
| **9** | 0.20 | 0.34 | -0.08 | N/A | 0.15 | -0.08 |
| **10** | 0.15 | 0.35 | -0.02 | N/A | 1.32 | -0.54 |
| **11** | 0.01 | 0.17 | -0.05 | N/A | 1.59 | -1.03 |
| **12** | 0.10 | 0.24 | 0.06 | N/A | 1.25 | -0.71 |
| **13** | -0.02 | 0.18 | 0.08 | N/A | 0.33 | -0.08 |

Table 5.5 summarizes the critical pile stresses caused by each live load condition. The critical stress was determined to be the largest negative stress in the pile due to the combined effects of axial load, weak-axis moment, strong-axis moment and torsion. Table 5.6 summarizes the total critical stress due to dead and live loads for each loading condition. These values does not include the additional residual stresses due to pile

driving, nor the stresses due to the load from the first portion of the abutments; the average stresses from the instrumented piles for these two events are -16 MPa (-2.32 ksi) and -15.6 MPa (-2.27 ksi), respectively. Table 5.7 summarizes the average portion of the critical stress due to dead load and live load for each of the internal forces. Table 5.8 summarizes the effects of dead load as determined prior to the application of live load, at 5:00 AM on Day 281.

**Table 5.5. Critical stresses (MPa) in piles due to live loading**

| | Stress (MPa) | | | | | |
|---|---|---|---|---|---|---|
| **Case** | **G1-S*** | **G2-S** | **G3-S** | **G2-N*** | **G3-N** | **G4-N*** |
| **1** | -10.18 | -1.00 | -4.76 | -13.16 | -7.22 | -7.94 |
| **2** | -18.60 | -9.36 | -6.63 | -10.68 | -4.14 | -4.80 |
| **3** | -15.71 | -9.78 | -7.64 | -2.70 | -1.46 | -3.99 |
| **4** | -7.39 | -1.62 | -3.36 | -7.51 | -6.38 | -12.93 |
| **5** | -10.60 | -6.49 | -6.67 | -6.77 | -4.96 | -9.03 |
| **6** | -11.47 | -7.58 | -7.91 | -4.50 | -0.97 | -3.52 |
| **7** | -18.50 | -2.67 | -1.92 | -21.09 | -8.44 | -0.43 |
| **8** | -35.32 | -13.29 | -1.33 | -21.10 | -8.98 | -0.90 |
| **9** | -41.20 | -17.13 | -1.77 | -8.39 | -1.40 | -2.57 |
| **10** | -34.64 | -18.30 | -3.07 | -17.83 | -11.08 | -3.47 |
| **11** | -12.90 | -6.97 | -1.79 | -18.41 | -14.88 | -9.51 |
| **12** | -24.59 | -15.96 | -4.06 | -14.39 | -11.14 | -6.77 |
| **13** | -23.40 | -18.48 | -5.96 | -4.84 | -3.09 | -2.18 |

**Table 5.6. Critical stresses (MPa) in piles due to dead load and live load**

| | Stress (MPa) | | | | | |
|---|---|---|---|---|---|---|
| **Case** | **G1-S*** | **G2-S** | **G3-S** | **G2-N*** | **G3-N** | **G4-N*** |
| **1** | -155.3 | -131.1 | -64.6 | -100.9 | -111.1 | -77.9 |
| **2** | -164.8 | -140.9 | -69.8 | -98.5 | -108.0 | -74.7 |
| **3** | -163.9 | -143.1 | -73.0 | -91.8 | -101.5 | -67.8 |
| **4** | -151.6 | -131.2 | -67.4 | -96.6 | -111.0 | -82.7 |
| **5** | -158.3 | -140.1 | -72.5 | -97.0 | -109.8 | -78.8 |
| **6** | -159.7 | -141.3 | -74.7 | -95.3 | -105.9 | -73.3 |
| **7** | -169.6 | -136.2 | -65.4 | -112.6 | -113.5 | -70.7 |
| **8** | -185.6 | -144.6 | -64.8 | -111.3 | -111.6 | -69.2 |
| **9** | -190.3 | -146.0 | -64.2 | -97.2 | -101.6 | -63.9 |
| **10** | -180.5 | -144.3 | -63.7 | -104.3 | -108.1 | -69.1 |
| **11** | -158.6 | -133.0 | -61.1 | -104.9 | -111.9 | -75.2 |
| **12** | -171.7 | -142.0 | -64.1 | -100.9 | -108.1 | -72.4 |
| **13** | -169.1 | -144.5 | -66.8 | -91.3 | -100.1 | -66.3 |

**Table 5.7. Summary of the average portion of the critical stress due to each of the internal forces due to live load and dead load**

| | G1-S* | G2-S | G3-S | G2-N* | G3-N | G4-N* |
|---|---|---|---|---|---|---|
| **% Axial Load** | 20% | 24% | 49% | 22% | 41% | 32% |
| **% Strong Axis Moment** | 23% | 11% | 15% | 5% | -2% | 10% |
| **% Weak Axis Moment** | 65% | 67% | 48% | 73% | 49% | 57% |
| **% Torsion** | -7% | -2% | -11% | 0% | 12% | 1% |

**Table 5.8. Summary of dead load effects on piles**

| | G1-S* | G2-S | G3-S | G2-N* | G3-N | G4-N* |
|---|---|---|---|---|---|---|
| **Axial Load (kN)** | -505.1 | -611.2 | -600.8 | -423.3 | -780.0 | -388.6 |
| **Strong Axis Mom (kN-m)** | -76.5 | -33.6 | -19.0 | -5.2 | -5.7 | -14.5 |
| **Weak Axis Moment (kN-m)** | -69.1 | -58.6 | -21.5 | -44.1 | -32.0 | -25.2 |
| **Torsion (kN-m)** | 1.95 | 1.01 | 2.75 | N/A | 3.53 | 0.35 |
| **Critical Stress (MPa)** | -144.1 | -120.7 | -60.1 | -82.9 | -90.2 | -58.6 |

The measured sum of the axial loads due to dead load at the time of the live load test for all of the instrumented piles is 3309 kN (744 kips). The calculated bridge weight, after completion, is 4392 kN (987 kips) excluding the lower part of the abutment and the to be installed guard rail (see Appendix B.3 for calculations). The weight is not distributed equally to the instrumented piles. The six instrumented piles are supporting 75.3% of the bridge's total weight. With time this percentage is likely to be higher. The measured axial load of 3309 kN likely does not carry all the pavement load, since all the pavement load may not have been transferred to the piles. In Table 4.3, all previous loads, like the deck concrete, transferred fully to the axial load after about one week. This delay was likely caused by initial support by the soil under the abutment which is gradually transferred to support by the piles. Based on an assumed equal load in each pile, they should be carrying 75% of the bridge weight. Based on dead loads applied proportionally to the tributary deck area, the pecentage in these piles should be 77.3 %.

The concurrence of the calculated axial loads in the six piles to the estimated dead loads for these six piles shows that the calculation method and the measurements appear to be reasonable.

In another comparison the weight of the bridge was distributed evenly to each abutment, and thus the weight on south and north abutments each is 2196 kN. The axial loads in the un-instrumented piles can be estimated by subtracting the measured axial loads in the instrumented piles from half the bridge weight. Based on this assumption, after completion of the bridge, but prior to live loading, piles G4-S and G1-N were determined to have 479 kN and 604 kN, respectively. It is expected that the acute pile would be less heavily loaded than the obtuse pile; this is the case for the estimate of pile G4-S, but not the case for pile G1-N (see Table 5.8).

### 5.2.3. Pile and Abutment Movements

The movements of the bridge under test loading indicate abutment rotation in the vertical and horizontal planes. The movements were measured by extensometers at the top of the piles, extensometers on the abutments and inclinometers on the piles. Tables 5.9 and 5.10 summarize the abutment and pile movements as determined by extensometers, for the south and north abutments, respectively. The abutment and pile extensometers are located 1.2 m and 3 m (4 ft and 9.8 ft) below the top of the deck, respectively, for both abutments. Positive movements indicate the lengthening of the extensometer, and thus contraction of the bridge deck. Negative movements indicate expansion of the bridge deck.

**Table 5.9. South abutment and pile movements (mm) during live loading**

| | Pile and Abutment Movements (mm) | | | | | |
|---|---|---|---|---|---|---|
| Case | G1-S, Abutment | G4-S, Abutment | G1-S, Pile | G2-S, Pile | G3-S, Pile | G4-S, Pile |
| 1 | 0.195 | 0.094 | 0.333 | 0.328 | 0.252 | 0.142 |
| 2 | 0.193 | 0.099 | 0.271 | 0.222 | 0.122 | -0.051 |
| 3 | 0.206 | 0.154 | 0.305 | 0.224 | 0.109 | -0.019 |
| 4 | 0.205 | 0.136 | 0.351 | 0.267 | 0.150 | 0.048 |
| 5 | 0.196 | 0.080 | 0.324 | 0.234 | 0.043 | -0.209 |
| 6 | 0.182 | 0.064 | 0.313 | 0.218 | 0.033 | -0.224 |
| 7 | 0.076 | 0.123 | 0.114 | 0.162 | 0.174 | 0.141 |
| 8 | -0.065 | 0.104 | -0.187 | -0.077 | 0.094 | 0.081 |
| 9 | -0.103 | 0.048 | -0.240 | -0.124 | 0.084 | 0.064 |
| 10 | -0.025 | 0.117 | -0.171 | -0.119 | 0.042 | 0.036 |
| 11 | -0.061 | -0.007 | -0.052 | -0.066 | 0.047 | 0.039 |
| 12 | -0.081 | -0.026 | -0.122 | -0.121 | -0.028 | -0.085 |
| 13 | -0.068 | -0.016 | -0.101 | -0.125 | -0.051 | -0.115 |

**Table 5.10. North abutment and pile movements (mm) during live loading**

| | Pile and Abutment Movements (mm) | | | | |
|---|---|---|---|---|---|
| Case | G1-N, Abutment | G4-N, Abutment | G1-N, Pile | G2-N, Pile | G4-N, Pile |
| 1 | 0.152 | 0.307 | 0.190 | 0.200 | 0.195 |
| 2 | 0.152 | 0.288 | 0.166 | 0.191 | 0.114 |
| 3 | 0.141 | 0.277 | 0.247 | 0.290 | 0.193 |
| 4 | 0.160 | 0.258 | 0.289 | 0.261 | 0.022 |
| 5 | 0.156 | 0.165 | 0.253 | 0.226 | -0.086 |
| 6 | 0.129 | 0.100 | 0.263 | 0.235 | -0.039 |
| 7 | 0.060 | 0.105 | -0.263 | -0.064 | 0.141 |
| 8 | 0.040 | 0.100 | -0.403 | -0.197 | 0.101 |
| 9 | -0.036 | 0.045 | -0.261 | -0.107 | 0.103 |
| 10 | 0.064 | 0.059 | -0.268 | -0.184 | 0.048 |
| 11 | 0.081 | 0.055 | -0.211 | -0.180 | -0.012 |
| 12 | 0.071 | 0.016 | -0.208 | -0.173 | -0.071 |
| 13 | 0.011 | -0.037 | -0.123 | -0.079 | -0.043 |

Inclinometer readings were taken during two live load positions, #5, and #8, and were compared to the surveys taken the day prior to live load testing. Due to technical difficulties, five surveys were not collected, piles G1-S, G2-S, G3-S, G2-N, and the south embankment, all during loading case #8. For plotting purposes, the inclinometer readings in the A-direction, parallel to the centerline of the bridge, are positive when the

movement is in the northerly direction and negative when the movement is in the southerly direction. For the south piles, negative displacement is consistent with deck expansion, while positive displacement for the north piles is consistent with deck expansion. Movements determined by inclinometer differ from those determined by extensometer, using the same reference point, by 4% to 54%.

### 5.2.4. Earth Pressures

The earth pressure cells indicate the resistance of the soil on each abutment. This reflects movement of the bridge abutment due to the live loading. Table 5.11 contains the change in earth pressure on the back face of the abutments for each live load case.

**Table 5.11. Change in earth pressure (kPa) due to live loading**

| | Change in Earth Pressure (kPa) | | | | | | | |
|---|---|---|---|---|---|---|---|---|
| **Case** | **SE, Lower** | **SE, Upper** | **SW, Lower** | **SW, Upper** | **NE, Lower** | **NE, Upper** | **NW, Lower** | **NW, Upper** |
| **1** | 0.12 | 1.16 | 0.12 | 0.56 | 4.50 | -0.09 | 0.36 | 0.53 |
| **2** | 2.38 | 1.18 | 1.46 | 0.51 | 4.73 | 0.09 | 0.53 | 0.61 |
| **3** | 1.79 | 1.29 | 0.11 | 0.50 | 2.15 | 0.22 | -0.15 | 0.91 |
| **4** | 1.00 | 1.18 | -0.50 | 0.56 | 4.74 | 0.21 | -0.43 | 0.63 |
| **5** | 5.25 | 1.20 | -0.30 | 0.51 | 5.28 | 0.61 | 0.07 | 0.75 |
| **6** | 5.85 | 1.23 | -0.38 | 0.53 | 3.54 | 1.02 | 0.54 | 0.98 |
| **7** | 0.07 | 1.22 | 3.76 | 0.71 | 1.27 | 0.54 | 4.18 | 0.71 |
| **8** | 0.80 | 1.34 | 8.27 | 1.15 | 1.83 | 0.71 | 5.07 | 0.68 |
| **9** | 0.84 | 1.41 | 9.67 | 1.25 | 2.06 | 1.73 | 3.83 | 1.16 |
| **10** | 1.92 | 1.37 | 8.27 | 1.29 | 4.16 | 1.07 | 3.98 | 0.74 |
| **11** | 2.45 | 1.53 | 5.79 | 2.18 | 4.73 | 1.03 | 3.56 | 0.71 |
| **12** | 4.61 | 1.36 | 7.76 | 1.95 | 5.12 | 1.22 | 3.40 | 0.81 |
| **13** | 5.33 | 1.36 | 6.60 | 1.68 | 3.55 | 1.94 | 2.48 | 1.15 |

The sign convention for the earth pressure cells is positive changes in pressure correspond to the abutment moving into the backfill, or deck expansion. Negative changes in earth pressure correspond to the abutment moving away from the backfill, or deck contraction.

### 5.2.5. Pore Pressures

The pore pressures in the north and south embankments were recorded during the live load testing. It appears that the load testing had no effect on the pore pressure; this is likely due to the granular soil deposits.

## 5.3. Discussion of Live Loading

This section discusses the pile stresses, pile and abutment movements and soil pressure for the live load testing. Observations of the effects of skew and the differences between the two abutments are made. The loadings which induce the largest stresses for each pile are examined. General trends observed for series of loadings are also discussed.

### 5.3.1. Pile Stresses

This section discusses trends seen in the piling with respect to several factors, including load distribution, critical stresses, effects of skew, and differences between short piles and long piles. The general trends of stresses along the length of the pile are also discussed.

#### 5.3.1.1. Distribution of Loads to the Piles due to Live Loading

The sums of measured pile loads due to the various cases of live loading are shown in Table 5.1. These do not include loads on piles G4-S or G1-N since these two piles were not instrumented. However, using the results in Table 5.1, an estimate can be made for the loads on the uninstrumented piles. Thus the total loads on all piling can be estimated.

Axial loads on the uninstrumented piles were estimated for the two loadings which are furthest from the two uninstrumented piles (loading cases #4 and #9). This minimizes the loads in the uninstrumented piles from the live loads and thus minimized the amount that the estimate may be off. Also, behavior away from the area of loading is more well behaved (in the sense of the pattern of load dissipation with distance). The two cases are also mirror image loadings, which gives a sense of the consistency of the results.

For load cases #4 and #9, the trucks are located in corners with instrumented piles. The uninstrumented piles (G4-S and G1-N) will carry significantly diminished portions of the load. For load case #4 (trucks at the north abutment over girder #4) it is expected that pile G4-N will have the largest load and the loads will diminish progressively along the abutment, with pile G1-N having the smallest load. This is the basis for estimating the load on pile G1-N. It should be less than G2-N* and continue the pattern from G3-N and G4-N*. Likewise, the load for G4-S in loading case #9 can be estimated. These estimated loads are -10 kN and -6 kN (-2.2 kips and -1.3 kips), respectively, for G1-N and G4-S.

Using a similar approach, the load on G4-S due to loading case #4 was estimated using the load on G4-N* due to load case #6. Likewise, the load on G1-N due to case #9 can be based on the load on G1-S* due to case #7. The estimated loads on G4-S and G1-N, for these load cases, are -40 kN and -70 kN (-9 kips and 15.8 kips), respectively.

The maximum value of the sum of the axial loads for the six instrumented piles is due to load case #10 with -335.1 kN (-75.3 kips) (refer to Table 5.1). This value exceeds

the totals for all eight piles for cases #4 and #9 (G4-S and G1-N were estimated). Applying the logic that piles further from the loading location will see reduced effects, the loads for piles G4-S and G1-N can be estimated. The estimates are -13 kN and -25 kN (-2.9 kips and -5.6 kips) for piles G4-S and G1-N, respectively. These estimates increase the total axial load applied to the piles to -373.1 kN (83.9 kips) for case #10.

The highest measured total load on the instrumented piles was 335.1 kN (75.3 kips), or 78% of the tributary live load on the instrumented piles, assuming an equally distributed load. When adding the estimated loads on piles G4-S and G1-N, the total load on the piles was estimated to be 373.1 kN; only 65% of the total applied live load is transferred to the piles. The abutment's contact with the soil must account for the remaining amount of the live load. This observation was also found during the construction sequence. Only a fraction of the weight of the deck was initially seen in the axial loads of the piles. The sum of the load in the piles from t he deck increased for eight days to six-eighths of the total load. Since the live loadings were only short term, each only lasted nine minutes, it is reasonable to believe that the remaining load was compensated by the abutment in either bearing and/or shear. If the loads were applied for a sufficiently long time, the total load could eventually be seen in the pilings.

#### 5.3.1.2. Critical Loadings for Each Pile

The critical loading is the loading that results in the largest negative stress for a given pile. The critical loading position for each pile is consistent with the critical loading position for the corresponding pile on the opposite abutment. For example, G1-S* and G4-N*, both obtuse corner piles, see the highest stress for obtuse corner loadings,

#9 and #4, respectively. The near-obtuse piles (G2-S, and G3-N) of the south and north abutments correspond to each other, as do the near-acute piles (G3-S and G2-N*). The near-obtuse, however, do not correspond to the near-acute piles of the same abutment. The difference is due to the skew effects.

Table 5.12 summarizes the breakdown of the critical stresses in the piles due to critical loadings.

**Table 5.12. Summary of the portion of the critical stress due to each of the internal forces for critical loadings (Live Load only)**

| | G1-S | G2-S | G3-S | G2-N | G3-N | G4-N |
|---|---|---|---|---|---|---|
| **Load Case** | # 9 | # 13 | # 6 | # 7 | # 11 | # 4 |
| **Critical Stress (MPa)** | -41.2 | -18.5 | -7.9 | -21.1 | -14.9 | -12.9 |
| **% Axial Load** | 20% | 24% | 61% | 23% | 35% | 50% |
| **% Strong Axis Moment** | 16% | 21% | 37% | 25% | 1% | -18% |
| **% Weak Axis Moment** | 65% | 58% | 3% | 53% | 35% | 42% |
| **% Torsion** | -1% | -3% | -1% | 0% | 29% | 25% |

The piles in the obtuse corners of the abutments experienced the highest stresses when the trucks are positioned with their rear bumpers touching, and located one-quarter deck length away from the abutment on the supported girder. The critical stress in pile G1-S occurred during loading case #9. The maximum compressive stress due to live loading was 41.20 MPa (5.98 ksi) at location #2 on the pile (see Figure 5.5). The critical stress in pile G4-N* occurs during loading case #4. The net compressive stress due to live loading was 12.93 MPa (1.88 ksi) at location #4 on the pile.

The piles in the acute corner are not instrumented, so the behavior of these piles can only be inferred from behavior of the instrumented near-acute piles. The near-acute piles (G3-S and G2-N*) experience the highest stress when the trucks are positioned in the acute corner. Piles G3-S and G2-N* are most severely loaded when the trucks are

positioned with their rear bumpers touching, and located over the girder supported by the acute pile. The critical stress for pile G3-S occurs during load case #6. The maximum compressive stress due to live loading was 7.91 MPa (1.15 ksi) at location #3. The critical stress for pile G2-N* occurs during both load case #7 and #8. The torsional moment was not computed as one of the strain gages at this location was faulty and the corrected valued determined by the least squares regression laid out in Section 4.3.1 did not produce a credible value. The net compressive stress due to live loading for both cases was 21.1 MPa (3.06 ksi) at location #4 (see Figure 5.5).

The near-obtuse piles were subjected to the highest stresses during the loading case where the trucks were one-quarter span length from the respective abutment, positioned with a truck centered in each of the two bridge lanes. The critical stress for pile G2-S occurred during load case #13. The net compressive stress due to live loading was 18.48 MPa (2.68 ksi) at location #2. The critical stress for pile G3-N occurs during load case #11. The net compressive stress due to live loading was 14.88 MPa (2.16 ksi) at location #3 (see Figure 5.5).

#### 5.3.1.3. Skew Effects

For centered loadings (#11-#13), the near-obtuse piles (G2-S and G3-N) sustain higher axial loads than the near-acute piles (G3-S and G2-N*). Piles G2-S and G3-N have axial loads of -53.0 kN and -55.2 kN (-11.9 kips and -12.4 kips), respectively for loading case #12 (see Figure 5.2.b). Piles G3-S and G2-N* see -38.2 kN and -22.3 kN (-8.6 kips and -5.0 kips), respectively for the same loading. However, for eccentric loadings in which the trucks are bumper to bumper in each corner of the bridge, the near-acute piles see larger loads for the acute loading than the near-obtuse piles see for obtuse

loadings. The near-acute piles (G3-S and G2-N*) see -93.4 kN and -93.7 kN (-21.0 kips and -21.1 kips) due to the acute corner loadings (case #6 and #7), respectively. The near-obtuse piles (G2-S and G3-N) see -68.4 kN and -59.0 kN (-15.4 kips and -13.3 kips) due to the obtuse corner loadings (case #9 and #4), respectively. This behavior implies (since the acute piles are not instrumented) that the obtuse pile sustains more loading when the loading is in the obtuse corner than the acute piles sustain when the loading is in the acute corner. This is a consequence of the skew.

#### 5.3.1.4. Fully Fixed Piles versus Piles to Shallow Bedrock

The comparisons made in Section 5.3.1.3 referring to the effects of skew can also be applied to the comparison of the differences between the two abutments. The critical stresses and axial loads for the near-obtuse and near-acute piles of the south and north abutment were compared for corresponding loadings (cases #4 and #9, cases #6 and #7, cases #11 and #13, and cases #2 and #10) (refer to Figure 5.2). The piles were also compared for the centered load case, #12. For corresponding loadings, the two abutments saw comparable loads.

The comparison of total stresses due to the live loads, however, shows a different trend. The near-obtuse pile of the south abutment (pile G2-S) consistently saw larger stresses than the near-obtuse pile of the north abutment (pile G3-N). Pile G3-S, however, saw smaller stresses than its northern counterpart, G2-N*; both near acute piles. The south obtuse pile (G1-S*) saw consistently higher axial loads than the north obtuse pile (G4-N*). The western piles of both abutments saw more stress than the eastern piles. The bedrock slopes downward from east to west. It is unclear if there is a connection between these two observations.

The overall stress along the length of the pile typically diminished with depth along the length of pile. The axial loads also tended to diminish along the length of the pile. Piles G2-N* and G4-N* were exceptions to this trend; the middle set of strain gages sees larger loads than the high set gages for pile G2-N* during load cases #7-#12 and during all load cases for pile G4-N*. The axial load diminished along the length of the pile to a much lesser degree along the north piles than the south piles. The south piles are 3 m to 4.3 m (10 ft to 14 ft) longer than their northern counterparts; therefore there were likely more frictional effects in the south piles. The north piles behaved like end-bearing piles. The long piles deformed in double curvature along the weak axis. The strong axis moment typically decreased with depth along the length of pile. Torsional effects were found to be insignificant for the south piles, but torsional effects accounted for up to 29% of the critical stress (Table 5.12) on the north piles.

### 5.3.2. Abutment and Pile Movements

The magnitudes of movement during live load testing, as recorded by the abutment and pile extensometers ranged from -0.403 mm (-0.016 in), corresponding to deck expansion, to 0.351 mm (0.014 in), corresponding to deck contraction.

#### 5.3.2.1. Skew

The movements determined from the corner pile and abutment extensometers as a result of the critical load cases for the corner piles were examined. The critical loadings for each test pile were determined in Section 5.3.1.1 based on pile stresses. Loading case #4 and #9 produced critical loadings for piles G4-N and G1-S, respectively. Piles G4-S and G1-N, both acute corner piles, were not instrumented with strain gages. The

corresponding load cases in the acute corners are assumed to cause critical loadings for the acute corner piles. The critical load cases were assumed to be case #6 for G4-S and case #7 for G1-N.

The extensometer on pile G1-S was compared with the SW abutment extensometer for load case #9 and the extensometer on pile G4-S was compared with the SE abutment extensometer for load case #6. In both cases, the pile extensometer had greater movements into the backfill than the abutment extensometer. This is consistent with the top of the abutment rotating inward due to the loading. This trend was also seen in the comparison between the extensometer on pile G1-N and the NW abutment extensometer for load case #7. The pile extensometer on pile G4-N had less movement into the backfill than the NE abutment extensometer for load case #4. Figures 5.7 a) and b) show an exaggerated sectional view of the movements of each corner pile under critical loading.

The extensometers on the south piles and abutment showed the abutment was rotating, or increasing the skew angle when the eastern girders of the bridge were being loaded (cases #1 - #6). When the load was applied to the western girders (loadings #7 - #10), the abutment tended to straighten out, or reduce the skew angle.

The north pile extensometers corresponded well with the south pile and abutment extensometers. The abutment tended to rotate when the eastern girders were being loaded while the abutment tended to straighten when the western girders were being loaded. The north abutment extensometers showed straightening of the abutment during load cases #1-#5, and #7-#9, and abutment rotation during loadings #6, and #10-#13.

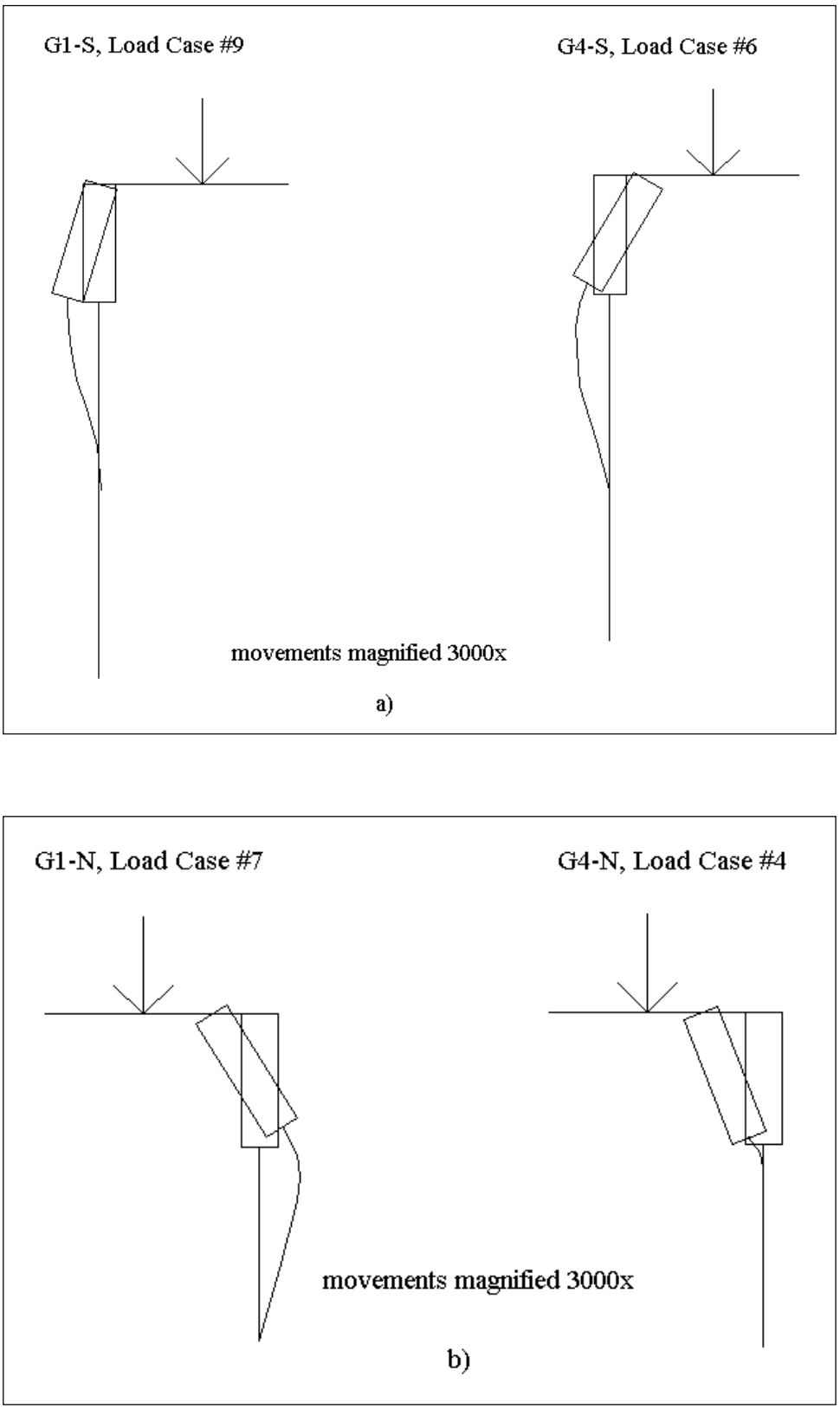


**Figure 5.7. Movements during critical loadings for G1-S, G4-S, G1-N and G4-N**

While the extensometers on the south piles and abutments both show rotating or straightening for the same load case, the extensometers on the north piles and abutments show contradicting abutment movements. Thus there is some complex movement of the skewed abutments during live loading.

5.3.2.2. Fully Fixed Piles versus Piles to Shallow Bedrock

Inclinometer surveys for piles G2-S and G3-N were compared during load case #5, and #8, respectively. These are corresponding piles, both near-obtuse, and corresponding loading cases. Figure 5.8 shows complementary movement, with both abutments showing rotation towards the bridge at the top of the abutment, and away from the bridge below the abutment. Pile G2-S is fixed at 6.4 m (21 ft) below final grade. Pile G3-N deforms in double curvature; it is not fully fixed, nor does it act like a true pinned support. This corresponds to the conclusions made by DeLano (2004). Figure 5.9 shows magnified pile movements from the finite element model created by DeLano (2004).

In Figure 5.8, the kink in G2-S at 1.5 m (5 ft) below finish grade corresponds to the cut off elevation of the pile. The steel inclinometer protective pipe is not continuous at this location and this is likely affecting the readings.

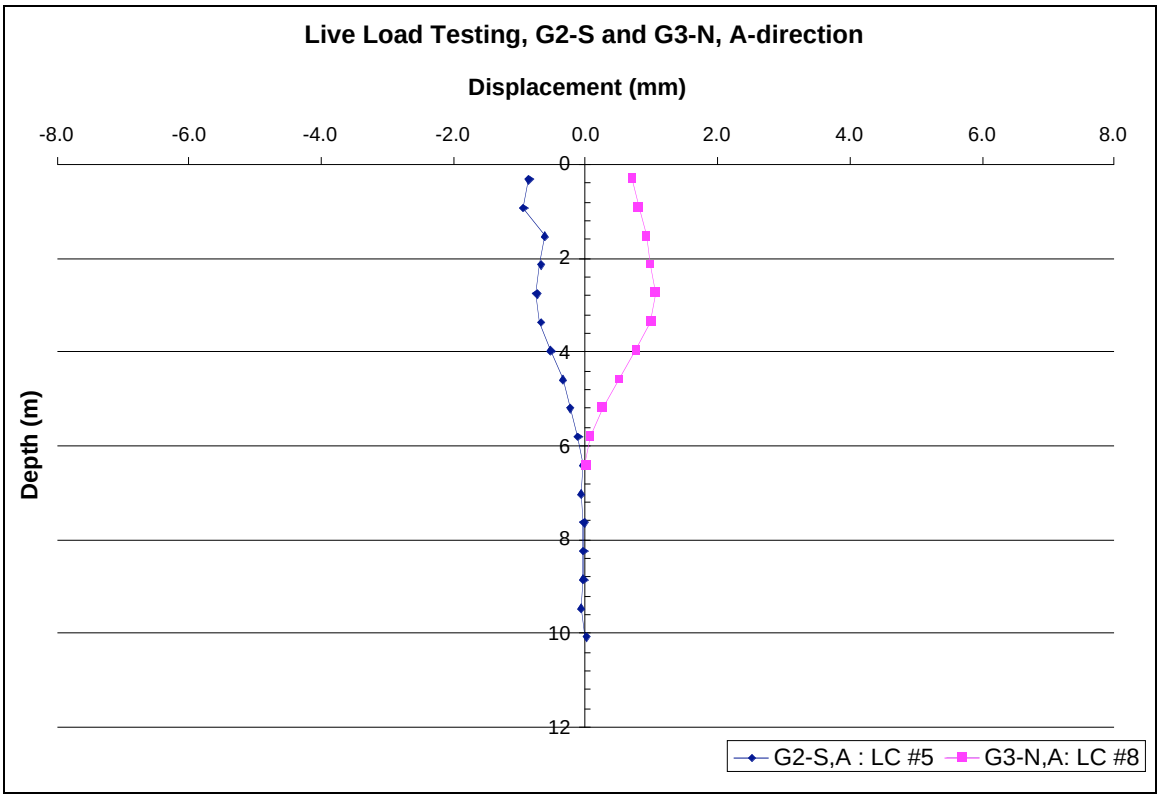


**Figure 5.8. Inclinometer data for piles G2-S and G3-N during live load testing**

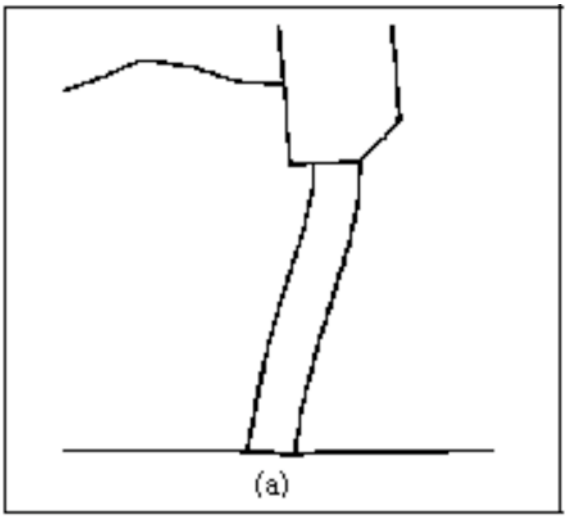


**Figure 5.9. Deflected shape of model pile (magnified 100x) (DeLano, 2004)**

### 5.3.3. Soil Pressures

The lower elevation pressure cells are located in the portion of the abutments below the construction joint, while the upper elevation cells are located in the portion of the abutments cast with the deck. The lower elevation cells are located 0.25 m (10 in) above the bottom of the concrete abutment, at elevation 378.20 and 378.05 for the south and north abutments, respectively. The upper elevation cells are located 0.25 m (10 in) above the construction joint, at elevation 379.40 and 379.25 for the south and north abutments, respectively. The upper cells for the south and north abutments are 0.6 m and 0.4 m (2 ft and 1.6 ft) below the bottom of the approach slabs, respectively. The position of each earth pressure cell on the face of the abutment can be seen in Figures 3.1 and 3.2.

#### 5.3.3.1. Vertical Rotation of Abutments

The lower elevation cells have considerably larger soil pressure increases due to the live load than the upper elevation cells, as shown in Table 5.11. The lower elevation pressure cells, on both abutments, indicate larger pressure increases when the live loading is near the pressure cells. This indicates the vertical rotation of the abutment similar to the movements shown in Figure 5.7.

#### 5.3.3.2. Skew

The lower elevation pressure cell on the obtuse corner of the north abutment indicates larger increases than the acute cell when the trucks are positioned near the obtuse corner (case #4), and vice versa (case # 7). The pressure decreases as the trucks move down the span, towards the opposite abutment. When the trucks are centered in the bridge lanes, loadings #11 - #13 (Figure 5.2.b), the obtuse cells show greater earth

pressure increases than the acute cells, as the load is applied closer to the obtuse corner of the abutment. Higher earth pressures at the obtuse corner indicate that the abutment moves into the earth more at the obtuse corner than at the acute corner.

The upper elevation pressure cells do not follow a specific trend as closely as the lower elevation cells. The cells on the north abutment indicate larger pressure increases on the corner opposite to loading, i.e. when the north obtuse corner is loaded, the north acute corner registers the larger soil pressure increases and when the north acute corner is loaded the north obtuse corner registers larger increases. The cells on the south abutment suggest a different trend. The acute corner registers larger pressure than the obtuse corner, during both acute and obtuse loadings.

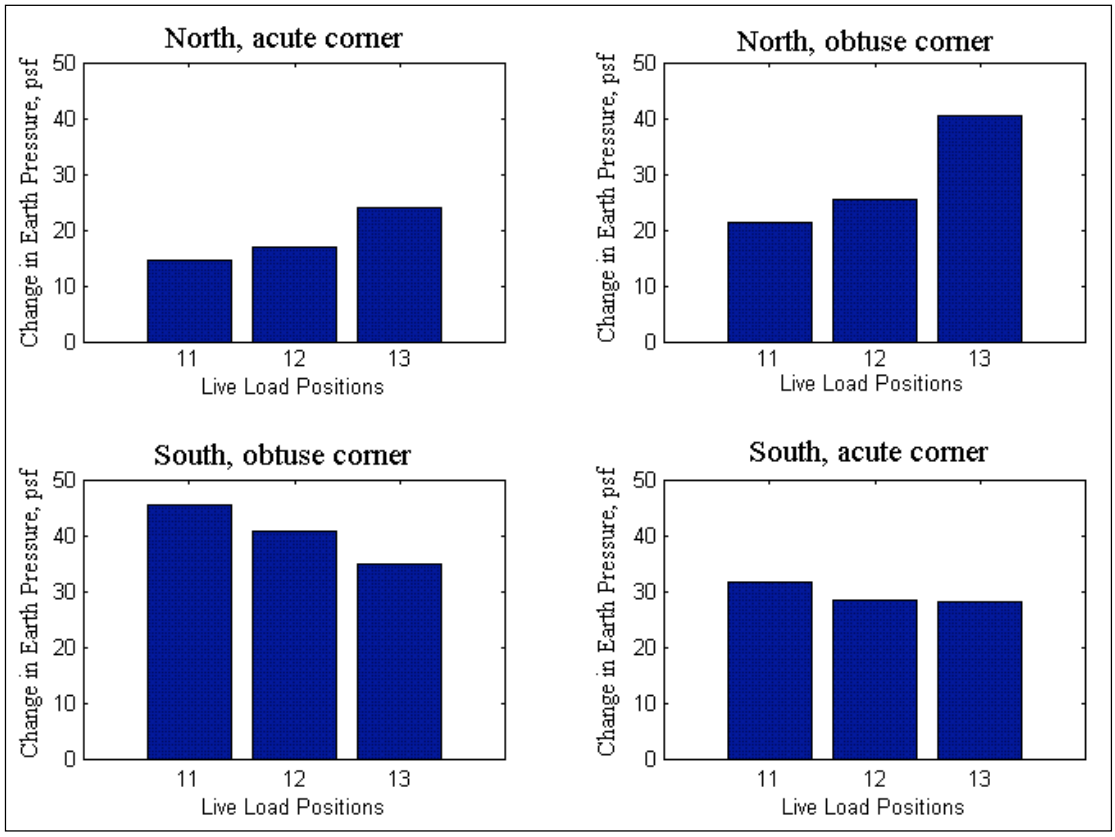


**Figure 5.10. Change in earth pressure on the upper portion of the abutments during loading cases #11, #12, and #13**

For loadings #11, #12, and #13, the upper elevation pressure cells agree with the lower elevation pressure cell sets; they show that the obtuse corners have considerably higher soil pressure increases than the acute corners, as seen in Figure 5.10. The earth pressure on each abutment increases as the truck moves towards the other abutment, i.e. the earth pressure behind the south abutment increase as the truck moves from the south abutment towards the north abutment.

The changes in earth pressure for the progression of a truck along the bridge corresponds to the increasingly negative weak axis moment, i.e. as the load nears a given abutment, the upper part of the abutment is pulled towards the centerline of the bridge.

5.3.3.3. Fully Fixed Piles versus Piles to Shallow Bedrock

The live loading caused greater pressure increases on the south abutment with fully fixed piles, than on the north abutment with short piles to shallow bedrock. For corresponding loadings of #4 (N) versus #9 (S), #7 (N) versus #6 (S), #5 (N) versus #8 (S), #2 (N) versus #10 (S), and #11 (N), versus #13 (S), the maximum change in pressure is always higher for the south abutment (Table 5.11). This indicates more movement into the soil on the south abutment than on the north abutment as a result of live loading.

For live load positions #11, #12, and #13 where the live load progresses from the north to the south, the south abutments have higher pressures in the upper pressure cells for corresponding load positions as shown in Figure 5.10. This indicates more rotation into the soil on the south abutment than on the north abutment, due to the live loading.

## 5.4. Conclusions

### 5.4.1. Pile Stresses

The critical stress was determined as the largest negative stress calculated at the edge of the flanges of the pile. The critical location on the cross-section of the pile followed an expected trend as well. The piles have the largest induced stresses when the trucks are positioned closest to the pile being studied. Overall stresses (due to dead load and live load) decreased, for the most part, as the trucks moved away from the given pile.

The largest critical stress due to dead and live loading was calculated to be -187.8 MPa (-27.2 ksi) for pile G1-S* under loading condition #9. Not included in this critical stress are residual stresses from pile driving and stresses caused by the weight of the portion of the abutment below the construction joint. The average stresses from the instrumented piles for these two events are -16 MPa (-2.32 ksi) and -15.6 MPa (-2.27 ksi), respectively. With an average measured yield stress of 407 MPa (-59 ksi) for the piles, there is ample of room for additional stress from thermal loading.

It was found that the skew affected the magnitude of axial load for different load positions. For centered loadings (#11-#13), the near-obtuse piles (G2-S and G3-N) see higher axial loads than the near-acute piles (G3-S and G2-N*). However, for eccentric loadings in which the trucks are bumper to bumper in each corner of the bridge (cases #4, #6, #7, and #9), the near-acute piles see larger loads for the acute loading than the near-obtuse piles see for obtuse loadings. This observation is significant because it implies that the acute piles may see larger axial loads during acute loadings than the obtuse piles saw during obtuse loadings. During the construction sequence, the near-obtuse piles (G2-

S and G3-N) experience the largest axial loads (refer to Chapter 4); this is likely due to the fact that loads are distributed more centrally during the construction sequence, i.e. no large, eccentric loadings.

During live loading, the sum of the axial loads in the instrumented piles was approximately 48% of the total live load, 571.4 kN (128.5 kips). This implies that the soil supporting the abutment in bearing and shear is supporting part of the live load. This trend was also found during the construction sequence with the casting of the deck. The tributary weight of the deck (assuming an equal load distribution) was not seen in the instrumented piles for eight days. The weight of the bridge and test loading trucks was calculated to be 4605 kN (1035 kips). The average measured axial load in the instrumented piles due to dead load and live load was 3633 kN (817 kips), or 79% of the total applied load.

Stresses tended to decrease with depth along the length of the piles. These stresses and loads diminished to a lesser degree on the north piles compared to the south piles. This is believed to be due to frictional losses along the pile; the south piles have a greater length for losses to develop. The north piles behaved like end-bearing piles. It was determined that the maximum stresses are no more severe in the north (short) piles than the south (long) piles.

The stresses were found to be greater in the western piles than the eastern piles, for both abutments; the western piles are slightly longer than the eastern piles. Piles G2-S and G3-N consistently saw larger stresses when compared to the corresponding pile on the opposite abutment. When the eastern girders (G3 and G4) were loaded, the stresses

were distributed more evenly than when the west girders (G1 and G2) were loaded. There was less difference in transverse distribution in the north piles than the south piles; there was also less difference in bedrock elevation between the four north piles as compared to the four south piles. Although the sloping bedrock may have affected pile stresses, the location of the temporary bridge on the eastern side of the new bridge may also have affected stresses on the piles on that side.

### 5.4.2. Pile and Abutment Movements

All extensometers installed on piles indicate the abutments were rotating (increasing the skew angle) when the acute side of the bridge was being loaded and the abutments are straightening out when the obtuse side of the bridge is being loaded. The results of the abutment extensometers were less clear. The south abutment extensometers results concurred with the pile extensometers, while the north abutment extensometers suggested abutment straightening for all loadings.

The corner pile and abutment extensometers were examined due to the critical load case for the corner being studied. The pile extensometers at the particular corner had greater movements into the backfill than the abutment extensometers for all corners except the north west corner. This is consistent with the top of the abutment rotating into the deck due to the loading, and the bottom of the abutment rotating into the backfill. The earth pressure cells agreed with this trend. The lower elevation pressure cells showed larger increases in pressure during critical loading than the upper elevation pressure cells, which concurs with the extensometer data.

While the magnitudes of the inclinometer movements differed from the extensometer movements, it is believed, however, that inclinometer results can be used to

accurately compare the deformed shape of the piles. The inclinometer data showed the longer south piles are fixed at some depth, while the short north piles do not develop full fixity, nor do they act as a true pinned support.

### 5.4.3. Earth Pressure

The lower earth pressure cells register larger pressures than their upper counterparts. Both north and south sets indicate higher pressure increases at the corner where the load is being applied, which agrees with the pile and south abutment extensometers. The upper pressure cells are inconsistent with regard to location of load and elevated earth pressure.

Both lower and upper sets of both abutments indicate higher earth pressures in the obtuse corner during lane-centered loadings (#11-#13). During lane-centered loadings, one truck is closer to the obtuse corner than the other truck is to the acute corner.

# Chapter 6

## SUMMARY, CONCLUSIONS AND RECOMMENDATIONS

This chapter provides a summary of the work completed on Phase II of the development of design guidelines for short piles supporting integral abutment bridges. Phase II covers the performance monitoring of a constructed bridge, the calibration of a finite element model from the performance data, and use of the monitoring results and the finite element model to develop final design guidelines. Under the first task of Phase II covered herein, the installation of instrumentation of an integral abutment bridge founded on short piles at the Coplin Plantation site is described. The first task includes performance monitoring during bridge construction and live load testing of the bridge. Conclusions drawn from the results of this research, as well as recommendations for areas of further study are also included.

### 6.1. Summary of Work Performed

The following sections provide a summary of the major components of this report. For a more detailed explanation of processes and results, please refer to the appropriate chapter.

#### 6.1.1. Construction of Integral Abutment Bridge

Results based on work completed by DeLano (2004) in Phase I of this study, including the development of the finite element modeling and parametric study, suggest that it is indeed feasible to construct integral abutments in some areas with shallow bedrock. As a means to gather more extensive data regarding the behavior of short piles

supporting integral abutment bridges, a bridge was constructed and instrumented over Nash Stream in Coplin Plantation, in western Maine. The Coplin Plantation site offered a unique opportunity to investigate possible differences in short and long pile behaviors, as well as the effects of a relatively large skew, 35-degrees. The south abutment has a depth of overburden sufficient to achieve pile fixity, while the north abutment has insufficient overburden to achieve pile fixity.

The bridge crossing Nash Stream in Coplin Plantation, ME spans 30 m (98 ft) and was 10 m (32.8 ft) wide. Each abutment was supported by four- HP360x132 (HP14x89) grade 50 steel H-piles driven to bedrock oriented with the weak axis perpendicular to the direction of traffic. The bedrock was found to slope from east to west beneath both abutments. The piles supporting the south abutment were 7 -8.7 m (23-28 ft) long while the piles supporting the north abutment were only 4.1 to 4.25 m (13.5-14 ft) long.

Site work commenced on Day 127 (May 6, 2004); the bridge was completed and opened to traffic on Day 281 (October 7, 2004). Instrumentation of the bridge included seventy-two strain gages, twelve extensometers, nine thermistors, eight pressure cells, eight inclinometers, two vibrating wire piezometers, and one standpipe piezometer.

Instrumentation of the bridge allowed the researchers to investigate the stresses in the piles, the movement of the piles and abutments, the soil pressure behind each abutment, the pore pressure behind each abutment, and the temperatures of the concrete deck, steel girders, and air.

### 6.1.2. Analysis of Construction Sequence

The stresses in the piles as derived from the strain gages, the movements of the piles and the abutments (extensometers and inclinometers), the soil pressures (pressure cells) were determined for each construction event. All readings were relative to some initial condition; the initial condition for the strain gages and extensometers on the piles was set when all instruments were operational to make comparisons easier. This time was after the portion of the abutments below the construction joint was cast, but before the girders were set in place. The stresses and movement changes before this initial time were based on fewer instruments.

A set of four linear equations was written to express the four internal pile forces (axial load, strong-axis bending, weak-axis bending and a torsional moment) as a function of strains, the pile elastic modulus, and cross-sectional member properties. The four equations were solved for the four member forces using the four strains from a set of gages. The system of linear equations was only valid if the stresses in the pile did not exceed the yield stress of the pile, which was always the case.

Of the 112 instruments installed, only four strain gages and one extensometer were lost during construction, giving a success rate of 96%. A least squares regression was developed to correct for the four faulty strain gages. This correction method was used for three of the faulty gages; it did not produce reasonable results for one of the incomplete strain gage sets. It was assumed that due to its rigidity, the abutment remained planar, and therefore the missing extensometer data could be linearly interpolated from other extensometer readings.

The effect of each construction event was found by comparing readings from before and after the event. Whenever possible, before and after readings were taken at 5:00 am on the day of the event and on the day after the event, respectively. Because the data acquisition systems were not fully functional until the day following the deck pour, the first few events do not have a complete set of data.

The weight of the bridge was calculated and compared to the axial loads seen in the instrumented piles. The weight of deck was not immediately transferred to piles; some load was transferred to the soil. The tributary load of the calculated bridge deck weight (assuming an equal load distribution) was steadily transferred to the instrumented piles over approximately eight days. The strong-axis moment was large immediately after the deck pour and eventually dissipated; the weak-axis moment increased as the strong-axis moment decreased. Upon completion of paving the bridge crossing Nash Stream in Coplin Plantation, the sum of the axial loads computed from the strain data for the six test piles was 3047 kN (685 kips). The corresponding calculated weight of the bridge for the six test piles assuming an equal load distribution was 2991.4 kN (672.5 kips), a 2% difference. However, loads are not equal in the piles.

The average critical stress breakdown at the end of construction for the instrumented piles is as follows: percentage due to axial load 37%, percentage due to strong-axis moment 6%, percentage due to weak-axis moment 56%, and percentage due to torsion 1%.

Throughout the construction process the interior piles of both abutments carried more dead load than the piles further from the centerline. The near-obtuse piles (G2-S

and G3-N) sustained the largest loads. The area of the bridge deck beyond the outside girders was less than one-half the area between the girders.

The inclinometers that monitored pile movement showed similar movements between the south and north piles. The top of the inclinometer pipe, which was cast in the abutment, shows contraction of the bridge deck, while the pile below the bottom of the abutment showed movement into the backfill. The south (long) piles were fixed at some depth, but the north (short) piles were not fully fixed, nor did they act like a true pinned support.

### 6.1.3. Live Load Testing

Live loading was completed on the bridge on Day 281 (October 7, 2004). The bridge was loaded using two Maine Department of Transportation (MaineDOT) dump trucks weighing a total of 571.4 kN (128.45 kips). Thirteen loading positions were chosen to magnify the difference in responses from the south abutment piles with sufficient fixity and those of the north abutment without fixity, as well as the effects of the large skew. Each position was held for nine minutes, allowing for three sets of data to be taken for each loading.

Diurnal temperature variations were found to significantly affect the live load data. To compensate for the temperature changes on the day of the test loading, the effects of temperature changes on days without test loading were obtained. Days 282 and 287 (October 8 and 13), days with no live load testing, have deck temperatures slightly higher and slightly lower, respectively, than Day 281. Data for all vibrating wire instruments was interpolated for Day 281 between the readings from Days 282 and 287

on the basis of the temperatures. These values were considered to reflect the in situ bridge conditions, if live loading had not taken place. The difference between the readings during the test loadings and the interpolated values for no live load was taken to be the result of live loading.

As expected, stresses tended to be largest in the pile closest to the load. The average breakdown for all instrumented piles under all load cases reveals that the weak-axis moment was the largest component at 50% of the critical stress. The axial load was the next largest component with 29%. The strong-axis moment and torsion made up the remaining 21%. The axial loads tended to decrease with depth along the length of the pile, especially for the southern, longer piles. Weak axis moments showed the piles deforming in double curvature. Strong axis moments proved to be significant is some cases.

The largest axial load, seen by pile G1-S* during loading case #9 (see Figure 5.2), was 162 kN (36 kips). The sums of the measured axial loads on the instrumented piles during live load testing were, on the average, only 48% of the total applied live load - 571.4 kN (128.5 kips).

## 6.2. Conclusions

The maximum measured pile stress due to the dead load and maximum test live load (axial, weak-axis bending, strong-axis bending and torsion) combined was -187.8 MPa (-27.2 ksi), in pile G1-S*. This value does not include the additional -16 MPa (-2.32 ksi) average stresses measured in the piles due to pile driving and -15.6 MPa (-2.27 ksi) average stresses measured for the lower portion of the abutments. The dead and live loads (including an average value for the lower portion of the abutment) gave significant

stresses to the piles, i.e., up to 59% of the nominal yield stress of -345 Mpa (-50 ksi) or 50% of the measured yield stress of -407 MPa (-59 ksi). The effect of the seasonal variation is not included and will be measured in the next task of Phase II monitoring.

Although many departments of transportation in the United States (Maine not included) design piles for axial load only (Kunin and Alampalli, 2000), axial load is only one component of dead load stress in piles. Further, for this bridge, stress from weak-axis bending (bending along centerline) was found to be the largest component of dead load stresses at an average 63% (51% to 78%) of the total stress. This bending arises from the pile rotation caused by abutment rotation from dead load on the girders. The next largest component was the axial load at 31% (20% to 47%) of the total, followed by strong-axis bending (bending perpendicular to centerline) at 9% (-2% to 25%), and torsion, -2% (-13% to 9%). For seasonal temperature changes, Girton et al. (1991) monitored two skewed bridges in Iowa supported by H-piles oriented with the weak axis movement parallel to the longitudinal direction. Girton et al. (1991) found weak-axis bending to induce the highest strains, similar to the results from the Coplin Plantation Bridge. Girton et al., however, found the second largest strains to be due to strong-axis bending, followed by relatively smaller axial and torsional strains. Thus it is expected that stress contributions from bending will continue to increase during seasonal temperature changes.

The abutments underwent vertical rotation with the extensometers on the abutments showing movements into the bridge, while extensometers on the top of the piles showed movements away from the bridge. This corresponded to the application of

weight to the bridge causing the deck to bend and to pull in the abutments. This caused the weak-axis bending stresses in the piles. This trend was also seen in the parametric studies using the finite element model created in Phase I of this study.

Of the construction events examined in this study, the casting of the deck concrete had the largest effect on the stresses in the piles. The weight of the deck induced a load to the supporting piles, and the bending moments changed significantly during this event. The axial and bending stresses continued to increase during eight days after the deck pour. The remaining construction events, including placing of girders, casting and backfilling the approach slabs, casting the curbs, and paving, all had additional smaller effects on the pile stresses. They also showed a time lag in the application of the load to the piling. It is believed that the time lag occurred since initially the load was carried by the soil bearing under the abutment and that this load was transferred with time to the piles.

The maximum stress in a pile from the live load test was -41.2 Mpa (-6.0 ksi) that was 28 % of the dead load stress. This stress occurred when the total live load of 572 kN (128 kips) was at an obtuse corner. The bending stress was the most significant part of total live load stress with the weak axis bending stress at 65 % and the strong axis stress at 16 %. The axial stress was only 20 % of the total live load stress. During the live load test, the piles carried only 60 % of the applied live load while bearing beneath the abutment carried the remaining portion.

There was significant variability in the axial loadings to individual piles at the Nash Stream site in Maine. Although part of this variability may be attributed to the 35˚

skew and the different fixity conditions for the piles, different soil conditions under the abutment may have also led to variability. The stresses were found to be greater in the western piles than the eastern piles, for both abutments. The western piles were slightly longer than the eastern piles. Additionally, the temporary bridge was located on the eastern side and may have caused unbalanced loading. During the construction sequence and centered live loadings, the near-obtuse piles (G2-S and G3-N) carried the largest axial loads as these piles have the largest tributary deck area near the piles. The obtuse piles would normally have the most induced load (most tributary deck area for equal spacing of girders), but the width of the cantilevered part of the deck is less than half the distance between girders. Directly after construction the maximum stress in one pile due to dead load was 1.55 the mean maximum stress for all piles, and the lowest stress was 0.63 of the mean stress.

Skew of the abutments affected the distribution of axial loadings to the piles as a result of the difference in tributary area of deck for a given pile as previously noted. Skew also appeared to be related to the stress in bending perpendicular to the centerline (strong-axis bending for this design) as this stress had a different direction of movement on each abutment corresponding to the different location of the obtuse corner on each abutment. A large positive moment in strong-axis bending occurred during the placing of the deck concrete that appeared to be related to the different weight of concrete on each side of the skewed deck at the abutments. During the construction process, the obtuse side of the abutments moved into the backfill more than the acute side, suggesting the abutment was straightening. This was seen in both the extensometers and earth pressure cells. During backfill behind the abutment and development of abutment rotation, a

negative moment occurred in strong-axis bending. The net result at the end of construction for the strong-axis bending was the sum of the large positive moment and an even larger negative moment resulting in a low negative moment by the end of construction. Since the sources of these two moments appear to be different, the conditions for both moments being about the same magnitude may not occur on other projects.

The inclinometer data showed the long south piles were fixed at some depth, while the short north piles did not develop fixity, nor did they act as a freely pinned support. It appeared that the contacts on the north end rotated at the rock with soil support above the rock providing some fixity. The stresses, especially the bending stresses, in the north (short) piles were less than the stresses in the south (long) piles. The variability of load appeared to be higher for the shorter north piles than for the south piles. The short north piles behaved more like end-bearing piles with less loss of stresses with depth as compared to the deeper south piles.

### 6.3. Recommendations

Stresses from bending developed by rotation of the abutment under the dead load should be included as part of the design load in the supporting piling for an integral abutment bridge.

When skew is present, stresses in piles from bending perpendicular to centerline should be included as part of the pile design load. Final design guidelines should account for the effects of skew under a variety of Maine conditions. A three-dimensional finite-element model will be required to account for skew.

Pile-to-pile variability of axial load and moment stresses due to dead load should be considered in the design of piles. The results of this investigation indicate that the maximum stress is approximately 1.5 of the mean stress and the minimum stress is approximately 0.67 of the mean stress for axial loads and moments.

Where bedrock is shallow, piles to bedrock at a depth less than that required to develop fixity do not see more stress under dead and live load than piles that develop fixity.

It is strongly suggested that in future bridge instrumentation the girders be instrumented with strain gages so that load distribution from the deck can be more accurately determined. Also, especially if the bridge is skewed, it is very important that all piles should be instrumented, at least at the top level.

## REFERENCES


AASHTO (1998). Standard Specifications for Highway Bridges. Washington, D.C. American Association of State Highway and Transportation Officials. 16th Edition.

Abendroth, R.E.; Greimann, L.F.; and Ebner, P.B. (1989). Abutment pile design for jointless bridges. Journal of Structural Engineering. Vol. 115, No. 11. pp. 2914-2929.

Alberta Transportation (2003). Appendix C – Guidelines for Design of Integral Abutments. Alberta Transportation Bridge Design Manual.

Amde, A.M.; Chini, S.A.; and Mafi, M. (1997). Model study of H-piles subjected to combined loading. Geotechnical and Geological Engineering. Vol. 15. pp. 343-355.

Arsoy, S.; Barker, R.M.; and Duncan, J.M. (1999). The behavior of integral abutment bridges. Virginia Transportation Research Council, Final Contract Report No. VTRC 00-CR3.

Arsoy, S.; Duncan, J.M.; and Barker, R.M. (2002). Performance of piles supporting integral bridges. Transportation Research Record #1808. pp. 162-167.

ASTM A 370-97a, "Standard Test Methods and Definitions for Mechanical Testing of Steel Products." ASTM International.

Broms, B.B. (1964a). Lateral resistance of piles in cohesive soils. Journal for Soil Mechanics and Foundation Engineering. Vol. 90, SM2. pp. 27-63.

Broms, B.B. (1964b). Lateral resistance of piles in cohesionless soils. Journal for Soil Mechanics and Foundation Engineering. Vol. 90, SM3. pp. 123-156.

Burdette, E.G.; Wasserman, E.P.; Goodpasture, D.W.; and Deatherage, J.H. (1999). Field performance of integral abutment bridges in Tennessee. Transportation Research Record #00404. pp. 1-11.

DeLano, J.G. (2004). Behavior of pile-supported integral abutment at bridge sites with shallow bedrock. M.S. Thesis, Department of Civil and Environmental Engineering, The University of Maine, May 2004.

Diceli, M.; Eng, P.; and Albhaisi, S.M. (2003). Maximum length of integral bridges supported on steel H-piles driven in sand. Engineering Structures. Vol. 25. pp. 1491-1504.

Duncan, J.M. and Arsoy, S. (2003). Effect of bridge-soil interaction on behavior of piles supporting integral bridges. Transportation Research Record #1849. pp. 91-97.

Ensoft, Inc. (2002). Computer program L-PILE Plus, Version 4.0M.

Faraji, S.; Ting, J.M.; Crovo, D.S.; and Ernst, H. (2001). Nonlinear analysis of integral bridges: finite element model. Journal of Geotechnical and Geoenvironmental Engineering. Vol. 127, No. 5. pp. 454-461.

Girton, D.D.; Hawkinson, T.R.; and Greimann, L.F. (1991). Validation of design recommendations for integral-abutment piles. Journal of Structural Engineering. Vol.117, No. 7. pp. 2117-2134.

Greimann, L.F.; Yang, P.; and Wolde-Tinsae, A.M. (1986). Nonlinear analysis of integral abutment bridges. Journal of Structural Engineering. Vol. 112, No. 10. pp. 2263-2280.

Greimann, L. and Wolde-Tinsae, A.M. (1988). Design model for piles in jointless bridges. Journal of Structural Engineering. Vol. 114, No. 6. pp. 1355-1369.

Greimann, L.F.; Abendroth, R.E.; Johnson, D.E.; and Ebner, P.B. (1987). Final report: Pile design and tests for integral abutment bridges. College of Engineering, Iowa State University.

Highways Agency (1996). The design of integral bridges. Design Manual for Roads and Bridges. The Highways Agency. London, U.K. Vol. 1, Section 3, Part 12. BA 42/96, Amendment #1.

Husain, I. and Bagnariol, D. (1996). Integral abutment bridges. Ministry of Transportation, Ontario, Canada. Structural Office Report No. SO-96-01.

Husain, I. and Bagnariol, D. (2000). Design and performance of jointless bridges in Ontario. Transportation Research Record #1696. pp. 109-121.

Ingram, E.E.; Burdette, E.G.; Goodpasture, D.W.; and Deatherage, J.H. (2003). Evaluation of applicability of typical column design equations to steel H-piles supporting integral abutments. AISC Engineering Journal. Q1, pp. 50-58.

Jorgenson, J.L. (1983). Behavior of abutment piles in an integral abutment in response to bridge movements. Transportation Research Record #903. pp. 72-79.

Krusinski, L. (2002). Project Research Progress Report: Design and Construction of Pile-Supported Integral Abutments at Bridge Sites with Shallow Bedrock. University of Maine, Department of Civil and Environmental Engineering. Unpublished, Volumes 1-3.

Kunin, J. and Alampalli, S. (2000). Integral abutment bridges: current practice in United States and Canada. Journal of Performance of Constructed Facilities. Vol. 14, No. 3. pp. 104-120.

Lawver, A.; French, C.; and Shield, C.K. (2000). Field performance of integral abutment bridges. Transportation Research Record #1740. pp. 107-117.

Lehane, B.M.; Keogh, D.M.; and O'Brien, E.J. (1999). Simplified elastic model for restraining effects of backfill soil on integral bridges. Computers and Structures. Vol. 73. pp. 303-313.

MacGregor, J.G. and Wight, J.K. (2005). Reinforced Concrete Mechanics and Design. 4th Ed. Upper Saddle River, NJ. Prentice Hall.

Mistry, V.C. (2000). Integral abutment and jointless bridges. Retrieved October 1, 2002, from http://www.nabro.unl.edu/articles/20002012/download/vasant.pdf

Mourad, S. and Tabsh, S.W. (1998). Pile forces in integral abutment bridges subjected to truck loads. Transportation Research Record #1633. pp. 77-83.

Roctest: Model ERI (2000). Instruction Manual for Vibrating Wire Fill Extensometer. pp.1-7.

Roctest: Model PWS (2000). Instruction Manual for Vibrating Wire Piezometer. pp.1-7.

Roctest: Model SM-5A (2000). Instruction Manual for Vibrating Wire Surface Strain Gage. pp.1-7.

Roctest: Model TH-T (2000). Instruction Manual for Temperature Sensor. pp.1-6.

Roctest: Model TPC (2000). Instruction Manual for Vibrating Wire Total Pressure Cell. pp.1-19.

Taylor, H.P.J. (1999). Progress with integral bridges in the United Kingdom. Preprint CD-ROM, TRB 1999 Annual Meeting, January 11-14, Washington, D.C.

Wang, S.T. and Reese, L.C. (1993). COM624P – Laterally Loaded Pile Analysis Program for the Microcomputer, Version 2.0. Washington, D.C. United States Department of Transportation, Federal Highway Administration.

Wasserman, E.P. and Walker, J.H. (1996). Integral abutments for steel bridges. Highway Structures Design Handbook. Structures Division, Tennessee Department of Transportation. Vol. 2, Chapter 5.

# APPENDIX

# Appendix A

## SITE INFORMATION

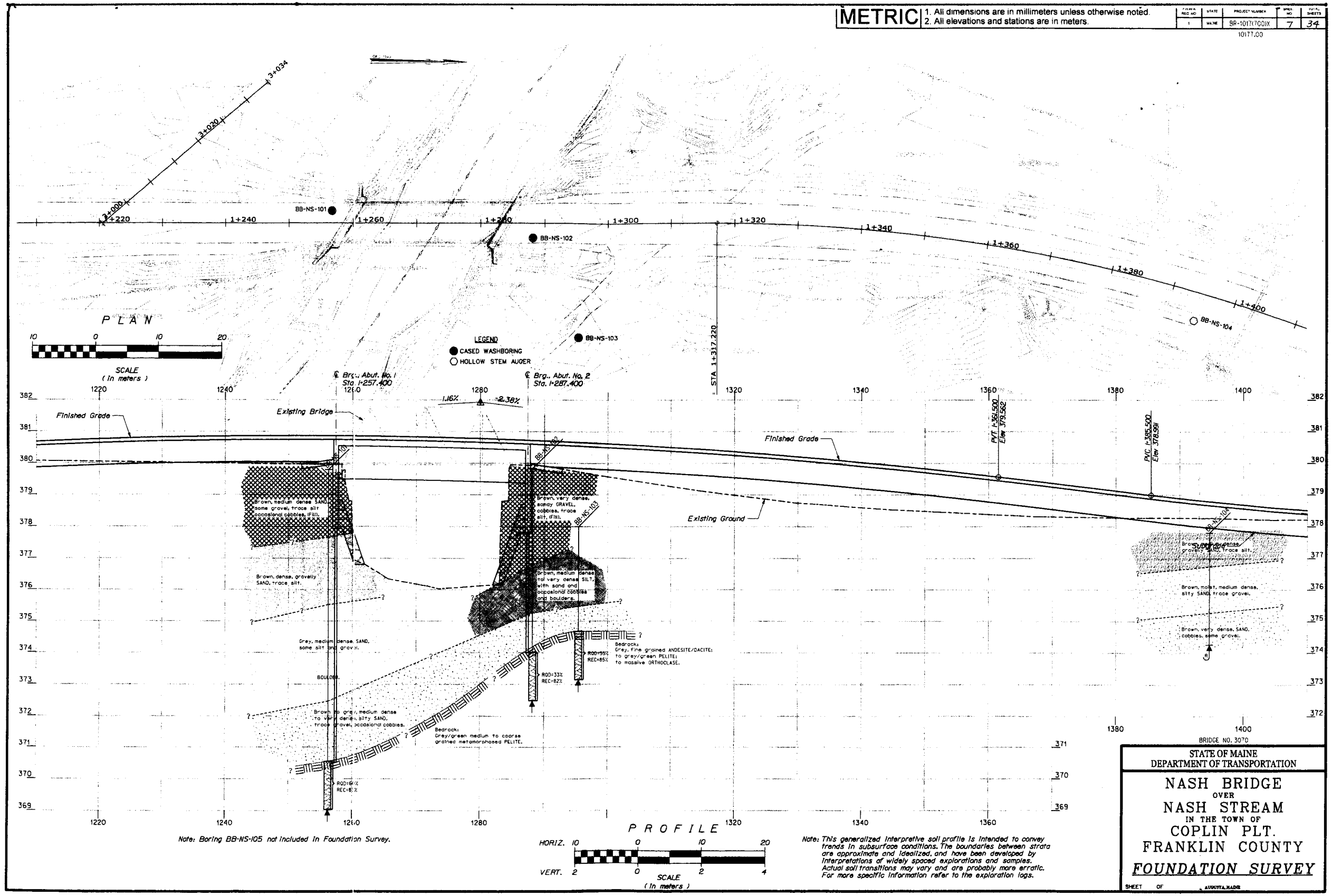


**Figure A.1. Plan and profile view of bridge in Coplin Plantation**

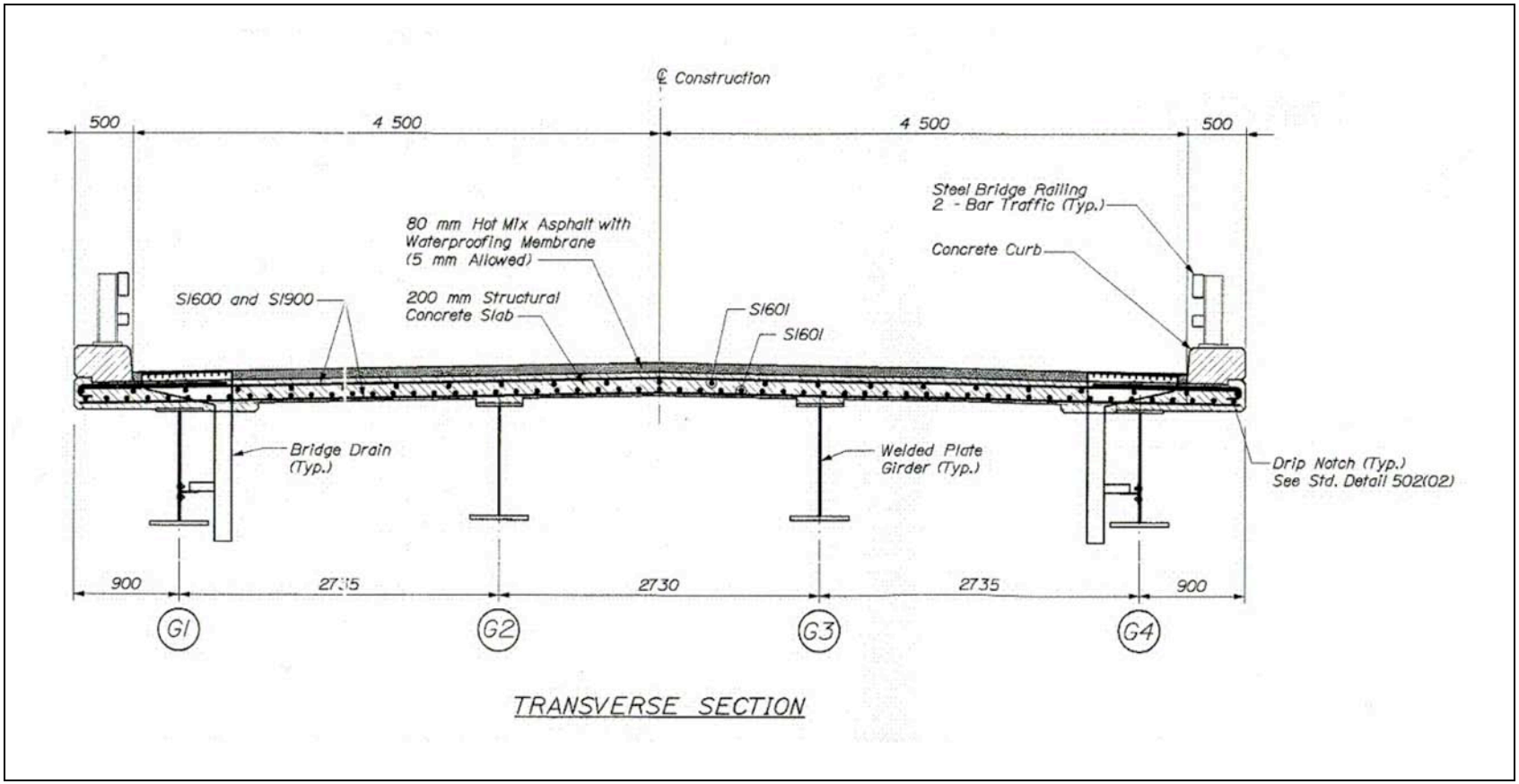


**Figure A.2. Typical cross-sectional view of bridge in Coplin Plantation, looking north**

**Maine Department of Transportation**

Soil/Rock Exploration Log
METRIC UNITS

**Project:** NASH STREAM BRIDGE, ROUTE 16
**Location:** COPLIN PLT.

**Boring No.:** BB-NS-101
**PIN:** 10177.00

| | | | | | |
|---|---|---|---|---|---|
| **Driller:** | MDOT | **Elevation (m):** | 379.84 | **Auger ID/OD:** | 100 mm |
| **Operator:** | C.MANN | **Datum:** | NGVD | **Sampler:** | STANDARD SPLIT SPOON |
| **Logged By:** | G.LIDSTONE | **Rig Type:** | CME 45C | **Hammer Wt./Fall:** | 63.5 kg/760 mm |
| **Date Start/Finish:** | 5/22/02-5/22/02 | **Drilling Method:** | CASED WASHBORING | **Core Barrel:** | NQ |
| **Boring Location:** | 1+256.2, 1.9 LT. | **Casing ID/OD:** | NW,75/88 mm | **Water Level*:** | 2.1 m BGS. |

Definitions:
D = Split Spoon Sample
MD = Unsuccessful Split Spoon Sample attempt
U = Thin Wall Tube Sample
R = Rock Core Sample
V = Insitu Vane Shear Test
SSA = Solid Stem Auger

Definitions:
$S_u$ = Insitu Field Vane Shear Strength (kPa)
$T_v$ = Pocket Torvane Shear Strength (kPa)
$q_p$ = Unconfined Compressive Strength (Pa)
$S_{u(lab)}$ = Lab Vane Shear Strength (kPa)
WOH = weight of 64 kg hammer
WOR = weight of rods

Definitions:
WC = water content, percent
LL = Liquid Limit
PL = Plastic Limit
PI = Plasticity Index
G = Grain Size Analysis
C = Consolidation Test

**Sample Information**

| Depth (m) | Sample No. | Type | Recovery (mm) | Penetration Resistance (Blows/0.15m) | Elev. (m) | Visual Description and Remarks | Laboratory Testing Results/ AASHTO and Unified Class. |
|---|---|---|---|---|---|---|---|
| 0 | | SSA | | | 379.75 | PAVEMENT. 0.09 | |
| | 1D | | 61.0/22.9 | 0.15 - 0.76 | 18/10/8/7 | 18 | Brown, dry, medium dense, fine to coarse SAND, some gravel, trace silt, (Fill). | |
| 1.2 | | | | | 378.47 | 1.37 | |
| | 2D | | 61.0/22.9 | 1.52 - 2.13 | 10/8/12/8 | 20 | Brown, dry, medium dense, gravelly SAND, occasional cobbles, trace silt, (Fill). | |
| 2.4 | | | | | 377.71 | 2.13 | Brown, wet, dense, gravelly fine to coarse SAND, trace silt. | |
| | 3D | | 61.0/20.3 | 3.05 - 3.66 | 11/12/18/25 | 30 | | G#98881 A-1-a, SW-SM WC=9.8% |
| 3.6 | | | | | 375.57 | 4.27 | Grey, moist, medium dense, fine to coarse SAND, some silt and gravel. | |
| | 4D | | 61.0/17.8 | 4.57 - 5.18 | 9/6/7/8 | 13 | | G#98882 A-2-4, SM WC=8.9% |
| 4.8 | | | | | | | | |
| 6 | | | | | | | | |
| | 5D | | 35.6/12.7 | 6.10 - 6.45 | 10/10/50(120) | --- | | |
| | R1 | NQ | 109.2/30.5 | 6.52 - 7.61 | | | 373.32 6.52 GRANITE BOULDER. R1: Core Times (min:sec) 6.52-6.8 (6:25) 6.8-7.1 (2:02) 7.1-7.4 (1:38) 7.4-7.61 (0:30) Rec'ed 100% | |
| 7.2 | | | | | 373.04 | 6.80 Grey, moist, medium dense, silty fine to coarse SAND, little gravel. | |
| | 6D | | 15.2/7.6 | 7.62 - 7.77 | 50 | --- | 372.52 7.32 Grey, damp, very dense, silty fine to coarse SAND, occasional cobbles, little gravel. Wased ahead of casing for 1.62 m. | |
| 8.4 | | | | | | | | |
| | 7D | | 10.2/5.1 | 9.14 - 9.25 | 50(100) | | 370.60 9.24 | |
| | R2 | | 152.4/127.0 | 9.24 - 10.76 | RQD = 60% | | Bedrock: Grey/green, medium grained metamorphosed PELITE: | |

**Remarks:**

Static water levels were not achieved.
Borings were located in field with tape.

Stratification lines represent approximate boundaries between soil types; transitions may be gradual.

* Water level readings have been made at times and under conditions stated. Groundwater fluctuations may occur due to conditions other than those present at the time measurements were made.

**Page 1 of aa**

**Boring No.:** BB-NS-101

**Figure A.3. Boring Log BB-NS-101**

| **Maine Department of Transportation**<br>Soil/Rock Exploration Log<br>METRIC UNITS | **Project:** NASH STREAM BRIDGE, ROUTE 16<br>**Location:** COPLIN PLT. | **Boring No.:** BB-NS-101<br>**PIN:** 10177.00 |
|---|---|---|

| | | | | | |
|---|---|---|---|---|---|
| **Driller:** | MDOT | **Elevation (m):** | 379.84 | **Auger ID/OD:** | 100 mm |
| **Operator:** | C.MANN | **Datum:** | NGVD | **Sampler:** | STANDARD SPLIT SPOON |
| **Logged By:** | G.LIDSTONE | **Rig Type:** | CME 45C | **Hammer Wt./Fall:** | 63.5 kg/760 mm |
| **Date Start/Finish:** | 5/22/02-5/22/02 | **Drilling Method:** | CASED WASHBORING | **Core Barrel:** | NQ |
| **Boring Location:** | 1+256.2, 1.9 LT. | **Casing ID/OD:** | NW,75/88 mm | **Water Level*:** | 2.1 m BGS. |

Definitions:
D = Split Spoon Sample
MD = Unsuccessful Split Spoon Sample attempt
U = Thin Wall Tube Sample
R = Rock Core Sample
V = Insitu Vane Shear Test
SSA = Solid Stem Auger

Definitions:
$S_u$ = Insitu Field Vane Shear Strength (kPa)
$T_v$ = Pocket Torvane Shear Strength (kPa)
$q_p$ = Unconfined Compressive Strength (Pa)
$S_{u(lab)}$ = Lab Shear Strength (kPa)
WOH = weight of 64 kg hammer
WOR = weight of rods

Definitions:
WC = water content, percent
LL = Liquid Limit
PL = Plastic Limit
PI = Plasticity Index
G = Grain Size Analysis
C = Consolidation Test

| Depth (m) | Sample No. | Type | Blows (0.15 m) | Recovery (%) | RQD | Elev. (m) | Visual Description and Remarks | Laboratory Testing Results/ AASHTO and Unified Class. |
|---|---|---|---|---|---|---|---|---|
| | | | Sample Information | | | | | |
| 9.6 | | | | | | | quartz, calcite, diopside and chlorite with trace pyrite.<br>R2: Core Times (min:sec)<br>9.24-9.5 (4:14)<br>9.5-9.8 (5:06)<br>9.8-10.1 (4:23)<br>10.1-10.4 (3:51)<br>10.4-10.76 (3:50) Rec'ed 83% | |
| 10.8 | | | | | | 369.08 | 10.76<br>**Bottom of Exploration at 10.76 m below ground surface.** | |
| 12 | | | | | | | | |
| 13.2 | | | | | | | | |
| 14.4 | | | | | | | | |
| 15.6 | | | | | | | | |
| 16.8 | | | | | | | | |
| 18 | | | | | | | | |

**Remarks:**

Static water levels were not achieved.
Borings were located in field with tape.

Stratification lines represent approximate boundaries between soil types; transitions may be gradual.

* Water level readings have been made at times and under conditions stated. Groundwater fluctuations may occur due to conditions other than those present at the time measurements were made.

**Page 2 of aa**

**Boring No.:** BB-NS-101

**Figure A.3. continued**

**Maine Department of Transportation**

Soil/Rock Exploration Log

METRIC UNITS

**Project:** NASH STREAM BRIDGE, ROUTE 16

**Location:** COPLIN PLT.

**Boring No.:** BB-NS-102

**PIN:** 10177.00

| | | | | | |
|---|---|---|---|---|---|
| **Driller:** | MDOT | **Elevation (m):** | 379.84 | **Auger ID/OD:** | 100 mm |
| **Operator:** | C.MANN | **Datum:** | NGVD | **Sampler:** | STANDARD SPLIT SPOON |
| **Logged By:** | G.LIDSTONE | **Rig Type:** | CME 45C | **Hammer Wt./Fall:** | 63.5 kg/760 mm |
| **Date Start/Finish:** | 5/21/02-5/21/02 | **Drilling Method:** | CASED WASHBORING | **Core Barrel:** | NQ |
| **Boring Location:** | 1+288.2, 2.3 RT. | **Casing ID/OD:** | NW,75/88 mm | **Water Level*:** | NONE OBSERVED |

Definitions:
D = Split Spoon Sample
MD = Unsuccessful Split Spoon Sample attempt
U = Thin Wall Tube Sample
R = Rock Core Sample
V = Insitu Vane Shear Test
SSA = Solid Stem Auger

Definitions:
$S_u$ = Insitu Field Vane Shear Strength (kPa)
$T_v$ = Pocket Torvane Shear Strength (kPa)
$q_p$ = Unconfined Compressive Strength (Pa)
$S_{u(lab)}$ = Lab Vane Shear Strength (kPa)
WOH = weight of 64 kg hammer
WOR = weight of rods

Definitions:
WC = water content, percent
LL = Liquid Limit
PL = Plastic Limit
PI = Plasticity Index
G = Grain Size Analysis
C = Consolidation Test

**Sample Information**

| Depth (m) | Sample No. | Type | Blows (0.15 m) | RQD (%) | Recovery (%) | Blows (0.30 m) | Elev. (m) | Visual Description and Remarks | Laboratory Testing Results/ AASHTO and Unified Class. |
|---|---|---|---|---|---|---|---|---|---|
| 0 | | | | | | SSA | 379.73 | PAVEMENT. 0.11 | |
| | 1D | 15.2/10.2 | 0.15 - 0.30 | 50 | --- | | | Brown, dry, very dense, sandy GRAVEL, cobbles, trace silt, (Fill). | |
| 1.2 | | | | | | | | | |
| | 2D | 61.0/15.2 | 1.52 - 2.13 | 16/21/19/16 | 40 | 65 | | | |
| | | | | | | 68 | | | |
| | | | | | | 103 | | | |
| 2.4 | | | | | | 60 | | | |
| | | | | | | 157 | | | |
| | 3D | 50.8/17.8 | 3.05 - 3.56 | 23/34/28/25(61) | +50 | 38 | 376.79 | 3.05 Brown, moist, very dense SILT, little sand, trace clay. Washed ahead 1.52 m. | G#98883 A-4, ML WC=31.8% |
| | | | | | | 42 | | | |
| 3.6 | | | | | | 67 | | | |
| | | | | | | 70 | | | |
| | | | | | | 64 | | | |
| | 4D | 61.0/22.9 | 4.57 - 5.18 | 24/13/13/18 | 26 | 52 | 375.27 | 4.57 Brown, moist, medium dense, silty fine to coarse SAND, trace gravel and clay. | G#98884 A-4, SM WC=11.6% |
| 4.8 | | | | | | 91 | | | |
| | | | | | | 265 | 374.66 | 5.18 Similar to above, except with cobbles. | |
| | | | | | | 200 | 374.20 | 5.64 | |
| | R1 | 152.4/124.5 | 5.82 - 7.35 | RQD = 33% | | NQ | 374.02 | Bedrock: Grey/green, medium to coarse grained, metamorphosed PELITE. Calcite clusters 2-3 mm in diameter with diopside reaction rims occur in a argillaceous groundmass. Washed ahead 0.18 m. 5.82 | |
| 6 | | | | | | | | R1: Core Times (min:sec) 5.82-6.1 (4:17) 6.1-6.4 (4:14) 6.4-6.7 (4:28) 6.7-7.0 (5:09) 7.0-7.35 (3:39) Rec'ed 82% | |
| 7.2 | | | | | | | 372.49 | 7.35 **Bottom of Exploration at 7.35 m below ground surface.** | |
| 8.4 | | | | | | | | | |

**Remarks:**

Static water levels were not achieved.
Borings were located in field with tape.

Stratification lines represent approximate boundaries between soil types; transitions may be gradual.

* Water level readings have been made at times and under conditions stated. Groundwater fluctuations may occur due to conditions other than those present at the time measurements were made.

**Page 1 of aa**

**Boring No.:** BB-NS-102

**Figure A.4. Boring Log BB-NS-102**

| **Maine Department of Transportation**<br>Soil/Rock Exploration Log<br>METRIC UNITS | **Project:** NASH STREAM BRIDGE, ROUTE 16<br>**Location:** COPLIN PLT. | **Boring No.:** BB-UMO-201<br>**PIN:** 10177.00 |
|---|---|---|

| | | | | | |
|---|---|---|---|---|---|
| **Driller:** | MaineDOT | **Elevation (m):** | 377.65 | **Auger ID/OD:** | N/A |
| **Operator:** | C.MANN | **Datum:** | NGVD | **Sampler:** | Standard Split Spoon |
| **Logged By:** | B. Wilder | **Rig Type:** | CME 45C | **Hammer Wt./Fall:** | 63.5 kg/760 mm |
| **Date Start/Finish:** | 8/2/04-8/2/04 | **Drilling Method:** | Cased Wash Boring | **Core Barrel:** | NQ |
| **Boring Location:** | ABT-1-G2 | **Casing ID/OD:** | HW & NW | **Water Level*:** | 1.22 m' bgs |

Definitions:
D = Split Spoon Sample
MD = Unsuccessful Split Spoon Sample attempt
U = Thin Wall Tube Sample
R = Rock Core Sample
V = Insitu Vane Shear Test
SSA = Solid Stem Auger

Definitions:
$S_u$ = Insitu Field Vane Shear Strength (kPa)
$T_v$ = Pocket Torvane Shear Strength (kPa)
$q_p$ = Unconfined Compressive Strength (Pa)
$S_{u(lab)}$ = Lab Vane Shear Strength (kPa)
WOH = weight of 64 kg hammer
WOR = weight of rods

Definitions:
WC = water content, percent
LL = Liquid Limit
PL = Plastic Limit
PI = Plasticity Index
G = Grain Size Analysis
C = Consolidation Test

| Depth (m) | Sample No. | Type | Recov./Pen. (mm) | Blows (0.15 m) | Qu (kPa) | Elev. (m) | Visual Description and Remarks | Laboratory Testing Results/ AASHTO and Unified Class. |
|---|---|---|---|---|---|---|---|---|
| 0 | | | | | | | | |
| | | | | | | 20 | | |
| | | | | | | 36 | | |
| | | | | | | 50 | | |
| | | | | | | 46 | | |
| 1.2 | | | | | | 42 | | |
| | 1D | | 61.0/38.1 | 1.52 - 2.13 | 11/12/21/20 | 33 | 21 | Brown, wet, dense, fine to coarse SAND, some gravel, (Fill). |
| | | | | | | 39 | | |
| | | | | | | 41 | | |
| 2.4 | | | | | | 35 | | |
| | | | | | | 200 | [a]Roller coned ahead to 3.66 m bgs. Boulder ? | |
| | | | | | | [a]RC | Dropped in NW Casing. | |
| 3.6 | | | | | | 7 | | |
| | | | | | | 14 | | |
| | | | | | | 40 | | |
| | | | | | | 54 | | |
| 4.8 | | | | | | 36 | | |
| | | | | | | 38 | | |
| | | | | | | 100 | [b]Roller coned ahead to 8.87 m bgs. | |
| | | | | | | [b]RC | Drove casing to 8.26 m bgs. | |
| 6 | | | | | | 19 | | |
| | | | | | | 43 | | |
| | | | | | | 41 | | |
| | | | | | | 43 | | |
| | | | | | | 44 | | |
| 7.2 | | | | | | 52 | | |
| | | | | | | 65 | | |
| | | | | | | 150 | Very dense from 7.99-8.88 m bgs. | |
| 8.4 | | | | | | [c]50 | [c]50 blows for 25 mm. | |
| | | | | | | | 368.87 / 368.78 — 8.78 | |
| | R1 | | 152.4/134.6 | 8.87 - 10.39 | | NQ CORE | Top of bedrock at 8.78 m bgs. Roller coned into bedrock to 8.87 m bgs. — 8.87<br>R1: Core Times (min:sec) | |

**Remarks:**

Stratification lines represent approximate boundaries between soil types; transitions may be gradual.

* Water level readings have been made at times and under conditions stated. Groundwater fluctuations may occur due to conditions other than those present at the time measurements were made.

**Page 1 of aa**

**Boring No.:** BB-UMO-201

**Figure A.5. Boring Log BB-NS-UMO-201**

| **Maine Department of Transportation**<br>Soil/Rock Exploration Log<br>METRIC UNITS | **Project:** NASH STREAM BRIDGE, ROUTE 16<br>**Location:** COPLIN PLT. | **Boring No.:** BB-UMO-201<br>**PIN:** 10177.00 |
|---|---|---|

| | | | | | |
|---|---|---|---|---|---|
| **Driller:** | MaineDOT | **Elevation (m):** | 377.65 | **Auger ID/OD:** | N/A |
| **Operator:** | C.MANN | **Datum:** | NGVD | **Sampler:** | Standard Split Spoon |
| **Logged By:** | B. Wilder | **Rig Type:** | CME 45C | **Hammer Wt./Fall:** | 63.5 kg/760 mm |
| **Date Start/Finish:** | 8/2/04-8/2/04 | **Drilling Method:** | Cased Wash Boring | **Core Barrel:** | NQ |
| **Boring Location:** | ABT-1-G2 | **Casing ID/OD:** | HW & NW | **Water Level*:** | 1.22 m' bgs |

Definitions:
D = Split Spoon Sample
MD = Unsuccessful Split Spoon Sample attempt
U = Thin Wall Tube Sample
R = Rock Core Sample
V = Insitu Vane Shear Test
SSA = Solid Stem Auger

Definitions:
$S_u$ = Insitu Field Vane Shear Strength (kPa)
$T_v$ = Pocket Torvane Shear Strength (kPa)
$q_p$ = Unconfined Compressive Strength (Pa)
$S_{u(lab)}$ = Lab Vane Shear Strength (kPa)
WOH = weight of 64 kg hammer
WOR = weight of rods

Definitions:
WC = water content, percent
LL = Liquid Limit
PL = Plastic Limit
PI = Plasticity Index
G = Grain Size Analysis
C = Consolidation Test

| Depth (m) | Type | Recovery (mm) | Blows (0.15 m) | Sample Information: Water Content (%) | Qu (kPa) | Blows/0.30 m | Elevation (m) | Visual Description and Remarks | Laboratory Testing Results/ AASHTO and Unified Class. |
|---|---|---|---|---|---|---|---|---|---|
| 9.6 | | | | | | | | 8.87-9.17 (4:00)<br>9.17-9.48 (4:00)<br>9.48-9.78 (7:00)<br>9.78-10.09 (4:00)<br>10.09-10.39 (5:00) 84% Recovery | |
| | | | | | | | 367.25 | **Bottom of Exploration at 10.39 m below ground surface.** | |
| 10.8 | | | | | | | | | |
| 12 | | | | | | | | | |
| 13.2 | | | | | | | | | |
| 14.4 | | | | | | | | | |
| 15.6 | | | | | | | | | |
| 16.8 | | | | | | | | | |
| 18 | | | | | | | | | |

**Remarks:**

Stratification lines represent approximate boundaries between soil types; transitions may be gradual.

* Water level readings have been made at times and under conditions stated. Groundwater fluctuations may occur due to conditions other than those present at the time measurements were made.

**Page 2 of aa**

**Boring No.:** BB-UMO-201

**Figure A.5. continued**

| **Maine Department of Transportation**<br>Soil/Rock Exploration Log<br>METRIC UNITS | **Project:** NASH STREAM BRIDGE, ROUTE 16<br>**Location:** COPLIN PLT. | **Boring No.:** BB-UMO-202<br>**PIN:** 10177.00 |
|---|---|---|

| | | | | | |
|---|---|---|---|---|---|
| **Driller:** | MaineDOT | **Elevation (m):** | 377.65 | **Auger ID/OD:** | N/A |
| **Operator:** | C.MANN | **Datum:** | NGVD | **Sampler:** | Standard Split Spoon |
| **Logged By:** | B. Wilder | **Rig Type:** | CME 45C | **Hammer Wt./Fall:** | 63.5 kg/760 mm |
| **Date Start/Finish:** | 8/2/04-8/2/04 | **Drilling Method:** | Cased Wash Boring | **Core Barrel:** | NQ |
| **Boring Location:** | ABT-1-G1 | **Casing ID/OD:** | HW | **Water Level*:** | 1.07 m bgs |

Definitions:
D = Split Spoon Sample
MD = Unsuccessful Split Spoon Sample attempt
U = Thin Wall Tube Sample
R = Rock Core Sample
V = Insitu Vane Shear Test
SSA = Solid Stem Auger

Definitions:
$S_u$ = Insitu Field Vane Shear Strength (kPa)
$T_v$ = Pocket Torvane Shear Strength (kPa)
$q_p$ = Unconfined Compressive Strength (Pa)
$S_{u(lab)}$ = Lab Vane Shear Strength (kPa)
WOH = weight of 64 kg hammer
WOR = weight of rods

Definitions:
WC = water content, percent
LL = Liquid Limit
PL = Plastic Limit
PI = Plasticity Index
G = Grain Size Analysis
C = Consolidation Test

| Depth (m) | Sample No. | Type | Recovery (mm) | Blows (0.15 m) | Water Content (%) | RQD | Elevation (m) | Soil Class | Visual Description and Remarks | Laboratory Testing Results/ AASHTO and Unified Class. |
|---|---|---|---|---|---|---|---|---|---|---|
| 0 | | | | | | | | 7 | | |
| | | | | | | | | 24 | | |
| | | | | | | | | 38 | | |
| | | | | | | | | 47 | | |
| 1.2 | | | | | | | | 63 | | |
| | | | | | | | | 157 | | |
| | | | | | | | | 402 | [a]Roller coned ahead to 4.57 m bgs. | |
| | | | | | | | | [a]RC | | |
| | | | | | | | | 19 | | |
| 2.4 | | | | | | | | 28 | Cobble from 2.44-2.5 m bgs.<br>Cobble from 2.56-2.68 m bgs. | |
| | | | | | | | | 24 | | |
| | | | | | | | | 17 | | |
| | | | | | | | | 18 | | |
| 3.6 | | | | | | | | 20 | | |
| | | | | | | | | 18 | | |
| | | | | | | | | 28 | | |
| | | | | | | | | 68 | | |
| 4.8 | | | | | | | | 52 | | |
| | | | | | | | | 76 | | |
| | | | | | | | | 92 | | |
| | | | | | | | | 198 | [b]Roller coned ahead to 8.72 m bgs. | |
| 6 | | | | | | | | [b]RC | | |
| | | | | | | | | 92 | | |
| | | | | | | | | 58 | | |
| | | | | | | | | 111 | | |
| 7.2 | | | | | | | | 263 | Cobble from 7.01-7.1 m bgs. | |
| | | | | | | | | 340 | | |
| | | | | | | | | 162 | | |
| | | | | | | | | 336 | Very dense layer from 7.86-8.72 m bgs. | |
| 8.4 | | | | | | | | 387 | | |
| | | | | | | | | [c]200 | [c]200 blows for 180 mm. | |
| | R1 | | 152.4/144.8 | 8.72 - 10.24 | | | 368.93 | NQ CORE | 8.72 | |
| | | | | | | | | | R1:Core Times (min:sec)<br>8.72-9.02 (6:15)<br>9.02-9.33 (5:30)<br>9.33-9.63 (5:00) | |

**Remarks:**

Stratification lines represent approximate boundaries between soil types; transitions may be gradual.

* Water level readings have been made at times and under conditions stated. Groundwater fluctuations may occur due to conditions other than those present at the time measurements were made.

**Page 1 of aa**

**Boring No.:** BB-UMO-202

**Figure A.6. Boring Log BB-NS-UMO-202**

| **Maine Department of Transportation**<br>Soil/Rock Exploration Log<br>METRIC UNITS | **Project:** NASH STREAM BRIDGE, ROUTE 16<br>**Location:** COPLIN PLT. | **Boring No.:** BB-UMO-202<br>**PIN:** 10177.00 |
|---|---|---|

| | | | | | |
|---|---|---|---|---|---|
| **Driller:** | MaineDOT | **Elevation (m):** | 377.65 | **Auger ID/OD:** | N/A |
| **Operator:** | C.MANN | **Datum:** | NGVD | **Sampler:** | Standard Split Spoon |
| **Logged By:** | B. Wilder | **Rig Type:** | CME 45C | **Hammer Wt./Fall:** | 63.5 kg/760 mm |
| **Date Start/Finish:** | 8/2/04-8/2/04 | **Drilling Method:** | Cased Wash Boring | **Core Barrel:** | NQ |
| **Boring Location:** | ABT-1-G1 | **Casing ID/OD:** | HW | **Water Level*:** | 1.07 m bgs |

Definitions:
D = Split Spoon Sample
MD = Unsuccessful Split Spoon Sample attempt
U = Thin Wall Tube Sample
R = Rock Core Sample
V = Insitu Vane Shear Test
SSA = Solid Stem Auger

Definitions:
$S_u$ = Insitu Field Vane Shear Strength (kPa)
$T_v$ = Pocket Torvane Shear Strength (kPa)
$q_p$ = Unconfined Compressive Strength (Pa)
$S_{u(lab)}$ = Lab Vane Shear Strength (kPa)
WOH = weight of 64 kg hammer
WOR = weight of rods

Definitions:
WC = water content, percent
LL = Liquid Limit
PL = Plastic Limit
PI = Plasticity Index
G = Grain Size Analysis
C = Consolidation Test

| Depth (m) | Sample No. | Type | Blows (0.15 m) | Recovery (%) | Elev. (m) | Graphic Log | Visual Description and Remarks | Laboratory Testing Results/ AASHTO and Unified Class. |
|---|---|---|---|---|---|---|---|---|
| 9.6 | | | | | | | 9.63-9.94 (4:30)<br>9.94-10.24 (4:30) 95% Recovery | |
| | | | | | 367.41 | | 10.24<br>**Bottom of Exploration at 10.24 m below ground surface.** | |
| 10.8 | | | | | | | | |
| 12 | | | | | | | | |
| 13.2 | | | | | | | | |
| 14.4 | | | | | | | | |
| 15.6 | | | | | | | | |
| 16.8 | | | | | | | | |
| 18 | | | | | | | | |

**Remarks:**

Stratification lines represent approximate boundaries between soil types; transitions may be gradual.

* Water level readings have been made at times and under conditions stated. Groundwater fluctuations may occur due to conditions other than those present at the time measurements were made.

**Page 2 of aa**

**Boring No.:** BB-UMO-202

**Figure A.6. continued**

**Maine Department of Transportation**

Soil/Rock Exploration Log

METRIC UNITS

**Project:** NASH STREAM BRIDGE, ROUTE 16

**Location:** COPLIN PLT.

**Boring No.:** BB-UMO-203

**PIN:** 10177.00

| | | | | | |
|---|---|---|---|---|---|
| **Driller:** | MaineDOT | **Elevation (m):** | 377.65 | **Auger ID/OD:** | 125 mm Solid Stem Auger |
| **Operator:** | C.MANN | **Datum:** | NGVD | **Sampler:** | Standard Split Spoon |
| **Logged By:** | B. Wilder | **Rig Type:** | CME 45C | **Hammer Wt./Fall:** | 63.5 kg/760 mm |
| **Date Start/Finish:** | 8/3/04-8/3/04 | **Drilling Method:** | Cased Wash Boring | **Core Barrel:** | NQ |
| **Boring Location:** | ABT-1-G3 | **Casing ID/OD:** | HW | **Water Level*:** | 1.16 m bgs |

Definitions:
D = Split Spoon Sample
MD = Unsuccessful Split Spoon Sample attempt
U = Thin Wall Tube Sample
R = Rock Core Sample
V = Insitu Vane Shear Test
SSA = Solid Stem Auger

Definitions:
$S_u$ = Insitu Field Vane Shear Strength (kPa)
$T_v$ = Pocket Torvane Shear Strength (kPa)
$q_p$ = Unconfined Compressive Strength (Pa)
$S_{u(lab)}$ = Lab Vane Shear Strength (kPa)
WOH = weight of 64 kg hammer
WOR = weight of rods

Definitions:
WC = water content, percent
LL = Liquid Limit
PL = Plastic Limit
PI = Plasticity Index
G = Grain Size Analysis
C = Consolidation Test

**Sample Information**

| Depth (m) | Sample No. | Type | Recovery (mm) | Blows (0.15 m) | Water Content (%) | Qu (kPa) | Qp (kPa) | Su(lab) (kPa) | Elevation (m) | Graphic Log | Visual Description and Remarks | Laboratory Testing Results/ AASHTO and Unified Class. |
|---|---|---|---|---|---|---|---|---|---|---|---|---|
| 0 | | | | | | | | | | SSA | | |
| 1.2 | | | | | | | | | | | | |
| 2.4 | | | | | | | | | | | Cobble from 2.13-2.23 m bgs. | |
| | | | | | | | | | | 24 | | |
| 3.6 | | | | | | | | | | 60 | | |
| | | | | | | | | | | 66 | | |
| | | | | | | | | | | 57 | | |
| 4.8 | | | | | | | | | | 114 | | |
| | | | | | | | | | | 100 | | |
| | | | | | | | | | | 98 | | |
| | | | | | | | | | | 155 | | |
| 6 | | | | | | | | | | 169 | | |
| | | | | | | | | | | 160 | | |
| | | | | | | | | | | a RC | aRoller coned ahead to 6.71 m bgs. | |
| 7.2 | R1 | 131.1/111.8 | 6.71 - 8.02 | | | | | | 371.00 / 370.94 | NQ CORE | Bedrock:<br>R1:Core Times (min:sec)<br>6.71-7.01 (4:38)<br>7.01-7.32 (3:00)<br>Void at 7.1-7.19 bgs.<br>7.32-7.62 (3:30)<br>7.62-7.92 (2:30)<br>7.92-8.02 (1:25) 85% Recovery | |
| 8.4 | | | | | | | | | 369.63 | | | |

6.64

6.71

8.02

**Bottom of Exploration at 8.02 m below ground surface.**

**Remarks:**

Stratification lines represent approximate boundaries between soil types; transitions may be gradual.

* Water level readings have been made at times and under conditions stated. Groundwater fluctuations may occur due to conditions other than those present at the time measurements were made.

**Page 1 of aa**

**Boring No.:** BB-UMO-203

**Figure A.7. Boring Log BB-NS-UMO-203**

**Maine Department of Transportation**

Soil/Rock Exploration Log

METRIC UNITS

**Project:** NASH STREAM BRIDGE, ROUTE 16

**Location:** COPLIN PLT.

**Boring No.:** BB-UMO-204

**PIN:** 10177.00

| | | | | | |
|---|---|---|---|---|---|
| **Driller:** | MaineDOT | **Elevation (m):** | 377.49 | **Auger ID/OD:** | 125 mm Solid Stem Auger |
| **Operator:** | C.MANN | **Datum:** | NGVD | **Sampler:** | Standard Split Spoon |
| **Logged By:** | B. Wilder | **Rig Type:** | CME 45C | **Hammer Wt./Fall:** | 63.5 kg/760 mm |
| **Date Start/Finish:** | 8/4/04-8/4/04 | **Drilling Method:** | Cased Wash Boring | **Core Barrel:** | NQ |
| **Boring Location:** | ABT-2-G2 | **Casing ID/OD:** | HW | **Water Level*:** | 0.91 m bgs |

Definitions:
D = Split Spoon Sample
MD = Unsuccessful Split Spoon Sample attempt
U = Thin Wall Tube Sample
R = Rock Core Sample
V = Insitu Vane Shear Test
SSA = Solid Stem Auger

Definitions:
$S_u$ = Insitu Field Vane Shear Strength (kPa)
$T_v$ = Pocket Torvane Shear Strength (kPa)
$q_p$ = Unconfined Compressive Strength (Pa)
$S_{u(lab)}$ = Lab Vane Shear Strength (kPa)
WOH = weight of 64 kg hammer
WOR = weight of rods

Definitions:
WC = water content, percent
LL = Liquid Limit
PL = Plastic Limit
PI = Plasticity Index
G = Grain Size Analysis
C = Consolidation Test

**Sample Information**

| Depth (m) | Sample No. | Type | Recovery (mm) | Blows (per 150 mm) | Qu (kPa) | Qp (kPa) | Wn (%) | Grain Size | Soil Class | Elev. (m) | Log | Visual Description and Remarks | Laboratory Testing Results/ AASHTO and Unified Class. |
|---|---|---|---|---|---|---|---|---|---|---|---|---|---|
| 0 | | | | | | | | SSA | | | | | |
| 1.2 | | | | | | | | | | | | | |
| 2.4 | | | | | | | | | | | | | |
| | | | | | | | | | | | | Till from 2.74-3.35 m bgs. | |
| | | | | | | | | 17 | | | | | |
| 3.6 | | | | | | | | 58 | | | | | |
| | | | | | | | | 75 | | | | Cobbles from 3.66-4.18 m bgs. | |
| | R1 | 152.4/139.7 | 4.21 - 5.73 | | | | | a50 bWA NQ CORE | | 373.31 373.28 | | a50 blows for 50 mm. bWash ahead from 4.02-4.21 m' bgs. 4.18 Bedrock: 4.21 R1:Core Times (min:sec) 4.21-4.51 (5:28) 4.51-4.82 (6:27) 4.82-5.12 (5:29) 5.12-5.43 (4:05) 5.43-5.73 (2:30) 92% Recovery | |
| 4.8 | | | | | | | | | | | | | |
| | | | | | | | | | | 371.76 | | 5.73 | |
| 6 | | | | | | | | | | | | **Bottom of Exploration at 5.73 m below ground surface.** | |
| 7.2 | | | | | | | | | | | | | |
| 8.4 | | | | | | | | | | | | | |

**Remarks:**

Stratification lines represent approximate boundaries between soil types; transitions may be gradual.

* Water level readings have been made at times and under conditions stated. Groundwater fluctuations may occur due to conditions other than those present at the time measurements were made.

**Page 1 of aa**

**Boring No.:** BB-UMO-204

**Figure A.8. Boring Log BB-NS-UMO-204**

**Maine Department of Transportation**

Soil/Rock Exploration Log

METRIC UNITS

**Project:** NASH STREAM BRIDGE, ROUTE 16

**Location:** COPLIN PLT.

**Boring No.:** BB-UMO-205

**PIN:** 10177.00

| | | | | | |
|---|---|---|---|---|---|
| **Driller:** | MaineDOT | **Elevation (m):** | 377.49 | **Auger ID/OD:** | 125 mm Solid Stem Auger |
| **Operator:** | C.MANN | **Datum:** | NGVD | **Sampler:** | Standard Split Spoon |
| **Logged By:** | B. Wilder | **Rig Type:** | CME 45C | **Hammer Wt./Fall:** | 63.5 kg/760 mm |
| **Date Start/Finish:** | 8/4/04-8/4/04 | **Drilling Method:** | Cased Wash Boring | **Core Barrel:** | NQ |
| **Boring Location:** | ABT-2-G3 | **Casing ID/OD:** | HW | **Water Level*:** | 0.91 m bgs |

Definitions:
D = Split Spoon Sample
MD = Unsuccessful Split Spoon Sample attempt
U = Thin Wall Tube Sample
R = Rock Core Sample
V = Insitu Vane Shear Test
SSA = Solid Stem Auger

Definitions:
$S_u$ = Insitu Field Vane Shear Strength (kPa)
$T_v$ = Pocket Torvane Shear Strength (kPa)
$q_p$ = Unconfined Compressive Strength (Pa)
$S_{u(lab)}$ = Lab Vane Shear Strength (kPa)
WOH = weight of 64 kg hammer
WOR = weight of rods

Definitions:
WC = water content, percent
LL = Liquid Limit
PL = Plastic Limit
PI = Plasticity Index
G = Grain Size Analysis
C = Consolidation Test

**Sample Information**

| Depth (m) | Sample No. | Type | Recovery (mm) | Blows (0.15 m) | Qu (kPa) | Qp (kPa) | Wn (%) | Sample Type | Elevation (m) | Soil Description | Visual Description and Remarks | Laboratory Testing Results/ AASHTO and Unified Class. |
|---|---|---|---|---|---|---|---|---|---|---|---|---|
| 0 | | | | | | | | SSA | | | GRAVEL. | |
| 1.2 | | | | | | | | | 375.97 | | 1.52 | |
| | | | | | | | | | | | Brown, moist, sandy SILT, trace gravel. | |
| 2.4 | | | | | | | | | 374.90 | | 2.59 | |
| | | | | | | | | | | | TILL. | |
| | | | | | | | | 35 | | | | |
| | | | | | | | | 110 | 374.14 | | 3.35 | |
| 3.6 | | | | | | | | | | | COBBLES. | |
| | | | | | | | | OPEN HOLE | | | Washed ahead from 3.66-3.96 m bgs. | |
| | R1 | 152.4/124.5 | 3.96 - 5.49 | | | | | NQ | 373.56 | | 3.93 | |
| | | | | | | | | | 373.53 | | Bedrock: 3.96 | |
| 4.8 | | | | | | | | | | | R1:Core Times (min:sec)<br>3.96-4.27 (3:50)<br>4.27-4.57 (8:01)<br>4.57-4.88 (6:21)<br>4.88-5.18 (6:46)<br>5.18-5.49 (6:24) 82% Recovery | |
| | | | | | | | | | 372.00 | | 5.49 | |
| | | | | | | | | | | | **Bottom of Exploration at 5.49 m below ground surface.** | |
| 6 | | | | | | | | | | | | |
| 7.2 | | | | | | | | | | | | |
| 8.4 | | | | | | | | | | | | |

**Remarks:**

Stratification lines represent approximate boundaries between soil types; transitions may be gradual.

* Water level readings have been made at times and under conditions stated. Groundwater fluctuations may occur due to conditions other than those present at the time measurements were made.

**Page 1 of aa**

**Boring No.:** BB-UMO-205

**Figure A.9. Boring Log BB-NS-UMO-205**

**Maine Department of Transportation**

Soil/Rock Exploration Log

METRIC UNITS

**Project:** NASH STREAM BRIDGE, ROUTE 16

**Location:** COPLIN PLT.

**Boring No.:** BB-UMO-206

**PIN:** 10177.00

| | | | | | |
|---|---|---|---|---|---|
| **Driller:** | MaineDOT | **Elevation (m):** | 377.49 | **Auger ID/OD:** | 125 mm Solid Stem Auger |
| **Operator:** | C.MANN | **Datum:** | NGVD | **Sampler:** | Standard Split Spoon |
| **Logged By:** | B. Wilder | **Rig Type:** | CME 45C | **Hammer Wt./Fall:** | 63.5 kg/760 mm |
| **Date Start/Finish:** | 8/3/04-8/4/04 | **Drilling Method:** | Cased Wash Boring | **Core Barrel:** | NQ |
| **Boring Location:** | ABT-2-G4 | **Casing ID/OD:** | HW | **Water Level*:** | 0.91 m bgs |

Definitions:
D = Split Spoon Sample
MD = Unsuccessful Split Spoon Sample attempt
U = Thin Wall Tube Sample
R = Rock Core Sample
V = Insitu Vane Shear Test
SSA = Solid Stem Auger

Definitions:
$S_u$ = Insitu Field Vane Shear Strength (kPa)
$T_v$ = Pocket Torvane Shear Strength (kPa)
$q_p$ = Unconfined Compressive Strength (Pa)
$S_{u(lab)}$ = Lab Vane Shear Strength (kPa)
WOH = weight of 64 kg hammer
WOR = weight of rods

Definitions:
WC = water content, percent
LL = Liquid Limit
PL = Plastic Limit
PI = Plasticity Index
G = Grain Size Analysis
C = Consolidation Test

| Depth (m) | Sample No. | Type | Blows (0.15 m) | Recovery (mm) | RQD (%) | Elev. (m) | Visual Description and Remarks | Laboratory Testing Results/ AASHTO and Unified Class. |
|---|---|---|---|---|---|---|---|---|
| 0 | | | | | | | GRAVEL. | |
| 1.2 | | | | | | 375.97 | 1.52 — Brown, moist, sandy SILT, trace gravel, trace clay. | |
| 2.4 | R1 | 61.0/33.0 | 2.59 - 3.20 | | | 374.90 | 2.59 — 0.09 and 0.18 COBBLE, 0.6 GRAVEL. Washed ahead from 2.59-3.26 m bgs. R1:Core Times (min:sec) 2.59-2.89 (6:30) 2.89-3.2 (2:30) 54% Recovery | |
| | R2 | 152.4/121.9 | 3.26 - 4.79 | | | 374.56 | | |
| 3.6 | | | | | | 374.23 | 2.93 — TILL. 3.26 — R2:Bedrock: R2:Core Times (min:sec) 3.26-3.57 (5:46) 3.57-3.87 (5:52) 3.87-4.17 (5:53) 4.17-4.48 (5:45) 4.48-4.79 (5:00) 80% Recovery | |
| 4.8 | | | | | | 372.70 | 4.79 — **Bottom of Exploration at 4.79 m below ground surface.** | |
| 6 | | | | | | | | |
| 7.2 | | | | | | | | |
| 8.4 | | | | | | | | |

**Remarks:**

Stratification lines represent approximate boundaries between soil types; transitions may be gradual.

* Water level readings have been made at times and under conditions stated. Groundwater fluctuations may occur due to conditions other than those present at the time measurements were made.

**Page 1 of aa**

**Boring No.:** BB-UMO-206

**Figure A.10. Boring Log BB-NS-UMO-206**

# Appendix B

## SAMPLE CALCULATIONS

## B.1. Strain Gage Analysis

Sample Calculation of four internal forces acting on the piles, based on four measured strains from strain gages.

P : Axial Load
Mx: x-axis bending (Strong Axis bending)
My : y-axis bending (Weak axis bending)
Mt : tortional moment

Assumptions:

Assume all loads exist through the center of gravity for the pile
Lateral bending for each flange is equal and opposite, net axial forced produced by restrained torsion is zero
Assume loads are applied through center of gravity in x-section due to confinement of abutment concrete
The effects of the pipe are not included for torsional Mf in bottom flange since it is stitch weded to flange and will not be fuly mobilized
Pipe stops at top of pile, and a new section is added from girder to road
Angles are included

Angles : 1.5 x 1.5 x 3/16

$r := 2.73\frac{kg}{m}$

$q := 45deg$

$Ixx := 0.0734\,10^{6}mm^{4}$ $\qquad Ixx = 0.176in^{4}$

$Iyy := 0.0734\,10^{6}mm^{4}$ $\qquad Iyy = 0.176in^{4}$

$Ixy := -0.0296\,10^{6}mm^{4}$ $\qquad Ixy = -0.071in^{4}$

$Izz := \frac{Ixx + Iyy}{2} + \frac{Ixx - Iyy}{2}\cos(2q) - Ixy\sin(2q)$ $\qquad Izz = 0.247in^{4}$

$Iqq := Ixx2 - Izz$ $\qquad Iqq = 0.105in^{4}$

$A\_angle := \frac{r}{7850\frac{kg}{m^{3}}}$ $\qquad A\_angle = 0.539in^{2}$

Pipe : 2.5 ID, Sch 90

$A\_pipe := 1.70\,in^2$

$I := 1.53\,in^4$

Pile : HP 14x89

$A := 26.1\,in^2$

$Ixx := 904\,in^4$

$Iyy := 326\,in^4$

Locate center of gravity:

$A\_total := 4A\_angle + A\_pipe + A$ $\qquad A\_total = 29.956\,in^2$

$Y := 6.62\,in$

$X := 7.49\,in$

$Ixx\_total := 1001\,in^4$

$Iyy\_total := 342.4\,in^4$

Bending due to rotation:

Iyy for top flange:

$$Iyy\_top := \frac{0.615\,14.7^3}{12} + 2\,0.176 + 2\,0.539\left(\frac{0.615}{2} + 1.047\right)^2 \qquad Iyy\_top = 165.127$$

$$S2t := \frac{Iyy\_top}{\frac{14.7}{2} - 2} \qquad S2t = 30.865 \qquad S2t := 30.865\,in^4$$

$S3t := 30.865\,in^4$

Iyy for bottom flange*:

*Did not include pipe, as it was stitch welded to flange and will not mobilize full section

$$Abott := 0.615\,in\,14.7\,in + 2\,0.539\,in^2 \qquad Abott = 10.118\,in^2$$

$$Ybott := \frac{\left(9.04\,\frac{14.7}{2} + 0.539\left(\frac{14.7 + 0.615}{2}\right) + 2.88 + 0.420\right) + 0.539\left(\frac{14.7 - 0.615}{2} - 1.047\right)}{10.118}$$

$Ybott = 7.47 \qquad Ybott := 7.47\,in$

$$It := 162.8 + 0.176 + 0.247 + 0.539\left(\frac{14.7 + 0.615}{2}\right) + 2.88 + .420 - 7.47^2 + 0.539\left(7.47 - \frac{14.7 - 0.615}{2} + 1.047\right)^2$$

$It = 170.951 \qquad It := 170.951\,in^4$

$$S4t := \frac{It}{14.7\,in - 7.47\,in - 2\,in} \qquad S4t = 32.687\,in^3$$

$$S1t := \frac{It}{7.47\,in - 2\,in} \qquad S1t = 31.252\,in^3$$

Due to x-axis bending:

$$S1x := \frac{Ixx\_total}{Y - 0.615in} \qquad S1x = 166.694in^3$$

$$S2x := \frac{Ixx\_total}{13.8in - Y - 0.615in} \qquad S2x = 152.475in^3$$

$$S3x := S2x \qquad S3x = 152.475in^3$$

$$S4x := S1x \qquad S4x = 166.694in^3$$

Due to y-axis bending:

$$S1y := \frac{Iyy\_total}{7.49in - 2in} \qquad S1y = 62.368in^3$$

$$S2y := S1y \qquad S2y = 62.368in^3$$

$$S3y := \frac{Iyy\_total}{14.7in - 7.49in - 2in} \qquad S3y = 65.72in^3$$

$$S4y := S3y \qquad S4y = 65.72in^3$$

Solve 4 equations to find 4 unknowns:

Basis: $$Stress := \frac{1}{E}\left(\frac{P}{A} + \frac{Mx}{Sx} + \frac{My}{Sy} + \frac{Mt}{St}\right)$$

$$a := \frac{1}{A\_total}$$

For South piles:

$$b1 := \frac{1}{S1x} \qquad c1 := \frac{1}{S1y} \qquad d1 := \frac{1}{S1t}$$

$$b2 := \frac{1}{S2x} \qquad c2 := c1 \qquad d2 := \frac{1}{S2t}$$

$$b3 := b2 \qquad c3 := \frac{1}{S3y} \qquad d3 := d2$$

$$b4 := b1 \qquad c4 := c3 \qquad d4 := \frac{1}{S4t}$$

For north piles: S1->N3; S2->N4; S3-> N1; S4-> N2

Four equations for strains:

$$e1 := \frac{1}{E}(-aP + b1\ Mx - c1\ My - d1\ Mt)$$

$$e2 := \frac{1}{E}(-aP - b2\ Mx - c2\ My + d2\ Mt)$$

$$e3 := \frac{1}{E}(-aP - b3\ Mx + c3\ My - d3\ Mt)$$

$$e4 := \frac{1}{E}(-aP + b4\ Mx + c4\ My + d4\ Mt)$$

*Sign convention: for south piles: + north, and + west

let: $P := \frac{EA(e1 + e2 + e3 + e4)}{4}$ $\qquad \frac{a\ P}{E} := \frac{P}{EA}$ $\qquad$ eave

$$\begin{bmatrix} b1 & -c1 & -d1 \\ -b2 & -c2 & d2 \\ -b3 & c3 & -d3 \\ b4 & c4 & d4 \end{bmatrix} \times \begin{bmatrix} Mx \\ My \\ Mt \end{bmatrix} \qquad \begin{bmatrix} e1 - eave \\ e2 - eave \\ e3 - eave \\ e4 - eave \end{bmatrix} E$$

(B) $\qquad$ (X) $\qquad$ $(e - eave)\ E$

BX = e-eave*E

B'BX = B'(e-eave)*E

**X = (B'B)' x B'(e-eave)*E**

## B.2. Correction for Faulty Strain Gages

**Process for determing the strain for a faulty strain gage including sample equation.**

Input: Strains for all working gages on Day 281 (Live Load Test), noon

South:

$AH1 := -441.60$ $BH1 := -461.02$

$AH2 := -711.33$ $BH2 := -586.05$

$AH3 := 0$ bad $BH3 := 101.24$

$AH4 := 466.04$ $BH4 := 279.88$

$CH1 := -255.53$

$CH2 := -289.58$

$CH3 := -108.48$

$CH4 := 30.71$

North:

$XH1 := -385.35$ $YH1 := -467.07$

$XH2 := 0$ bad $YH2 := -382.08$

$XH3 := 129.98$ $YH3 := -94.90$

$XH4 := 201.84$ $YH4 := 32.72$

$ZH1 := -195.21$

$ZH3 := -270.62$

$ZH3 := 0$ bad

$ZH4 := 66.72$

For good piles (B,C, Y), find average and normalize

$$Bavg := \frac{(BH1 + BH2 + BH3 + BH4)}{4} \qquad Bavg = -166.487$$

$$B1 := \frac{BH1 - Bavg}{Bavg} \qquad B3 := \frac{BH3 - Bavg}{Bavg} \qquad B1 = 1.769 \qquad B3 = -1.608$$

$$B2 := \frac{BH2 - Bavg}{Bavg} \qquad B4 := \frac{BH4 - Bavg}{Bavg} \qquad B2 = 2.52 \qquad B4 = -2.681$$

$$Cavg := \frac{(CH1 + CH2 + CH3 + CH4)}{4} \qquad Cavg = -155.72$$

$$C1 := \frac{CH1 - Cavg}{Cavg} \qquad C3 := \frac{CH3 - Cavg}{Cavg} \qquad C1 = 0.641 \qquad C3 = -0.303$$

$$C2 := \frac{CH2 - Cavg}{Cavg} \qquad C4 := \frac{CH4 - Cavg}{Cavg} \qquad C2 = 0.86 \qquad C4 = -1.197$$

$$Yavg := \frac{(YH1 + YH2 + YH3 + YH4)}{4} \qquad Yavg = -227.832$$

$$Y1 := \frac{YH1 - Yavg}{Yavg} \qquad Y3 := \frac{YH3 - Yavg}{Yavg} \qquad Y1 = 1.05 \qquad Y3 = -0.583$$

$$Y2 := \frac{YH2 - Yavg}{Yavg} \qquad Y4 := \frac{YH4 - Yavg}{Yavg} \qquad Y2 = 0.677 \qquad Y4 = -1.144$$

For Bad Gage: AH3

Say A3 = B3: B3 = (BH3-Bave)/Bave = (AH3-Aave)/Aave : AH3 = B3*Aave+Aave
And: 4*Aave = AH1 + AH2 + AH4 +(B3*Aave + Aave)

Therefore : Aave = (AH1 + AH2 +AH4)/(3-B3)
and AH3 = B3*Aave + Aave

Find Aave and AH3 based on each complete set of data:

$$Aave\_B := \frac{(AH1 + AH2 + AH4)}{3 - B3} \qquad Aave\_B = -149.062$$

$$AH3\_B := B3\ Aave\_B + Aave\_B \qquad AH3\_B = 90.643$$

$$Aave\_C := \frac{(AH1 + AH2 + AH4)}{3 - C3} \qquad Aave\_C = -207.936$$

$$AH3\_C := C3\ Aave\_C + Aave\_C \qquad AH3\_C = -144.856$$

$$Aave\_Y := \frac{(AH1 + AH2 + AH4)}{3 - Y3} \qquad Aave\_Y = -191.683$$

$$AH3\_Y := Y3\ Aave\_Y + Aave\_Y \qquad AH3\_Y = -79.843$$

Determind factors for good gages of incomplete set:

$$A1\_B := \frac{AH1 - Aave\_B}{Aave\_B} \qquad A1\_B = 1.963$$

$$A2\_B := \frac{AH2 - Aave\_B}{Aave\_B} \qquad A2\_B = 3.772$$

$$A4\_B := \frac{AH4 - Aave\_B}{Aave\_B} \qquad A4\_B = -4.126$$

$$A1\_C := \frac{AH1 - Aave\_C}{Aave\_C} \qquad A1\_C = 1.124$$

$$A2\_C := \frac{AH2 - Aave\_C}{Aave\_C} \qquad A2\_C = 2.421$$

$$A4\_C := \frac{AH4 - Aave\_C}{Aave\_C} \qquad A4\_C = -3.241$$

$$A1\_Y := \frac{AH1 - Aave\_Y}{Aave\_Y} \qquad A1\_Y = 1.304$$

$$A2\_Y := \frac{AH2 - Aave\_Y}{Aave\_Y} \qquad A2\_Y = 2.711$$

$$A4\_Y := \frac{AH4 - Aave\_Y}{Aave\_Y} \qquad A4\_Y = -3.431$$

Determine error based on least squares:

$$B := \sqrt{\frac{(A1\_B - B1)^2}{|B1|} + \frac{(A2\_B - B2)^2}{|B2|} + \frac{(A4\_B - B4)^2}{|B4|}} \qquad B = 1.193$$

$$C := \sqrt{\frac{(A1\_C - C1)^2}{|C1|} + \frac{(A2\_C - C2)^2}{|C2|} + \frac{(A4\_C - C4)^2}{|C4|}} \qquad C = 2.586$$

$$Y := \sqrt{\frac{(A1\_Y - Y1)^2}{|Y1|} + \frac{(A2\_Y - Y2)^2}{|Y2|} + \frac{(A4\_Y - Y4)^2}{|Y4|}} \qquad Y = 3.278$$

Since the error for the comparison to set B is the smallest, use this set.

$$AH3 := AH3\_B \qquad AH3 = 90.643$$

## B.3. Calculation of the Weight of the Bridge

Units: $pcf := \frac{lb}{ft^3}$

Structural steel: Includes girders, diaphragms, stiffners and cross bracing

Girders (4):

$top := 25mm\ 400mm$ — Area of top flange

$web := 14mm\ 945mm$ — Area of web

$bottom := 35mm\ 500mm$ — Area of bottom flange

$Lspan := 30m$ — Bridge span

$\gamma_{steel} := 490pcf$ — Unit weight of structural steel

$Wgirders := \left(\left(top + web + bottom\right) Lspan\ \gamma_{steel}\right) 4$ — Weight of 4 girders

$Wgirders = 8.458 \cdot 10^4\ lb$

Diaphragms (6): Type MB - W 610x82

$ldia := 3.33m$ — Diaphram length: distance between girders, w/skew

$Wdiaphragm := \left(82 \frac{kg}{m}\ ldia\right) 6$ — Weight of 6 diaphragms

$Wdiaphragm = 3.612 \cdot 10^3\ lb$

Stiffners (40): PL16x175

$t := 16mm$ — Stiffner thickness

$w := 175mm$ — Stiffner width

$l := 945mm$ — Stiffner length

$Wstiff := \left(t\ w\ l\ \gamma_{steel}\right) 40$ — Weight of stiffner

$Wstiff = 1.831 \cdot 10^3\ lb$

Cross Bracing: 6-Type MH, 3-Type MG

Straight:WT 100x13.3

$lstraight := 2.735m$ — Cross bracing lenth, transverse distance between girders

$Wstraight := \left(13.3 \frac{kg}{m}\ lstraight\right) 6$ — Weight of 6 straight bars

$Wstraight = 481.166lb$

Angled: L76x76x7.9

$L := 2.816m$ — Length of angle crossing girders

$Wangle := 7.9 \frac{kg}{m} L \cdot 18$ — Weight of angles, 18 total

$Wangle = 882.809lb$

Total structural steel:

$Wbracing := Wdiaphragm + Wstiff + Wstraight + Wangle$

$Wbracing = 6.807 \times 10^{3} lb$

$\frac{Wbracing}{Wgirders} = 8.049\%$ — Percent bracing steel

First Portion of Abutment: Not used in comparison to measured load

$t := 0.75m$ — Abutment thickness

$h := 1.2m$ — Abutment height

$l := 19.4m$ — Abutment length, including wingwalls

$\gamma conc := 150pcf$ — Unit weight of reinforced concrete

$Wabut1 := (t \cdot h \cdot l \cdot \gamma conc) \cdot 2$ — Weight of first portion of abutments

$Wabut1 = 1.85 \times 10^{5} lb$

Second Portion of Abutment: including wingwalls

$Volume := (t \cdot 0.51m \cdot l) + (t \cdot 1.25m \cdot 13.4m) + (t \cdot 1.25m \cdot 6m)$ — Volume of second portion of abutment

$Wabut2 := (Volume \cdot \gamma conc) \cdot 2$ — Weight of second portion of abutments

$Wabut2 = 2.713 \times 10^{5} lb$

Deck:

$t := 8in$ — Concrete deck thickness

$w := 10m$ — Width of deck

$Wdeck := (t \cdot w \cdot Lspan \cdot \gamma conc)$ — Weight of Deck

$Wdeck = 3.229 \times 10^{5} lb$

Approach Slab:

Concrete:

$t := 205mm$ Thickness of approach slab

$w := 10m$ Width of approach slab

$ltrib := 2.5m$ Length of approach slab which might induce load on seat

$Wconc := (t \cdot w \cdot ltrib \cdot \gamma conc) \cdot 2$ Weight of 2 concrete approach slabs

$Wconc = 5.43 \cdot 10^4 lb$

Backfill:

$t := 356mm$ Thickness of backfill

$\gamma soil := 120pcf$ Unit weight of backfill

$Wbackfill := (t \cdot w \cdot ltrib \cdot \gamma soil) \cdot 2$ Weight of backfill over 2 approach slabs

$Wbackfill = 7.543 \cdot 10^4 lb$

Pavement:

$t := 80mm$ Pavement thickness

$\gamma pavement := 150pcf$ Unit weight of asphalt pavement

$Wapppave := (t \cdot w \cdot ltrib \cdot \gamma pavement) \cdot 2$ Weight of pavement over 2 approach slabs

$Wapppave = 2.119 \cdot 10^4 lb$

$Wapproach := Wconc + Wbackfill + Wapppave$ Total weight of approach slabs

$Wapproach = 1.509 \cdot 10^5 lb$

Curbs:

$t := 9in$ Thickness of curbs

$w := 0.5m$ Width of curbs

$Wcurbs := (t \cdot w \cdot Lspan \cdot \gamma conc) \cdot 2$ Weight of curbs

$Wcurbs = 3.633 \cdot 10^4 lb$

Pavement:

$t := 80mm$ Pavement thickness

$w := 9m$ Width of paved deck

$Wpavement := t \cdot w \cdot Lspan \cdot \gamma pavement$ Weight of Pavement

$Wpavement = 1.144 \cdot 10^5 lb$

Guardrail: 2- Type Bridge Rail

50 lb/ft: Bridge Design Guide Table 3-1

$$Wrail := 50\frac{lb}{ft}\ 100ft\ 2$$ Weight of 2 guardrails

$$Wrail = 1 \times 10^{4}\ lb$$

**Total Weight of Bridge** :

$$DL := Wgirders + Wbracing + Wabut2 + Wdeck + Wapproach + Wcurbs + Wpavement + Wrail$$

$$DL = 9.973 \times 10^{5}\ lb$$

DL = 906.7 kips

Load applied to 6 test piles: 6/8 DL = 680 kips

# Appendix C

# RESULTS

## C.1. Tensile Testing

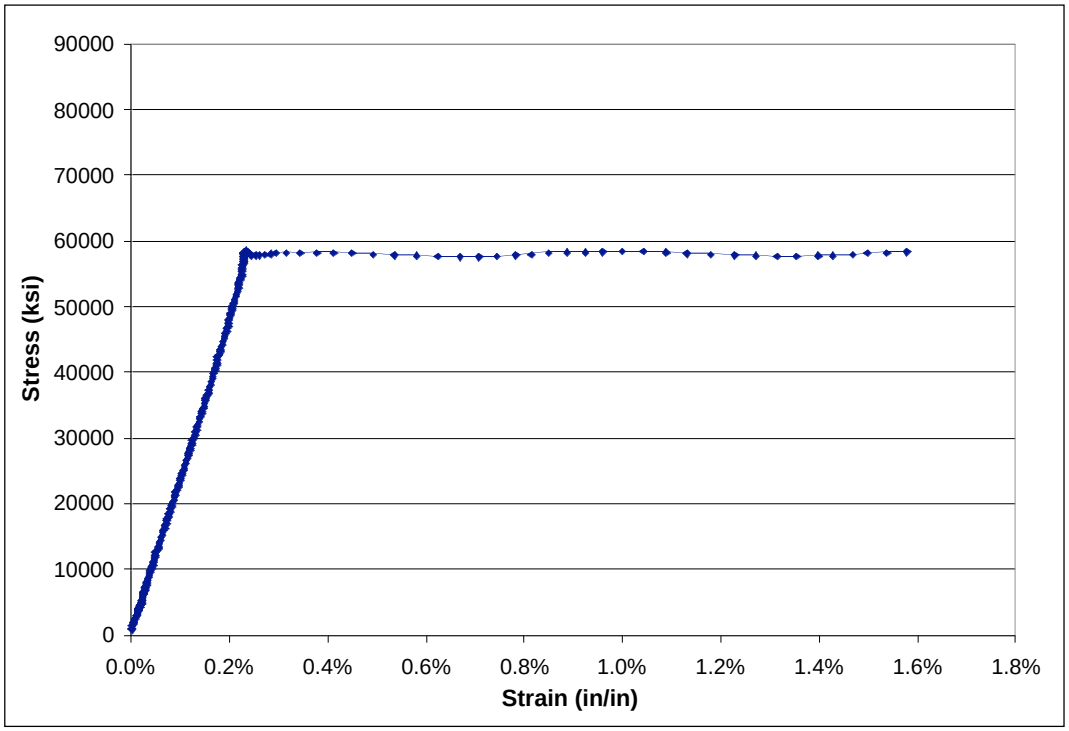


**Figure C.1. Stress-strain curve for the web of pile G2-N (and G3-S) (testing error)**

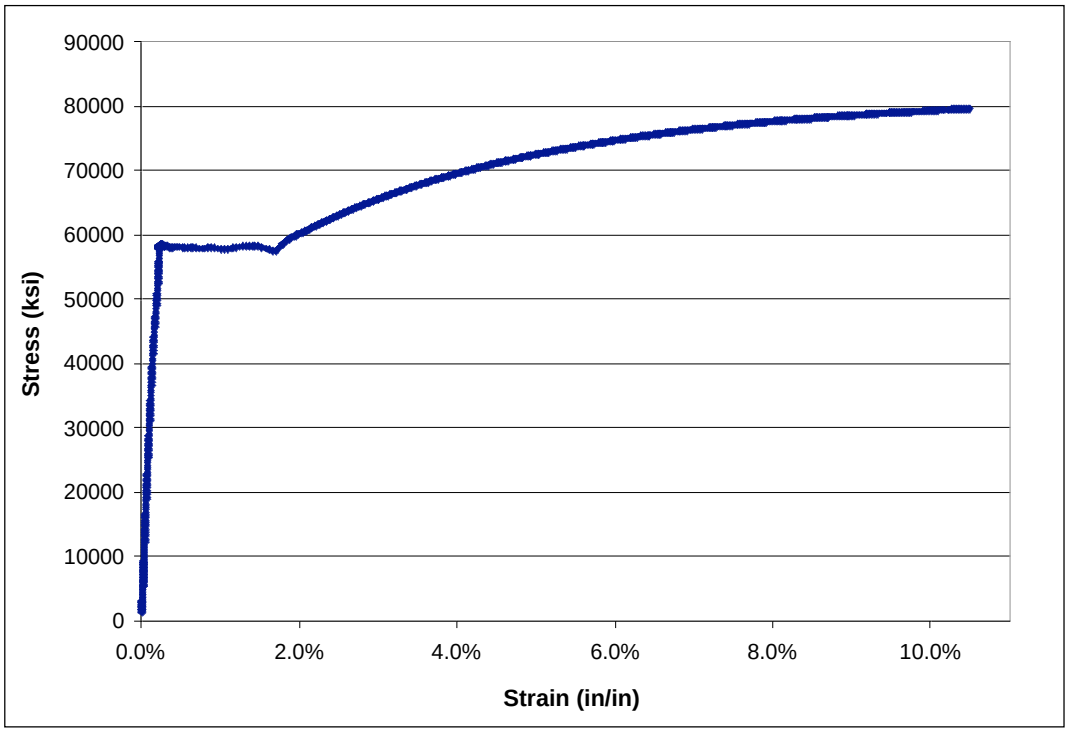


**Figure C.2. Stress-strain curve for the flange of pile G2-N (and G3-S)**

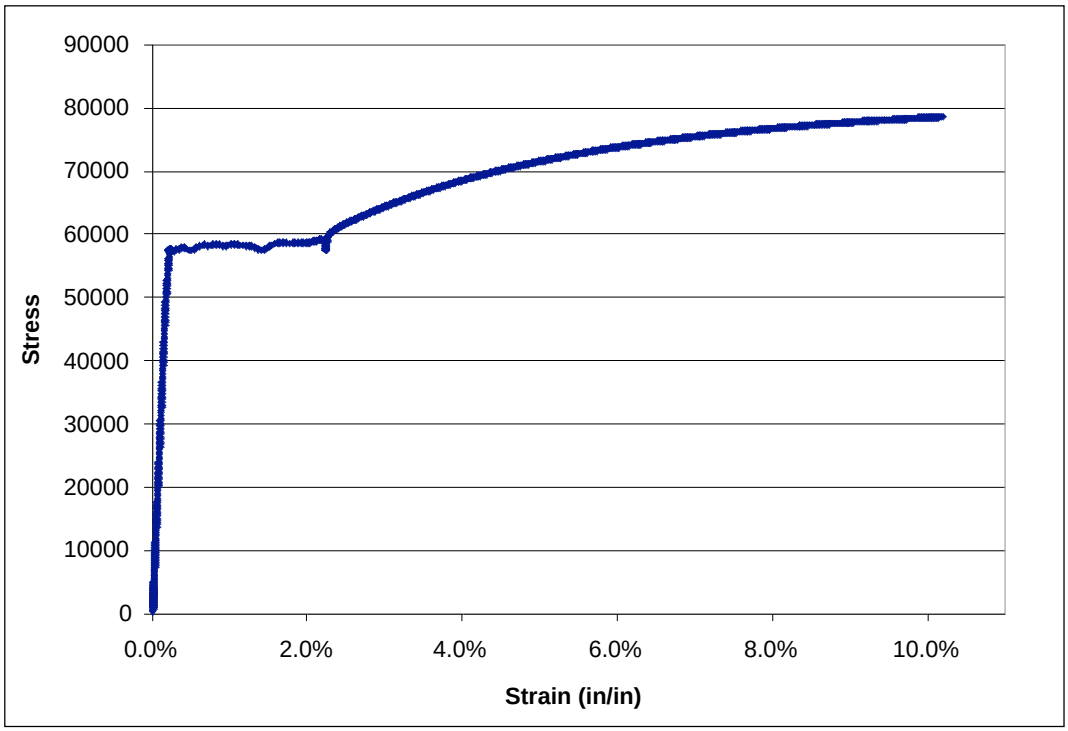


**Figure C.3. Stress-strain curve for the web of pile G3-N (and G2-S)**

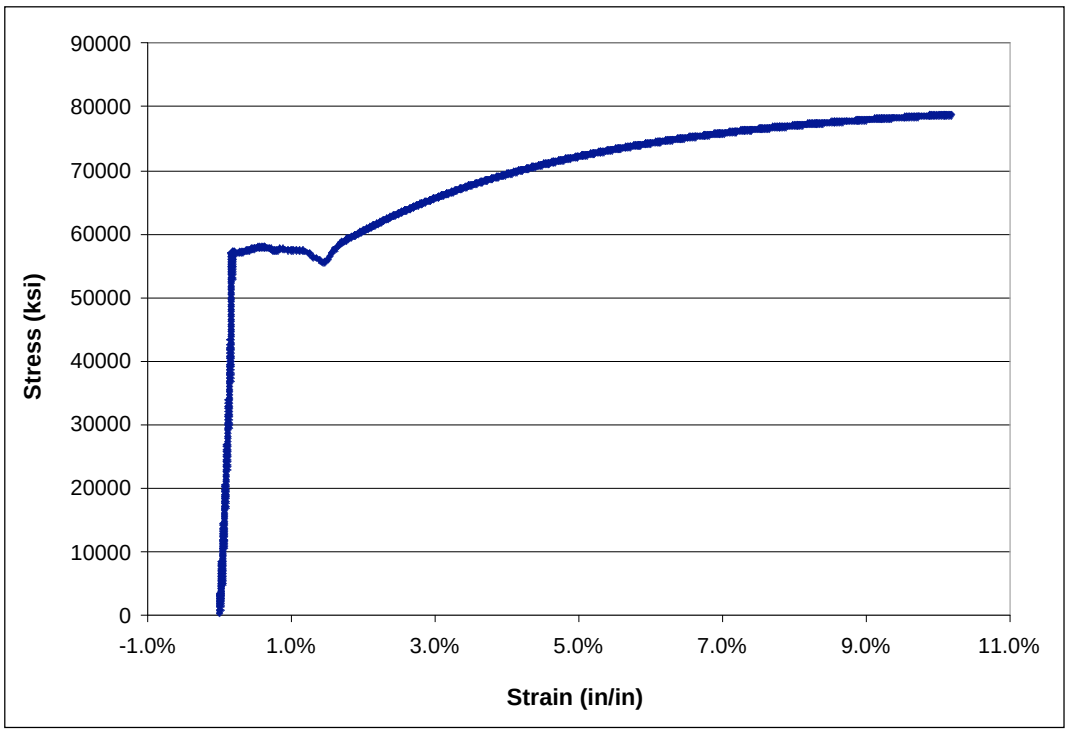


**Figure C.4. Stress-strain curve for the flange of pile G3-N (and G2-S)**

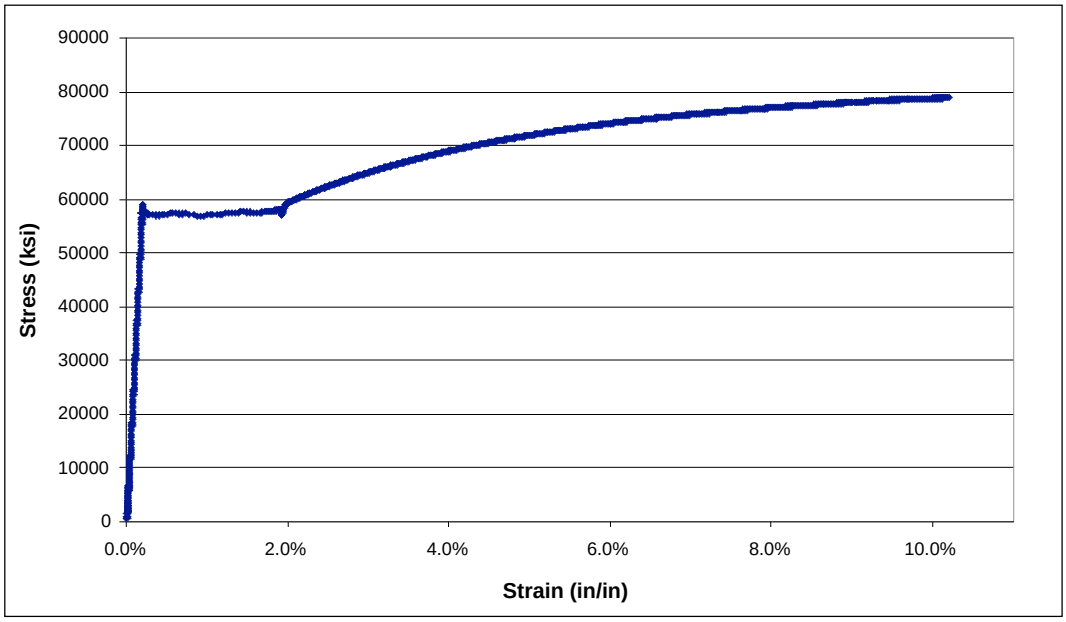


**Figure C.5. Stress-strain curve for the web of pile G4-N (and G1-S)**

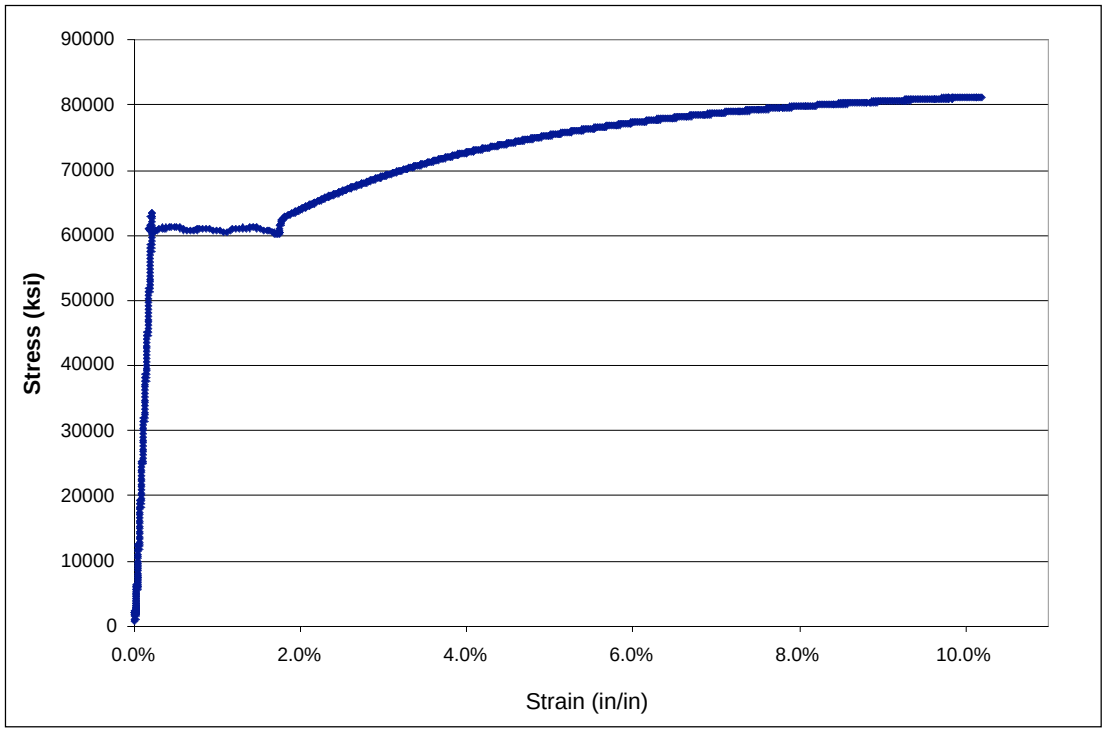


**Figure C.6. Stress-strain curve for the flange of pile G4-N (and G1-S)**

## C.2. Construction Results

**Table C.1. Effects of dead load along length of pile G1-S**

| | | | G1-S | | | |
|---|---|---|---|---|---|---|
| **Julian Day** | **Time** | **Gage Set** | **P (kN)** | **Mx (kN-m)** | **My (kN-m)** | **Mz (kN-m)** |
| 238 | 1200 | | | | | |
| 257 | 1301 | High | -79.9 | 0.32 | -1.44 | -0.03 |
| | | Middle | -80.4 | -2.68 | -1.35 | -0.03 |
| | | Low | -74.6 | -2.21 | -0.43 | 0.23 |
| 259 | 1301 | High | -276.8 | 58.89 | -5.60 | -0.87 |
| | | Middle | -237.9 | 20.84 | 9.55 | 1.14 |
| | | Low | -205.5 | -7.65 | -1.45 | 0.62 |
| 260 | 501 | High | -288.8 | 43.19 | -1.65 | 0.21 |
| | | Middle | -274.8 | 20.36 | 7.43 | 0.99 |
| | | Low | -234.1 | -8.71 | -1.73 | 0.70 |
| 261 | 501 | High | -346.7 | 19.98 | -10.87 | -0.50 |
| | | Middle | -270.0 | 12.27 | 7.62 | 1.32 |
| | | Low | -232.7 | -9.09 | -1.82 | 0.72 |
| 266 | 501 | High | -272.9 | -55.04 | -33.84 | 0.19 |
| | | Middle | -186.2 | -20.20 | 2.39 | 1.20 |
| | | Low | -166.2 | -7.37 | -1.84 | 0.51 |
| 267 | 501 | High | -322.7 | -40.26 | -34.74 | 0.35 |
| | | Middle | -221.9 | -15.72 | 2.19 | 1.43 |
| | | Low | -192.7 | -7.94 | -1.86 | 0.61 |
| 268 | 501 | High | -319.2 | -55.13 | -36.18 | -0.16 |
| | | Middle | -247.9 | -20.20 | 0.45 | 1.48 |
| | | Low | -218.6 | -8.43 | -1.95 | 0.65 |
| 271 | 501 | High | -339.1 | -68.19 | -44.10 | 0.09 |
| | | Middle | -268.0 | -24.84 | -1.85 | 1.55 |
| | | Low | -232.9 | -8.77 | -2.03 | 0.71 |
| 272 | 501 | High | -374.9 | -60.23 | -45.81 | 0.51 |
| | | Middle | -286.9 | -23.98 | -1.60 | 1.62 |
| | | Low | -249.4 | -8.80 | -2.18 | 0.69 |
| 275 | 501 | High | -393.9 | -54.09 | -46.85 | 0.75 |
| | | Middle | -302.3 | -24.78 | -2.29 | 1.52 |
| | | Low | -266.9 | -9.26 | -2.29 | 0.74 |
| 276 | 501 | High | -433.2 | -32.48 | -44.03 | 1.08 |
| | | Middle | -356.0 | -16.09 | -2.89 | 1.60 |
| | | Low | -309.9 | -10.40 | -2.75 | 0.91 |
| 277 | 501 | High | -490.8 | -50.22 | -56.26 | 1.27 |
| | | Middle | -408.4 | -22.42 | -4.70 | 1.77 |
| | | Low | -351.1 | -11.77 | -3.35 | 1.07 |

**Table C.2. Effects of dead load along length of pile G2-S**

| | | | G2-S | | | |
|---|---|---|---|---|---|---|
| **Julian Day** | **Time** | **Gage Set** | **P (kN)** | **Mx (kN-m)** | **My (kN-m)** | **Mz (kN-m)** |
| 238 | 1200 | | | | | |
| 257 | 1301 | High | -81.8 | 1.83 | -0.92 | -0.02 |
| | | Middle | -87.2 | -2.48 | -1.13 | 0.10 |
| | | Low | -75.2 | 0.50 | -0.59 | -0.14 |
| 259 | 1301 | High | -129.9 | 42.24 | 2.36 | -0.15 |
| | | Middle | -142.5 | 11.08 | 12.60 | 1.04 |
| | | Low | -125.0 | 0.21 | -1.15 | -0.15 |
| 260 | 501 | High | -166.4 | 34.95 | 3.53 | -0.20 |
| | | Middle | -171.9 | 10.79 | 11.42 | 1.03 |
| | | Low | -138.8 | -0.07 | -1.05 | -0.17 |
| 261 | 501 | High | -282.0 | 21.12 | -7.99 | 0.08 |
| | | Middle | -291.9 | 3.58 | 9.81 | 1.50 |
| | | Low | -212.6 | 0.27 | -1.11 | -0.17 |
| 266 | 501 | High | -508.9 | -14.68 | -30.83 | 0.86 |
| | | Middle | -536.2 | -16.37 | -0.19 | 1.80 |
| | | Low | -401.2 | 1.84 | -2.16 | -0.35 |
| 267 | 501 | High | -474.6 | -6.51 | -31.78 | 0.82 |
| | | Middle | -503.1 | -13.97 | 0.57 | 1.89 |
| | | Low | -384.3 | 2.09 | -2.20 | -0.32 |
| 268 | 501 | High | -534.2 | -16.18 | -33.94 | 0.81 |
| | | Middle | -562.8 | -16.58 | -1.46 | 1.95 |
| | | Low | -427.0 | 2.02 | -2.04 | -0.38 |
| 271 | 501 | High | -541.8 | -25.24 | -40.76 | 1.12 |
| | | Middle | -570.5 | -19.34 | -3.37 | 1.97 |
| | | Low | -436.8 | 2.24 | -2.21 | -0.40 |
| 272 | 501 | High | -547.1 | -19.51 | -41.51 | 1.02 |
| | | Middle | -578.7 | -19.43 | -2.78 | 2.04 |
| | | Low | -452.4 | 2.70 | -2.23 | -0.34 |
| 275 | 501 | High | -528.0 | -16.29 | -41.45 | 0.98 |
| | | Middle | -566.0 | -19.99 | -3.60 | 1.99 |
| | | Low | -451.0 | 3.31 | -2.67 | -0.36 |
| 276 | 501 | High | -500.8 | -6.09 | -38.08 | 0.80 |
| | | Middle | -536.4 | -14.56 | -2.97 | 2.10 |
| | | Low | -426.1 | 2.42 | -2.58 | -0.47 |
| 277 | 501 | High | -570.7 | -16.74 | -48.36 | 0.86 |
| | | Middle | -608.7 | -19.16 | -5.21 | 2.25 |
| | | Low | -487.1 | 3.22 | -2.66 | -0.37 |

**Table C.3. Effects of dead load along length of pile G3-S**

| | | | G3-S | | | |
|---|---|---|---|---|---|---|
| **Julian Day** | **Time** | **Gage Set** | **P (kN)** | **Mx (kN-m)** | **My (kN-m)** | **Mz (kN-m)** |
| 238 | 1200 | | | | | |
| 257 | 1301 | High | -83.2 | -1.07 | -0.02 | 0.09 |
| | | Middle* | N/A | N/A | N/A | N/A |
| | | Low | -15.4 | 2.28 | -0.88 | 0.41 |
| 259 | 1301 | High | -114.0 | 27.15 | 9.26 | 0.92 |
| | | Middle* | -124.9 | 6.22 | 11.88 | -0.20 |
| | | Low | -26.6 | 3.82 | -1.51 | 0.72 |
| 260 | 501 | High | -140.0 | 24.27 | 8.20 | 0.86 |
| | | Middle* | -148.4 | 6.16 | 11.10 | -0.25 |
| | | Low | -29.6 | 4.18 | -1.66 | 0.80 |
| 261 | 501 | High | -267.8 | 16.37 | 3.70 | 1.29 |
| | | Middle* | -221.9 | 9.73 | 14.31 | 0.61 |
| | | Low | -51.1 | 7.10 | -2.85 | 1.34 |
| 266 | 501 | High | -475.3 | -1.46 | -9.45 | 1.94 |
| | | Middle* | -310.2 | 16.39 | 16.76 | 3.05 |
| | | Low | -87.6 | 12.51 | -4.91 | 2.36 |
| 267 | 501 | High | -458.1 | 1.80 | -8.96 | 2.10 |
| | | Middle* | -320.6 | 12.39 | 17.15 | 2.45 |
| | | Low | -86.3 | 12.34 | -4.83 | 2.33 |
| 268 | 501 | High | -504.0 | -2.60 | -11.30 | 2.08 |
| | | Middle* | -367.6 | 11.14 | 15.26 | 2.28 |
| | | Low | -92.9 | 13.28 | -5.20 | 2.51 |
| 271 | 501 | High | -504.4 | -8.13 | -14.32 | 2.24 |
| | | Middle* | -372.6 | 8.43 | 14.84 | 2.09 |
| | | Low | -92.7 | 13.25 | -5.18 | 2.50 |
| 272 | 501 | High | -532.6 | -6.93 | -13.85 | 2.33 |
| | | Middle* | -404.8 | 6.93 | 15.63 | 2.07 |
| | | Low | -99.9 | 14.32 | -5.58 | 2.71 |
| 275 | 501 | High | -517.1 | -6.68 | -14.53 | 2.33 |
| | | Middle* | -425.8 | 0.91 | 13.16 | 1.31 |
| | | Low | -98.7 | 14.21 | -5.52 | 2.68 |
| 276 | 501 | High | -508.1 | -1.10 | -12.95 | 2.40 |
| | | Middle* | -431.6 | -0.28 | 13.06 | 1.04 |
| | | Low | -97.0 | 13.91 | -5.42 | 2.63 |
| 277 | 501 | High | -556.5 | -7.63 | -16.27 | 2.69 |
| | | Middle* | -468.7 | -1.01 | 14.52 | 1.08 |
| | | Low | -104.8 | 15.05 | -5.85 | 2.85 |

**Table C.4. Effects of dead load along length of pile G2-N**

| | | | G2-N | | | |
|---|---|---|---|---|---|---|
| **Julian Day** | **Time** | **Gage Set** | **P (kN)** | **Mx (kN-m)** | **My (kN-m)** | **Mz (kN-m)** |
| 240 | 700 | | | | | |
| 245 | 541 | High* | -53.8 | -3.62 | -1.37 | 0.00 |
| | | Middle | -56.3 | -1.69 | -0.66 | -0.10 |
| | | Low | -46.5 | 2.94 | -0.33 | 0.24 |
| 258 | 1001 | High* | -205.0 | 2.78 | -0.12 | 0.00 |
| | | Middle | -216.9 | 1.96 | 3.16 | -0.31 |
| | | Low | -221.5 | 12.32 | -1.61 | 0.49 |
| 259 | 1301 | High* | -134.1 | 43.45 | 2.38 | 0.00 |
| | | Middle | -136.9 | 20.08 | 12.44 | 0.23 |
| | | Low | -163.8 | 8.47 | 0.96 | -0.01 |
| 260 | 501 | High* | -163.2 | 40.57 | 5.21 | 0.00 |
| | | Middle | -167.4 | 19.21 | 10.39 | 0.19 |
| | | Low | -187.5 | 9.33 | 1.27 | 0.05 |
| 261 | 501 | High* | -215.5 | 30.51 | -5.69 | 0.00 |
| | | Middle | -232.0 | 13.86 | 8.12 | -0.05 |
| | | Low | -237.9 | 11.87 | 2.03 | 0.08 |
| 266 | 501 | High* | -350.6 | 8.83 | -21.37 | 0.00 |
| | | Middle | -392.0 | -0.91 | -2.41 | -0.65 |
| | | Low | -368.7 | 19.01 | 1.77 | 0.57 |
| 267 | 501 | High* | -340.8 | 15.29 | -22.94 | 0.00 |
| | | Middle | -386.2 | 1.15 | -1.82 | -0.37 |
| | | Low | -365.7 | 17.36 | 2.69 | 0.38 |
| 268 | 501 | High* | -385.1 | 7.34 | -25.61 | 0.00 |
| | | Middle | -439.0 | -2.85 | -5.03 | -0.61 |
| | | Low | -406.7 | 20.03 | 2.33 | 0.60 |
| 272 | 501 | High* | -361.4 | 3.05 | -32.62 | 0.00 |
| | | Middle | -421.6 | -6.66 | -8.42 | -0.53 |
| | | Low | -385.9 | 18.34 | 4.06 | 0.40 |
| 273 | 501 | High* | -409.5 | 2.45 | -33.18 | 0.00 |
| | | Middle | -471.1 | -7.28 | -8.45 | -0.65 |
| | | Low | -434.0 | 19.93 | 2.93 | 0.64 |
| 275 | 501 | High* | -390.7 | 9.78 | -29.77 | 0.00 |
| | | Middle | -448.5 | -5.34 | -7.39 | -0.52 |
| | | Low | -418.6 | 17.94 | 2.30 | 0.69 |
| 276 | 501 | High* | -383.5 | 19.25 | -24.87 | 0.00 |
| | | Middle | -433.5 | -0.68 | -6.19 | -0.22 |
| | | Low | -413.3 | 16.04 | 2.51 | 0.64 |
| 277 | 501 | High* | -401.7 | 9.70 | -33.51 | 0.00 |
| | | Middle | -464.3 | -5.18 | -8.31 | -0.55 |
| | | Low | -432.4 | 18.01 | 3.16 | 0.76 |

**Table C.5. Effects of dead load along length of pile G3-N**

| | | | G3-N | | | |
|---|---|---|---|---|---|---|
| **Julian Day** | **Time** | **Gage Set** | **P (kN)** | **Mx (kN-m)** | **My (kN-m)** | **Mz (kN-m)** |
| 240 | 700 | | | | | |
| 245 | 541 | High | -54.7 | 2.29 | -0.95 | -0.09 |
| | | Middle | -41.9 | -1.51 | -0.82 | 0.04 |
| | | Low | -32.4 | 1.26 | -0.12 | -0.06 |
| 258 | 1001 | High | -233.5 | 3.40 | 3.44 | -2.59 |
| | | Middle | -227.2 | 3.49 | 5.95 | -0.20 |
| | | Low | -222.4 | 7.18 | 2.44 | -0.95 |
| 259 | 1301 | High | -153.3 | 1.46 | 8.38 | -7.26 |
| | | Middle | -159.6 | 13.94 | 13.48 | -0.07 |
| | | Low | -158.4 | 5.89 | 4.77 | -1.29 |
| 260 | 501 | High | -173.1 | 2.47 | 9.34 | -6.94 |
| | | Middle | -173.6 | 14.94 | 12.00 | -0.12 |
| | | Low | -173.5 | 6.41 | 4.78 | -1.32 |
| 261 | 501 | High | -265.1 | 1.06 | 2.14 | -4.98 |
| | | Middle | -258.4 | 11.17 | 12.51 | 0.05 |
| | | Low | -254.9 | 8.91 | 6.30 | -1.52 |
| 266 | 501 | High | -541.7 | -2.78 | -11.91 | 0.13 |
| | | Middle | -512.8 | -2.99 | 7.28 | 0.30 |
| | | Low | -514.1 | 21.04 | 12.53 | -3.18 |
| 267 | 501 | High | -530.0 | -3.45 | -12.80 | -0.72 |
| | | Middle | -505.4 | -1.80 | 8.05 | 0.47 |
| | | Low | -504.8 | 19.03 | 13.59 | -3.34 |
| 268 | 501 | High | -618.5 | -3.21 | -15.95 | 0.96 |
| | | Middle | -584.1 | -4.21 | 6.32 | 0.58 |
| | | Low | -585.6 | 23.60 | 14.53 | -3.62 |
| 272 | 501 | High | -614.7 | -4.30 | -21.59 | 1.86 |
| | | Middle | -579.7 | -6.79 | 4.71 | 0.80 |
| | | Low | -579.5 | 24.16 | 17.05 | -3.96 |
| 273 | 501 | High | -691.3 | -4.65 | -22.25 | 2.12 |
| | | Middle | -653.9 | -7.45 | 4.69 | 0.77 |
| | | Low | -659.2 | 26.50 | 17.52 | -4.20 |
| 275 | 501 | High | -639.4 | -5.80 | -20.12 | 0.80 |
| | | Middle | -607.2 | -6.62 | 4.87 | 0.72 |
| | | Low | -608.7 | 24.92 | 17.76 | -4.34 |
| 276 | 501 | High | -594.2 | -5.74 | -16.89 | -1.26 |
| | | Middle | -566.2 | -1.89 | 5.52 | 0.82 |
| | | Low | -567.2 | 21.52 | 17.49 | -4.38 |
| 277 | 501 | High | -688.6 | -5.35 | -23.14 | 0.55 |
| | | Middle | -650.7 | -4.30 | 5.19 | 1.02 |
| | | Low | -656.1 | 25.26 | 19.67 | -4.70 |

**Table C.6. Effects of dead load along length of pile G4-N**

| | | | G4-N | | | |
|---|---|---|---|---|---|---|
| **Julian Day** | **Time** | **Gage Set** | **P (kN)** | **Mx (kN-m)** | **My (kN-m)** | **Mz (kN-m)** |
| 240 | 700 | | | | | |
| 245 | 541 | High* | 8.7 | -6.31 | -2.03 | -0.10 |
| | | Middle | 3.7 | -2.66 | -0.35 | 0.04 |
| | | Low | N/A | 0.00 | 0.00 | 0.00 |
| 258 | 1001 | High* | -117.0 | 23.53 | 5.24 | -0.39 |
| | | Middle | -151.5 | 3.98 | 8.24 | -0.37 |
| | | Low | -150.3 | -5.33 | 1.30 | 0.30 |
| 259 | 1301 | High* | -95.0 | 44.80 | 7.49 | -0.35 |
| | | Middle | -164.3 | 12.69 | 14.11 | -0.35 |
| | | Low | -170.2 | -6.65 | 3.48 | 0.43 |
| 260 | 501 | High* | -137.4 | 42.27 | 7.48 | 0.08 |
| | | Middle | -188.6 | 14.42 | 11.59 | -0.30 |
| | | Low | -192.8 | -5.69 | 3.19 | 0.50 |
| 261 | 501 | High* | -165.8 | 33.12 | 2.85 | 0.19 |
| | | Middle | -208.6 | 11.91 | 13.62 | -0.01 |
| | | Low | -213.9 | -4.54 | 4.44 | 0.44 |
| 266 | 501 | High* | -117.8 | -3.38 | -5.71 | -0.49 |
| | | Middle | -141.6 | -2.73 | 14.48 | -0.02 |
| | | Low | -148.2 | -0.41 | 8.28 | 0.65 |
| 267 | 501 | High* | -140.6 | 2.96 | -6.53 | -0.26 |
| | | Middle | -169.5 | -2.35 | 15.24 | -0.05 |
| | | Low | -174.6 | -3.51 | 9.48 | 0.68 |
| 268 | 501 | High* | -167.5 | -5.58 | -9.52 | -0.38 |
| | | Middle | -192.0 | -3.91 | 13.77 | 0.18 |
| | | Low | -196.8 | -1.65 | 9.56 | 0.69 |
| 272 | 501 | High* | -191.0 | -9.71 | -14.50 | -0.18 |
| | | Middle | -201.1 | -6.71 | 13.45 | 0.15 |
| | | Low | -205.0 | -2.62 | 12.31 | 0.94 |
| 273 | 501 | High* | -247.9 | -10.32 | -17.44 | -0.03 |
| | | Middle | -257.3 | -6.97 | 11.34 | 0.47 |
| | | Low | -281.4 | -1.90 | 11.15 | 1.09 |
| 275 | 501 | High* | -233.8 | -4.88 | -16.44 | -0.07 |
| | | Middle | -244.9 | -7.26 | 11.74 | 0.17 |
| | | Low | -268.9 | -4.75 | 11.23 | 1.22 |
| 276 | 501 | High* | -287.8 | 10.79 | -16.42 | 0.44 |
| | | Middle | -303.2 | -1.99 | 11.37 | 0.01 |
| | | Low | -316.6 | -8.12 | 11.13 | 1.38 |
| 277 | 501 | High* | -337.5 | 8.38 | -20.75 | 0.05 |
| | | Middle | -353.9 | -2.22 | 12.93 | 0.14 |
| | | Low | -362.8 | -6.88 | 12.39 | 1.60 |

## C.3. Live Load Results

**Table C.7 Effects of live load along length of pile G1-S**

| | | G1-S | | | |
|---|---|---|---|---|---|
| **Load Case** | **Gage Set** | **P (kN)** | **Mx (kN-m)** | **My (kN-m)** | **Mz (kN-m)** |
| 1 | High* | -60.6 | -1.38 | -4.93 | 0.39 |
| 1 | Middle | -6.2 | 0.28 | 4.43 | 0.58 |
| 1 | Low | 11.6 | 0.52 | 0.48 | -0.10 |
| 2 | High* | -91.2 | -6.70 | -9.88 | 0.75 |
| 2 | Middle | -32.5 | -1.81 | 4.39 | 0.58 |
| 2 | Low | -3.3 | 0.26 | 0.48 | -0.07 |
| 3 | High* | -85.9 | -7.87 | -7.54 | 0.74 |
| 3 | Middle | -36.5 | -2.54 | 3.56 | 0.56 |
| 3 | Low | -7.4 | 0.28 | 0.47 | -0.05 |
| 4 | High* | -36.0 | 0.63 | -2.70 | 0.61 |
| 4 | Middle | 10.3 | -0.01 | 3.73 | 0.44 |
| 4 | Low | 19.3 | 0.53 | 0.51 | -0.08 |
| 5 | High* | -51.4 | -2.79 | -5.25 | 0.79 |
| 5 | Middle | 1.9 | -1.77 | 3.75 | 0.50 |
| 5 | Low | 15.2 | 0.55 | 0.50 | -0.08 |
| 6 | High* | -53.7 | -3.65 | -5.73 | 0.97 |
| 6 | Middle | 6.7 | -2.09 | 3.64 | 0.52 |
| 6 | Low | 17.0 | 0.45 | 0.50 | -0.09 |
| 7 | High* | -72.8 | -7.25 | -10.39 | 0.77 |
| 7 | Middle | -32.3 | -0.44 | 3.21 | 0.29 |
| 7 | Low | -7.0 | 0.13 | 0.44 | -0.05 |
| 8 | High* | -114.2 | -16.03 | -18.23 | 0.52 |
| 8 | Middle | -88.5 | -1.44 | 2.22 | 0.01 |
| 8 | Low | -46.6 | -0.65 | 0.12 | 0.04 |
| 9 | High* | -162.0 | -16.17 | -20.10 | 0.20 |
| 9 | Middle | -144.8 | -2.23 | 1.50 | 0.06 |
| 9 | Low | -88.7 | -1.33 | -0.11 | 0.15 |
| 10 | High* | -113.0 | -17.70 | -16.52 | 0.15 |
| 10 | Middle | -101.8 | -2.88 | 0.85 | 0.05 |
| 10 | Low | -62.9 | -1.17 | -0.13 | 0.09 |
| 11 | High* | -41.8 | -5.88 | -6.28 | 0.01 |
| 11 | Middle | -39.5 | -0.28 | 0.37 | -0.10 |
| 11 | Low | -25.0 | -0.66 | 0.00 | 0.05 |
| 12 | High* | -84.8 | -11.10 | -11.99 | 0.10 |
| 12 | Middle | -77.1 | -1.93 | 0.76 | 0.00 |
| 12 | Low | -46.5 | -0.93 | -0.08 | 0.08 |
| 13 | High* | -100.1 | -11.10 | -10.26 | -0.02 |
| 13 | Middle | -92.9 | -2.74 | 0.23 | 0.02 |
| 13 | Low | -57.8 | -0.96 | -0.11 | 0.10 |
| 14 | AH | -6.8 | 2.11 | 2.73 | -0.02 |
| 14 | AM | -14.2 | 1.14 | -0.44 | -0.22 |
| 14 | AL | -12.6 | -0.32 | -0.03 | 0.00 |

**Table C.8. Effects of live load along length of pile G2-S**

| | | G2-S | | | |
|---|---|---|---|---|---|
| Load Case | Gage Set | P (kN) | Mx (kN-m) | My (kN-m) | Mz (kN-m) |
| 1 | High | -8.33 | 0.43 | 0.31 | 0.14 |
| 1 | Middle | -3.07 | 1.43 | 3.56 | 0.20 |
| 1 | Low | 8.89 | -0.39 | 0.36 | 0.03 |
| 2 | High | -44.42 | -4.57 | -4.16 | 0.13 |
| 2 | Middle | -37.34 | -0.36 | 3.52 | 0.24 |
| 2 | Low | -13.98 | -0.40 | 0.39 | 0.03 |
| 3 | High | -64.44 | -6.13 | -3.27 | 0.15 |
| 3 | Middle | -59.46 | -1.35 | 2.87 | 0.23 |
| 3 | Low | -31.64 | -0.19 | 0.33 | 0.04 |
| 4 | High | 0.65 | 0.49 | 1.29 | 0.09 |
| 4 | Middle | 1.78 | 0.55 | 2.76 | 0.12 |
| 4 | Low | 9.81 | -0.27 | 0.35 | -0.01 |
| 5 | High | -33.71 | -3.87 | -2.59 | 0.10 |
| 5 | Middle | -26.91 | -1.53 | 3.06 | 0.14 |
| 5 | Low | -11.08 | -0.40 | 0.34 | -0.03 |
| 6 | High | -40.52 | -4.68 | -2.89 | 0.10 |
| 6 | Middle | -33.17 | -2.24 | 2.98 | 0.12 |
| 6 | Low | -15.39 | -0.19 | 0.42 | 0.02 |
| 7 | High | -5.37 | -1.63 | -1.77 | 0.27 |
| 7 | Middle | -1.59 | 0.51 | 3.02 | 0.10 |
| 7 | Low | -0.44 | 0.30 | -0.05 | 0.10 |
| 8 | High | -30.62 | -7.07 | -7.35 | 0.36 |
| 8 | Middle | -26.66 | -0.62 | 2.15 | 0.11 |
| 8 | Low | -16.12 | 0.10 | 0.20 | 0.07 |
| 9 | High | -68.43 | -7.53 | -8.58 | 0.34 |
| 9 | Middle | -61.72 | -1.12 | 1.55 | 0.16 |
| 9 | Low | -41.51 | -0.29 | 0.25 | 0.01 |
| 10 | High | -59.67 | -10.52 | -8.92 | 0.35 |
| 10 | Middle | -55.19 | -1.72 | 1.40 | 0.18 |
| 10 | Low | -35.37 | 0.06 | 0.40 | 0.08 |
| 11 | High | -20.04 | -3.97 | -3.59 | 0.17 |
| 11 | Middle | -17.42 | -0.24 | 1.19 | 0.11 |
| 11 | Low | -3.65 | -1.21 | 0.69 | -0.17 |
| 12 | High | -53.03 | -8.32 | -7.87 | 0.24 |
| 12 | Middle | -48.47 | -1.59 | 1.55 | 0.20 |
| 12 | Low | -31.62 | 0.16 | 0.27 | 0.08 |
| 13 | High | -85.15 | -9.51 | -8.02 | 0.18 |
| 13 | Middle | -80.46 | -2.37 | 1.18 | 0.25 |
| 13 | Low | -51.34 | -0.24 | 0.43 | 0.03 |
| 14 | BH | -14.23 | 1.00 | 2.31 | 0.00 |
| 14 | BM | -14.00 | 0.68 | 0.68 | 0.05 |
| 14 | BL | -3.04 | -1.27 | 0.73 | -0.19 |

**Table C.9. Effects of live load along length of pile G3-S**

| | | G3-S | | | |
|---|---|---|---|---|---|
| **Load Case** | **Gage Set** | **P (kN)** | **Mx (kN-m)** | **My (kN-m)** | **Mz (kN-m)** |
| 1 | High | -18.45 | 0.02 | 2.72 | 0.08 |
| 1 | Middle* | -10.76 | 2.54 | 1.84 | -0.05 |
| 1 | Low | -6.55 | -0.43 | 0.24 | 0.00 |
| 2 | High | -54.73 | -3.96 | 1.54 | 0.02 |
| 2 | Middle* | -30.10 | 3.74 | 3.60 | 0.02 |
| 2 | Low | -29.36 | -0.44 | 0.21 | 0.00 |
| 3 | High | -82.83 | -5.13 | 0.93 | -0.02 |
| 3 | Middle* | -50.57 | 4.54 | 3.38 | 0.15 |
| 3 | Low | -53.11 | -0.23 | 0.16 | 0.00 |
| 4 | High | -19.39 | -1.28 | 1.57 | -0.06 |
| 4 | Middle* | -16.14 | 1.52 | 1.29 | -0.14 |
| 4 | Low | -10.23 | -0.16 | 0.15 | -0.01 |
| 5 | High | -67.71 | -5.62 | 0.61 | -0.02 |
| 5 | Middle* | -44.50 | 3.10 | 3.35 | -0.01 |
| 5 | Low | -41.93 | -0.06 | 0.16 | 0.01 |
| 6 | High | -93.36 | -6.65 | 0.20 | -0.02 |
| 6 | Middle* | -60.21 | 3.84 | 3.69 | 0.12 |
| 6 | Low | -61.46 | -0.06 | 0.10 | 0.01 |
| 7 | High | 3.89 | 0.32 | 1.04 | -0.16 |
| 7 | Middle* | 7.88 | 1.53 | 0.49 | -0.03 |
| 7 | Low | 4.95 | 0.19 | 0.09 | 0.02 |
| 8 | High | -3.05 | -1.40 | 0.65 | -0.07 |
| 8 | Middle* | 4.91 | 1.20 | 1.28 | -0.10 |
| 8 | Low | 3.27 | 0.14 | 0.11 | 0.02 |
| 9 | High | -15.97 | -1.73 | 0.30 | -0.05 |
| 9 | Middle* | 0.26 | 1.78 | 1.65 | 0.05 |
| 9 | Low | -6.23 | 0.14 | 0.09 | 0.02 |
| 10 | High | -28.42 | -3.62 | 0.05 | -0.01 |
| 10 | Middle* | -13.85 | 1.57 | 1.68 | -0.08 |
| 10 | Low | -13.81 | 0.03 | 0.11 | 0.00 |
| 11 | High | -9.74 | -1.34 | 0.64 | -0.03 |
| 11 | Middle* | -8.81 | 0.04 | 0.76 | -0.21 |
| 11 | Low | -2.14 | 0.09 | 0.08 | 0.00 |
| 12 | High | -38.18 | -4.06 | 0.11 | 0.04 |
| 12 | Middle* | -24.67 | 1.13 | 2.29 | -0.13 |
| 12 | Low | -19.17 | 0.08 | 0.14 | 0.00 |
| 13 | High | -70.71 | -5.14 | -0.33 | 0.05 |
| 13 | Middle* | -43.36 | 2.53 | 2.89 | 0.04 |
| 13 | Low | -43.23 | -0.11 | 0.13 | -0.01 |
| 14 | High | -21.68 | 1.01 | 0.66 | -0.12 |
| 14 | Middle* | -9.37 | 2.18 | 0.44 | 0.17 |
| 14 | Low | -18.94 | -0.06 | -0.01 | 0.00 |

**Table C.10. Effects of live load along length of pile G2-N**

| | | G2-N | | | |
|---|---|---|---|---|---|
| **Load Case** | **Gage Set** | **P (kN)** | **Mx (kN-m)** | **My (kN-m)** | **Mz (kN-m)** |
| 1 | High* | -49.05 | -5.71 | -6.23 | 0.00 |
| 1 | Middle | -46.08 | 1.04 | 3.64 | -0.25 |
| 1 | Low | -41.48 | 3.56 | -0.56 | -0.04 |
| 2 | High* | -25.21 | -4.54 | -5.65 | 0.00 |
| 2 | Middle | -20.81 | 1.42 | 3.74 | -0.20 |
| 2 | Low | -19.32 | 2.77 | -0.37 | -0.08 |
| 3 | High* | -14.03 | -0.50 | -1.33 | 0.00 |
| 3 | Middle | -7.57 | 2.46 | 3.53 | -0.10 |
| 3 | Low | -8.75 | 2.22 | -0.58 | -0.07 |
| 4 | High* | -25.99 | -2.71 | -3.80 | 0.00 |
| 4 | Middle | -20.61 | 1.86 | 3.31 | -0.16 |
| 4 | Low | -19.43 | 2.48 | -0.55 | -0.08 |
| 5 | High* | -9.92 | -2.08 | -4.06 | 0.00 |
| 5 | Middle | -5.92 | 1.89 | 3.40 | -0.08 |
| 5 | Low | -3.70 | 2.28 | -0.40 | -0.17 |
| 6 | High* | -1.95 | -0.15 | -3.25 | 0.00 |
| 6 | Middle | 1.04 | 2.12 | 3.22 | 0.01 |
| 6 | Low | 3.38 | 2.04 | -0.25 | -0.24 |
| 7 | High* | -93.43 | -12.83 | -8.30 | 0.00 |
| 7 | Middle | -104.10 | -2.59 | 1.47 | -0.56 |
| 7 | Low | -89.63 | 4.55 | 0.04 | 0.23 |
| 8 | High* | -58.47 | -13.01 | -9.61 | 0.00 |
| 8 | Middle | -69.97 | -2.96 | 0.50 | -0.53 |
| 8 | Low | -56.94 | 3.18 | 1.00 | 0.13 |
| 9 | High* | -14.17 | -5.48 | -4.08 | 0.00 |
| 9 | Middle | -17.97 | -0.98 | 0.16 | -0.31 |
| 9 | Low | -14.34 | 1.22 | 0.98 | 0.06 |
| 10 | High* | -43.59 | -11.72 | -8.12 | 0.00 |
| 10 | Middle | -51.81 | -2.54 | 0.04 | -0.42 |
| 10 | Low | -41.33 | 2.47 | 1.02 | 0.10 |
| 11 | High* | -58.05 | -11.51 | -8.06 | 0.00 |
| 11 | Middle | -67.34 | -2.83 | -0.31 | -0.43 |
| 11 | Low | -55.09 | 2.70 | 0.98 | 0.11 |
| 12 | High* | -22.14 | -9.35 | -7.10 | 0.00 |
| 12 | Middle | -28.28 | -2.08 | -0.07 | -0.33 |
| 12 | Low | -21.27 | 1.65 | 1.07 | 0.05 |
| 13 | High* | 1.67 | -3.42 | -2.66 | 0.00 |
| 13 | Middle | -0.19 | -0.59 | -0.03 | -0.19 |
| 13 | Low | 1.37 | 0.36 | 0.88 | 0.02 |
| 14 | High* | 6.10 | -0.67 | 1.06 | 0.00 |
| 14 | Middle | 8.30 | 0.20 | -0.18 | -0.11 |
| 14 | Low | 7.22 | -0.05 | 0.51 | 0.06 |

**Table C.11. Effects of live load along length of pile G3-N**

| | | G3-N | | | |
|---|---|---|---|---|---|
| **Load Case** | **Gage Set** | **P (kN)** | **Mx (kN-m)** | **My (kN-m)** | **Mz (kN-m)** |
| 1 | High | -63.74 | -0.02 | -1.43 | 0.75 |
| 1 | Middle | -61.42 | 0.44 | 3.58 | -0.10 |
| 1 | Low | -57.01 | 0.70 | -1.12 | 0.22 |
| 2 | High | -22.55 | -0.10 | -1.21 | 0.51 |
| 2 | Middle | -23.00 | 0.77 | 3.51 | -0.12 |
| 2 | Low | -18.37 | 0.46 | -0.91 | 0.22 |
| 3 | High | 17.46 | 0.24 | 1.28 | -0.23 |
| 3 | Middle | 14.54 | 1.56 | 2.49 | -0.15 |
| 3 | Low | 18.22 | -0.25 | -1.40 | 0.24 |
| 4 | High | -59.04 | 0.10 | -1.39 | 0.53 |
| 4 | Middle | -56.81 | 1.01 | 3.15 | -0.18 |
| 4 | Low | -54.01 | 0.74 | -0.83 | 0.18 |
| 5 | High | -23.53 | 0.06 | -1.78 | 0.50 |
| 5 | Middle | -23.37 | 1.12 | 3.03 | -0.18 |
| 5 | Low | -19.72 | 0.66 | -0.44 | 0.18 |
| 6 | High | 7.22 | 0.36 | -0.81 | 0.04 |
| 6 | Middle | 5.04 | 1.21 | 2.30 | -0.17 |
| 6 | Low | 7.82 | -0.03 | -0.28 | 0.19 |
| 7 | High | -63.73 | 0.65 | -1.47 | 1.06 |
| 7 | Middle | -59.39 | -0.96 | 2.35 | -0.09 |
| 7 | Low | -56.75 | 0.70 | -0.40 | 0.17 |
| 8 | High | -54.15 | 0.22 | -2.36 | 1.08 |
| 8 | Middle | -52.27 | -1.06 | 2.37 | -0.03 |
| 8 | Low | -49.62 | 0.54 | 0.12 | 0.14 |
| 9 | High | -6.84 | 0.19 | -0.41 | 0.15 |
| 9 | Middle | -9.30 | 0.20 | 1.81 | -0.03 |
| 9 | Low | -7.05 | -0.36 | -0.01 | 0.15 |
| 10 | High | -64.41 | 0.37 | -2.99 | 1.32 |
| 10 | Middle | -62.84 | -0.57 | 2.48 | 0.02 |
| 10 | Low | -60.00 | 0.98 | 0.43 | 0.09 |
| 11 | High | -100.02 | 0.48 | -3.87 | 1.59 |
| 11 | Middle | -96.10 | -0.81 | 2.31 | 0.03 |
| 11 | Low | -94.34 | 1.38 | 0.73 | 0.03 |
| 12 | High | -55.19 | 0.21 | -3.58 | 1.25 |
| 12 | Middle | -54.81 | -0.35 | 2.26 | 0.03 |
| 12 | Low | -52.68 | 0.97 | 0.82 | 0.05 |
| 13 | High | -7.28 | 0.26 | -1.27 | 0.33 |
| 13 | Middle | -10.33 | 0.43 | 1.52 | -0.01 |
| 13 | Low | -8.94 | 0.01 | 0.42 | 0.08 |
| 14 | YH | 15.59 | 0.61 | 0.86 | -0.21 |
| 14 | YM | 12.95 | 0.82 | 0.51 | -0.04 |
| 14 | YL | 12.54 | -0.67 | -0.18 | 0.13 |

**Table C.12. Effects of live load along length of pile G4-N**

| | | G4-N | | | |
|---|---|---|---|---|---|
| Load Case | Gage Set | P (kN) | Mx (kN-m) | My (kN-m) | Mz (kN-m) |
| 1 | High* | -87.75 | 4.64 | -2.26 | -0.84 |
| 1 | Middle | -118.61 | 1.93 | 3.20 | 0.24 |
| 1 | Low | -109.07 | 0.60 | -2.01 | -0.36 |
| 2 | High* | -59.94 | 3.53 | -1.11 | -0.62 |
| 2 | Middle | -80.92 | 2.18 | 3.92 | 0.18 |
| 2 | Low | -76.36 | 0.93 | -1.42 | -0.33 |
| 3 | High* | -20.86 | 2.14 | 1.61 | 0.01 |
| 3 | Middle | -24.50 | 2.12 | 2.46 | 0.15 |
| 3 | Low | -26.68 | 0.75 | -1.55 | -0.36 |
| 4 | High* | -124.79 | 5.22 | -4.04 | -1.19 |
| 4 | Middle | -153.96 | 2.33 | 2.98 | 0.16 |
| 4 | Low | -141.79 | 0.84 | -1.44 | -0.17 |
| 5 | High* | -81.94 | 2.26 | -2.52 | -0.87 |
| 5 | Middle | -95.53 | 2.52 | 3.70 | 0.13 |
| 5 | Low | -90.72 | 1.50 | -0.51 | -0.12 |
| 6 | High* | -37.73 | 0.55 | -0.55 | -0.39 |
| 6 | Middle | -38.37 | 1.99 | 2.85 | 0.08 |
| 6 | Low | -38.68 | 1.25 | -0.09 | -0.09 |
| 7 | High* | 8.98 | -1.97 | 0.51 | -0.29 |
| 7 | Middle | 7.43 | -0.31 | 0.60 | 0.07 |
| 7 | Low | 16.38 | -0.72 | -1.17 | 0.15 |
| 8 | High* | 6.57 | -0.70 | 0.37 | -0.39 |
| 8 | Middle | 2.69 | -0.50 | 1.14 | 0.04 |
| 8 | Low | 4.74 | -0.06 | -0.56 | -0.03 |
| 9 | High* | 10.62 | 0.84 | 1.99 | -0.08 |
| 9 | Middle | 13.97 | 0.52 | 1.14 | 0.01 |
| 9 | Low | 12.64 | -0.02 | -0.42 | -0.10 |
| 10 | High* | -25.77 | -0.07 | -0.50 | -0.54 |
| 10 | Middle | -32.85 | 0.31 | 1.88 | 0.06 |
| 10 | Low | -31.68 | 0.79 | -0.40 | -0.10 |
| 11 | High* | -65.46 | 1.97 | -3.12 | -1.03 |
| 11 | Middle | -87.86 | 0.06 | 1.97 | 0.06 |
| 11 | Low | -83.54 | 0.70 | -0.49 | -0.09 |
| 12 | High* | -50.65 | 1.61 | -2.17 | -0.71 |
| 12 | Middle | -64.50 | 0.72 | 2.59 | 0.06 |
| 12 | Low | -62.39 | 0.77 | -0.02 | -0.08 |
| 13 | High* | -23.03 | 0.55 | 0.43 | -0.08 |
| 13 | Middle | -19.43 | 1.12 | 1.97 | 0.05 |
| 13 | Low | -20.99 | 0.48 | 0.02 | -0.08 |
| 14 | ZH | 0.89 | 0.26 | 1.73 | 0.19 |
| 14 | ZM | 9.84 | 0.97 | 0.39 | 0.03 |
| 14 | ZL | 7.52 | 0.07 | -0.42 | -0.09 |


**Maine Department of Transportation**
**Bureau of Planning**
**Transportation Research Division**
**16 State House Station**
**Augusta, Maine 04333**
**tel. 207-624-3305**
**Fax 207-624-3301**


**For more information on all of our studies visit our website at:**
**http://www.maine.gov/mdot/Trans-Planning.php**

**Federal Highway Administration**